2015

Vibration and acoustic emission-based condition monitoring and prognostic methods for very low speed slew bearing

Wahyu Caesarendra
University of Wollongong

UNIVERSITY OF WOLLONGONG

School of Mechanical, Materials and Mechatronic Engineering

Faculty of Engineering and Information Sciences

Vibration and acoustic emission-based condition monitoring and prognostic methods for very low speed slew bearing

Wahyu Caesarendra

M.Eng. (Mechanical)
B.Eng. (hons.) (Mechanical)

A thesis submitted in fulfilment for the

award of the degree of

Doctor of Philosophy

from

University of Wollongong

March 2015

ABSTRACT

Heavy industries such as mining and steel mill rely on machinery that has a number of rotating parts. When unforeseen failure occurs, the plant may suffer from significant production loss. One of the most important rotating parts is slew bearing that supports highly loaded rotation. In order to prevent failure and reduce maintenance cost, a condition monitoring method for early damage detection of the slew bearing is required.

It is more difficult and complicated to analyse the condition of slew bearings that operate at a very low speed than to analyse that of typical rolling element bearings. Slew bearing signal has a low energy. It is non-stationary, chaotic and practically hard to analyse. Due to its low energy, the signal is masked by a higher background noise level. Therefore, it is difficult to extract the pertinent bearing signal. It is necessary to have reliable condition monitoring parameters or features that could extract accurate information about the bearing condition from the signal.

Recently, there has been increasing number of studies on slew bearing-based condition monitoring and fault detection. The studies mainly focused on the identification of bearing fault frequencies signalling the occurrence of the damaged bearing parts. However, a study on an entire slew bearing service life has not been presented. This thesis focuses on the slew bearing service life, and aims to investigate reliable features and to develop a methodology for slew bearing health assessment. To collect condition monitoring data for the entire bearing life, two laboratory tests were conducted. The tests were performed on a slew bearing test rig rotating at 1 rpm. The first laboratory test produced run-to-failure vibration data from slew bearing rotating in one direction. The second test produced vibration and acoustic emission (AE) data from reversibly rotated bearing.

To address the above-mentioned research challenges such as the difficulty in extracting features for slew bearing condition monitoring and prognostics, this thesis is divided into three parts: (1) vibration-based condition monitoring; (2) acoustic emission-based condition monitoring; and (3) integrated condition monitoring and prognostic method.

Part (1) includes a review of recent study on vibration condition monitoring of rolling element bearings and feature extraction methods. In the past five years, studies have been conducted on bearings operated at speed greater than 600 rpm with artificially defective bearings instead of bearings with natural defect. In terms of feature extraction methods, six categories are reviewed, namely (i) time-domain feature extraction; (ii) frequency-domain feature extraction; (iii) time-frequency representation; (iv) phase-space dissimilarity measurement; (v) complexity measurement; and (vi) other features. Among the six categories, time-domain feature extraction method is found to be the most dominant method in typical rolling element bearings. In addition, methods in the third and fourth categories are suitable for non-stationary, non-linear and chaotic signals. Therefore, a method of the fourth category, Largest Lyapunov Exponent (LLE) algorithm is selected and employed in this thesis.

The LLE algorithm can detect changes in the condition of the bearing. It demonstrated a better tracking of the progressive deterioration of the bearing during the test than comparable methods in the first category such as root mean square (RMS), skewness and kurtosis. This algorithm is also better than a method in the third category, empirical mode decomposition (EMD) method. The application of the method has been demonstrated with laboratory and industrial slew bearing condition monitoring data.

The thesis also develops a new feature extraction method based on circular domain analysis. The method employed data reduction process by adopting piecewise aggregate approximation (PAA) to detect frequency alteration in the bearing signal during the occurrence of the fault. From the processed data, circular domain features were extracted and monitored. The method can identify the incipient slew bearing damage; it is also compared to RMS, skewness, kurtosis, EMD and wavelet decomposition.

Part (2) presents a review of AE and complexity analysis of rolling element bearing. The review include (a) the application of AE in typical rolling element bearings running at different speed levels, i.e. high speed (> 600 rpm), low speed (10 – 600 rpm) and very low speed (< 10 rpm); (b) the commonly used AE hit parameters in rolling element bearings; and (c) AE signal processing, feature extraction and pattern recognition

methods. While most AE studies focus on high and low speed, this thesis focuses on very low speed. In addition, the commonly used AE hit parameters such as counts, energy, duration and RMS were tested and found to be effective monitoring parameters in high and low speed bearings.

This thesis investigates the AE hit parameters for slew bearing signals. In the experiment, significant changes in the slew bearing condition were detected from these parameters after the new bearing had run continuously for approximately 15 months. However, these changes are drastic and in practice cannot provide adequate warning for the maintenance engineers. The LLE algorithm, which has been effectively used with vibration signals, was also employed to extract feature of the AE waveform signals. It was shown that LLE algorithm can detect sign of failure earlier and demonstrate better progressive trend of the defect than AE hit parameters. At the end of the experiment, the slew bearing was dismantled and the surface defect / wear was analysed.

Part (3) presents a brief review of four prognostic approaches in rolling element bearings: (i) model-based approaches; (ii) reliability-based methods and probability models; (iii) data-driven approaches; and (iv) combined data-driven and reliability-based methods.

This thesis also develops an integrated condition monitoring and prognostic method based on multivariate state estimation technique (MSET), sequential probability ratio test (SPRT) and kernel regression. Both MSET and SPRT were used to analyse the recorded reliable features obtained from a previous work and clearly picked up the sign of early bearing damage. After the early damage detection signal had been acquired, kernel regression was used to predict the future condition of the bearing.

In summary, this thesis presents six major contributions to the study on very low speed slew bearing condition monitoring and prognosis: (1) review of studies on vibration and AE-based condition monitoring of rolling element bearing; (2) selection of reliable features for slew bearing condition monitoring parameters from features that were reported in the literatures; (3) development of alternative features based on circular domain analysis and LLE algorithm; (4) development of incipient damage

detection method based on MSET and SPRT; (5) development of future state prediction using kernel regression method; and (6) implementation of online monitoring system based on File Transfer Protocol (FTP).

Keywords: Acoustic emission-based condition monitoring, Feature extraction, Low speed slew bearing, Vibration-based condition monitoring, Prognostics

ACKNOWLEDGEMENTS

This thesis is a result of a three-and-a-half-years journey at the School of Mechanical, Materials and Mechatronic Engineering of University of Wollongong. Definitely, this doctoral thesis would never come true without support and help of some people. First and foremost, I would like to express my deepest gratitude to my principal supervisor, Dr. Buyung Kosasih, for his invaluable guidance, scholarly insight and genuine encouragement during my study. My sincere appreciation is also extended to my co-supervisor, Professor Anh Kiet Tieu, for his advice and his brilliant ideas. Without their supervision, this doctoral thesis would not be accomplished within 3.5 years.

My special thanks go to workshop staff in particular Mr. Stuart Rodd, Mr. Kevin Brown, Mr. Sean Ritchie and Mr. Keith Maywald for all help in slew bearing experimental works. I also wish to take the opportunity to thank Dr. Qiang Zhu and Dr. Kong Ning for their help on SEM, and Dr. Madeleine Strong Cincotta for language editing in some parts of the thesis.

I would like to convey my gratitude to the University of Wollongong for financial support through University Postgraduate Award (UPA) and International Postgraduate Tuition Award (IPTA) during this study.

Many thanks for all of my friends in University of Wollongong, especially to Dr. Craig A.S. Moodie, Mr. Yasa, Dr. Syamsul Hadi, Mrs. Ika Damayanti and Mr. Irshadi. My thanks also go to my colleagues in Diponegoro University in particular Dr. Berkah Fajar, Dr. Achmad Widodo, Dr. Joga Dharma Setiawan and Mr. Mochammad Ariyanto.

I would like to present my special acknowledgement to my beloved wife, Nia, for her love, faithful support and patience during the completion of this thesis. My two lovely “little princesses”, Zee zee and Zivara, who were born in Wollongong and make my day colourful. I would also like to express my deepest gratitude to my parents and my mother-in-law for their prayer and motivation as well as my family members and relatives in my hometown for their indirect support.

I apologize if I unintentionally forget to acknowledge persons who supported me to get this achievement.

LIST OF PUBLICATIONS

Journal articles

1. **W. Caesarendra**, J.H. Park, P.B. Kosasih, B.K. Choi, Condition monitoring of low speed slewing bearings based on ensemble empirical mode decomposition, Transactions of Korean Society on Noise and Vibration Engineering 23 (2) (2013) 141-153.
2. **W. Caesarendra**, P.B. Kosasih, A.K. Tieu, C.A.S. Moodie, B.K. Choi, Condition monitoring of naturally damaged slow speed slewing bearing based on ensemble empirical mode decomposition, Journal of Mechanical Science and Technology 27 (8) (2013) 2253-2262.
3. **W. Caesarendra**, B. Kosasih, A.K. Tieu, C.A.S. Moodie, Circular domain features based condition monitoring for low speed slewing bearing, Mechanical Systems and Signal Processing 45 (1) (2014) 114-138.
4. B. Kosasih, **W. Caesarendra**, K. Tieu, A. Widodo, C.A.S. Moodie, Degradation trend estimation and prognosis of large low speed slewing bearing lifetime, Applied Mechanics and Materials 493 (2014) 343-348.
5. **W. Caesarendra**, B. Kosasih, A.K. Tieu, C.A.S. Moodie, Application of the largest Lyapunov exponent algorithm for feature extraction in low speed slew bearing condition monitoring, Mechanical Systems and Signal Processing 50-51 (2015) 116-138.
6. **W. Caesarendra**, B. Kosasih, A.K. Tieu, C.A.S. Moodie, Integrated condition monitoring and prognosis method for incipient defect detection and remaining life prediction of low speed slew bearings, submitted to Mechanical Systems and Signal Processing (under review with Paper ID MSSP14-393).
7. S. Hadi, A.K. Tieu, C. Lu, H. Yu, **W. Caesarendra**, A.S.K. Parisianto, The effect of bulged punch on wrinkles reduction in micro deep drawing, submitted to Journal of Material Processing Technology (Accepted for publication).
8. **W. Caesarendra**, B. Kosasih, A.K. Tieu, H. Zhu, C.A.S. Moodie, Acoustic emission-based condition monitoring methods: Review and Application for low speed slew bearing, submitted to Mechanical Systems and Signal Processing (accepted for publication with paper ID MSSP14-741).

9. **W. Caesarendra**, B. Kosasih, A.K. Tieu, A review study of feature extraction for low speed slew bearing condition monitoring, Mechanical Systems and Signal Processing (under review with paper ID MSSP15-655).
10. **W. Caesarendra**, G.D. Haryadi, M. Ariyanto, B.H. Ahn, B.K. Choi, An application of mathematical morphology operators as feature extraction method for low speed slew bearing condition monitoring, Journal of Robotics and Mechanical Engineering Research (accepted for publication with paper ID JRMER-15-RA-111).

Conference proceedings

1. **W. Caesarendra**, P.B. Kosasih, A.K. Tieu, M. Arijanto, Vibration online condition monitoring system for slow speed slewing bearing based on file transfer protocol and web, In: Proceedings of 1st International Joint Conference on Advance Engineering, Indonesia, 2012.
2. **W. Caesarendra**, B. Kosasih, B.K. Choi, K. Tieu, C.A.S. Moodie, Condition monitoring of Naturally damaged slewing bearing based on EMD and EEMD methods, In: Proceedings of the 7th World Congress on Engineering Asset Management (WCEAM), Daejon, South Korea, October 8-9, 2012, pp. 125-136.
3. **W. Caesarendra**, B. Kosasih, A.K. Tieu, C.A.S. Moodie, Condition monitoring of low speed slewing bearing based on largest Lyapunov exponent algorithm and circular-domain feature extractions, In: Proceeding of the 26th International Congress of Condition Monitoring and Diagnostic Engineering Management (COMADEM), Helsinki, Finland, June 11-13, 2013, pp. 312-319, ISBN 978-952-67981-0-3.
4. **W. Caesarendra**, B. Kosasih, K. Tieu, C.A.S. Moodie, An application of nonlinear feature extraction – A case study for low speed slewing bearing condition monitoring and prognosis, In: Proceeding of the 12th IEEE/ASME International Conference on Advanced Intelligent Mechatronics, Wollongong, Australia, July 9-12, 2013, pp. 1713-1718.
5. **W. Caesarendra**, B. Kosasih, K. Tieu, A. Widodo, C.A.S. Moodie, Degradation trend estimation and prognosis of large low speed slewing bearing lifetime, In: Proceeding of 1st International Conference on Mechanical Engineering, Lombok, Indonesia, September 12-14, 2013.

6. **W. Caesarendra**, J.M. Lee, J.M. Ha, B.K. Choi, In: Proceeding of the 14th IEEE/ASME International Conference on Advanced Intelligent Mechatronics, Busan, South Korea, July 7-11, 2015, pp. 1161-1166.

Book chapter

1. **W. Caesarendra**, B. Kosasih, B.K. Choi, K.Tieu, C.A.S. Moodie, Chapter 12: Condition Monitoring of Naturally Damaged Slewing Bearing Based on EMD and EEMD. In: W.B. Lee, B.K. Choi, L. Ma, J. Mathew, eds. *Towards Integration and Interoperability in Engineering Asset Management*, Springer.

TABLE OF CONTENTS

DECLARATION OF AUTHORSHIP i

ABSTRACT ii

ACKNOWLEDGEMENTS vi

LIST OF PUBLICATIONS vii

TABLE OF CONTENTS x

LIST OF FIGURES xiii

LIST OF TABLES xix

LIST OF ABBREVIATIONS AND ACRONYMS xxi

NOMENCLATURE xxiv

Chapter 1 Introduction 1

1.1 Background and motivation 1

1.2 Scope of research 5

1.3 Scientific contributions 6

1.4 Thesis outline 7

Chapter 2 Review of vibration-based condition monitoring and feature extraction 10

2.1 Review of vibration-based condition monitoring 10

2.1.1 Vibration-based condition monitoring in general 10

2.1.2 Very low rotational speed 11

2.2 Review of feature extraction methods 15

2.2.1 Category 1: Time-domain feature extraction 17

2.2.2 Category 2: Frequency-domain feature extraction 30

2.2.3 Category 3: Time-frequency representation 33

2.2.4 Category 4: Phase-space dissimilarity measurement 42

2.2.5 Category 5: Complexity measurement 46

2.2.6 Category 6: Other features 48

2.2.7 Conclusion 49

Chapter 3 Laboratory experiment and industrial measurement 50

3.1 Laboratory slew bearing experiment 50

3.1.1 Slew bearing with continuous rotation (first laboratory test) 51

3.1.2 Slew bearing with reversible rotation (second laboratory test) 51

3.2 Industrial measurement 56
3.2.1 Coal bridge reclaimer 56
3.2.2 Slew bering data from industrial company in Korea 57
Chapter 4 Condition monitoring based on feature extraction 59
4.1 Circular domain features-based condition monitoring 60
4.1.1 Introduction 60
4.1.2 Angular resampling 61
4.1.3 Piecewise Aggregate Approximate (PAA) 63
4.1.4 Circular features analysis 75
4.1.5 Discussion 86
4.2 Largest Lyapunov Exponent (LLE) feature 88
4.2.1 Introduction 88
4.2.2 The LLE algorithm 89
4.2.3 LLE feature 98
4.2.4 LLE feature applied in bridge reclaimer data 104
4.2.5 Evaluation criteria in tracking progressive slew bearing failure 108
4.3 Conclusion 114
Chapter 5 Incipient defect detection method and damage analysis 116
5.1 Introduction 116
5.2 Multivariate State Estimation Technique (MSET) 116
5.3 Sequential Probability Ratio Test (SPRT) 119
5.4 Results and discussion 121
5.5 Damage analysis 127
5.6 Conclusion 132
Chapter 6 Acoustic emission-based condition monitoring 133
6.1 Introduction 133
6.2 AE-based condition monitoring in rolling element bearings 136
6.2.1 AE hit parameters 136
6.2.2 AE signal processing, feature extraction and pattern recognition 140
6.3 Results and discussion 148
6.3.1 AE hit parameters 148
6.3.2 Complexity analysis of AE signals 150

6.4 Conclusion 157
Chapter 7 Prognostic method for slew bearing 159
7.1 Review of prognostic methods 159
7.1.1 Classification of prognostic approaches 160
7.1.2 Prognostic methods for rolling element bearings 163
7.2 Integrated condition monitoring and prognostic method 171
7.2.1 Kernel regression 173
7.2.2 Results and discussion 178
7.3 Conclusion 186
Chapter 8 Conclusions and recommendations for future work 187
8.1 Conclusions 187
8.1.1 Vibration-based condition monitoring 187
8.1.2 Vibration feature extraction 188
8.1.3 AE-based condition monitoring 189
8.1.4 AE feature extraction 189
8.1.5 Integrated condition monitoring and prognostic method 190
8.2 Recommendations for future work 190
References 192
Appendix A The formula for calculating bearing fault frequencies 209
Appendix B Circular domain feature analysis 210
Appendix C Physical meaning of the reconstruction delay, *J* 213
Appendix D MATLAB codes 214
Appendix E Wideband differential AE sensor calibration chart 248
Appendix F Implementation of online monitoring system based on FTP 249

LIST OF FIGURES

Figure 1.1	Photo of axial/radial bearing, YR260.	2
Figure 2.1	Recent bearing vibration condition monitoring studies classified in two different speed levels and damage types. (Note: the year of publication is limited from 2009 to 2014, extensive literature for specific topics will be presented in different chapters).	12
Figure 2.2	Flowchart of CECDFFT method.	14
Figure 2.3	Statistical time-domain features: RMS, skewness, kurtosis, shape factor, crest factor, entropy, histogram upper bound and histogram lower bound extracted from the vibration slew bearing signal.	20
Figure 2.4	AR features (up to 8 coefficients) extracted from the vibration slew bearing signal.	22
Figure 2.5	Impulse factor and margin factor feature extracted from the vibration slew bearing signal.	23
Figure 2.6	Hjorts' parameters: activity, mobility and complexity extracted from the vibration slew bearing signal.	25
Figure 2.7	Illustration of four MM operators: (a) the original 1D signal, (b) the effect of erosion, (c) the effect of dilation, (d) the effect of closing and (e) the effect of opening. (Note: the solid blue line is the original signal and the dashed red line is the signal after being processed or transformed by the MM operators).	27
Figure 2.8	RMS feature extracted from MM operators for 0.9T (T = 1/BPFI): (a) erosion, (b) dilation, (c) closing and (d) opening.	29
Figure 2.9	RMS feature extracted from MM operators for 0.9T (T = 1/BPFO): (a) erosion, (b) dilation, (c) closing and (d) opening.	29
Figure 2.10	RMS feature extracted from MM operators for 0.9T (T = 1/BSF): (a) erosion, (b) dilation, (c) closing and (d) opening.	30
Figure 2.11	Frequency-domain features: FC, RMSF and RVF extracted from the vibration slew bearing signal.	31
Figure 2.12	Schematic visualization of block-based processing: the input signal with the input sample index i is split into overlapping	32

blocks of length B_L and block index n; the hop size H_S is the distance from the start of one block and the following block.

Figure 2.13 STFT of the vibration slew bearing signal (data May 3rd). 35

Figure 2.14 Three level wavelet decompositions of the vibration slew bearing signal. 37

Figure 2.15 Statistical-based features: mean, variance, skewness and kurtosis extracted from D3 signal of wavelet decomposition. 38

Figure 2.16 (a) A view of damaged rollers in axial plane; (b) outer raceway damage. 40

Figure 2.17 Statistical-based features: mean, variance, skewness and kurtosis extracted from EMD decomposition. 41

Figure 2.18 Fractal dimension, correlation dimension and approximate entropy feature extracted from the vibration slew bearing signal. 46

Figure 2.19 KS test feature extracted from the vibration slew bearing signal. 47

Figure 2.20 Sample entropy feature extracted from the vibration slew bearing signal 48

Figure 3.1 A photo of slew bearing laboratory test rig. 50

Figure 3.2 A photo of control mechanism to enable reversible rotation. 52

Figure 3.3 Illustration of reversible rotation from top view. 52

Figure 3.4 Schematic of laboratory slew bearing rig. (a) A larger front view of test rig showing a slew bearing attached on the drive ring and the applied load from hydraulic jack and (b) sensors placement. 53

Figure 3.5 A detailed sketch of accelerometers and AE sensors location. 54

Figure 3.6 An illustration of eccentric loading. 55

Figure 3.7 Slew bearing under test: (1) driving motor, (2) motor gear, (3) slew bearing gear and (4) sensor placement (radial). 57

Figure 4.1 One cycle of sinusoidal signal (1 Hz) sampled with 64Hz 64

sampling frequency is shown with solid blue curve. The data is divided into 8 frames (solid red line). The calculated mean value of sampled data in each frame is shown in yellow square shape. All mean values notated by the vector of $\mathbf{x} = (x_1, x_2, ..., x_8)$ are the PAA results. The index $w1, w2, ..., w8$ is the equal window size or "frame".

Figure 4.2 Neighborhood correlation plots of 1Hz and 5Hz sinusoidal signals with window size = 2. 66

Figure 4.3 Neighborhood correlation plots of 1Hz and 5Hz sinusoidal signals with window size = 4. 66

Figure 4.4 Neighborhood correlation plots of 1Hz and 5Hz sinusoidal signals with window size = 8. 67

Figure 4.5 Sinusoidal signal and PAA process (left) and neighbourhood correlation plot based on PAA result (right) for different frequencies with fix window size of 4: (a) 1Hz; (b) 2Hz; (c) 3Hz; (d) 6Hz. 67

Figure 4.6 Results of PAA data reduction of the laboratory test data: (a) March 2007; (b) May 2007; (c) August 2007; and results of coal bridge reclaimer data: (d) May 2004; (e) January 2005; (f) September 2006. 70

Figure 4.7 Simulated 5Hz signal with added white noise for different amplitude ratio; (b) PAA result or data reduced representation plotted in neighbourhood correlation plot. 71

Figure 4.8 Progression of simulated bearing signal degradation and the detection of fault occurrence using PAA. This signal is simulated with sampling frequency of 4880 and PAA window size of 40. Stage I: 5Hz signal + white noise for amplitude ratio of 0.1. Stage II: 5Hz signal + white noise for amplitude ratio of 0.4. Stage III: 55Hz signal + white noise for amplitude ratio of 0.4. Stage IV: 5Hz signal + white noise for amplitude ratio of 1. The four neighbourhood plots show the evolution of the ellipsoid and its orientation change. 72

Figure 4.9 Illustration of signal processing based on PAA method and ellipse least-square fitting method using vibration data acquired on May 25th (the 90th day). 74

Figure 4.10 Illustration of PAA method as frequency alteration identification and time domain to circular domain transformation using the vibration data acquired on May 25th 77

(the 90th day).

Figure 4.11 First laboratory slew bearing data acquired on March 1 (the 9th day): (a) vibration data in circular domain; (b) the 'occurrence' results plotted in circular domain (in radian); (c) circular histogram (in degree) (note: blue line and red line is circular histogram and resultant vector length (R), respectively); (d) circular feature extraction results. 81

Figure 4.12 First Laboratory slew bearing data acquired on May 25 (the 90th day): (a) vibration data in circular domain; (b) the 'occurrence' results plotted in circular domain (in radian); (c) circular histogram (in degree) (note: blue line and red line is circular histogram and resultant vector length (R), respectively); (d) circular feature extraction results. 81

Figure 4.13 Circular-domain feature extraction results and comparable methods (time-domain features, wavelet decomposition and EMD) from February to August 2007 (139 days measurement). 83

Figure 4.14 Shift factor value for different frequency alteration and different window size. 85

Figure 4.15 FFT of slew bearing data on May 25 data i.e. 90 days after the start. 86

Figure 4.16 The flowchart of preparatory LLE algorithm (note: N=15, J=2 and m=6). 91

Figure 4.17 (a) The initial Euclidean distance $\mathbf{d}_0$ at I = 1; (b) The new initial Euclidean distance value $\mathbf{d}_{0\_new}$ at i = 1. 95

Figure 4.18 (a) The initial Euclidean distance $\mathbf{d}_0$ at i = 64; (b) The new initial Euclidean distance value $\mathbf{d}_{0\_new}$ at i = 64. 96

Figure 4.19 (a) The initial Euclidean distance $\mathbf{d}_0$ at i = 128; (b) The new initial Euclidean distance value $\mathbf{d}_{0\_new}$ at i = 128. 96

Figure 4.20 Vibration data acquired on 30 August: (a) raw vibration data and (b) FFT. 100

Figure 4.21 One day LLE result (data April 26): (a) at the 9th second (stable condition, negative λ_1); (b) at the 16th second (non-linear condition, positive λ_1). 102

Figure 4.22 Number of positive λ_1 over the 139 measurement days from 103

February to August 2007.

Figure 4.23 Comparison condition monitoring performance between the LLE feature and other features: time domain features of raw vibration data and features of EMD: (a) features before smoothing; (b) features after smoothing of 100 samples. 104

Figure 4.24 FFT of coal bridge reclaimer: (a) data 28 July 2003; (b) data 16 September 2004 and (c) data 14 September 2005. 106

Figure 4.25 Comparison between time domain features and LLE feature extracted from the coal bridge reclaimer data: (a) RMS feature; (b) skewness feature; (c) kurtosis feature and (d) LLE feature. The measurement in the *x*-axis is related to Table 4.7. 107

Figure 4.26 Count of peaks of features extracted from laboratory slew bearing data. 109

Figure 4.27 Peaks identification of features extracted from laboratory slew bearing data. 110

Figure 4.28 First peak detection of features extracted from laboratory slew bearing data. 111

Figure 4.29 Interval between peaks of features extracted from lab slew bearing data. 112

Figure 5.1 Flowchart of the proposed combined MSET and SPRT method in step (1). 121

Figure 5.2 (a) Circular kurtosis; (b) Time-domain kurtosis; (c) Wavelet kurtosis; (d) EMD kurtosis; (e) The LLE feature. Note: t = dayth. 123

Figure 5.3 The SPRT index result for detecting impending bearing deterioration. 127

Figure 5.4 RMS, skewness, kurtosis and entropy features extracted from slew bearing data from the second laboratory test. 129

Figure 5.5 Naturally generated outer race damage photographs. 130

Figure 5.6 Naturally generated inner race damage photographs. 130

Figure 5.7 Naturally generated roller damage photographs and SEM images: (a) a photo of roller number 40; (b) a SEM of roller 131

number 40; (c) a photo of roller number 81 and (d) a SEM of roller number 81. Note that the total number of roller is 82. The roller was marked in clockwise direction.

Figure 6.1 AE hit parameters on one event. 138

Figure 6.2 AE hit parameters extracted from AE data at clockwise rotational directional. 150

Figure 6.3 The illustration of one AE measurement in a clockwise rotation. 154

Figure 6.4 (a) AE signal on 30 May 2013; (b) FFT. 155

Figure 6.5 (a) AE signal on 24 December 2013; (b) FFT. 155

Figure 6.6 LLE feature of AE channel 2. 156

Figure 7.1 A general prognostic approach or method selection for specific needs. 163

Figure 7.2 The integrated condition monitoring and prognostic method for low speed slew bearing. 172

Figure 7.3 Kurtosis extracted from the original vibration signal. The well-known kurtosis value for normal bearing is 3. The alarm threshold is set at 4 x 3 = 12. 174

Figure 7.4 Regression model of three data points and one-step-ahead prediction. 175

Figure 7.5 One-step-ahead prediction based on modified kernel regression. 176

Figure 7.6 Calculation of evaluation criterion, *E*: (a) time domain kurtosis feature; (b) LLE feature. 179

Figure 7.7 Kernel regression model and three-step-ahead prediction 181

Figure 7.8 Prediction of modified Kernel regression: (a) Time-domain kurtosis; (b) Wavelet kurtosis; (c) LLE feature; (d) PDF of the predicted failure day of the slew bearing. 135.2 is the peak value of the normal distribution (Note: the defect threshold is set differently to capture the abnormal peak of a particular feature; different feature may have different defect threshold value). 184

LIST OF TABLES

Table 1.1	Dimensions and properties of axial/radial bearings.	3
Table 2.1	Feature classification in wide range applications.	16
Table 2.2	Brief review of common time-domain feature extraction applied in condition monitoring of typical rolling element bearings.	18
Table 2.3	Fault frequencies of slew bearing (run at 1 rpm and 4.3 rpm for slew bearing test rig and slew bearing bridge reclaimer, respectively.	39
Table 2.4	Decomposition result of EMD method for slew bearing data on February 24.	39
Table 2.5	Decomposition result of EMD method for slew bearing data on May 3.	39
Table 2.6	Decomposition result of EMD method for slew bearing data on August 30.	40
Table 3.1	Specification of slew bearing used in coal bridge reclaimer.	56
Table 3.2	Fault frequencies of coal bridge reclaimer (Rothe Erde) bearing rotating at a nominal speed 4.3 rpm.	56
Table 3.3	Frequency content of slew bearing from industrial company in Korea.	58
Table 4.1	The effect of different window sizes on different unknown frequencies.	85
Table 4.2	Comparison methods in identifying the initial onset of damage.	87
Table 4.3	Comparison methods in estimating the progressive deterioration.	88
Table 4.4	The LLE algorithm showing the subroutines of *i* and *j* in order to calculate the new Euclidean distance $\mathbf{d}_{0\_new}$.	95
Table 4.5	The algorithm to calculate $\mathbf{d}_{\mathbf{new}}(i)$ based on *k* iteration and the index of minimum value, $\Delta_b(i)$.	98
Table 4.6	The LLE result (λ_1) at one second intervals during the 30	101

second vibration signal (data April 26).

Table 4.7 Details of LLE result (λ_1) related to the measurement dates. 108

Table 4.8 Evaluation comparison result for laboratory slew bearing data. 113

Table 4.9 Evaluation comparison result for coal bridge reclaimer data. 113

Table 5.1 Normalized $\mathbf{R}_{\mathrm{N}}$ matrix. 125

Table 5.2 Mean (M) values of normal state. 125

Table 5.3 Standard deviation (σ) values of normal state. 125

Table 5.4 Hypotheses for SPRT. 126

Table 5.5 Example calculation of L_i in one day observation. 127

Table 6.1 AE application in rolling element bearing for different speed levels and damage types. 135

Table 6.2 Seven common AE hit parameters based on two speed classification. 139

Table 6.3 Classification of AE-based condition monitoring and fault diagnosis methods. 147

Table 7.1 Classification of prognostic approaches extracted from literatures. 162

Table 7.2 Prognostic methods for rolling element bearing. 164

Table 7.3 Data points with non-uniform interval. 174

Table 7.4 Kernel regression model for 1-step-ahead prediction of time-domain kurtosis. 177

Table 7.5 The prediction of failure day. 183

Table 7.6 Original and predicted data points of time-domain kurtosis. 185

Table 7.7 Original and predicted data points of WD kurtosis. 185

Table 7.8 Original and predicted data points of LLE feature. 185

LIST OF ABBREVIATIONS AND ACRONYMS

Condition Monitoring and Prognostic

ALT	Accelerated Life Test
CBM	Condition-Based Maintenance
CM	Condition Monitoring
DI	Degradation Index
RUL	Remaining Useful Life

General

AE	Acoustic Emission
AI	Artificial Intelligence
ALE	Adaptive Line Enhancer
ANN	Artificial Neural Network
APCA	Adaptive Piecewise Constant Approximation
AR	Autoregressive
ARIMA	Autoregressive Integrated Moving Average
BPFI	Ball Pass Frequency of Inner race
BPFO	Ball Pass Frequency of Outer race
BSF	Ball Spin Frequency
CDF	Cumulative Distribution Function
CF	Crest Factor
CPH	Cox-Proportional Hazard
DAQ	Data acquisition
ECG	Electrocardiography
EEG	Electroencephalography
EMD	Empirical Mode Decomposition

EEMD	Ensemble Empirical Mode Decomposition
FC	Frequency Centre
FCO	Fault Characteristic Order
FFNN	Feed-Forward Neural Network
FFT	Fast Fourier Transform
GA	Genetic Algorithm
HHT	Hilbert Huang Transform
HMM	Hidden Markov Model
IF	Impulse Factor
IMF	Intrinsic Mode Function
KS	Kolmogorov-Smirnov
LLE	Largest Lyapunov Exponent
LPF	Low Pass Filter
MD	Mahalanobis Distance
MF	Margin Factor
MM	Mathematical Morphology
MSET	Multivariate State Estimation Technique
NN	Neural Network
PAA	Piecewise Aggregate Approximation
PCA	Principal Component Analysis
PCM	Principal Covariate Model
PDF	Probability Density Function
PHM	Proportional Hazard Model
PIM	Proportional Intensity Model
PMM	Power ratio of Maximum defective frequency to Mean

RCF	Rolling Contact Fatigue
RLS	Recursive Least Square
RMS	Root Mean Square
RMSF	Root Mean Square Frequency
RVF	Root Variance Frequency
RVM	Relevance Vector Machine
SE	Structuring Element
SK	Spectral Kurtosis
SOM	Self-Organizing Map
SPC	Statistical Process Control
SPRT	Sequential Probability Ratio Test
SS	Spectral Skewness
STFT	Short-time Fourier Transform
SVM	Support Vector Machine
SVR	Support Vector Regression
WPD	Wavelet Packet Decomposition
WVS	Wigner-Ville Spectrum

NOMENCLATURE

Nomenclature for circular domain features

C	number of occurrence of circular domain analysis
fs	sampling frequency
i^{th}	occurrence data point
k	circular kurtosis feature
m	circular skewness feature
N	number of data points of vibration signal
n	length of reduced-data in PAA method, $n = N / w$
$\mathrm{A_{RMS}}$	RMS of white noise amplitude
r	radius of circular plane
R	resultant vector length
S	number of samples for a half sinusoidal signal $\mathbf{x}$
$\mathbf{t}$	time discrete vector, $\mathbf{t} = (t_1, t_2, ..., t_N)$
$t_{\max}$	total time, $t_{\max} = t_N$
V	circular variance feature
$\mathrm{V_{RMS}}$	RMS of original vibration signal of slew bearing
w	window size in PAA method
$\mathbf{x}$	reduce-data in PAA method, $\mathbf{x} = (x_1, x_2, ..., x_n)$
$\mathbf{y}$	sampled vibration data, $\mathbf{y} = (y_1, y_2, ..., y_N)$
Z_i	circular plane of angular domain α_i

Nomenclature for largest Lyapunov exponent (LLE) algorithm

$\mathbf{d}_0$	initial Euclidean distance between phase space matrix $\mathbf{X}$ and the replicated matrix $\mathbf{X}_{rep}$
$\mathbf{d}_{0\_\text{new}}$	new Euclidean distance $\mathbf{d}_0$
$\mathbf{d}$	measured distance
$\mathbf{d_{new}}$	new measured distance
i	time duration of the acquired vibration data, ($i = 30$ seconds)
J	number of samples delay to construct the phase space matrix $\mathbf{X}$
M	number of rows of the phase-space matrix $\mathbf{X}$
m	embedding dimension of the phase-space matrix $\mathbf{X}$
N	number of sampled data points of vibration data $\mathbf{x}$
n	number of measurement days, $n = 139$
S_i	initial separation of original LLE algorithm
$\mathbf{X}$	phase-space matrix of LLE algorithm
$\mathbf{X}_{rep}$	row-vector replication of the phase space matrix $\mathbf{X}$
$\mathbf{x}$	vibration data, $\mathbf{x} = (x_1, x_2, ..., x_N)$
Δt	sampling period of vibration data $\mathbf{x}$
δ	elements of Euclidean distance calculation, $\left\|\mathbf{X} - \mathbf{X}_{rep}\right\|$
λ_1	largest Lyapunov exponent (LLE)
μ	number of nearest neighbors after and before the zero value
Δ_a	minimum value of $\mathbf{d}_{0\_\text{new}}$
Δ_b	identifier of the minimum value Δ_a

Nomenclature for MSET

$\mathbf{D}$	memory matrix
i	one measurement day, $i = 1, 2, ..., n$
$\mathbf{L}$	remaining training matrix
$\mathbf{L}_{\text{est}}$	health estimate matrix
m	number of features
n	number of measurement days, $n = 139$
n_T	number of days used in the training matrix $\mathbf{T}$
n_D	number of days used in the memory matrix $\mathbf{D}$
n_L	number of days used in the remaining training matrix $\mathbf{L}$
$\mathbf{P}$	data matrix
$\mathbf{P}_{\text{obs}}$	observation matrix or testing matrix
$\mathbf{P}_{\text{est}}$	actual estimate matrix
$\mathbf{R}_{\text{M}}$	monitored residual matrix
$\mathbf{R}_{\text{N}}$	normal residual matrix
$\mathbf{T}$	training matrix
$\mathbf{w}_1$	weight vector of health state
$\mathbf{w}_2$	weight vector of actual state
$\otimes$	nonlinear operator of MSET (e.g. Euclidean distance)

Nomenclature for SPRT

H_0	null hypothesis for healthy or normal condition
H_z	alternative hypothesis for unhealthy or anomaly condition, where z is a number of alternative hypothesis, e.g. $\mathrm{H}_1, \mathrm{H}_2, \mathrm{H}_3, \mathrm{H}_4$
i	one measurement day, $i = 1, 2, \ldots, n$
L_i	likelihood or probability ratio
M	mean of observation feature at i^{th} measurement day
s_i	statistical properties of the observed features of one measurement day, i.e. mean and standard deviation
z	number of alternative hypothesis
σ	standard deviation of observation feature at i^{th} measurement day

Nomenclature for kernel regression

A_p	accuracy of prediction
$\mathbf{K}_j$	Gaussian kernel vector
i	one measurement day, $i = 1, 2, ..., n$
k	*k*-step-ahead prediction
p	number of data points with non-uniform interval
t_a	actual final failure day
t_p	Predicted final failure day
$\mathbf{w}$	weight vector of kernel regression
$\mathbf{x}$	expanded non-uniform data point
X_j	one data point of kernel regression at j^{th} order
Y_j	feature level (y -axis value) of one data point X_j
$\hat{Y}_j$	future state prediction or predicted data point
α	kernel width
ε	sum square error

Chapter 1 - Introduction

"You don't have to be great to start, but you have to start to be great"
(Zig Ziglar)

1.1 Background and motivation

Steelmaking industry has many critical processes that rely on low rotating slew bearings. The bearings often endure harsh conditions and have high replacement costs with long delivery lead time. Therefore, it is important that their conditions are monitored at all times. However, due to their low speed operating condition and low energy vibration signal, traditional vibration analysis methods are unable to accurately process the signal and extract information about the bearing condition. As a result, some mills either run the bearings to failure or replace them after predetermined number of hours of operation. Both approaches lead to a high level of risk and the sub-utilization of the bearing. To avoid sudden bearing failure and to optimise the use of the bearing, it is necessary to have a condition monitoring method for the early damage detection.

It is more difficult and complicated to analyse the condition monitoring of slew bearings than to analyse that of typical rolling element bearings. This is because slew bearings are used at a much lower speed than typical rolling element bearings. Additionally, they are geometrically different from typical rolling element bearings. Slew bearings are large thrust bearings that are commonly used in large industrial machineries such as turntables, steel mill cranes, offshore cranes, rotatable trolleys, excavators, reclaimers, stackers, swing shovels and ladle cars. They typically support high axial and radial loads. The outer diameter of slew bearings can vary from 200 mm to 8000 mm and weigh up to 11.3 tonne [1].

Slew bearings are typically operated at very low rotational speed ranging from 0.5 to 15 rpm in continuous, intermittent and reversible rotation modes. Three axis slew

bearing was used in the experimental work of the thesis. The bearing is designed to support high axial and radial loads. Two slew bearings, YRT260 from Schaffler (Germany) and YR260 from Dalian Goldbull (China) were applied in this thesis. The bearings have an inner diameter of 260 mm and an outer diameter of 385 mm. A photograph of slew bearing YR260 is shown in Figure 1.1. Table 1.1 shows the detailed specifications of the slew bearing.

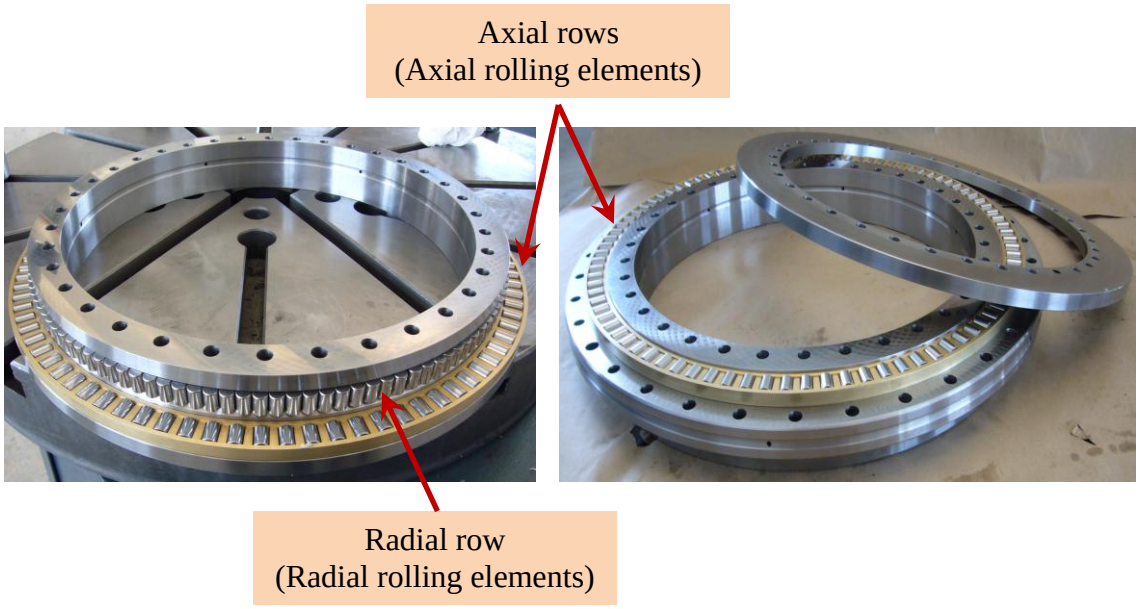

Figure 1.1 Photo of axial/radial bearing, YR260.

To monitor the daily condition of the degrading highly loaded slew bearings, parameters termed “features” are required to represent the bearing condition. For typical bearings, when spall occurs, the bearing emits detectable energy that will result in a significant level of vibration signal. Different from this, the vibration signal on a slew bearing is hard to detect. Therefore, the commonly accepted features used for monitoring typical bearings tend to be less effective when applied to slew bearings. This is because at low speed, the vibration amplitude of the bearing signal from the impact between the rotating elements and the defect is lower than the background noise signal. When some commonly accepted features applied in the signal with high amplitude noise level, the condition of the bearing is hard to detect. These features will show obvious changes when the damage is large. Once the damage is large, the vibration bearing signal is stronger than the background noise. This is why the features

show obvious changes. Once the damage is large, the vibration bearing signal is stronger than the background noise. However, by this stage the slew bearing has already been severely damaged. Therefore, the condition monitoring and prognostic systems for slew bearing need appropriate, sensitive and reliable features.

Table 1.1 Dimensions and properties of axial/radial bearings.

Dimension or Property	YRT260	YR260
Inner diameter (*Di*)	260 mm	260 mm
Outer diameter (*Do*)	385 mm	385 mm
Width (*w*)	55 mm	55 mm
Mass (*m*)	18.3 kg	19.5
Basic dynamic load rating (*C*)	109 kN (axial)	109 kN (axial)
	102 kN (radial)	102 kN (radial)
Basic static load rating (*Co*)	810 kN (axial)	810 kN (axial)
	310 kN (radial)	310 kN (radial)
Number of rolling element (*z*)	161 (axial)	119 (axial)
	66 (radial)	82 (radial)
Diameter of rolling element (*dr*)	6 mm (axial)	8 mm (axial)
	5 mm (radial)	8 mm (axial)
Pressure angel (α)	0^o (axial)	0^o (axial)
	90^o (radial)	90^o (radial)
Mean bearing diameter (*dm*)	325.6 mm (axial)	325.1 mm (axial)
	304 mm (radial)	307.82 mm (radial)

Recently, there have been an increasing number of studies on slew bearing-based condition monitoring and early fault detection. The studies employed a range of different methods such as vibration analysis [2-4], finite element method (FEM) [5-10] and oil analysis [11, 12]. The brief review of each research outcome is described below.

Slew bearing damage identification-based vibration analysis. Žvokelj et al. [3] proposed combined ensemble empirical mode decomposition (EEMD) and multi-scale principal component analysis (MSPCA) vibration analysis method. EEMD has been used to decompose signals into different time scales or intrinsic mode functions (IMFs). The significant IMFs are determined by features such as the kurtosis and crest factor of the signals. MSPCA is used to extract useful information from a large IMFs database. The

combined method is then used to control the time scale of the decomposition, the multivariate and multi-scale filtering or the reconstruction of the filtered signal.

An experiment has been designed to simulate a localized (single-point) defect. The double-row four-point contact ball bearing slewing ring with external gear was used as the test bearing. The test was conducted at 8 rpm. Ref. [4] is the extension work of Ref. [3] using the combination of EEMD with kernel PCA. Although the proposed vibration analysis method presented in [3] and [4] were successful, the method was only applied for the case of slew bearing with an artificial single defect. Further studies on the slew bearing with a natural defect need to be conducted. In addition, due to the extreme working conditions such as low rotational speed, reversible rotation and high load that are applied on slew bearing, in practice, slew bearing usually experiences multiple defects rather than single defect.

Slew bearing research based on finite element method or finite element analysis. Kania [5] analyses the deformation of slew roller bearing using finite element model. There are two objectives for the study: (1) the maximum roller-raceway contact force and (2) the maximum deformation of the bearing parts (raceway-roller-raceway) at the maximum force. The applied slew bearing was three-row roller bearing. Static load had been considered and applied on the radial and axial directions. Göncz et al. [6] develops a numerical model for fatigue life estimation of three-row slew bearing raceway based on a stress-life approach. In another study, Göncz et al. [7] presents a calculation procedure for the determination of dynamic load capacity of a large three-row roller slew bearing. Gang et al. [8] presents the finite element analysis (FEA) of a large-scale cross-roller bearing used in special propeller under the eccentric axial load. The objective is to calculate the contact stress between the rollers and the rings. The result of FE analysis has been compared to the theoretical analysis result. Glodež et al. [9] proposes a comprehensive computational model for determination of static capacity and the fatigue life of raceways of large slew bearing. Aguirrebeitia et al. [10] presents a mathematical model of the static load-carrying capacity of a three row roller slew bearings under axial load and tilting-moment. The critical value of the loads acting on a three row roller slew bearing is estimated based on the model.

Slew bearing condition monitoring-based oil analysis. Liu [11] proposes the condition monitoring of low speed heavily loaded bearing based on grease analysis. Bai et al. [12] presents the condition monitoring of a large slew bearing based on the oil analysis method by ferrography and spectrometric analysis. The oil analysis was considered in the study due to the difficulty in conducting vibration monitoring on slew bearing of ship loader and stacking crane in the Port. This method can detect element concentration of wear particle and contaminant as well as characterize and analyse the wear debris morphology that exist in lubricant. The element trace and the wear debris characteristics can indicate the running conditions of slew bearing. The three-row roller slew bearing with a large outer diameter of 5400mm was used. The rolling elements of this bearing are made of bearing steel and the cage is made of high polymer materials.

According to the above preliminary reviews, it can be highlighted that recent slew bearing studies have mainly focused on finite element method or finite element analysis to determine stress or strain for failure detection and prediction. The vibration analysis based on slew bearing condition monitoring is still being studied without a definite recommended guideline.

1.2 Scope of research

From the literature review in Chapter 2, it can be concluded that condition monitoring and prognostic methods for rolling element bearings have predominantly focused on speeds higher than 600 rpm and artificially generated single defect. This thesis focuses on the condition monitoring of bearing operating at 1 rpm with naturally generated multiple defects. The term naturally means that the defect is generated by introducing contaminants in the form of coal dust particles. The condition monitoring employed vibration and acoustic emission (AE) measurements. This study involves two laboratory accelerated life tests. The first test produced run-to-failure vibration data from slew bearing test rig rotating in one direction. The contamination was inserted in the bearing during the experiment. The second test produced the vibration and AE data from reversible test rig rotation (180 degree), and under dynamic and eccentric loading.

This thesis identifies appropriate features for slew bearing condition monitoring. Some features have been investigated using slew bearing vibration signals collected from the first test. It can be concluded from the results that most of the features have shown no obvious degradation trend of bearing condition. However, some features such as impulse factor, margin factor, approximate entropy and largest Lyapunov exponent (LLE) algorithm have been found to be appropriate for slew bearing condition monitoring. In particular, the LLE algorithm was further investigated in this thesis. This thesis also proposes a new feature extraction methods based on circular domain analysis and piecewise aggregate approximation (PAA).

This thesis also develops an integrated condition monitoring and prognostic method. The method employed combines multivariate state estimation technique (MSET) and sequential probability ratio test (SPRT) as an early damage detection method. Based on the incipient damage detection results, kernel regression was applied to predict the future condition of slew bearing.

This thesis also presents a review of AE in rolling element bearings and complexity analysis of AE waveform signal. The AE hit parameters were examined using slew bearing AE signals. Based on the results, the LLE algorithm was employed for feature extraction method.

1.3 Scientific contributions

Contribution 1: There have been a number of studies in vibration and AE-based condition monitoring of rolling element bearing. However, most of them focused on high rotational speed with artificially generated bearing defects, and a limited number of studies on very low speed with naturally defective bearing can be found. Rotating machinery running in very low rotational speed has been increasingly used with the development of more sophisticated technology. Bearing plays a major part in maintaining the sustainability of those machines. Therefore, it is important to develop an effective condition monitoring method for very low speed bearings.

Contribution 2: Monitoring of the slew bearing condition requires selection and extraction of features from both vibration and AE signals. Based on the study on feature extraction methods that have been reported in literatures, it is difficult to

select the most appropriate features for condition monitoring of slew bearings. This thesis reviews existing features and their extraction techniques in areas such as vibration signal, biomedical signal and financial time series data. Based on the literature review, LLE algorithm has been applied for slew bearing feature extraction method. However, it has not been used in bearing vibration signal generated from low rotational speed. This thesis also presents a new feature extraction technique based on piecewise aggregate approximation (PAA) and circular domain analysis.

Contribution 3: The outcome of Contribution 2 produces several reliable features for slew bearing condition monitoring. These features are processed in the integrated condition monitoring and prognostic method. The method employ MSET and SPRT on the recorded reliable features and provide a sign of early bearing damage. Based on the early damage detection warning, kernel regression is used to predict the future condition of slew bearing.

Contribution 4: A comprehensive review of AE method in rolling element bearing in three different speed levels (high speed, low speed and very low speed) is presented. While most AE studies focuses on high and low speed, this thesis focuses on very low speed. This thesis presents the investigation of AE hit parameters for slew bearing signals. In the experiment, significant changes in the slew bearing condition have been detected from the changes in the values of these parameters after the new bearing had run continuously for approximate 15 months. However, these changes, are drastic, and practically cannot provide adequate warning for the maintenance engineers. Based on the results, the LLE algorithm, which has been used effectively with vibration signals, was also employed for feature extraction of AE waveform signals. It is shown that LLE algorithm can detect signs of failure earlier and demonstrate better progressive trend of the defect than the AE hit parameters.

1.4 Thesis outline

This thesis includes 8 chapters. The subtopics contained in each chapter and how they are interlinked are described as follows.

Chapter 1 introduces the background and motivation of the research including slew bearing overview, literature review in slew bearing studies, scope of research and scientific contributions.

Chapter 2 first presents a comprehensive review of rolling element bearing vibration-based condition monitoring and feature extraction methods. The review presents the classification of literatures which is categorized into two different speed levels i.e. speed less than 600 rpm and greater than 600 rpm. Each category is divided into two types of damages i.e. natural (seeded) damage and artificial damage. The literature review then provides the investigation result of existing feature extraction methods or algorithms in wide range applications such as vibration analysis, time series analysis, bio-medical engineering and time series analysis. Some features are tested using vibration slew bearing data of the first laboratory test. The result of chapter 2 is the selected reliable features such as impulse factor, margin factor, approximate entropy and LLE.

Chapter 3 describes experimental work on the low speed slew bearing and presents the details of laboratory slew bearing test rig. The experiment consists of two laboratory tests. The first laboratory test produced run-to-failure vibration data from slew bearing test rig rotating in one direction. The second test produced the vibration and AE data from reversible test rig rotation (180 degree). This chapter also describes the slew bearing data obtained from industrial companies.

Chapter 4 proposes a new feature extraction-based condition monitoring method for low speed slew bearing. The method employs data reduction process using piecewise aggregate approximation (PAA) to detect frequency alteration in the bearing signal during the occurrence of fault. From the processed data, circular domain features such as circular mean, circular variance, circular skewness and circular kurtosis are calculated and monitored. This chapter demonstrates the application of the LLE algorithm for feature extraction method in low speed slew bearing condition monitoring. The LLE algorithm is employed to measure the degree of non-linearity of the vibration signal that is hard to be monitored by existing methods.

Chapter 5 applies the selected feature extraction results such as circular-domain kurtosis, time-domain kurtosis, wavelet decomposition (WD) kurtosis, empirical mode

decomposition (EMD) kurtosis and LLE feature that have been previously presented in Chapter 4. An application of multivariate state estimation technique (MSET) and sequential probability ratio test (SPRT) for early damage detection of slew bearing is also presented in this chapter. In addition, the chapter provides the damage analysis of slew bearing subject to high load, irregular greasing and eccentric loading.

Chapter 6 presents a review of AE in rolling element bearings and complexity analysis. The review includes (a) the application of AE in typical rolling element bearings running at different speed levels, i.e. high speed (> 600 rpm), low speed (10 – 600 rpm) and very low speed (< 10 rpm); (b) the commonly used AE hit parameters in rolling element bearings; and (c) AE signal processing, feature extraction and pattern recognition methods. This chapter also presents the investigation of AE hit parameters for slew bearing signals. Based on the investigation results, the LLE algorithm which has been effectively applied with vibration signals was employed for feature extraction of AE waveform signals.

Chapter 7 presents a review of prognostic methods applied in rolling element bearings. The review starts with the classification of prognostic approaches from the previously published studies. From the classification results, detailed prognostic classifications including the prognostic methods, their aims and the condition monitoring and prognostic features are summarized. A review of recent studies on slew bearing service life prediction is also presented. This chapter also presents the prediction of the selected features' trends and the estimation of the remaining useful life (RUL) of the slew bearing using kernel regression. This prognostic method is linked to condition monitoring features presented in Chapter 5.

Chapter 8 presents the conclusions of the work conducted to date and the essential future work.

Chapter 2 - Review of vibration-based condition monitoring and feature extraction

"A journey of a thousand miles begins with a single step"
(Chinese philosopher Laozi)

In order to identify the research gap and make the scientific contributions, this thesis conducts literature review on three areas: (1) vibration-based condition monitoring and feature extraction methods in Chapter 2, (2) acoustic emission-based condition monitoring in Chapter 6 and (3) prognostic approaches for rolling element bearings in Chapter 7.

2.1 Review of vibration-based condition monitoring

2.1.1 Vibration-based condition monitoring in general

For decades, vibration analysis has been used as a condition-based maintenance (CBM) tool by maintenance engineers to investigate whether a part or equipment is suitable for further use. Randall (2011, p3) [13] states that machines generate vibrations even in good condition. However, if faults occur, the machine's vibration signals will differ from standard vibration signals. In addition, vibration analysis distinguishes between the vibration signature during standard conditions and faulty conditions. A pioneering study on machines in standard conditions has been presented by Braun [14], which proposes the term 'mechanical signature analyses'.

A commonly used method for bearing vibration analysis and fault diagnosis is spectral analysis [15]. Yang and Widodo [15] claim that the spectral analysis of vibration signal is the most reliable method of assessing the rotating machine condition particularly the bearing condition. Usually, when bearings operate in rotating machines, coupled parts of machines, including the bearing, transmit the vibration

signals. From the vibration signals, related frequency spectrum that characterizes standard machine condition can be identified using spectral analysis. When a bearing either wears or becomes damaged, some frequency components in the spectrum will change. In fact, each fault in a machine produces vibrations with distinctive characteristics that can be measured and compared with standard condition in order to perform the fault detection and diagnosis.

As the technology involved becomes more sophisticated, the rotating machinery that uses rolling element bearings to support their operational work is also more complex. It is because the machine is sometimes operating at low speed and in non-stationary condition. This will generate chaotic vibration signals emanating from a nonlinear system. In this particular case, it is necessary to have an appropriate condition monitoring method, especially feature extraction method.

2.1.2 Very low rotational speed

According to the SPM (Shock Pulse Measurement) HD company website [16]:

"*Condition monitoring on machinery operating at low speed is more complicated than on industrial machinery in general. Signals originating from bearing and gear problems are typically low in energy content, jumbled up and practically unanalyzable. Distinguishing these signals from background noise in order to extract meaningful bearing information can be a very difficult task. Measurement data collected at low speeds are often mistakenly dismissed as being "just noise". Hence, bearing wear and damage often goes undetected until it is too late*."

The challenge of bearing condition monitoring at very low speed as mentioned above is the main problem addressed in this thesis. In order to narrow the literature review, the classification of bearing speeds should be initially determined. Although there is no accepted standard criterion for speed classification of rotating machinery, some literatures mentioned that speed below 600 rpm is "low rotating speed machinery" [17-19] and speed greater than 600 rpm is "high speed machinery" [20, 21]. Hence, the review on the two speed classifications: (1) low speed (lower than 600 rpm) and (2) high speed (greater than 600 rpm) are used in this thesis.

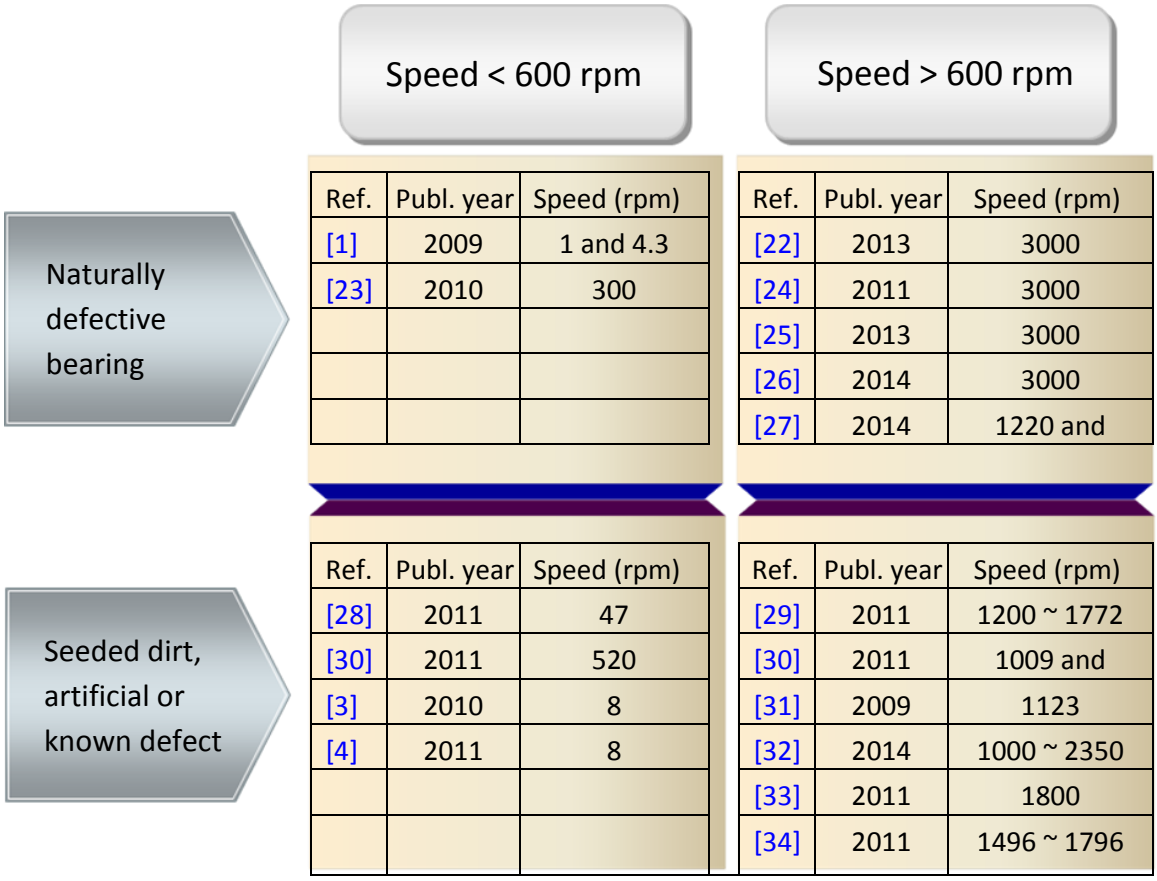

Ref.	Publ. year	Speed (rpm)
[1]	2009	1 and 4.3
[23]	2010	300

Ref.	Publ. year	Speed (rpm)
[22]	2013	3000
[24]	2011	3000
[25]	2013	3000
[26]	2014	3000
[27]	2014	1220 and

Ref.	Publ. year	Speed (rpm)
[28]	2011	47
[30]	2011	520
[3]	2010	8
[4]	2011	8

Ref.	Publ. year	Speed (rpm)
[29]	2011	1200 ~ 1772
[30]	2011	1009 and
[31]	2009	1123
[32]	2014	1000 ~ 2350
[33]	2011	1800
[34]	2011	1496 ~ 1796

Figure 2.1 Recent bearing vibration condition monitoring studies classified into two different speed levels and damage types. (Note: the year of publication is limited from 2009 to 2014, extensive literature for specific topics will be presented in different chapters).

Rotational speed greater than 600 rpm

Figure 2.1 indicates that a number of studies on bearing speed greater than 600 rpm in the past five years are still greater than that below 600 rpm. In the category of bearing with a natural defect, methods such as support vector regression (SVR) [22], Kolmogorov-Smirnov test [24], singular value decomposition (SVD) [25] and correlation dimension and approximate entropy [26] have been used. These methods have been applied in vibration data collected from bearing accelerated life test rotating at 3000 rpm. In addition, an online detection method for naturally progressing defect bearing was presented by Shakya et al. [27] based on Mahalanobis distance (MD). Due to the difficulties and the time issue in obtaining the entire bearing service life data (normal-fault-failure condition), the bearing accelerated life test was considered in more studies. In conclusion, there have been more studies on artificially damaged bearings

than on naturally defective bearings. The research in vibration analysis of rolling element bearing has mainly focused on high speed bearings with artificially damaged bearings so far. The methods include e.g. *K*-means clustering [29], mathematical morphology (MM) method [30], difference histograms [31], fault characteristic order (FCO) analysis [32] and antisymmetric real Laplace wavelet [33]. The bearing speeds in the above mentioned papers were varied from 1000 to 2350 rpm.

Rotational speed below 600 rpm

Very few studies on low speed bearings below 600 rpm, particularly the studies on naturally defective bearings, have been found during the past five years. The vibration signals generated from low speed bearings are more difficult to analyse than those generated from high speed bearings. Thus, acoustic emission (AE) is the preferred method used in analysing low speed bearings than the vibration analysis.

Prior to the present slew bearing study, an investigation into the condition monitoring of low speed slew bearings was initiated by Moodie [1]. The study focuses on (1) the design and construction of experimental slew bearing rig and (2) the detection of bearing fault frequencies such as ball pass frequency outer race (BPFO), ball pass frequency inner race (BPFI) and ball spin frequency (BSF) based on spectral analysis. Some novel signal processing methods including symmetric wave decomposition (SWD), compressed eigenvector deconvolution spectral analysis (CEDSA) and ring matric fault values (RMFV) were proposed for slew bearing condition monitoring. The SWD combined with fast Fourier transform (FFT) has been formed into one integrated method called SWDFFT. The CEDSA and RMFV methods are integrated into a method named CECDFFT (compressed eigenvalue compressed discrete fast Fourier transform). The result shows that SWDFFT can identify the BPFO, BPFI and BSF. Based on these findings, the progression of bearing fault frequencies is presented. However, the discussion on the selection of the number of wave (*nwave*) in SWD method is not presented, thus the operator needs to select the *nwave* arbitrarily, and this is time consuming. In addition, the study uses two different sampling frequencies of 4880 Hz and 625000 Hz. The result of SWDFFT indicates that the progression of bearing fault frequencies from 625000 Hz sampled data is clearer than that from 4880 Hz sampled data. However, using 625000 Hz sampled data will affect the

computational time. Similarly, CECDFFT has also been used initially to calculate the bearing fault frequencies followed by the calculation of the progressions of bearing fault based on the fault frequencies amplitude. However, the analysis of vibration data with 625000 Hz sampling rate; and the selection method of a number of upsampling (times) and downsampling (times) were not studied. In addition, both SWDFFT and CECDFFT are less applicable in practice due to their complex computational procedures. For example, the CECDFFT have to pass several methods to calculate the bearing fault frequencies as shown in Figure 2.2.

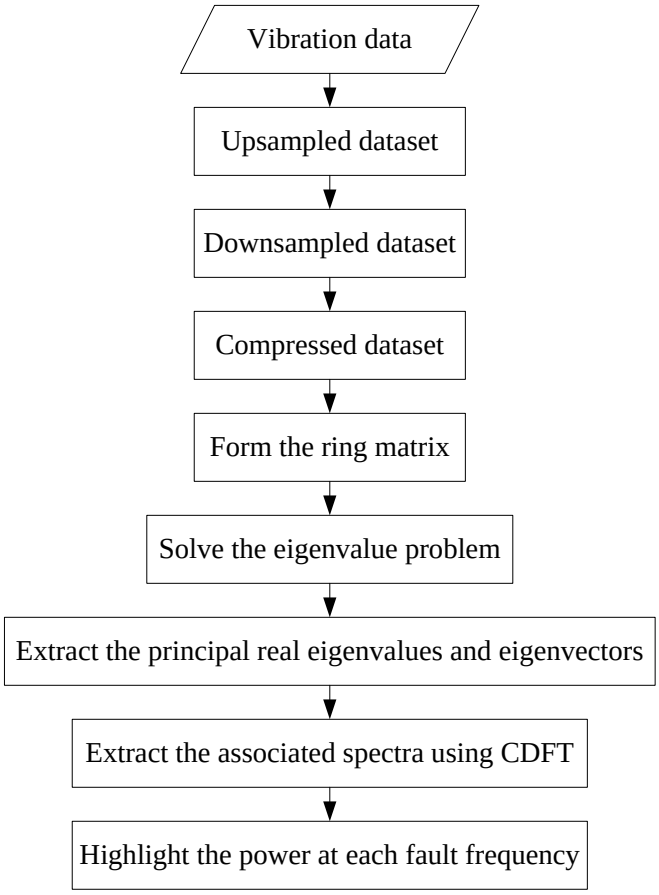

Figure 2.2 Flowchart of CECDFFT method [1].

One other study of very low speed bearing condition monitoring utilizing vibration signal was presented by Žvokelj et al. [3] and [4]. A review of these studies has been presented in Chapter 1. The methods work effectively for slew bearing vibration signals with artificial single defects [3] and [4]. However, further studies on multiple defects are necessary because the multiple defects are the common issue in practice

due to the extreme slew bearing operating conditions such as low speeds, reversible rotations and high loads.

Another study in low speed below 600 rpm presents the angular resampling method for the study on bearing in the wind turbines operating at 47 rpm under non-linear speed fluctuations [28]. The morphological method employed in bearing speed at 520 rpm is presented in [30].

As condition monitoring methods requires reliable features, a review on feature extraction methods is conducted in this thesis. This will be described further in Section 2.2.

2.2 Review of feature extraction methods

The terms and the utilization of features have been widely applied in some areas such as in vibration analysis [19], [29], [35], biomedical engineering [36], [37] and time series analysis [38]. In vibration analysis, especially for bearing condition monitoring, features can be defined as representative values to indicate bearing conditions. This is because the features are extracted from raw vibration signals acquired from rolling element bearing. The features identifying certain values indicate whether the condition of the bearing is normal or failing. The classification and the summary of features in a wide range application are presented in Table 2.1.

Table 2.1 Feature classification in wide range applications.

Category	Name of Features	References
Time-domain feature extraction	Mean, peak value and peak-to-peak	[19],[39],[40],[41],[18],[42],[43]
	Standard deviation and variance	[29],[19] ,[39],[40]
	Root mean square (RMS)	[29],[19] ,[39],[41],[18],[44],[42],[45],[46]
	Skewness	[29],[19] ,[39],[40],[41],[18],[42]
	Kurtosis	[29],[19] ,[39],[40],[41],[18],[42],[45],[46],[47]
	Crest factor	[29],[19],[41],[18],[42],[43]
	Shape factor	[29],[19] ,[43]
	Entropy estimation	[19],[40],[41]
	Upper, lower and difference histogram	[31],[19],[41]
	Autoregressive (AR) coefficients	[41],[48],[49]
	1^{st} Hjort parameter (activity)	[36],[50]
	2^{nd} Hjorth parameter (mobility)	[36],[50]
	3^{rd} Hjorth parameter (complexity)	[36],[50]
	Mathematical morphology operators	[30],[35],[51],[52]
	5^{th} to 9^{th} central moment	[29]
	Impulse factor (IF)	[29],[42],[43]
	Clearance factor or margin factor (MF)	[29],[42],[43]
	Zero-crossing	[53]
Frequency-domain feature extraction	Discrete and fast Fourier transform	[54]
	Mean frequency or frequency centre (FC)	[19],[41],[55],[43]
	Root mean square frequency (RMSF)	[19],[41],[43]
	Median frequency	[36]
	Root variance frequency (RVF)	[19],[41],[43]
	Spectral entropy	[36],[50],[56]
	Shannon entropy	[36],[57]
	Spectral skewness	[58]
	Spectral kurtosis	[58],[59],[60],[61]
	Energy	[29]
	Residual energy	[62]
	Power ratio of max defective frequency to mean (PMM)	[42],[63]
Time-frequency representation	Short-time Fourier transform (STFT)	[39]
	Wigner-Ville spectrum (WVS) and Wigner-Ville distribution (WVD)	[64]
	Instantaneous power spectrum distribution	[65]
	Wavelet transform	[39],[66],[67]
	Empirical mode decomposition (EMD)	[68],[69]
	Ensemble EMD (EEMD)	[70]
	S transform	[71]
Phase-space dissimilarity measurement	Fractal dimension	[36],[72],[73]
	Correlation dimension	[26],[74]
	Approximate entropy	[26],[36],[75],
	Largest Lyapunov exponent	[36],[37]
	Permutation entropy	[76]
Complexity measurement	Kolmogorov-Smirnov test	[26]
	Sample entropy	[77]
Other features	Singular value decomposition	[66],[78]
	Piecewise aggregate approximation	[38],[79]
	Adaptive piecewise constant approximation	[78]
	Particle filter	[55]
	Mahalanobis distance	[27]

2.2.1 Category 1: Time-domain feature extraction

Statistical-based features

Statistical features such as mean, root mean square (RMS), standard deviation and variance were usually used in past studies to identify the differences between one vibration signal and another. These features are called time-domain dimensional features, because they are calculated directly from the vibration signals (in time-domain). More advanced statistical-based features such as skewness and kurtosis can be applied to the signal which is not purely stationary. These features examine the probability density function (PDF) of the signal. It is a well-known fact that if the condition of the bearing changes, the PDF also changes, thus the skewness and kurtosis might be able to detect the changes. Furthermore, skewness is used to measure whether the signal is negatively or positively skewed. Kurtosis measures the peak value of the PDF and indicates that the signal is impulsive in nature. Based on the definition of moment, skewness is equal to zero for a signal with a normal distribution i.e. normal bearing signal. A negative value is due to skewness towards lower value while a positive value indicates non-symmetry towards higher values.

In addition, kurtosis, as the fourth-order moment is obtained from the peak of the PDF of the vibration signal, while skewness is obtained from the mean value of the PDF of the vibration signal. It is well known that the vibration signal of normal bearing has the kurtosis value of three [80] and the skewness value of approximately zero. Then, when the vibration signal changes due to faults, the kurtosis value will increase to greater than three and the skewness value will shift to either negative or positive. In higher order statistics (HOS), the kurtosis and skewness based on the definition of cumulant have value zero for Gaussian signals. Other features which can be calculated from PDF of the vibration signal includes: entropy, which calculates the histogram of the PDF and measures the degree of randomness of the vibration signal; lower bound and upper bound histogram, which measure the lower and upper values of the PDF respectively.

Aside from the time-domain dimensional features, there are other non-dimensional features such as shape factor (defined as RMS divided by mean) and crest factor

(defined as standard deviation divided by RMS). Both features will change as the mean, RMS and standard deviation change. The summary of these features is presented in Table 2.2.

Table 2.2 Brief review of common time-domain feature extraction applied in condition monitoring of typical rolling element bearings [81]**.**

Feature Name	Description	
	Brief Definition	Formula
RMS	As fault developed the RMS value will increase progressively. However, RMS has the shortcoming that it is unable to provide the information of incipient fault stage while it increases with the fault development [45].	$RMS = \sqrt{\frac{1}{N}\sum_{i=1}^{N} x_i^2}$
Variance	Variance quantifies the dispersion of a signal or a data set around their mean reference.	$\sigma^2 = \frac{\sum_{i=1}^{N}(x_i - m)^2}{(N-1)\sigma^2}$
Skewness	Skewness measures the asymmetry of probability density function (pdf) of vibration signal.	$Sk = \frac{\sum_{i=1}^{N}(x_i - m)^3}{(N-1)\sigma^3}$
Kurtosis	Kurtosis measures the degree of flatness of the probability density function (pdf) near its centre. In high speed bearing rotation, the kurtosis value of bearing normal is well-recognized as 3.	$Ku = \frac{\sum_{i=1}^{N}(x_i - m)^4}{(N-1)\sigma^4}$
Shape factor	Refers to a value that is affected by an object's shape but is independent of its dimensions [29].	$SF = \frac{\sqrt{\frac{1}{N}\sum_{i=1}^{N} x_i^2}}{\frac{1}{N}\sum_{i=1}^{N} \lvert x_i \rvert}$
Crest factor	Crest factor (CF) is a measure of how much impact. CF is appropriate for "spiky signals" [29].	$CF = \frac{\max \lvert x_i \rvert}{\sqrt{\frac{1}{N}\sum_{i=1}^{N} x_i^2}}$
Entropy	Entropy, $e(p)$, is a measure of the uncertainty and randomness of a sampled vibration data. Given a set of probabilisties, $(p_1, p_2, \ldots, p_n)$, the entropy can be calculated using the formulas as shown in the right column.	$e(p) = -\sum_{i=1}^{n} p(z_i)\log_2 p(z_i)$

Upper and lower bound of histogram

The histograms or a discrete probability density function, is calculated in the following way [15]. Let d be the number of divisions that is desired to divide the ranges into, and let h_i with $0 \le i < d$ be the columns of the histogram. For the time x_i

$$h_i = \sum_{j=0}^{n} r_i(x_i), \forall i, 0 \le i < d \tag{2.1}$$

$$r_i = \begin{cases} 1, & if \ \dfrac{i(\max(x_i) - \min(x_i))}{d} \le x < \dfrac{(i+1)(\max(x_i) - \min(x_i))}{d} \\ 0, & otherwise \end{cases} \tag{2.2}$$

The upper bound h_U and lower bound h_L of histogram are defined as

$$h_U = \max(x_i) + \Delta/2 \tag{2.3}$$

$$h_L = \max(x_i) - \Delta/2 \tag{2.4}$$

where $\Delta = (\max(x_i) - \min(x_i))/(n-1)$.

According to the feature extraction results presented in Figure 2.3, some features show the fluctuation in the last measurement day approximately from the 90th day to the 139th day such as RMS, variance, kurtosis and histogram lower. These indicate that some features are sensitive to the slew bearing condition whilst others are less appropriate. The fluctuation is associated with roller and outer race defects as shown later in Figure 2.16. However, more appropriate and reliable features are necessary for the condition monitoring of slew bearing to detect an impending damage and to estimate the degradation index for prognostics.

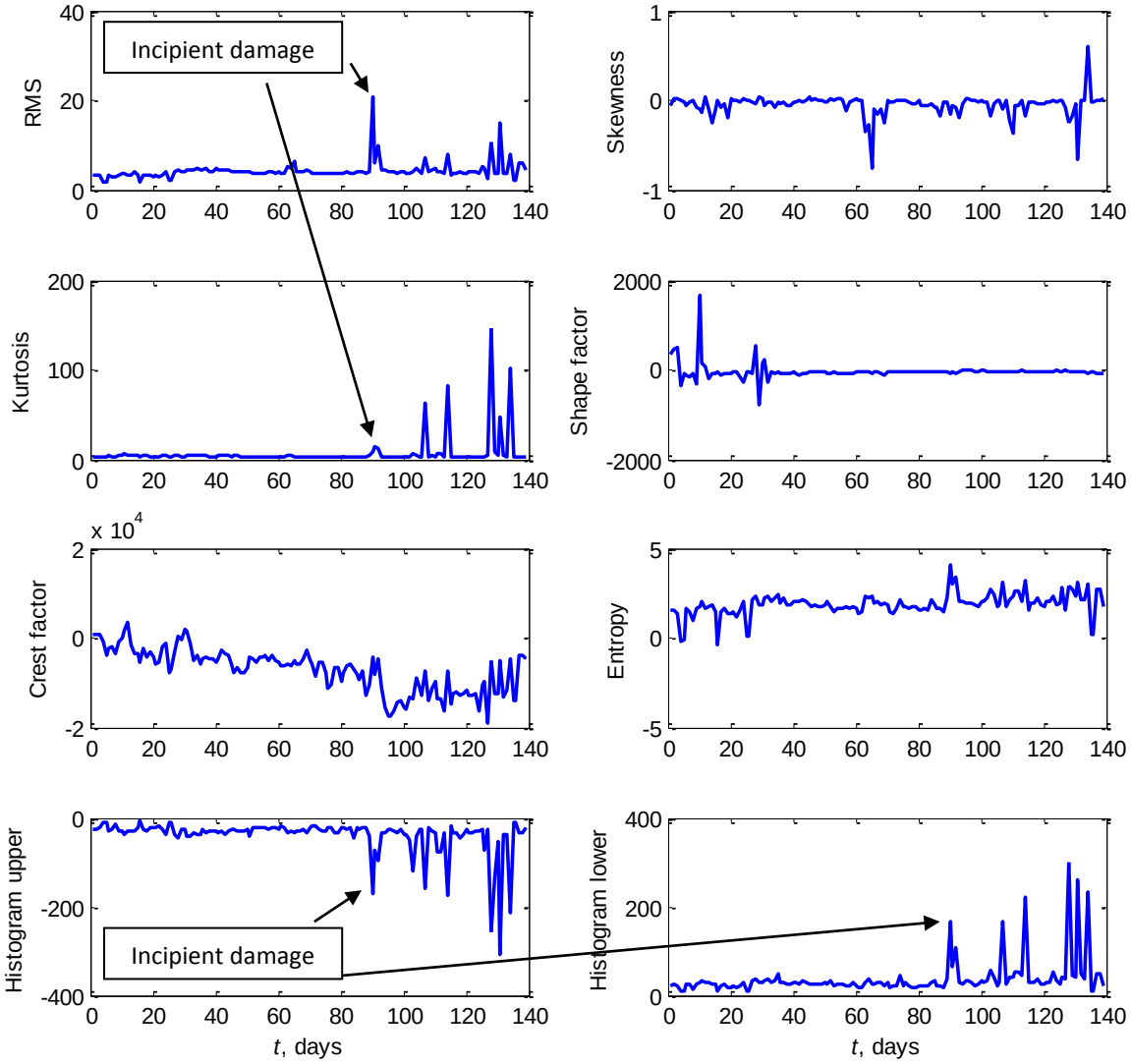

Figure 2.3 Statistical time-domain features: RMS, skewness, kurtosis, shape factor, crest factor, entropy, histogram upper bound and histogram lower bound extracted from the vibration slew bearing signal.

Autoregressive (AR) coefficients

In other studies, the autoregressive (AR) coefficients of the vibration signal are calculated and used as a bearing vibration feature. It is known that faulty vibration signal of typical rolling element bearings produces different autoregressive coefficients from normal vibration signal. Coefficients of AR models are selected through Burg's lattice-based method using the harmonic mean of forward and backward squared

prediction errors [15]. A common approach for modelling univariate time series is the AR model as follows:

$$y_t = a_1 y_{t-1} + a_2 y_{t-2} + \ldots + a_n y_{t-n} + \varepsilon_t = \sum_{i=1}^{n} a_i y_{t-1} + \varepsilon_t \quad (2.5)$$

where a_1 to a_n are the autoregressive coefficients, y_t is the time series under investigation, n is the order of the AR model ($n=8$) and ε is the residual which always assumed to be Gaussian white noise. An AR model (Eq. 2.5) is simply a linear regression of the current value of the series against one or more prior values of the series [15].

The RMS, skewness, kurtosis, entropy and AR coefficients have been tested using vibration datasets from induction motor [48] and rolling element bearing [19]. These papers have made great contributions to the research areas on the bearing condition monitoring and fault diagnosis. However, the features were tested for artificially bearing damage. In practice, the damage is typically developed naturally rather than artificially.

The AR coefficient results are presented in Figure 2.4. It is shown that most of features are less appropriate to represent the slew bearing condition except AR coefficient 4 which is shown to be fluctuating in the last measurement.

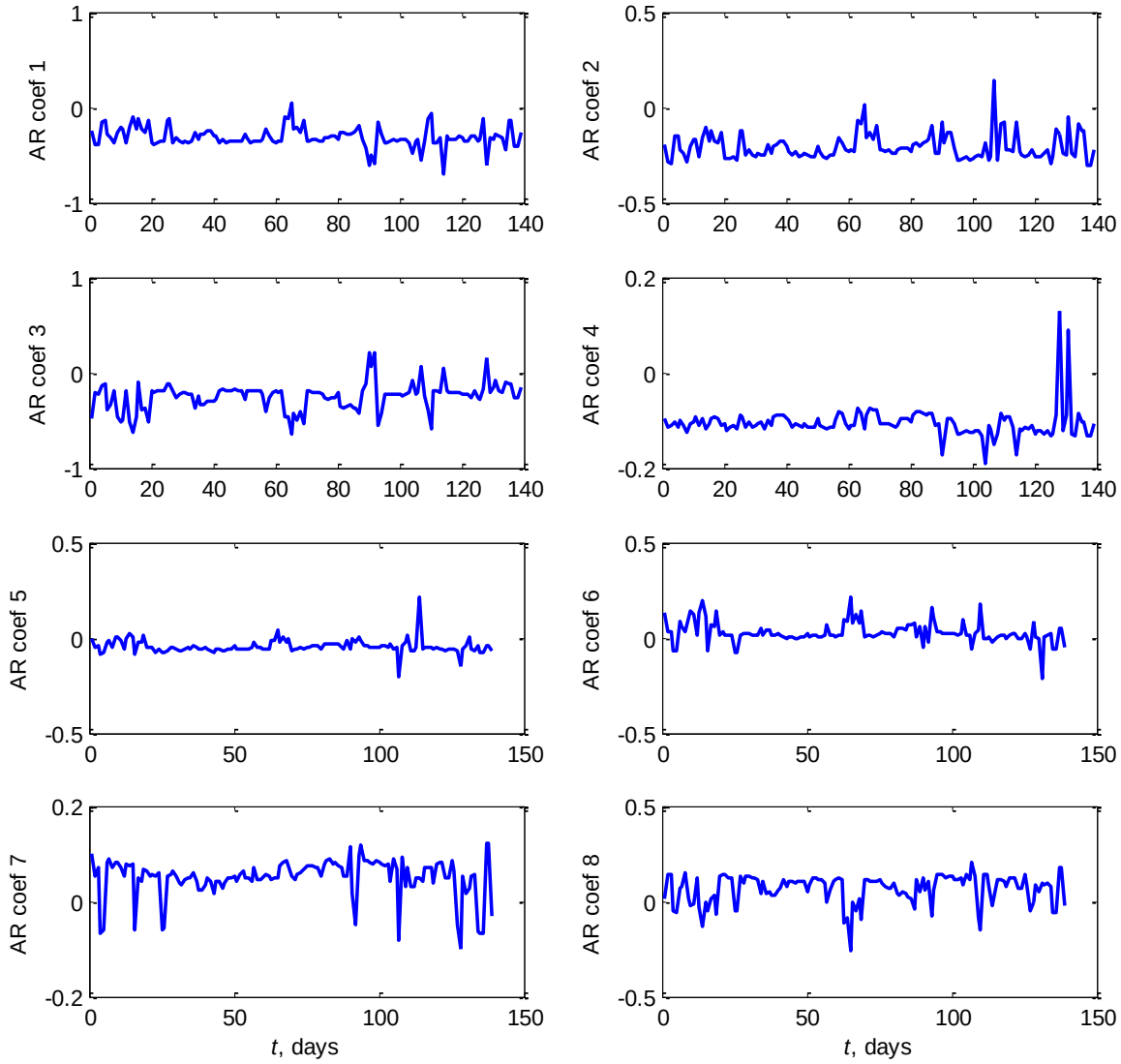

Figure 2.4 AR features (up to 8 coefficients) extracted from the vibration slew bearing signal.

Other time domain features such as impulse factor, margin factor or clearance factor have been recently used [29, 42, 43]. Similar to crest factor (CF), impulse factor (IF) is used to measure how much impact is generated from the bearing defect. CF measures the impact by dividing the maximum absolute value of vibration data and RMS value, while IF divides the maximum absolute value by the mean of absolute value. The formula is defined as follows:

$$IF = \frac{\max|x_i|}{\frac{1}{N}\sum_{i=1}^{N}|x_i|} \tag{2.6}$$

Margin factor (MF) or clearance factor is used to measure the level of impact. MF is calculated using the maximum absolute value of the vibration signal divided by the square of the mean of the square root of the absolute values of the vibration signal. The formula is defined as follows:

$$MF = \frac{\max|x_i|}{\left(\frac{1}{N}\sum_{i=1}^{N}\sqrt{|x_i|}\right)^2} \tag{2.7}$$

The progression of slew bearing deterioration of IF and MF features are clearer than RMS, variance, kurtosis and histogram lower features as presented in Figure 2.5.

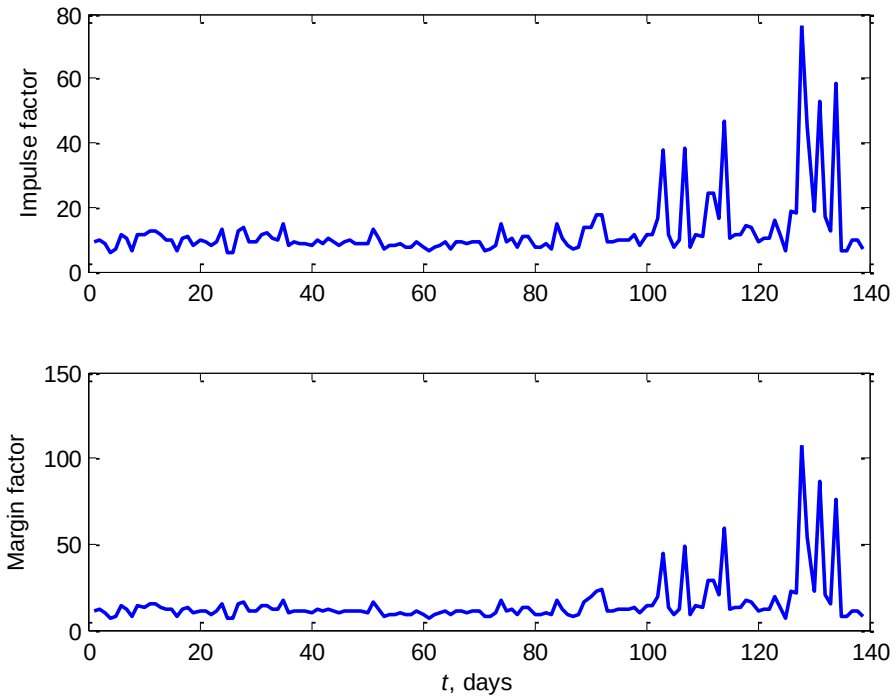

Figure 2.5 Impulse factor and margin factor feature extracted from the vibration slew bearing signal.

Hjort's parameter

In addition to the time-domain features mentioned above, Hjort's parameter can also be put into this category [58]. The first Hjorth's parameter is called 'activity'. The

activity of vibration signal can be computed by simply calculating the variance of the vibration signal amplitude $\sigma_x{}^2$, where σ_x is the standard deviation of the sampled vibration signal $\mathbf{x} = (x_1, x_2, x_3, ..., x_N)$, and N is the number of samples.

The second parameter is termed 'mobility' and defined as the standard deviation of the first derivative of the vibration signal and the standard deviation of the vibration signal.

$$\text{mobility} = \frac{\sigma_{x'}}{\sigma_x} \tag{2.8}$$

In the time series context, the numerical values for the derivatives are obtained as the differences between samples as follows. Note that the derivatives without normalisation are dimensional and will depend on the arbitrary sampling frequency.

$$x' = x_{(i+1)} - x_i \qquad i = 1, ..., N-1 \tag{2.9}$$

The third parameter called 'complexity' which is defined as the ratio of mobility of the first derivative and the mobility of the vibration signal.

$$\text{complexity} = \frac{\sigma_{x''} / \sigma_{x'}}{\sigma_{x'} / \sigma_x} \tag{2.10}$$

These parameters have been used in electroencephalography (EEG) signals to detect the epileptic seizures [36]. They have never been used in vibration bearing signal except for activity feature which is similar to the variance feature in the time domain feature extraction. It can be seen from Figure 2.6 that the progression of bearing condition is difficult to track using mobility and complexity. In contrast, the activity or variance feature shows one highest peak at approximately the 90th day and continue fluctuation on the last measurement days.

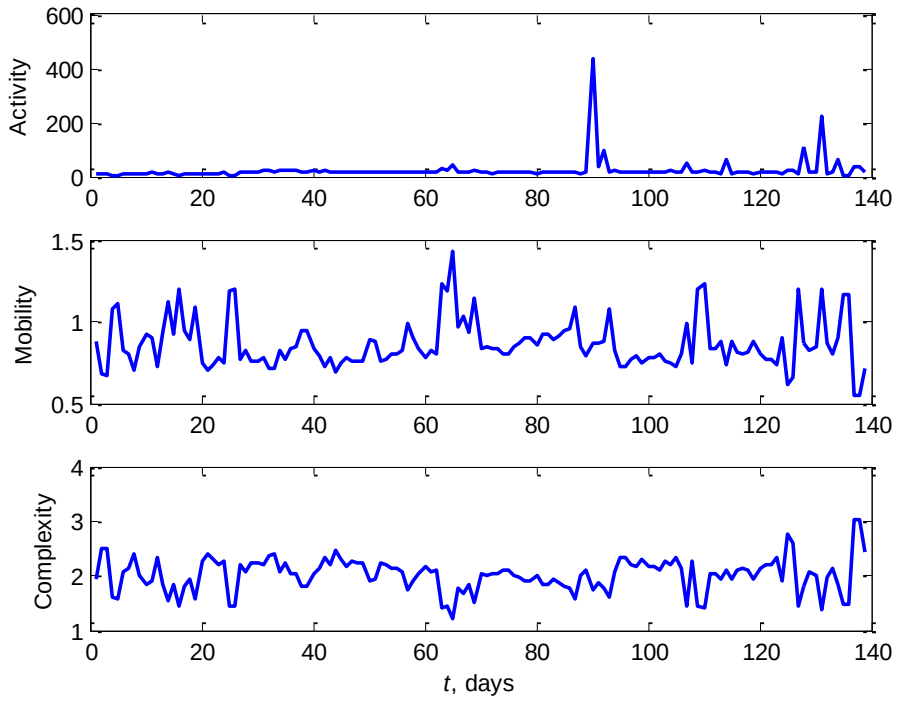

Figure 2.6 Hjorts' parameters: activity, mobility and complexity extracted from the vibration slew bearing signal.

Mathematical morphology (MM) operators

Mathematical morphology (MM) was initially introduced as a non-linear image processing method to analyse two dimensional (2D) image data including binary images and grey-level images based on set theory [82]. The basic principle of the MM method is to modify the shape of the original signal by transforming it through its intersection with another object called the 'structuring element' (SE). Four operators including erosion, dilation, closing and opening are used to achieve the transformation.

After having been applied successfully in 2D image processing, the MM method has been used in biomedical research field to analyse one dimensional (1D) EEG signals [83-85] and electrocardiography (ECG) signals [86]. The first known study of MM in 1D vibration signals was presented by Nikolaou and Antoniadis [52], who used the MM method for vibration data with inner race and outer race faults. The effects of four morphological operators on the enveloping impulse-type signals were examined. The result shows that the 'closing' operator is more suitable for extracting the impulse signal corresponding to the bearing fault type. The SE value was empirically

investigated within the range of 0.2T to 1.2T. The optimum SE for a signal with additive noise was selected as 0.6T (0.6 times the pulse repetition period).

The original discrete one dimensional (1D) signal and structuring element (SE) have to be first determined to use the four basic operators in the MM method. Suppose the discrete 1D vibration signal $\mathbf{x}(n)=\{x(1),x(2),...,x(N)\}$, which functions over a domain $n=(1,2,...,N)$. Let $S(m)=\{S(1),S(2),...,S(M)\}$ be the SE, which is the discrete function over a domain $m=(1,2,...,M)$, where N and M are integers and $N \geq M$. Then, the four morphology operators for the discrete 1D vibration signal can be defined as follows:

- *Erosion*: also refer to as min filter.

$$(x\Theta S)(n)=\min\left(x(n+m)-S(m)\right) \tag{2.11}$$

- *Dilation*: also refer to as max filter.

$$(x\oplus S)(n)=\max\left(x(n-m)+S(m)\right) \tag{2.12}$$

- *Closing*: Dilates 1D signal and then erodes the dilated signal using the same structuring element for both operations.

$$(x\bullet S)(n)=\left((x\oplus S)\Theta S\right)(n) \tag{2.13}$$

- *Opening*: Erodes 1D signal and then dilates the eroded signal using the same structuring element for both operations.

$$(x\circ S)(n)=\left((x\Theta S)\oplus S\right)(n) \tag{2.14}$$

where $n\in(1,2,...,N)$ and $m\in(1,2,...,M)$, the notations Θ, $\oplus$, $\bullet$, $\circ$ denote the erosion operator or Minkowski subtraction, dilation operator or Minkowski addition, closing operator and opening operator in the MM method, respectively.

The original simulated 1D signal is shown in Figure 2.7(a). The various effects of the basic MM operators application in the simulated 1D vibration signal are presented in Figures 2.7(b)-(e). The simulated signal has zero mean value which is typical of 1D vibration signals. The work principle of the basic MM operators can be summarized as follows: erosion of $x(n)$ by the structuring element $A(m)$ reduces the positive part and enlarges the negative part of $x(n)$, while dilation of $x(n)$ by the structuring

element $A(m)$ reduces the negative part and enlarges the positive part of $x(n)$. In addition, closing of $x(n)$ smoothens the signal $x(n)$ by cutting down any impulses in the negative part and opening $x(n)$ smoothens the signal $x(n)$ by cutting down its impulses in the positive part.

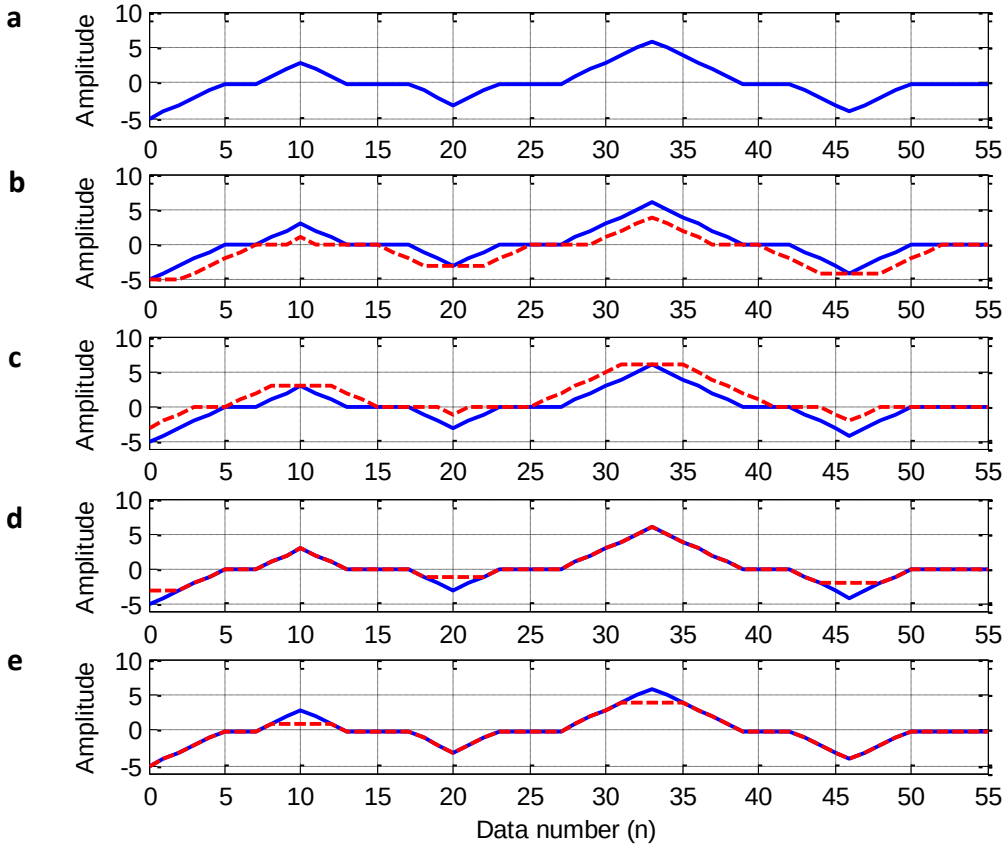

Figure 2.7 Illustration of four MM operators: (a) the original 1D signal, (b) the effect of erosion, (c) the effect of dilation, (d) the effect of closing and (e) the effect of opening. (Note: the solid blue line is the original signal and the dashed red line is the signal after being processed or transformed by the MM operators).

In rolling element bearing, the MM method has been studied. The multi-scale morphological analysis was developed by Zhang et al. [51]. The method shows independency of empirical rules in terms of SE selection, but the technique is quite complex. The vibration bearing data used in this paper was gathered from open access data from Case Western Reserve. Wang et al. [87] proposed an improved morphological filter for the feature extraction of periodic impulse signals. An average weighted combination of open-closing and close-opening morphological operators was

employed to eliminate the statistical deflection of amplitude and to extract the impulse component from the original signal. To optimize the SE, they used a new criterion called impulse attenuation (IMA). Dong et al. [30] presented the fault diagnosis of rolling element bearings using the modified morphological method. The morphological operator used in their method was the average weight combination of the closing and opening operator. They proposed a new criterion called SNR criterion to optimize the length of SE. Another recently published research on MM was presented by Raj and Murali [88]. The authors combined the MM operators with fuzzy inference to classify the bearing faults. The vibration data from the artificially defective bearing used in the paper are similar to Zhang et al. [51].

The effectiveness of the MM application in detecting the bearing fault frequencies from among impulsive-type signals have been demonstrated [30, 51, 87, 88]. These signals are generated from known bearing conditions such as inner and/or outer race faults. It has been acknowledged that the signals from artificial defect are easier to be identified than those from naturally defective bearing. Besides, typically, the impulse-type signals are easily identified visually without any additional tool or processing step [30]. The application of MM method to the naturally defective slew bearing in this thesis is presented in Figure 2.8 to Figure 2.10.

The MM method has been used effectively for the damage detection of high speed rolling bearing. It is because when the damage occurred, the contact between the damage spot and rolling element generates detectable impulse. In the case of naturally degraded low speed slew bearing, the multiple damage e.g. outer race, inner race and roller typically occurred at close sequence time and the magnitude of impulse is very low. Thus it is difficult to identify the origin of impulse from outer race, inner race or roller damage. Therefore, the feature extraction result of MM for the three conditions: BPFO, BPFI and BSF present an identical figure.

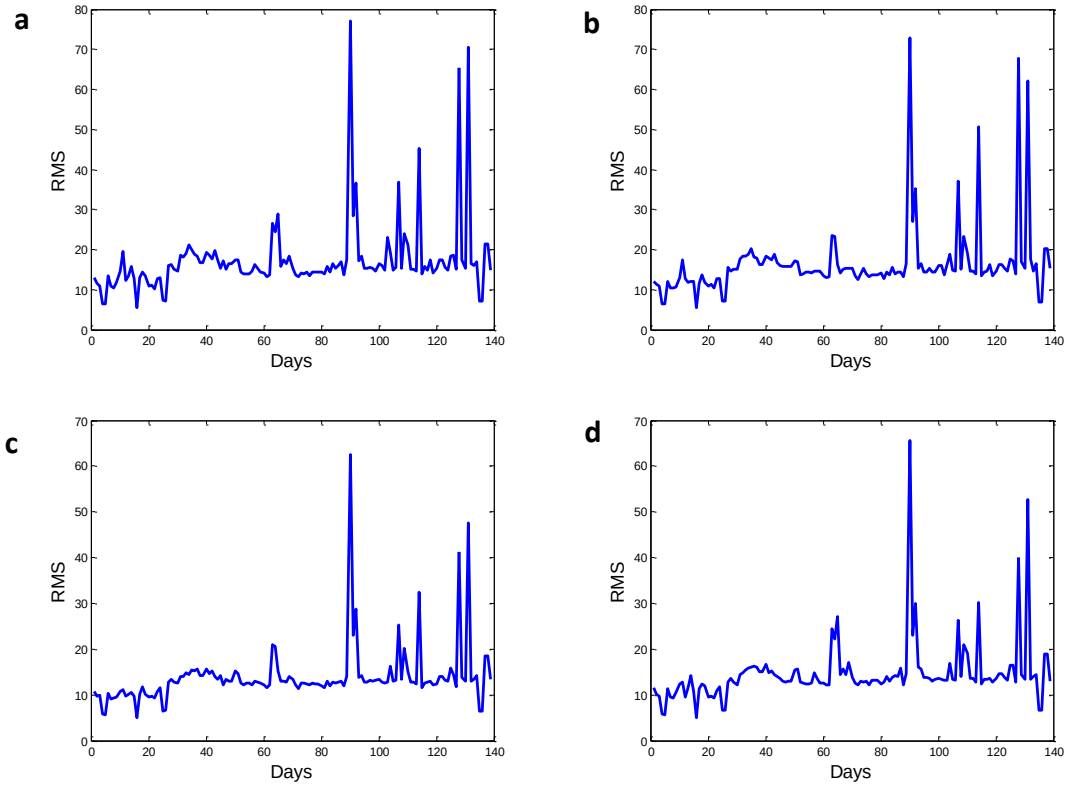

Figure 2.8 RMS feature extracted from MM operators for 0.9T (T = 1/BPFI): (a) erosion, (b) dilation, (c) closing and (d) opening.

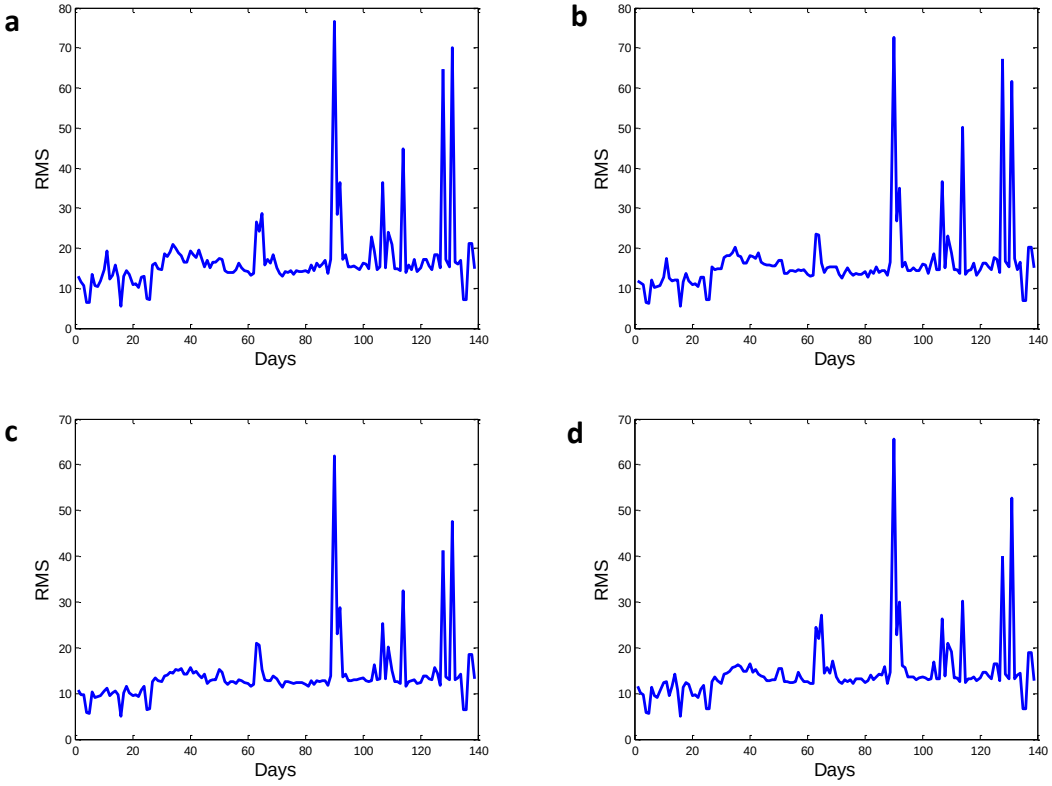

Figure 2.9 RMS feature extracted from MM operators for 0.9T (T = 1/BPFO): (a) erosion, (b) dilation, (c) closing and (d) opening.

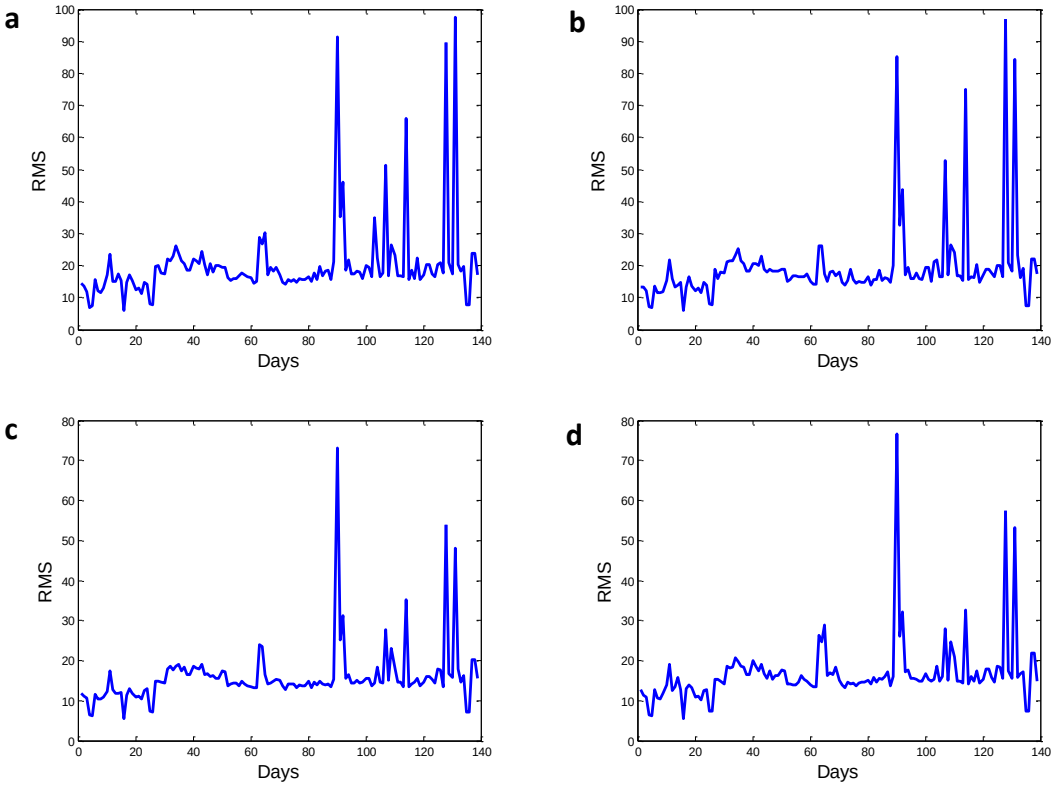

Figure 2.10 RMS feature extracted from MM operators for 0.9T (T = 1/BSF): (a) erosion, (b) dilation, (c) closing and (d) opening.

2.2.2 Category 2: Frequency-domain feature extraction

To apply frequency-domain features, the time-domain vibration signals must initially be converted into frequency-domain signals using Fast Fourier Transform (FFT). FFT is a common method in vibration analysis for bearing fault detection. FFT performs effectively in stationary periodic signals, however, it is less effective for non-stationary signals that arise from time-dependent events [89]. For sinusoids, FFT can be used to identify the dominant frequency event if the sinusoids plus noise. In practice, FFT has a limitation to measures the dominant frequency of the repetitive impulse period of certain faults due to the contact between rolling elements and defective spot. It is because the impulse responses are measured instead of the forcing impulses, in terms of acceleration, which contain almost nothing additive at the fault repetition frequencies. Frequency analysis of the demodulated envelope, does give clear information of the repetition frequencies, even if they come from resonances.

Other frequency-domain features such as frequency centre (FC), root mean square frequency (RMSF) and root variance frequency (RVF), have been studied in [15]. When fault exists, the frequency element changes, and the values of the FC, RMSF and RVF also change. The FC and RMSF indicate the position changes of main frequencies, while the RVF shows the convergence of the power spectrum. Another feature called median frequency is sometimes used. Graphically, the median frequency is the frequency which divides the area of the amplitude spectrum into equal halves. These features can be calculated as follows:

$$FC = \frac{\sum_{i=2}^{N} x_i' x_i}{2\pi \sum_{i=1}^{N} x_i^2} \tag{2.15}$$

$$MSF = \frac{\sum_{i=2}^{N} (x_i')^2}{4\pi^2 \sum_{i=1}^{N} x_i^2} \tag{2.16}$$

$$RMSF = \sqrt{MSF} \tag{2.17}$$

$$RVF = \sqrt{MSF - FC^2} \tag{2.18}$$

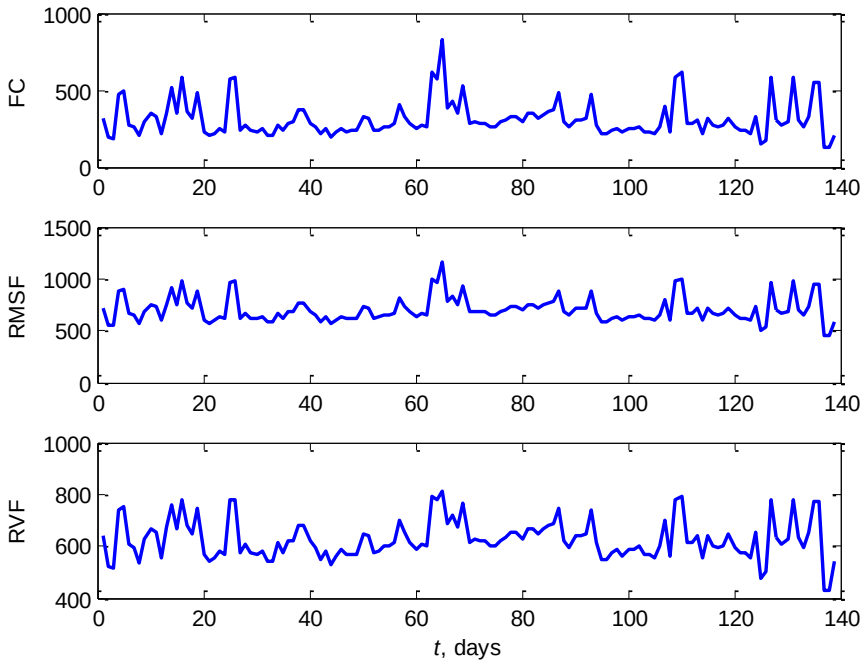

Figure 2.11 Frequency-domain features: FC, RMSF and RVF extracted from the vibration slew bearing signal.

Recently, new methods such as spectral skewness, spectral kurtosis, spectral entropy and Shannon entropy have been developed which are included in frequency-domain features category. Spectral skewness (SS) and spectral kurtosis (SK) are the statistical measures applied to the amplitude spectrum. In fact, the mean frequency (FC) can be interpreted as the first-order moment of the Fourier spectrum, RVF as the second-order moment, SS as the third-order moment and SK as the fourth-order moment of the Fourier spectrum [58].

The SS measures the symmetry of the distribution of the spectral magnitude values around their arithmetic mean [90]. It is defined by

$$SS(n) = \frac{2\sum_{k=0}^{B_L/2-1}(|X(k,n)| - \mu_{|X|})^3}{B_L \cdot \sigma_{|X|}^3} \tag{2.19}$$

The SK measures whether the distribution of the spectral magnitude values is shaped like a Gaussian distribution or not. It is defined by

$$SK(n) = \frac{2\sum_{k=0}^{B_L/2-1}(|X(k,n)| - \mu_{|X|})^4}{B_L \cdot \sigma_{|X|}^4} - 3 \tag{2.20}$$

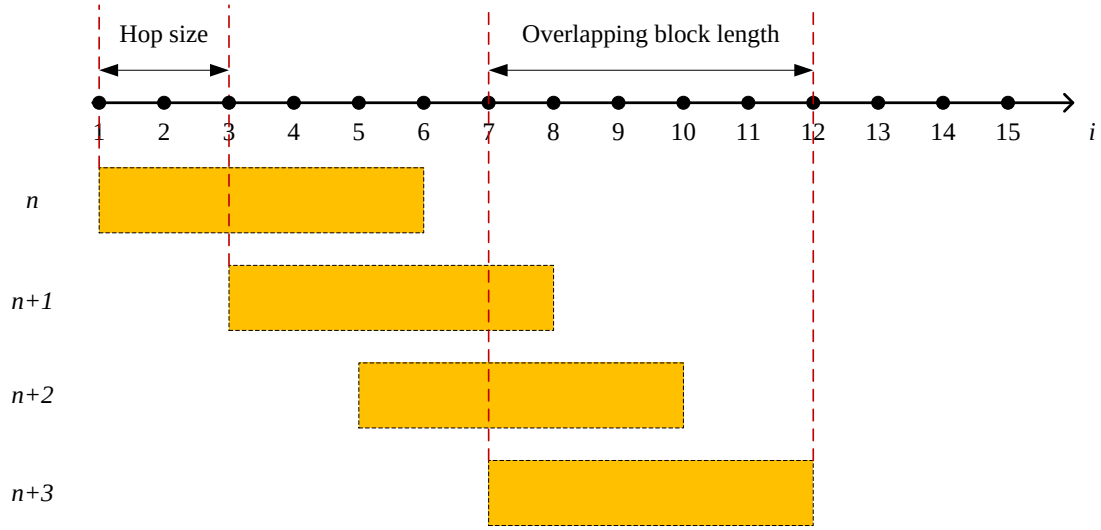

Figure 2.12 Schematic visualization of block-based processing: the input signal with the input sample index i is split into overlapping blocks of length B_L and block index n; the hop size H_s is the distance from the start of one block and the following block.

Antoni and Randall [60] presents the development of classical kurtosis analysis called spectral kurtosis (SK) to deal with the transient behaviour in a signal. SK can be used to detect incipient faults even in the presence of strong masking noise. The concept of spectral statistic is adopted in this method to supplement the classical power spectral density (PSD). PSD ideally gives zeros values at those frequencies when the signal has stationary Gaussian noise, and it gives high positive values at those frequencies during the occurrence of the transients. When the noise-to-signal ratio is high, the transient signal will be buried in the background noise, thus the incipient fault cannot be clearly detected. SK can overcome this problem by analysing the whole frequency domain to find out in which frequency bands the fault signal can be best detected.

2.2.3 Category 3: Time-frequency representation

Time-frequency domain representation methods such as short-time Fourier transform (STFT), wavelet transform and Wigner-Ville distribution (WVD) are commonly used for non-stationary or transient signal. These methods perform a mapping of one-dimensional time-domain signals to a two-dimensional function of time and frequency. The objective is to provide a true time-frequency representation of a signal. A recent review of time-frequency analysis methods for machinery fault diagnosis has been presented by Feng et al. [91].

Short-time Fourier transform (STFT)

Due to its low computational complexity and definite physical meaning, STFT is often used as an initial pre-processing tool to analyse non-stationary vibration signals. The STFT maps the vibration signal into a two-dimensional (2D) function of time and frequency [92]. STFT divides a non-stationary signal into small windows of equal time. The Fourier transformation is then applied to the time segment. Unlike FFT where the frequency transformation includes the whole original signal, in STFT original signal is decomposed using FFT at pre-defined time intervals. By doing this, the defect signal frequency can be identified in a particular window of time. The key to this method is the selection of the time interval. The difficulty in using the STFT is that the accuracy of extraction frequency information is limited by the length of the window relative to the

duration of the signal. Once the window function is defined, the area (time-bandwidth product) of the window function in the time-frequency plane remains fixed. This means that the time and frequency resolutions cannot be increased simultaneously. The STFT can be expressed as follows [93]:

$$STFT(f,t) = \int_{t-T/2}^{t+T/2} w(t-\tau)\, x(\tau) e^{j2\pi f \tau}\, d\tau \tag{2.21}$$

where $STFT(f,t)$ is short term frequency spectrum, t is the time variable, f is frequency, $w(t-\tau)$ is the shifted window, $x(\tau)$ denotes the input vibration signal, $\exp(j2\pi f \tau)$ is the complex exponential, T is the window interval and $w(\tau)$ is the windowing function which satisfies $w(\tau) = 0$ for $|\tau| => T/2$.

Using the STFT transform (2.21), an energy density can be achieved by computing the spectrogram $S(t, f)$, which is the squared magnitude of the STFT

$$S(t, f) = |STFT(t, f)|^2 \tag{2.19}$$

which represents the energy density of the original signal $x(\tau)$ windowed by $w(\tau)$.

The STFT result of one day slew bearing signal measurement is shown in Figure 2.13. Figure 2.13 is the STFT result for 10 seconds vibration signal with window length of 2048, hop size of 256 and number of FFT points of 16384. It can be seen that during 10 seconds sampled signal, the amplitudes of lower frequencies were higher than the amplitude of high frequencies (approximately 1300 Hz and 1750 Hz). This indicates that slew bearing frequencies were dominated by low frequency contents.

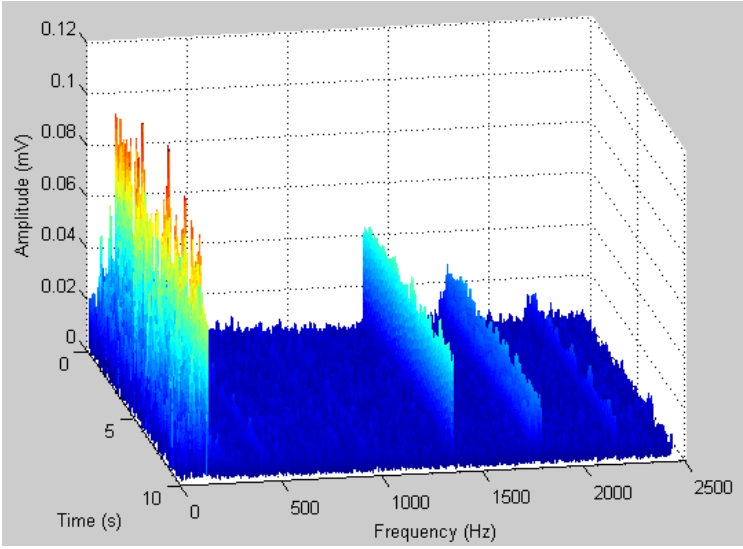

Figure 2.13 STFT of the vibration slew bearing signal (data May 3rd).

Wavelet transform and wavelet decomposition

It has been studied that wavelet transform is an appropriate method to analyse non-stationary and transient signal [34, 48]. Wavelet transformation employs wavelet instead of sinusoidal functions as the basis function. It adds a scale variable in addition to the time variable in the inner product transformation [91]. For any limited energy signal $x(t) \in L^2(R)$, the wavelet function is defined as [91]

$$\mathrm{WT}_x(t,a) = \frac{1}{\sqrt{a}} \int_{-\infty}^{+\infty} x(\tau) \psi\left(\frac{\tau - t}{a}\right) d\tau \tag{2.23}$$

where wavelet $\psi[(\tau - t)/a]$ is derived by dilating and translating the wavelet basis $\psi(t)$, a is the scale parameter $(a > 0)$, t is the time shift and $1/\sqrt{a}$ is a normalisation factor to maintain energy conservation.

A review of the wavelet transform applications in machine condition monitoring and fault diagnostics is presented by Peng et al. [94]. Apart from the original intention of the wavelet transform for the analysis of non-stationary signals, another very important and successful application of wavelets in machine fault diagnostics is fault feature extraction [94]. Since the wavelet transformations have good energy concentration properties due to the uses of the basis function; the wavelet transform can represent the signal with a certain number of coefficients. The process is usually called wavelet decomposition.

Wavelet decomposition decomposes a non-stationary input signal into a linear combination of time-scale units. It decomposes and organizes original signal into several signal components according to the translation of the mother wavelet (or wavelet basis function). This changes the scale and shows the transition of each frequency component [95]. Through this decomposition, a selected coefficient can be used directly as the fault feature. In wavelet decomposition, the input signal is basically decomposed into two coefficients. The input signal that passes through the low-pass filter becomes the 'approximation coefficient'. The input signal which passes through the high-pass filter becomes the 'detail coefficient.' Since the low-frequency content is the most important part, the 'approximate coefficient' is passed to the next wavelet decomposition loop in multilevel wavelet decomposition process. Figure 2.14 shows three level wavelet decomposition structure. The structure illustrates the decomposition of slew bearing vibration signal into approximate coefficient (A) and detailed coefficient (D) at each level. For further processing, features such as mean, variance, skewness and kurtosis can be extracted from the detailed coefficients of level 3 (D3) [96]. The feature extraction results are presented in Figure 2.15. From the feature extraction result, it can be seen that kurtosis can predict the damage compared to mean, variance and skewness extracted from signal D3 of the wavelet decomposition.

Niu et al. [97] employs wavelet decomposition for fault diagnosis of induction motor using transient stator current signal. Statistical features have also been used to extract the fault information from the selected coefficients. Another study that uses the wavelet coefficients as fault features for ball bearing has been presented by Liu et al. [98].

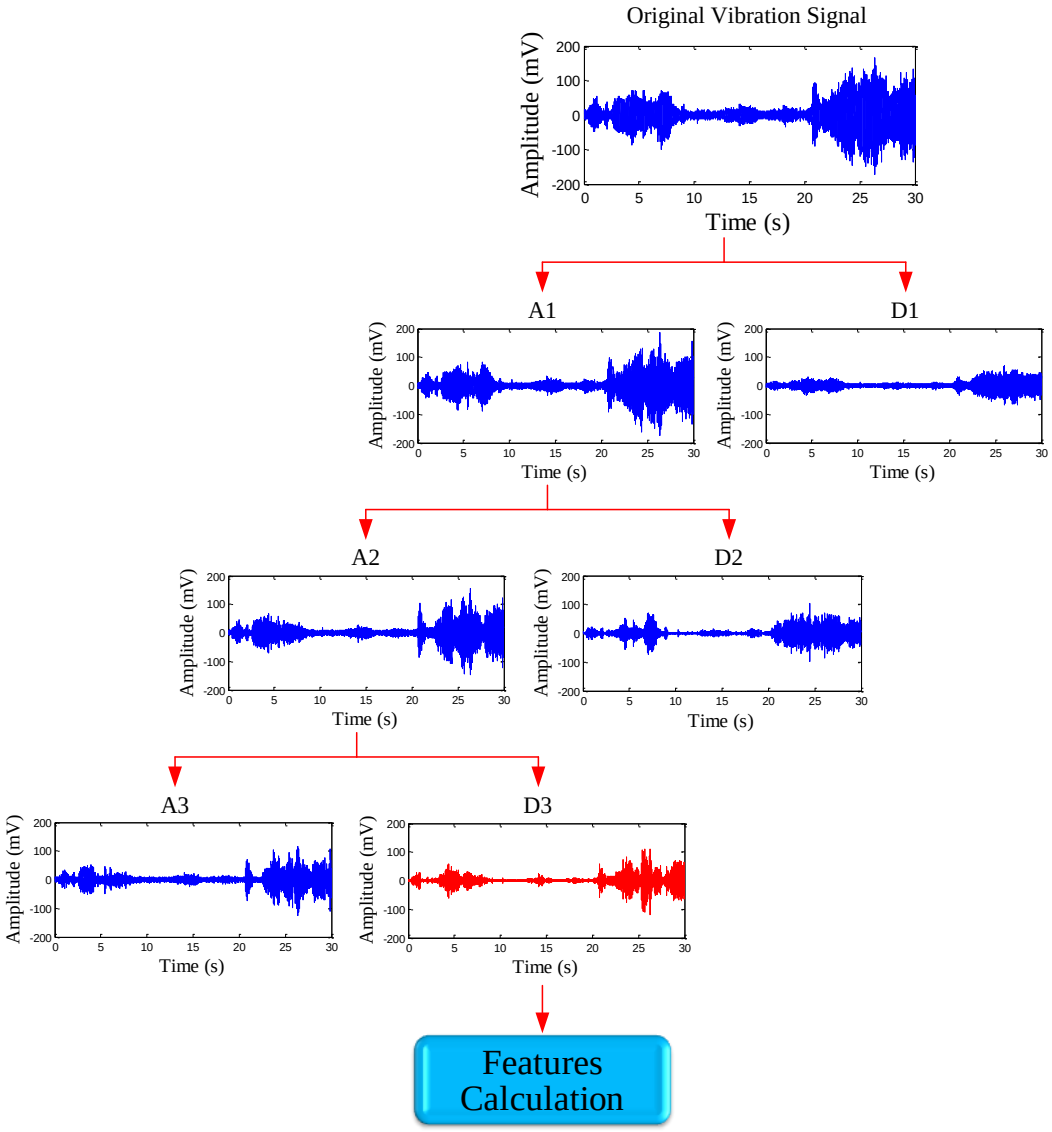

Figure 2.14 Three level wavelet decompositions of the vibration slew bearing signal.

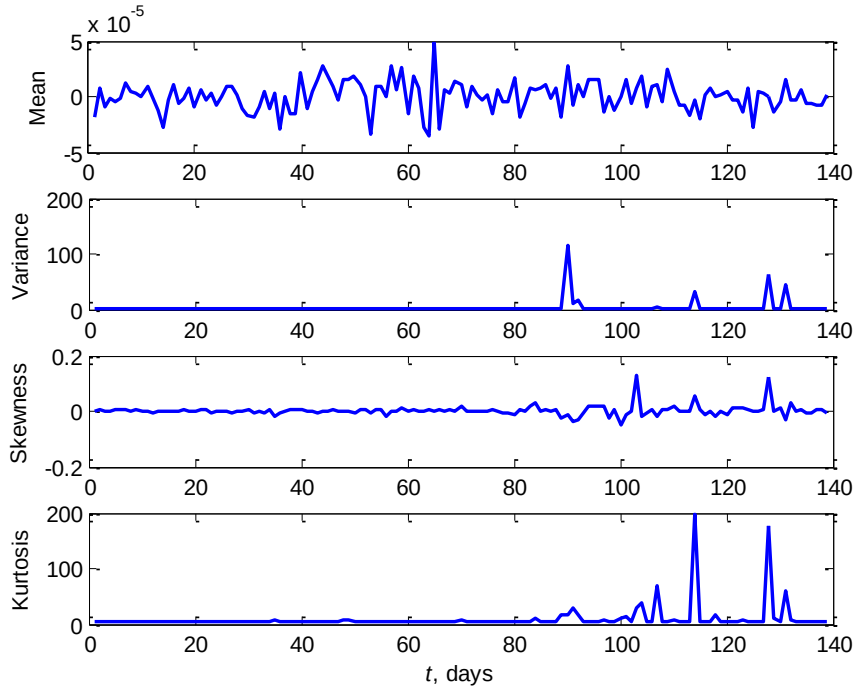

Figure 2.15 Statistical-based features: mean, variance, skewness and kurtosis extracted from D3 signal of wavelet decomposition.

Empirical mode decomposition-based Hilbert Huang transform

Empirical mode decomposition (EMD) [99] has been shown to be adaptable in applications where the signal is non-stationary (e.g. Braun and Feldman [68]). A recent review of EMD applications in fault diagnosis of rotating machinery is discussed in [100]. The review gives a detailed introduction to EMD application in various areas such as bearings, gears and rotors etc. The authors also reviewed existing EMD methodologies and classified them into three different groups namely: (1) original EMD method alone, (2) improved EMD methods and (3) combinations of EMD with other methods such as artificial neural network and support vector machine.

The main function of EMD is to decompose the original vibration signal into several signals which have specific frequency called intrinsic mode functions (IMFs) based on the enveloping technique (Hilbert-Huang transform). The results of IMFs are from high frequencies to low frequencies. In condition monitoring of rolling element bearing, EMD is used to reveal the frequency content of vibration signal by decomposing the original signal into several IMFs. The aim is to determine whether the bearing signal has a specific frequency content that corresponds to the bearing fault frequencies or

not. In preliminary studies on condition monitoring [96, 101], the original EMD [69] is used for non-stationary slew bearing data. A bearing fault such as outer race, inner race or rolling element fault has occurred when one of the IMF frequencies is identical to one of the bearing fault frequencies (for example as shown in Table 2.3) [101].

Table 2.3 Fault frequencies of slew bearing (run at 1 rpm and 4.3 rpm from the slew bearing test rig and slew bearing bridge reclaimer, respectively).

Defect mode	Fault frequencies (Hz) (calculation is given in Appendix A)			
	Slew bearing test-rig		Slew bearing Bridge Reclaimer	
	Axial	Radial	Axial	Radial
Outer ring (BPFO)	1.32	0.55	13.41	11.38
Inner ring (BPFI)	1.37	0.55	13.58	11.56
Rolling element (BSF)	0.43	0.54	5.65	4.87

Table 2.4 Decomposition result of EMD method for the slew bearing test-rig data on February 24.

IMFs of EMD (Hz) (vibration data on February 24th)					
IMF2	641.807	IMF7	52.591	IMF12	1.439
IMF3	694.521	IMF8	18.831	IMF13	0.687
IMF4	390.350	IMF9	9.019	IMF14	0.327
IMF5	190.387	IMF10	4.849	IMF15	1.990
IMF6	89.751	IMF11	2.474	IMF16	0.106

Table 2.5 Decomposition result of EMD method for the slew bearing test-rig data on May 3.

IMFs of EMD (Hz) (vibration data on May 3rd)					
IMF2	702.880	IMF7	69.199	IMF12	1.227
IMF3	684.340	IMF8	17.568	IMF13	0.638
IMF4	346.227	IMF9	8.570	IMF14	**0.432**
IMF5	1371.492	IMF10	4.026	IMF15	0.194
IMF6	74.370	IMF11	2.042	IMF16	0.069

Table 2.6 Decomposition result of EMD method for the slew bearing test-rig data on August 30.

IMFs of EMD (Hz) (vibration data on August 30th)					
IMF2	651.717	IMF7	28.891	IMF12	0.682
IMF3	679.862	IMF8	13.682	IMF13	0.331
IMF4	245.923	IMF9	6.464	IMF14	0.099
IMF5	121.319	IMF10	3.052		
IMF6	63.554	IMF11	**1.374**		

According to Table 2.4 to Table 2.6, the bearing fault frequencies were not identified on February 24th. In contrast, the fault frequency of rolling element (BSF axial) appeared on May 3rd with 0.432 Hz. This frequency is associated with roller defects as shown in Figure 2.16(a). Interesting result was obtained from data on August 30th. The fault frequency of rolling element disappeared and another fault frequency in the outer raceway of 1.37 Hz emerged. The reason could be that the amplitude of signal 0.432 Hz is weak and is buried in the background noise. The photo of the outer raceway damage is shown in Figure 2.16(b). The roller and outer race damage photo was taken after final failure upon dismantling on September 2nd. The detailed vibration data used from the slew bearing test rig is presented in Chapter 3. Statistical features from the extraction results of EMD method are shown in Figure 2.17. The mean, variance, skewness and kurtosis features are extracted from the summation of the low IMF frequencies (from IMF 9 to the lowest IMF with frequency band from 100 to 0.01 Hz) of the EMD results. The selection of these IMFs is based on the characteristic of slew bearing signal being dominated by low frequency components as presented previously in STFT result.

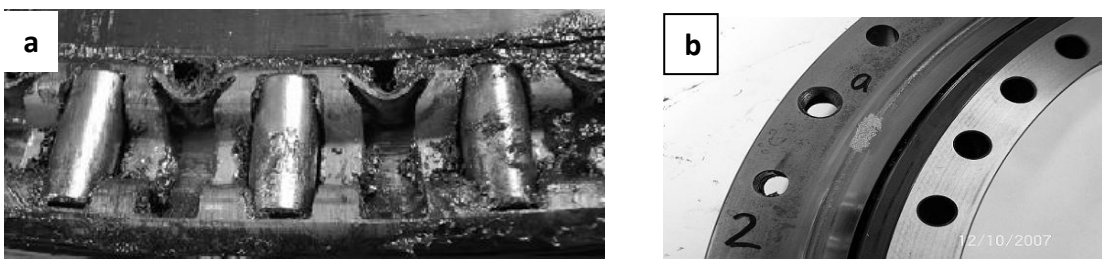

Figure 2.16 (a) A view of damaged rollers in axial plane; (b) outer raceway damage.

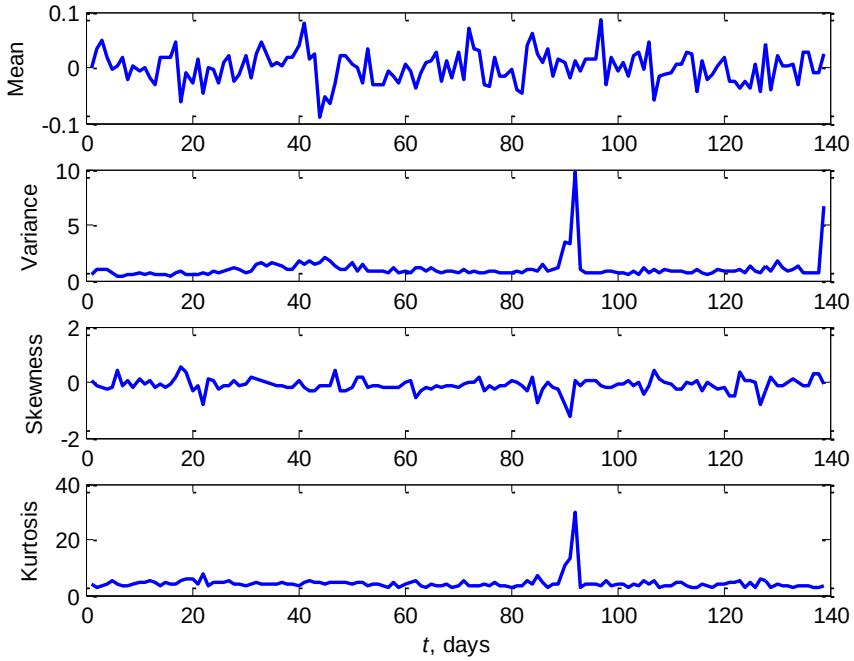

Figure 2.17 Statistical-based features: mean, variance, skewness and kurtosis extracted from EMD decomposition.

Wigner-Ville distribution (WVD)

The Wigner distribution (WD) can be derived by generalising the relationship between the power spectrum and the autocorrelation function for non-stationary, time-variant processes [102]. The correlation function is a product of the function at a past time with the function at a future time [103]. The original WD for real signal $x(t)$ is defined as [104]

$$W_x(t, f) = \int_{-\infty}^{+\infty} x^*\left(t - \frac{\tau}{2}\right) x\left(t + \frac{\tau}{2}\right) e^{-j2\pi f\tau} d\tau \tag{2.24}$$

The symbol $(*)$ in Eq. (2.24) denotes the complex conjugate.

When the WD is applied for the analytical signal $x_A(t)$, it is called the Wigner-Ville distribution (WVD). The analytical signal is defined as

$$x_A(t) = x(t) + jx_h(t) \tag{2.25}$$

where $x_h(t)$ is the Hilbert transform of $x(t)$ being

$$H[x(t)] = x_h(t) = \frac{1}{\pi}\int_{-\infty}^{+\infty} x(\tau)\frac{1}{t-\tau}d\tau\,. \tag{2.26}$$

The WVD has been used for gear fault detection [102, 103] and it is recently used for rolling element bearing to represent the time-frequency features of signals [64].

2.2.4 Category 4: Phase-space dissimilarity measurement

Phase-space dissimilarity measurements, such as fractal dimension, correlation dimension approximate entropy and largest Lyapunov exponent (LLE), are developed based on the chaos theory. These methods have been applied in biomedical engineering studies [36, 37] and vibration signals [74, 105]. Present studies have conducted investigations into these methods in the slew bearing condition monitoring for feature extraction. The motivation is that multiple defects occur more frequently than single defects in slew bearings, therefore the phase-space dissimilarity measurements can be used to analyse the irregular or chaotic vibration signals. The phase-space can be computed as follows:

$$\mathbf{X} = \begin{bmatrix} y_1 & y_{1+J} & y_{1+2J} & \cdots & y_{1+(m\text{-}1)J} \\ y_2 & y_{2+J} & y_{2+2J} & \cdots & y_{2+(m\text{-}1)J} \\ y_3 & y_{3+J} & y_{3+2J} & \cdots & y_{3+(m\text{-}1)J} \\ . & . & . & & . \\ . & . & . & & . \\ . & . & . & & . \\ y_M & y_{M+J} & y_{M+2J} & \cdots & y_{M+(m\text{-}1)J} \end{bmatrix} \tag{2.27}$$

where J represents reconstruction delay and can be computed by time lag $/\Delta t$, m represents the embedding dimension and M represents the number of reconstructed vectors. The relation between N, J, m and M can be defined in the following form: $N = M + (m\text{-}1)J$ or $M = N\text{-}(m\text{-}1)J$. Thus the dimension of phase-space is a $M \times m$ matrix.

Fractal dimension

Fractal dimension is used to quantify the complexity of signals by characterizing fractal patterns. The complexity can be quantified by examining the dynamical behaviours of phase-space or reconstruction vectors. The commonly used algorithm of

fractal dimension was proposed by Higuchi [106]. The field is rapidly growing as estimated fractal dimensions for statistically self-similar phenomena. These may have many practical applications in various fields including image analysis [107], neuroscience [72, 108], medicine [109], physics [110] and acoustics [111]. The application of fractal dimension in vibration signal of rolling element bearing has been presented in [73, 81]. The algorithm of fractal dimension is shown in Eq. (2.25) [81]. Once the phase-space matrix, $\mathbf{X}$ is obtained (2.27), the mean absolute length between j^{th} and ($j^{th}-1$) element of $\mathbf{X}$ is defined as follows:

$$\begin{aligned} &for\ i=1:J \\ &\quad for\ \ j=2:m \\ &\qquad L_1(i,j\text{-}1)=\left|\mathbf{X}(i,j)\text{-}\mathbf{X}(i,(j\text{-}1))\right| \\ &\qquad L_m(i,j\text{-}1)=mean(L_1) \\ &\quad end \\ &end \end{aligned} \tag{2.28}$$

where J represents reconstruction delay and m is embedding dimension. Assuming that L_m is proportional to m^{-D}, then take the logarithmic natural of $(1/m)$ and L_m. Hence, the fractal dimension D can be computed using standard least-square fitting method.

Correlation dimension

Correlation dimension provides a tool to quantify self-similarity. A larger correlation dimension corresponds to a larger degree of complexity and less-similarity. An earlier application of correlation dimension in bearing fault diagnosis was proposed by Logan and Mathew [74]. The correlation dimension was applied for vibration signals acquired from four different conditions: (1) normal (new bearing), (2) outer race fault, (3) inner race fault, and (4) roller fault. The damages were artificially introduced to the bearing parts. The bearing was operated at 3000 rpm. The method is able to identify the four different bearing conditions.

The frequently used procedure to estimate the correlation dimension was introduced by Grassberger and Procaccia [112]. To calculate correlation dimension, the reconstructed matrix Eq. (2.27) are used as the input for the correlation dimension algorithm. The correlation dimension formula is given by:

$$C(l) = \lim_{M \to \infty} \left[\frac{2}{M^2} \sum_{i=1}^{M-k} \sum_{j=i+k}^{M} \Theta \left(l - \left| X_i - X_j \right| \right) \right] \tag{2.29}$$

where X_i and X_j are the position vectors on attractor, l is the distance under consideration, $\Theta(x)$ is the Heaviside step function, $\Theta(x) = 0$ if $X \leq 0$, $\Theta(x) = 1$ if $X > 0$, k is the summation offset, M is the number of reconstructed vectors from the original vibration signal and $C(l)$ is the correlation dimension.

Approximate entropy

The approximate entropy computes the value of regularity in the signal. Smaller value indicates more regular behaviour, while higher value of it indicates less regularity on the data set. An earlier application of approximate entropy in bearing signal was proposed by Yan et.al. [75]; however, the method is applied in high speed rolling element bearing signal. Yan et al. [75] mentioned that the deterioration of machine condition was followed by the increase of number of frequency components. This condition will decrease the regularity and increase the corresponding approximate entropy value. Similar to fractal dimension and correlation dimension, approximate entropy also uses phase-space matrix, $\mathbf{X}$ in Eq. (2.27) as an input. According to [75] the initial step of approximate entropy is to measure the distance $d(X(i), X(j))$ between two vectors $X(i)$ and $X(j)$ which can be defined as the maximum difference in their respective corresponding elements:

$$d(X(i), X(j)) = \max_{k=1,2,\ldots,m} (|x(i+k-1) - x(j+k-1)|) \tag{2.30}$$

where $i = 1, 2, \ldots, N-m+1$, $j = 1, 2, \ldots, N-m+1$ and N is the number of data points contained in the time series. For each vector $X(i)$, a measure that describes the similarity between the vector $X(i)$ and all other vectors $X(j)$, where $j \neq i$ can be constructed as

$$C_i^m(r) = \frac{1}{N-(m-1)} \sum_{j \neq i} \Theta\{ r - d[X(i), X(j)] \} \tag{2.31}$$

the Heaviside step function, $\Theta(x)$ is similar to the symbol in correlation dimension where $\Theta(x) = 0$ if $X \leq 0$, $\Theta(x) = 1$ if $X > 0$.

The symbol r in (2.28) denotes a predetermined tolerance value, defined as

$$r = k \,.\, std(\mathbf{Y}) \tag{2.32}$$

where $std(\mathbf{Y})$ means is the standard deviation of original time series or vibration signal, $\mathbf{Y}$ and k is a constant $(k > 0)$. By defining

$$\phi^m(r) = \frac{1}{N - m + 1} \sum_i \ln\left[C_i^m(r)\right], \quad i = 1, 2, \ldots, N - m + 1 \tag{2.33}$$

the approximate entropy value of time series can be calculated as

$$ApEn\,(m, r) = \lim_{N \to \infty} [\phi^m(r) - \phi^{m+1}(r)] \tag{2.34}$$

Largest Lyapunov exponent

The largest Lyapunov exponent (LLE) algorithm is an old method and has been used in some areas such as biomedical engineering field especially in the analysis of electroencephalography (EEG) signal [36]. The LLE algorithm measures the exponential divergence (positive or negative) of two initial neighbouring trajectories in a phase-space. The objective is to quantify the appearance of disturbances corresponding to the signal abnormality. In other words, the LLE algorithm measures the degree of chaos in certain time due to any disturbances. In this thesis the term disturbances refers to any local instability vibration signal due to the dynamic contact between rolling elements and defect spots. A detailed description and further study of LLE algorithm for feature extraction of low speed slew bearings signals are presented in Chapter 4.

The feature extraction result for correlation dimension, fractal dimension and approximate entropy extracted from slew bearing vibration data is presented in Figure 2.18. It can be seen that approximate entropy shows better result in presenting the degradation condition of the slew bearing than correlation dimension and fractal dimension. A fluctuation in approximate entropy Figure in the last measurement (after the 90th day) indicates the slew bearing condition has changed.

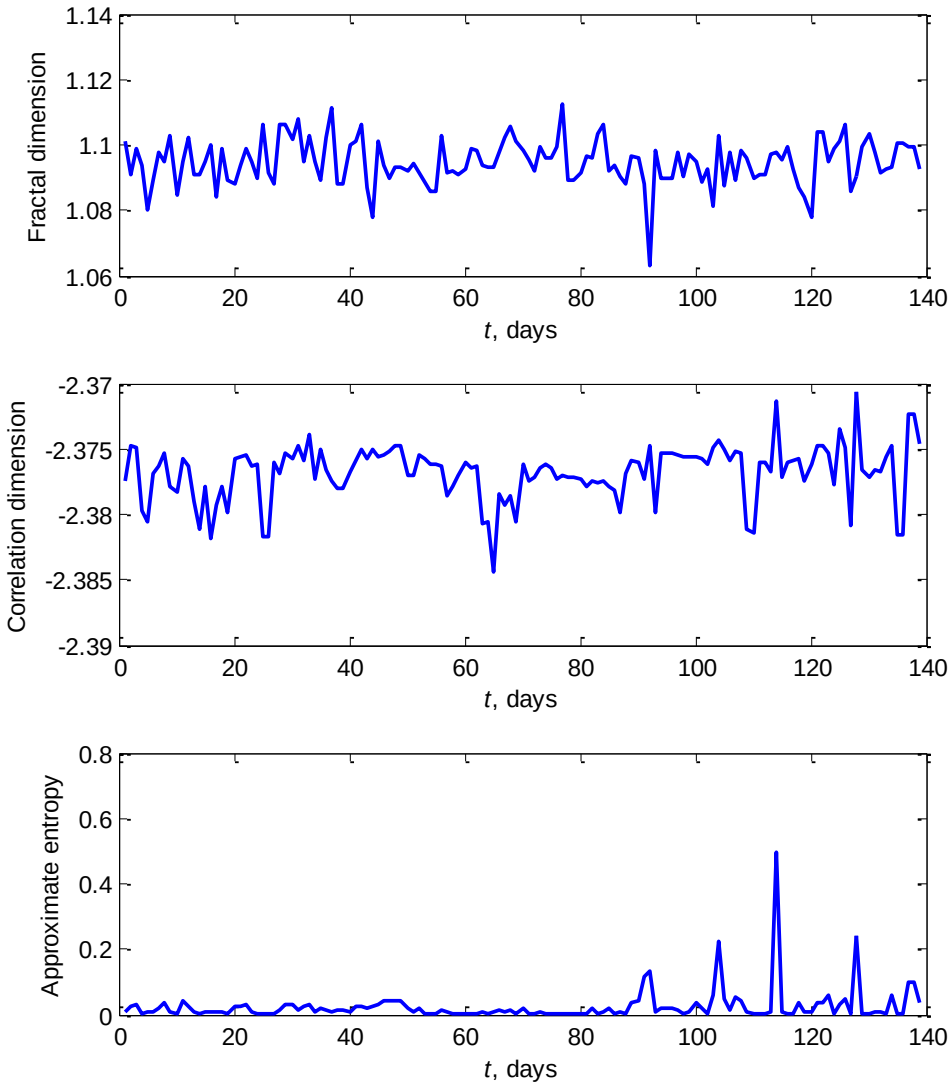

Figure 2.18 Fractal dimension, correlation dimension and approximate entropy features extracted from the vibration slew bearing signal.

2.2.5 Category 5: Complexity measurement

Kolmogorov-Smirnov test

The Kolmogorov-Smirnov (KS) test is a nonparametric test which can be used to compare or to measure the similarity of two cumulative distribution functions (CDFs), $\mathrm{T}(x)$ and $\mathrm{R}(x)$ [113]. $\mathrm{T}(x)$ is a target CDF and $\mathrm{R}(x)$ is a reference CDF. Because the signature of bearing condition can be identified by its CDF, therefore the K-S test can be applied in bearing condition monitoring to distinguish bearing health signal and

faulty signal. In order to distinguish the two CDFs, $\mathrm{T}(x)$ and $\mathrm{R}(x)$, a statistical distance D is calculated. We can define this distance D as the maximum absolute distance between $\mathrm{T}(x)$ and $\mathrm{R}(x)$. Mathematically, this is represented as follows

$$D = \max_{-\infty<x<\infty} \left| T(x) - R(x) \right| \tag{2.35}$$

The KS feature of slew bearing vibration data is presented in Figure 2.19. The '0' represents normal condition and '1' represent abnormal condition. It can be seen that at the beginning of the measurement, the condition of bearing was still normal. Then it changed to abnormal condition when bearing had run for a couple of days. This result needs further investigation as the abnormal detection was too early.

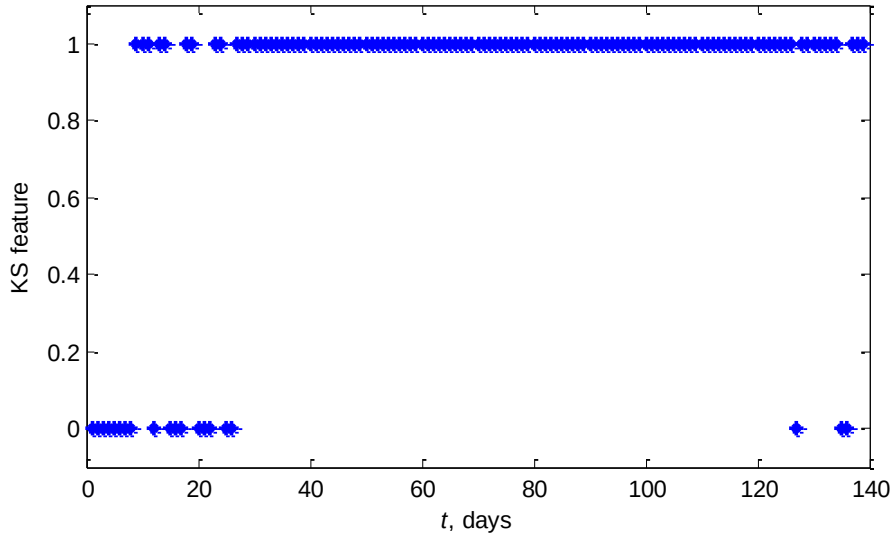

Figure 2.19 KS test feature extracted from the vibration slew bearing signal.

Sample entropy

Sample entropy has been proposed by Richman and Moorman [114] to improve approximate entropy. The sample entropy is applied for feature extraction of gearbox vibration signals by Chen et al. [115]. However, the application of sample entropy for bearing vibration signal is still limited [116]. The sample entropy feature for slew bearing vibration data is shown in Figure 2.20. It can be seen from Figure 2.20, the sample entropy feature is not effective for slew bearing damage detection.

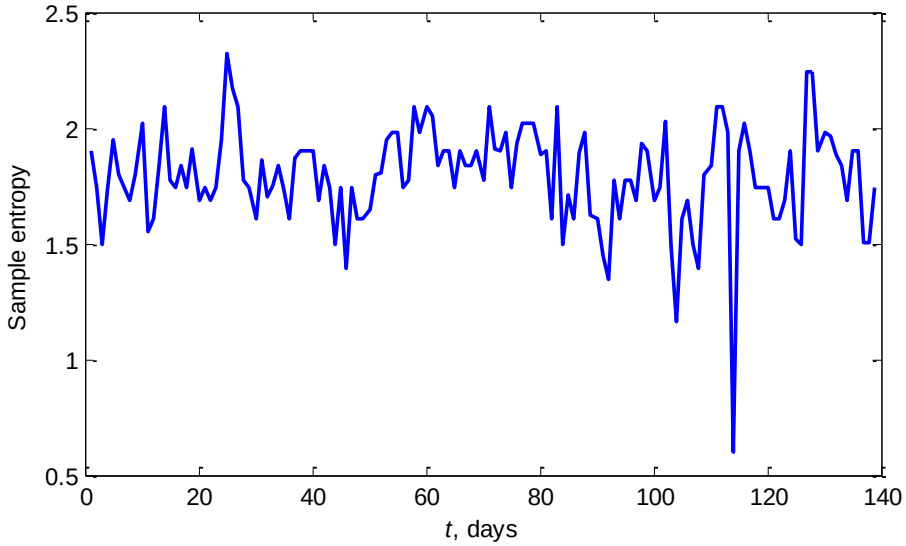

Figure 2.20 Sample entropy feature extracted from the vibration slew bearing signal.

2.2.6 Category 6: Other features

Singular value decomposition (SVD)

SVD is usually applied to detect the periodicity of the time series [117]. A comparison study [118] has been shown that SVD is more powerful and sensitive than Fourier decomposition in terms of information content and robustness. Formula of SVD can be found in [66].

Piecewise aggregate approximation (PAA) and adaptive piecewise constant approximation (APCA)

In online bearing condition monitoring cases, the changes of bearing condition can be effectively identified by measuring the similarity between two vibration signals (i.e. normal or reference and monitored signal) using Euclidean distance. However, the size of the measured data is a problem in Euclidean distance method. The most promising similarity search methods are techniques that perform dimensionality data reduction methods such as PAA [38, 79] and APCA [119]. APCA [119], is another approach of PAA that allows arbitrary length segments. PAA and APCA have some advantages. For example, PAA has twice as many approximating segments, and APCA is able to place a single segment in an area of low activity and many segments in areas of high activity

[119]. PAA is applied in this thesis for data pre-processing stage of circular domain feature extraction. The detailed discussion and the application of PAA in slew bearing vibration data is presented in Chapter 4.

2.2.7 Conclusion

Feature extraction methods in wide range application including mechanical area (bearing vibration signals), biomedical engineering area (EEG and ECG signals) and finance area (time series signal) have been presented. According to their basic principles, the methods were classified in six categories: (1) time-domain feature extraction; (2) frequency-domain feature extraction; (3) time frequency representation; (4) phase-space dissimilarity measure; (5) complexity measure; and (6) other features. Most of feature extraction methods in each category have been investigated and tested using real slew bearing vibration signal. It was shown that some features do not show bearing degradation trend clearly and the others are shown to be potential slew bearing condition parameters. The potential features are: impulse factor, margin factor, MM operators, wavelet kurtosis and approximate entropy.

Some contents of Chapter 2 have been published in the following papers:

- W. Caesarendra, P.B. Kosasih, A.K. Tieu, C.A.S. Moodie, B.K. Choi, Condition monitoring of naturally damaged slow speed slewing bearing based on ensemble empirical mode decomposition, Journal of Mechanical Science and Technology 27 (8) (2013) 2253-2262.
- W. Caesarendra, B. Kosasih, A.K. Tieu, C.A.S. Moodie, Circular domain features based condition monitoring for low speed slewing bearing, Mechanical Systems and Signal Processing 45 (2014) 114-138.
- W. Caesarendra, B. Kosasih, A.K. Tieu, C.A.S. Moodie, Application of the largest Lyapunov exponent algorithm for feature extraction in low speed slew bearing condition monitoring, Mechanical Systems and Signal Processing 50-51 (2015) 116-138.

Chapter 3 - Laboratory experiment and industrial measurement

"The whole purpose of education is to turn mirrors into windows"
(Sydney J. Haris)

3.1 Laboratory slew bearing experiment

The experimental run-to-failure bearing data, vibration and AE data used in this study were collected from a slew bearing test rig [1]. The test rig is designed to simulate real working conditions of a local steel making company such as high applied load and very low rotational speed. The rotational speed of the lab test rig can be varied from 1 to 12 rpm by using an inverted motor controller. This low rotational speed variation was achieved using two devices: (1) a motor to main gear reducer double vee belt system and (2) a final drive polychain belt drive. The test rig design specifications such as design rationale, safety, test rig stress frame design specifications, stress frame loading, speed requirements, power requirements, drive strength requirements and vibration isolation were explained in detail in [1]. A photo of the test rig is shown in Figure 3.1.

Figure 3.1 A photo of slew bearing laboratory test rig.

The laboratory slew bearing experiment consists of two measurements: (1) slew bearing with continuous rotation and (2) slew bearing with reversible rotation. Each measurement operates the bearing from new to damage.

3.1.1 Slew bearing with continuous rotation (first laboratory test)

The vibration data for continuous rotation was acquired from four accelerometers installed on the inner radial surface at 90^{o} to each other with the sampling rates of 4880 Hz and 620 kHz [1]. The accelerometers were IMI 608A11 ICP type sensors. The accelerometers were connected to a high speed Pico scope DAQ (PS3424). The bearing was subjected to axial load of 15 tonne. The bearing began running in 2006, however in order to provide continuous monitoring and produce run-to-failure bearing data, the bearing data was collected from February to August 2007 (139 days). In order to accelerate the bearing service life, coal dust was injected into the bearing in mid-April 2007 (58 days from the beginning). In practice, especially in steel making companies, the slew bearing is located in the open air where the bearing is exposed to a dusty environment. For this reason, the coal dust was inserted in mid-April to simulate the real working conditions.

3.1.2 Slew bearing with reversible rotation (second laboratory test)

The similar test rig used in continuous rotation measurement was also used for reversible rotation experiment. The test rig was also operated at 1 rpm, but this time the bearing was run continuously in reversible rotation at 180 angle rotation. To enable reversible rotation, which is one of the typical movements of slew bearing applications in practice, the test rig was then modified by adding a control mechanism, as shown in Figure 3.2. Each day, the vibration and AE data were collected from the reversible rotation (clockwise and anti-clockwise). The illustration of reversible rotation is presented in Figure 3.3.

Figure 3.2 A photo of control mechanism to enable reversible rotation.

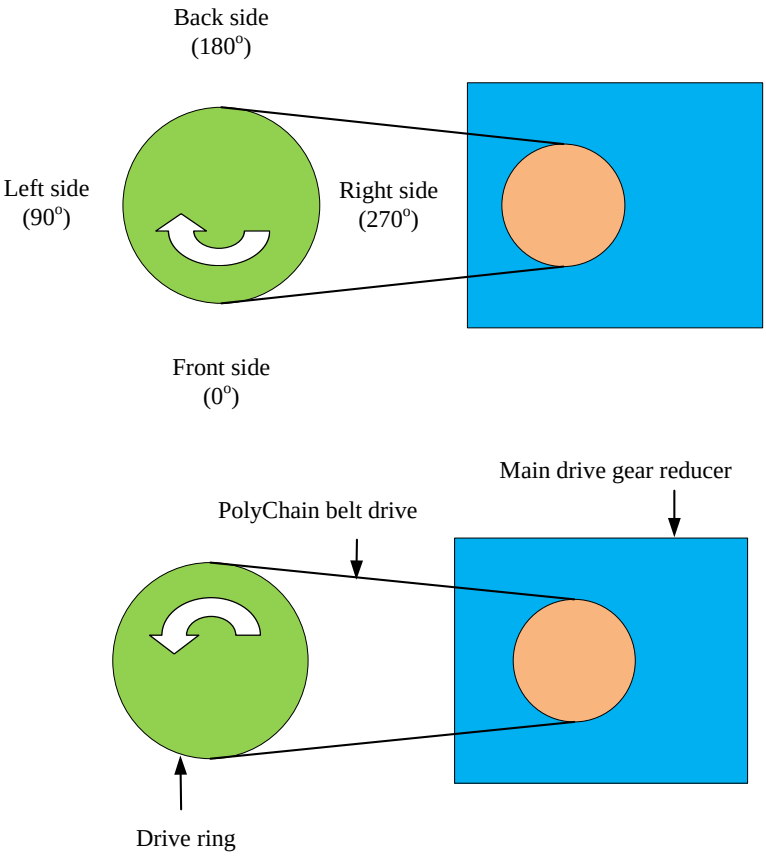

Figure 3.3 Illustration of reversible rotation from top view.

Vibration data

Four accelerometers, two AE sensors and four temperature sensors were used during the experiment. Two accelerometers of IMI 608A11 ICP type sensors with sensitivity 100mV/g and frequency range 0.5 to 10 kHz, and two accelerometers of IMI 626B02 ICP type sensors with sensitivity 500mV/g and frequency range 0.2 to 6 kHz

were used. The IMI 608A11 ICP type sensors were installed on the inner radial surface at 180 degrees to each other and the IMI 626B02 ICP type sensors were attached on the axial surface at 180 degrees to each other. Similar to the measurement in continuous rotation, these accelerometers were connected to a high speed Pico scope DAQ (PS3424). The IMI 626B02 ICP type accelerometers were selected because of the minimum frequency range of 0.2Hz and because the sensitivity is higher than that of the IMI 626B02 ICP type accelerometer. The vibration signal was acquired using 4880 Hz sampling rate. Figure 3.4 shows the schematic of the slew bearing test rig including the main drive gear reducer, the hydraulic load and how the bearing is attached. A detailed sensors placement is presented in Figure 3.5.

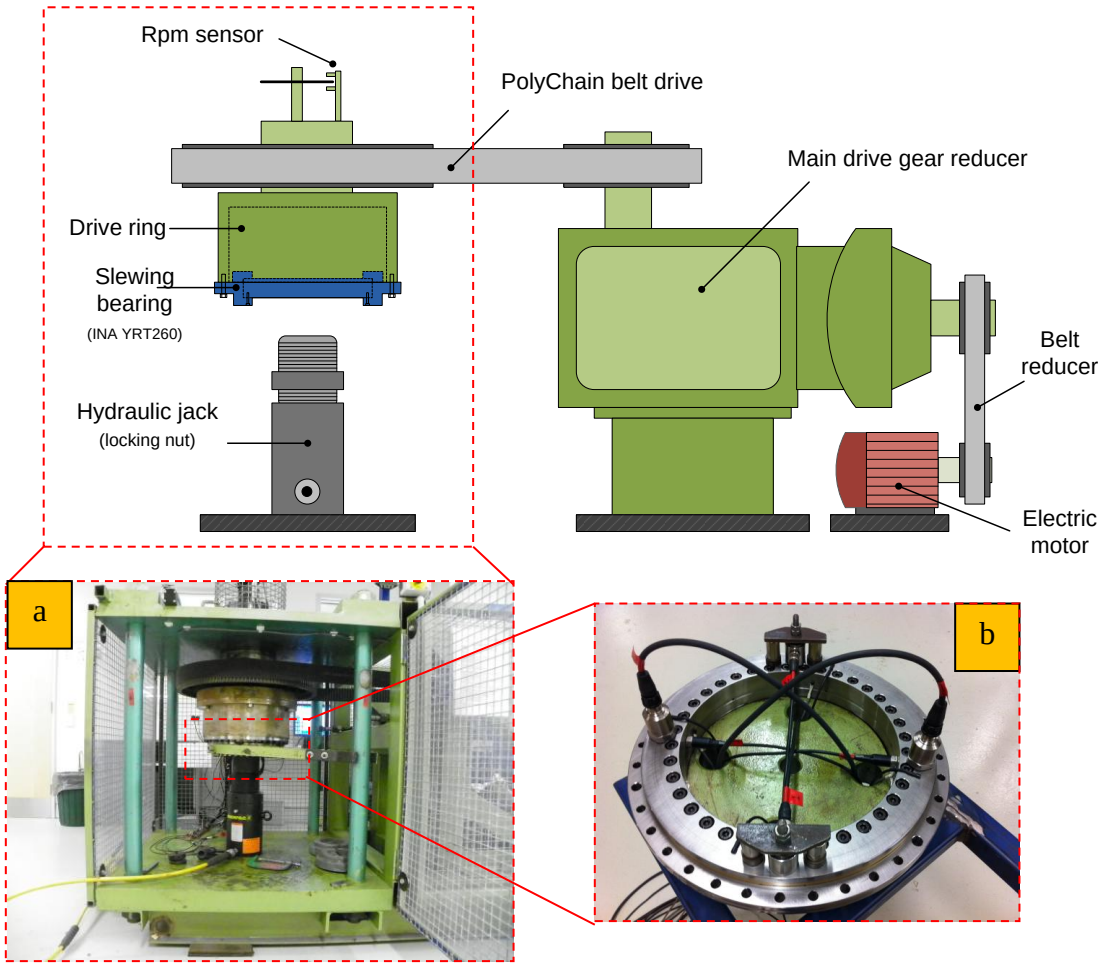

Figure 3.4 Schematic of laboratory slew bearing rig. (a) A larger front view of test rig showing a slew bearing attached on the drive ring and the applied load from hydraulic jack and (b) sensors placement.

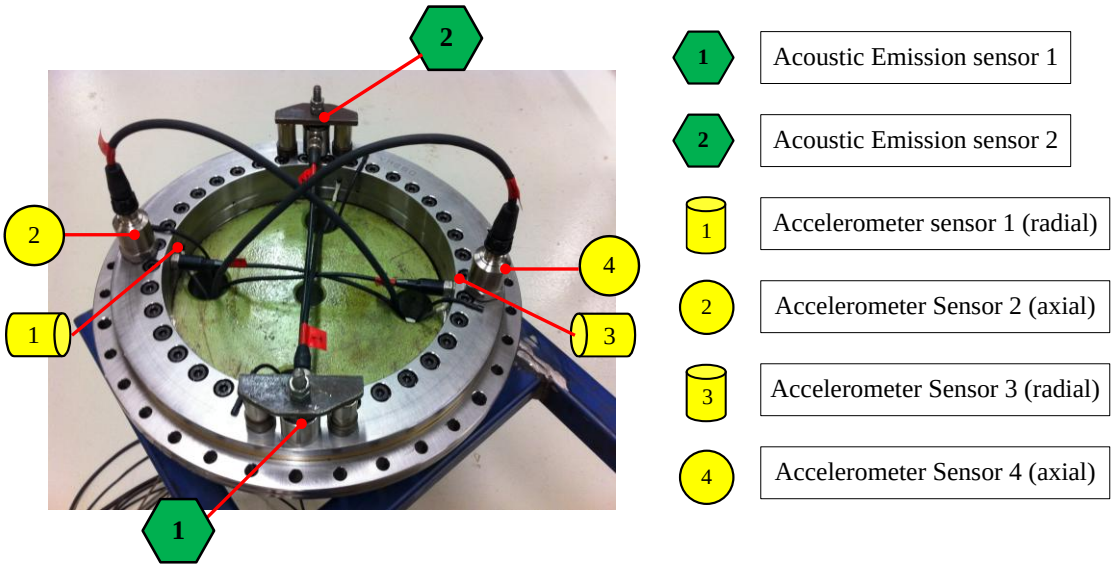

Figure 3.5 A detailed sketch of accelerometers and AE sensors location.

Acoustic emission data

Two integral AE PAC WD35A type sensors with a frequency range from 200 kHz to 1 MHz were used. These sensors are attached using magnetic mounting onto the top outer raceway of the slew bearing in the axial direction with 180 degrees to each other, as shown in Figure 3.5. Each integral sensor has internally installed preamplifier. These sensors were connected directly to an AE PCI-2 card with 2 channel inputs, 18 bit A/D conversion and 40 MS/second acquisition using coaxial cable with specified impedance (RG-58). The AE PCI-2 card was inserted into the computer. Similar to the vibration measurement, two data sets: clockwise and anti-clockwise, were acquired each day. Each data set was acquired for 35 seconds. The 35-second timeframe was determined based on the rotational speed of the slew bearing (1 rpm) and the reversible rotation angle (180^{o}). In order to obtain an accurate condition monitoring and damage detection result, the recording time must encompass sufficient shaft revolutions in a data set. Hence, the 35 second measurement was selected. The parameter set-up of AE measurement on an AEwin data acquisition software was as follows: the fixed threshold level was 30 dB, pre-amp 40 dB, lower analog filter 1 kHz and upper analog filter 2 kHz. In the waveform set-up: sample rate was 1 MSPS, pre-

trigger 5120 and 5k length were predefined. For low rotational speed rolling element bearings, the threshold has been studied and suggested to be 30 dB by Kim et al. [120].

Accelerated failure mechanism

The bearing run started on 22 November 2012. To accelerate failure, irregular greasing was applied in the following procedures. First, when the bearing was ordered and purchased, the slew bearing had already been lubricated by the manufacturer. Second, the slew bearing was relubricated after it had run continuously for two months from the commissioning of the lab experiment. A third lubrication was done after the slew bearing had run for 5 months. The type of grease for lubricating the slew bearing was Lithium base grease. During the experiment, dynamic load ranging from 7 to 15 tonnes was applied to the slew bearing through the hydraulic jack to accelerate the damage. This load is still below the maximum range of slew bearing requirement as shown in Table 1.1. The slew bearing was also subjected to an eccentric load about 10 mm to the right as illustrated in Figure 3.6. The measurement was stopped on 30 January 2014 for the identification of incipient damage which is already detected by time-domain feature extraction from the monitoring process. The bearing was then cleaned, and the damages on outer race, inner race and roller were analysed. The feature extraction results such as RMS, skewness, kurtosis and entropy was presented in Chapter 5. The bearing is assembled and attached to the test-rig. The second measurement was conducted from August to November 2014. The potential cause of the accelerated damage is investigated and the result is presented in section 5.5.

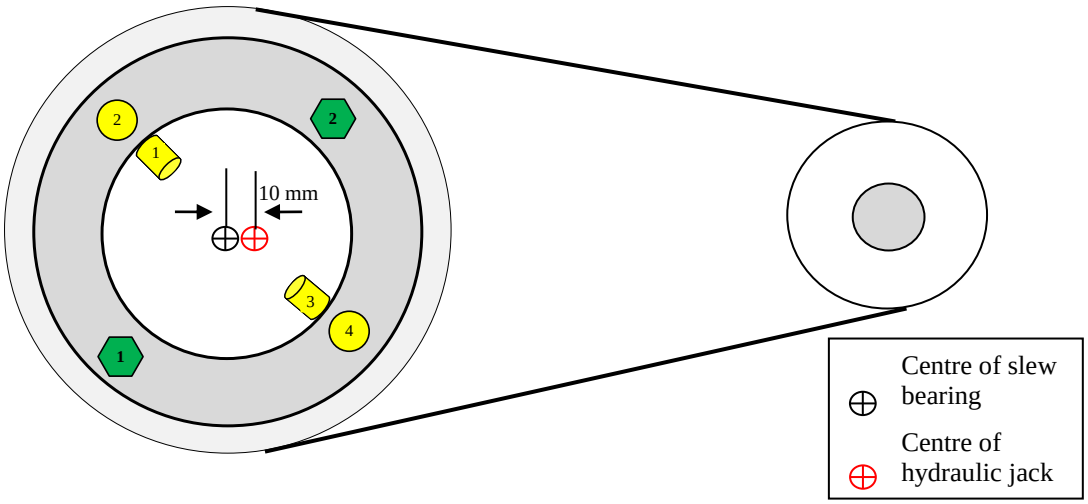

Figure 3.6 An illustration of eccentric loading.

3.2 Industrial measurement

3.2.1 Coal bridge reclaimer

Industrial bearing data used in this study was acquired from a slew bearing used in a coal bridge reclaimer. The bearing usually rotates at approximately 4.3 rpm. The type of slew bearing used is Rothe Erde 4.2 m diameter. The accelerometers are IMI512, 500 mV/g ICP type piezoelectric. Data was collected from 2003 to 2006 at each sample point, approximately once per month. It was captured via an industrialized portable DAQ unit (NI 5102) with a sampling rate of 240 Hz. The bearing specification is shown in Table 3.1.

Table 3.1 Specification of slew bearing used in coal bridge reclaimer.

Specification	Description	
	Dimension	Row
Outer diameter (D_0)	4.2m	
Number of rollers (z)	306	(axial)
	360	(radial)
Diameter of rollers (d_r)	32mm	(axial)
	28mm	(radial)
Pitch circle diameter (PCD) of rollers	4159mm	(axial)
	4224mm	(radial)

The fault frequencies of the bearing are presented in Table 3.2.

Table 3.2 Fault frequencies of coal bridge reclaimer (Rothe Erde) bearing rotating at a nominal speed 4.3 rpm [calculation is given in Appendix A].

Defect mode	Fault frequencies (Hz)	
	Axial	Radial
Rotating race speed	0.075	0.075
Outer ring (BPFO)	13.41	11.38
Inner ring (BPFI)	13.58	11.56
Rolling element (BSF)	5.65	4.87
Rolling element (BSF)	0.037	0.037

3.2.2 Slew bearing data from industrial company in Korea

The vibration data used in this study is acquired from an industrial company in Korea. The Wilcox accelerometer used during the data acquisition has a sensitivity of 100 mV/g. This sensor is installed on the radial direction of the slew bearings, as shown in Figure 3.7. The slew bearing under test is a single-row Koyo from Japan with an inner and outer diameter of 1093 mm and 1107 mm, respectively. The bearing runs continuously in one direction at a rotational speed of 15 rpm. The 15 rpm is achieved using a gear reducer mechanism. The driving motor rotational speed is 1800 rpm and the gear ratio is 17:1. The output shaft speed of the driving motor is 106 rpm. The gear motor has 18 gear teeth and the slew bearing has 123 gear teeth. Thus, the 15 rpm speed can be obtained. A figure of the slew bearing under test and the sensor placement is presented in Figure 3.7.

This bearing had been used for seven years. The maintenance engineer of the bearing company informed that it must be changed after years in use. Therefore, these data are treated as bearing damage data, supposedly including outer race, inner race or ball damage. If there is a fault in the outer race, inner race or even in the rolling element, the bearing fault frequencies must appear in the FFT. The bearing fault frequencies were calculated and presented in Table 3.3, where the gear mesh frequency is denoted by GMF.

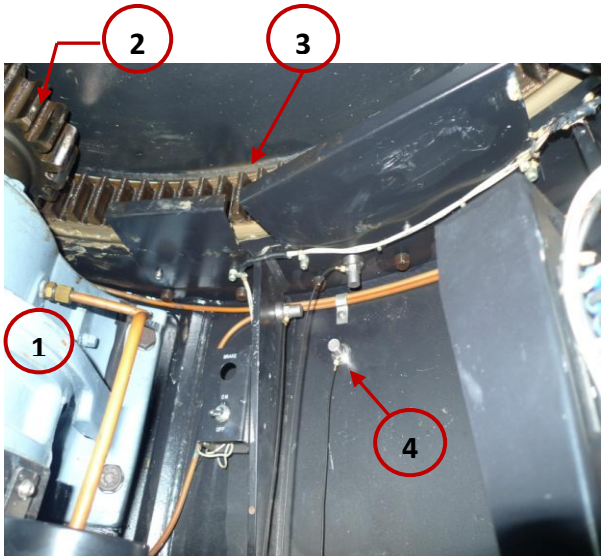

Figure 3.7 Slew bearing under test: (1) driving motor, (2) motor gear, (3) slew bearing gear and (4) sensor placement (radial).

Table 3.3 Frequency content of slew bearing signal from Korea.

FTF	0.24Hz	GMF	30Hz
BSF	5.16Hz	2x GMF	60Hz
BPFO	11.31Hz	3x GMF	90Hz
BPFI	11.87Hz	Bearing speed	0.24Hz

Four data sets were acquired on 26 May 2010, 7 December 2010, 19 July 2011 and 1 November 2011. These data are acquired within 1.6 seconds with a sampling frequency of 20480 Hz.

Chapter 4 - Condition monitoring based on feature extraction

"If you can't stand the fatigue of study, you will feel the poignant of stupidity"
(Imam Syafi'ie)

There has been no standard criterion for speed classification of rotating machinery so far. However, some published literatures have found that a rotating speed lower than 600 rpm is categorized as "low rotating speed machinery" [17-19] and a speed greater than 600 rpm is considered as "high speed" [20, 21]. Based on the above claim and the literature review presented in Chapter 2, this chapter classifies the speed in more details into three levels: (1) high speed (greater than 600 rpm), (2) low speed (below 600 rpm) and (3) very low speed (below 10 rpm). The literature review presented in Chapter 2 indicates that studies in low speed bearing condition monitoring (< 600 rpm) especially in case of naturally defective bearings has not been reported as widely as for high speed bearing with artificial damage. In the cases of high speed rolling element bearing, vibration analysis is a more commonly used method than AE method in both industrial application and research. It can be compared to the simpler and well developed data acquisition and analysis of vibration method. In contrast, recent studies claim that the application of the AE method for low speed bearing condition monitoring and early failure detection have offered an advantage compared with vibration analysis [19, 121, 122]. This project conducted both vibration and AE measurement to study the most effective and useful method for low speed slew bearing. In fact, both vibration and AE analysis required appropriate features in order to monitor the bearing condition. This chapter focuses on the development and application of feature extraction for low speed slew bearing vibration data.

Two feature extraction methods have been developed in this study. The first developed method employs data reduction process using PAA to detect frequency

alteration in the bearing signal. From the processed data, circular domain features are extracted and monitored. The second developed method applied one of the phase-space dissimilarity measures to analyse the chaotic characteristic of slew bearing vibration signal. Detailed introduction of each method is presented in the following sub-chapters.

4.1 Circular domain features-based condition monitoring

4.1.1 Introduction

There have been extensive studies on vibration analysis and feature extraction for condition monitoring, fault diagnosis and prognosis of high speed rolling element bearing [123-126]. The results show that these techniques can effectively monitor the changes of bearing condition. In high speed rolling bearing, once a fault has initiated, the bearing can deteriorate rapidly within a few hundreds or thousands of revolutions. This will result in changes of vibration within a very short time from the onset of the fault [126]. In this case, the use of feature extraction methods such as time domain and frequency domain feature calculation is effective to distinguish the bearing condition. However, the methods and features suitable for a high speed bearing cannot be effectively applied for identifying the abnormal condition of low rotational speed bearings [18] particularly in extremely low rotational speed (≈ 1 rpm) slewing bearings [1]. This is because the low impact energy emission from the rotating elements are in contact with a defect spot and might not show an obvious change in vibration signature corresponding to the bearing damage condition. Thus they will become hardly detectable using conventional vibration analysis [127]. Moreover, the bearing signal is also deeply masked by the background noise. Therefore, although time domain features [123-126] are extracted from the signal where the noise is dominant, the onset of bearing fault is still undetectable [1]. Eventually the amplitude is greater than the background noise. However, the features' value will have increased substantially by this stage. This shows that a significant change of bearing condition has already occurred. Typically, the bearing condition is already close to unsustainable operation or near failure by then.

This study presents a novel application of circular domain feature extraction based condition monitoring methods for low speed slewing bearings. The aim of the study is to investigate alternative features to identify the incipient fault and prevent the occurrence of a sudden breakdown. In contrast to the previous angle and cyclic domain analysis discussed in §4.1.2, this study employed circular analysis to extract the circular domain features. Different from general time domain statistical analysis, circular analysis is a sub-class of the field of statistics. In circular analysis the statistical features such as mean, variance, skewness and kurtosis are calculated from the data distributed in circular domain or angular domain. Circular features were initially introduced in biological and medical science fields [128-130].

This study combines piecewise aggregate approximation (PAA) data reduction processes and circular feature calculations (inspired by Berens [130]) as the monitored variables. The study demonstrates the efficiency of the proposed method in detecting the onset of slew reversible bearing fault. A reversible slew bearing alternately rotates in clockwise and anti-clockwise directions. The general steps of the proposed method are illustrated in Figure 4.1. The method consists of three main steps; (i) reduction of the vibration data using PAA process and construction of neighborhood correlations from the reduced data, (ii) determination of the shape of the neighborhood correlations using ellipse least-square fitting for pattern classification and (iii) plotting the distribution of the ellipse shape in the angular domain, and calculating the circular domain features (in this thesis, the first laboratory slew bearing data was used as the test case). The detailed description of Figure 4.1, especially the signals output between the boxes from original vibration signal to ellipsoid pattern classification, is presented in §4.6. The proposed method is compared to time domain features and advanced signal processing methods such as wavelet decomposition and empirical mode decomposition (EMD).

4.1.2 Angular resampling

Angular resampling is a useful signal processing methodology in vibration analysis. It has been proven to work well in rotational machineries with variable speed. The first known attempt used angular resampling by means of angle domain analysis [131]. The paper demonstrates the different results obtained from simulated sinusoidal signal

sampled at time domain and angular domain. Moreover, the sinusoidal signal is simulated with impulse signal that represents the bearing fault and varying speed using mathematical function. It is shown that the simulated fault is clearly identified in angular domain analysis even though the speed changes. Many researchers have used angular resampling to perform order domain analysis or order tracking method [132, 133].

Unlike frequency domain analysis which reveals the dominant frequency content of the vibration signal, the order domain analysis or order tracking method calculates multiple running speed content of the variable shaft rotation. Fyfe and Munck [132] stated that speed-related vibrations can be easily identified using order tracking method. The authors presented the two existing order tracking methods, namely conventional order tracking and computed order tracking. The conventional order tracking employed special instrumentations such as ratio synthesizer and anti-aliasing tracking filter to directly sample the analog vibration signal at constant increment angle (i.e. $\Delta\theta$). Computed order tracking method resamples the acquired discrete vibration data that are sampled at uniform Δt into constant angular increments $\Delta\theta$. Once a specified block of data sampled at constant $\Delta\theta$ (angle domain samples) from both methods has been obtained, the order spectrum is computed using Fast Fourier Transform (FFT). Moreover, the effect of various factors on the accuracy of the computed order tracking method was investigated. However, the data used for computing the order tracking is the simulation data. These are generated from run-up simulation model instead of actual data. An extended work of the two previous order tracking methods described in [132] was proposed by Bosssley et al. [133]. The focus of these works was to assess the accuracy of the three different order tracking methods: conventional order tracking, computed order tracking and hybrid of the two. The methods were applied in simulation vibration signals produced from a power station gas turbine shaft.

Case studies of angular resampling application include rolling element bearing [134, 135], gearbox [136-138], wind turbine [139, 140], and induction motor [141] analyses. The angular resampling application in [136] used the acceleration signals directly, and it does not require an encoder signal. The resampling algorithms developed in the

above published literatures [136-138] are applicable for small speed fluctuation cases. Ref. [139] offered an improved angular resampling algorithm for variable speed machineries such as wind turbine. A recent and promising method for natural roller bearing fault detection based on instantaneous angular speed measurement has been presented by Renaudin et al. [135]. The instantaneous angular speed measurement with a true angular sampling is conducted using magnetic and optical encoders. The instantaneous angular speed measures the kinematics of the device using the principle of pulsed timing method. This study proved that instantaneous angular speed exhibits small periodic fluctuations in the angular frequency domain in time of the occurrence of spall damage.

The application of angular resampling in 'slew bearing' has been considered in 1990 [142] as an internal steel metal making company report. However, the report only presented the theoretical analysis without any example in real case. To date, there have been limited literatures that discuss the application of angular resampling in slew bearing cases.

4.1.3 Piecewise Aggregate Approximation (PAA)

Theory

PAA data reduction process was introduced by Yi and Faloutsos [143] and Keogh et al. [144] independently. It was first developed as a data reduction technique for large time series data whilst keeping its characteristic. To reduce the data length, one sequence of sampled vibration data, $\mathbf{y} = (y_1, y_2, ..., y_N)$ with N number of data points is divided into w window of equal size termed 'frames'. The mean value of the data in each frame and the vector of these mean values becomes the reduced data representation or PAA result. The mean value of data in one frame is given as follow:

$$x_n = \frac{1}{w} \sum_{j=w(n-1)+1}^{wn} y_j \tag{4.1}$$

The PAA result of Eq. (4.1) is the vector $\mathbf{x} = (x_1, x_2, ..., x_n)$. One cycle of sinusoidal signal and the reduced data representation are shown in Figure 4.1. In the next step, the PAA result is used as processed data to identify the frequency alteration.

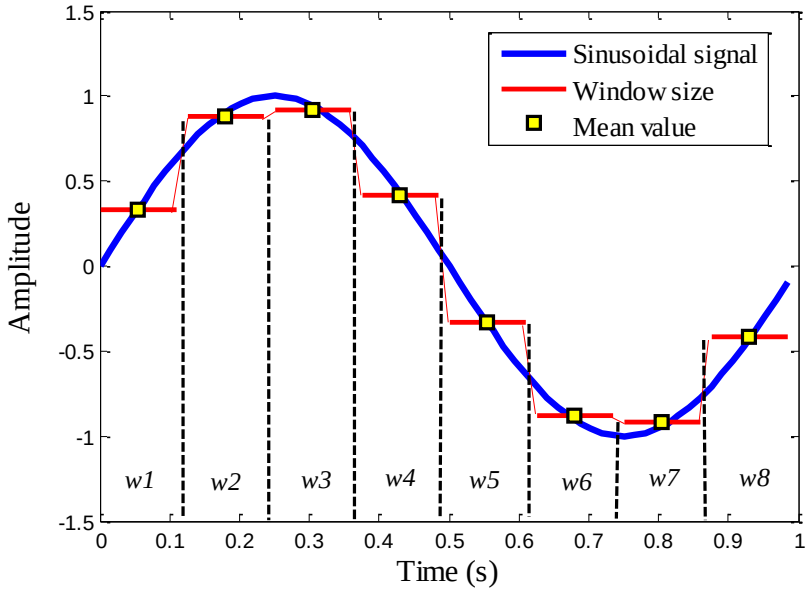

Figure 4.1 One cycle of sinusoidal signal (1 Hz) sampled with 64Hz sampling frequency is shown with solid blue curve. The data is divided into 8 frames (solid red line). The calculated mean value of sampled data in each frame is shown in yellow square shape. All mean values notated by the vector of $\mathbf{x} = (x_1, x_2, ..., x_8)$ are the PAA results. The index $w1, w2, ..., w8$ is the equal window size or "frame".

The saved vibration data are obtained from extremely low rotating speed bearing (≈ 1 rpm) that is acquired at certain sampling rate over one minute or more. The data reduction process is required for these saved data. In this study, PAA data processing is used to reduce the saved data but still can extract the high frequency component from short-duration signal (1 second). This is suitable for the present analysis, because slew bearing signal were sampled few times over long-duration each day during the months long experiment duration. The high frequency signal indicates the presence of fault initiation. The more high frequency component identified in one data set indicates that the bearing condition deteriorates further.

In addition, when slew bearing condition is normal, the bearing vibration signal amplitude is much lower than the background noise amplitude. As bearing condition deteriorates and the onset of damage occurs, the bearing signal amplitude will increase, but it may still be lower than the background noise amplitude. Therefore, if time-domain features are calculated from this signal, the feature values are still indistinguishable from normal condition bearing feature values. When bearing

condition is close to unsustainable operation, the bearing signal becomes stronger. Sometime later, the signal will be greater than the background noise. At this stage the time-domain features will be more sensitive. With PAA method combined with circular-domain features calculation, the onset of damage can be identified. This will allow an appropriate planning of the preventive maintenance program.

Identification of frequency alteration from the shift of the ellipsoid orientation

The question regarding the application of PAA is how frequency alteration is detected. The investigation is conducted using simulated data. Two different signals (1Hz and 5Hz frequency) sampled with sampling frequency of 64Hz are shown in Figures 4.2 to 4.4. Signals with amplitude 1 are simulated in one second. Each signal is analyzed using PAA method with equal frame or window size. Three different window sizes namely 2, 4 and 8 are used in Figures 4.2, 4.3 and 4.4 respectively. The reduced data or PAA result, $\mathbf{x} = (x_1, x_2, ..., x_n)$ is plotted in the form of neighborhood correlation plot, $x(n+1)$ against $x(n)$. For 1Hz signal, the neighborhood correlation plots show the ellipsoid axis is oriented at 45 degree angle as depicted in Figures 4.2(a) to 4.4(a) for window size of 2, 4 and 8. While, in case of 5Hz signal, the ellipsoid still inclines at 45 degree angle with window size of 2, but it changes to 135 degree angle when window sizes of 4 and 8 are used. Based on the result, it can conclude that the frequency alteration is highly dependent on the window size used. A detailed discussion of the selection of window sizes is presented in Appendix B.

Moreover, the effect of different frequency with fixed window size is investigated with four different frequencies namely 1Hz, 2Hz, 3Hz and 6Hz sampled at 64Hz. A window size of 4 is employed for each signal. It can be seen in Figure 4.5 in the neighborhood correlation plots, the ellipsoid of frequency 1Hz, 2Hz, and 3Hz is oriented at 45 degree angle (*right ellipsoid pattern*). But it is shifted to 135 degree (*left ellipsoid pattern*) when the frequency is 6Hz. This implies that frequency alterations can change the angle of the ellipsoid axis of the reduced data obtained from PAA process. The frequency alterations mean the apparent of one or more bearing fault frequency in the vibration signal and/or the apparent of high frequency content

excited from the bearing damage. In addition the impact between the damage spot and rolling element will also generates the signal with high frequency. Therefore, the used of PAA process can detect this sudden change.

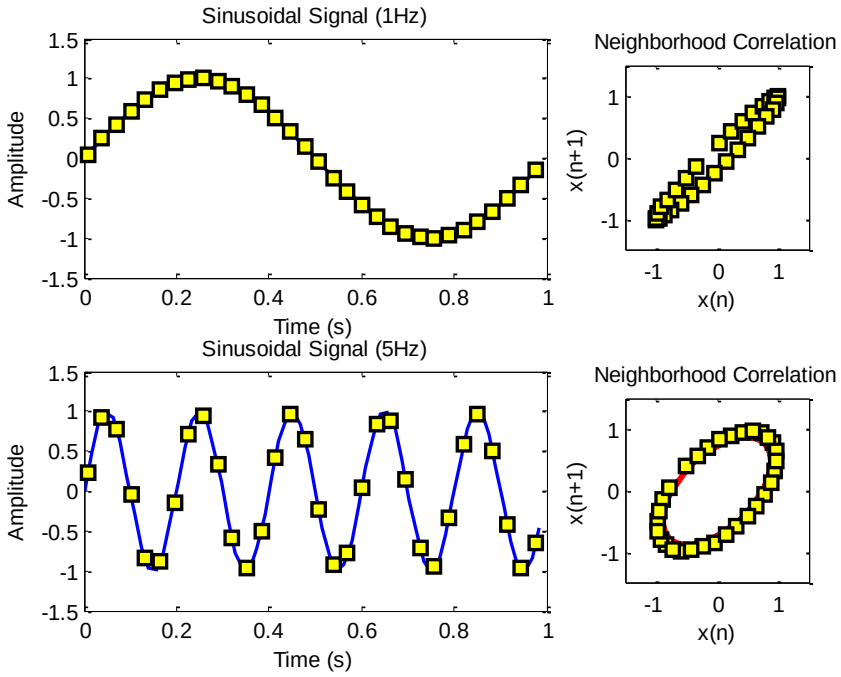

Figure 4.2 Neighborhood correlation plots of 1Hz and 5Hz sinusoidal signals with window size = 2.

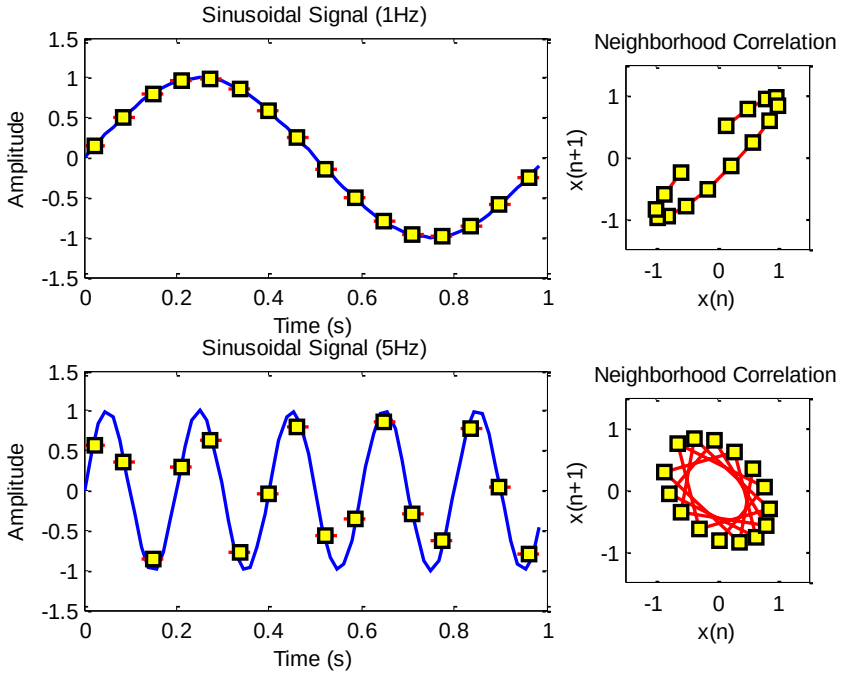

Figure 4.3 Neighborhood correlation plots of 1Hz and 5Hz sinusoidal signals with window size = 4.

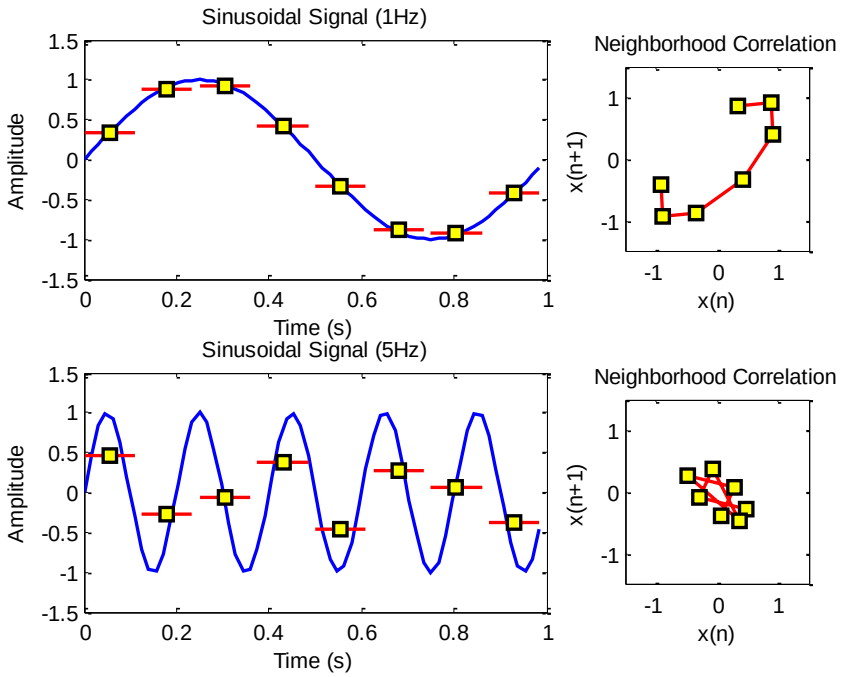

Figure 4.4 Neighborhood correlation plots of 1Hz and 5Hz sinusoidal signals with window size = 8.

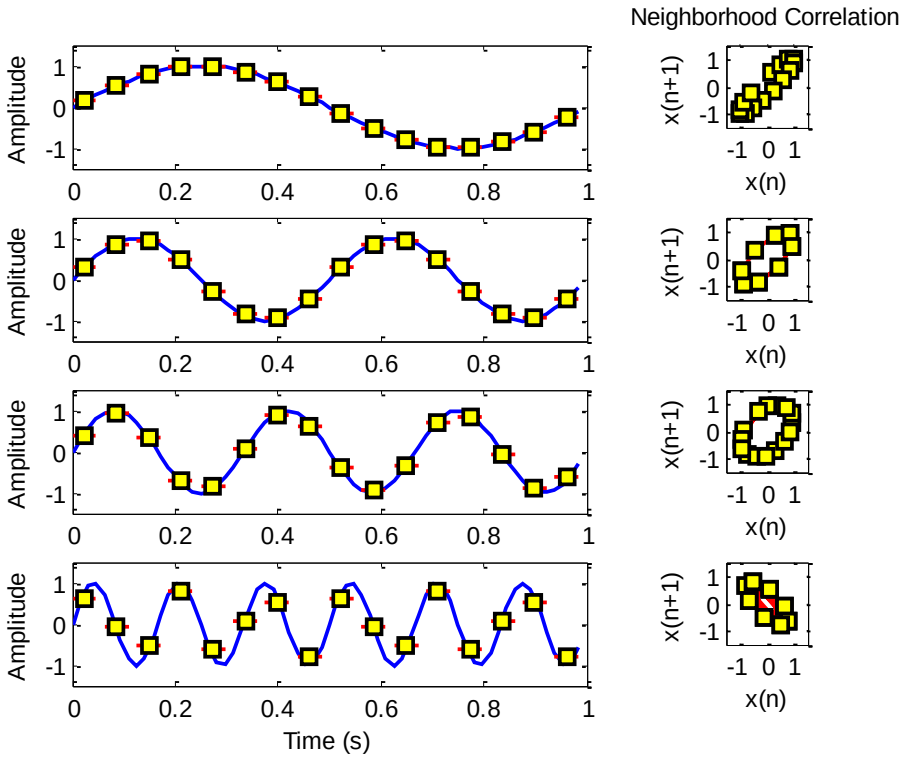

Figure 4.5 Sinusoidal signal and PAA process (left) and neighborhood correlation plot based on PAA result (right) for different frequencies with fix window size of 4: (a) 1Hz; (b) 2Hz; (c) 3Hz; (d) 6Hz.

PAA application in laboratory slew bearing rig and coal bridge reclaimer data

PAA data reduction process with w = 32 and 16 were used in processing the laboratory slew bearing data and the reclaimer data, respectively. The result is plotted in neighborhood correlation plot, $x(n+1)$ against $x(n)$ as shown in Figure 4.6. Three different neighborhood plot orientations are clearly visible namely (1) centered; (2) left shifted at 135 degree; and (3) right shifted at 45 degree. When the bearing is in good condition, the neighborhood plot appears to have centered orientation; when the condition starts to deteriorate, the ellipsoid is oriented to 135 degree (*left shifted*); and when the condition of bearing is close to failure the neighborhood plot is at 45 degree (*right shifted*). The 135 degree (*left shifted*) and 45 degree (*right shifted*) are the result in the plotting of neighborhood correlation plot. The question is what triggers the change of the orientation. The answer is the change of frequency explained in subsection 4.2. Furthermore, the data scattered in neighborhood plot with centered orientation is due to the background noise. The background noise is the common issue in practice. When the acquired signal contains dominant background noise, the neighborhood plot produce centered orientation. When the bearing is in good condition, the bearing signal is very weak and is deeply masked by the background noise. This is because the low amplitude of bearing signal is associated with good bearing condition.

To demonstrate the effect of the change of bearing signal magnitude, another simulated signal is produced as shown in Figure 4.7. The 5Hz frequency signal is sampled with sampling frequency identical to the sampling frequency of laboratory slew bearing rig data i.e. 4880Hz for 2sec. The first one-second signal contains the sinusoidal signal plus white noise where the amplitude of sinusoidal signal is greater than the amplitude of white noise shown with blue signal. The last one-second simulates the weak 5Hz signal that is deeply buried in white noise as shown in red in (Figure 4.7(a)). A window size of 40 was used for each type of signal resulting in 122 segments. When the 122 reduced data in the form of neighborhood correlations plot, $x(n+1)$ against $x(n)$, the data is scattered in the right ellipsoid orientation (45^o) as shown in the left plot in Figure 4.7(b).

When the amplitude of background noise is larger than the bearing signal, the data is scattered in circular formation. This demonstration illustrates the suitability of neighborhood correlation plot for bearing signal detection. An amplitude ratio denoted in Figure 4.7 was computed by V_{RMS} / A_{RMS}, where V_{RMS} is the root mean square of vibration signal amplitude and A_{RMS} is the root mean square of white noise amplitude. The green color signal is the PAA reduced data.

Elliptical least-square fitting method for PAA results

The right or left ellipsoid oriented patterns presented in Figures 4.2-4.5 only occur in pure sinusoidal signal. In practice, the PAA result or data reduced representation is scattered in neighborhood correlation plots as shown in Figure 4.6. Even though the PPA result is scattered but it still has ellipsoid outline. Thus, to establish the ellipsoid outline curve from the scattered data, direct least-square fitting method of ellipses [145] is used. This method [145] has a high computational efficiency compared to conventional elliptical fitting method [146, 147].

From the fitted ellipse three possible ellipsoid orientations are obtained labelled as ′0′ for centred orientation, ′1′ for right shifted orientation (45 degree) and ′2′ for left shifted orientation (135 degree). This method is used as the ellipsoid classification recognition in the circular feature analysis.

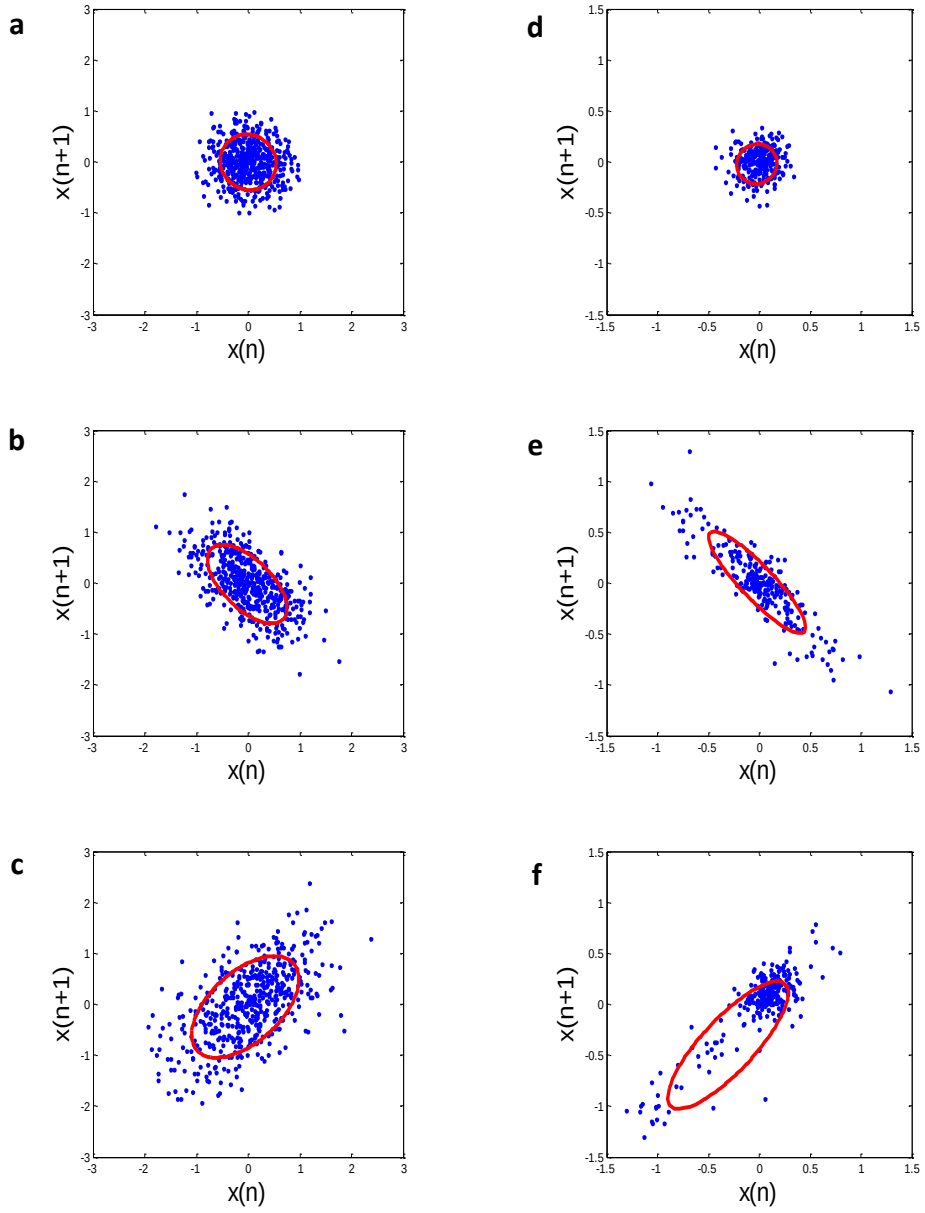

Figure 4.6 Results of PAA data reduction of the laboratory test data: (a) March 2007; (b) May 2007; (c) August 2007; and results of coal bridge reclaimer data: (d) May 2004; (e) January 2005; (f) September 2006.

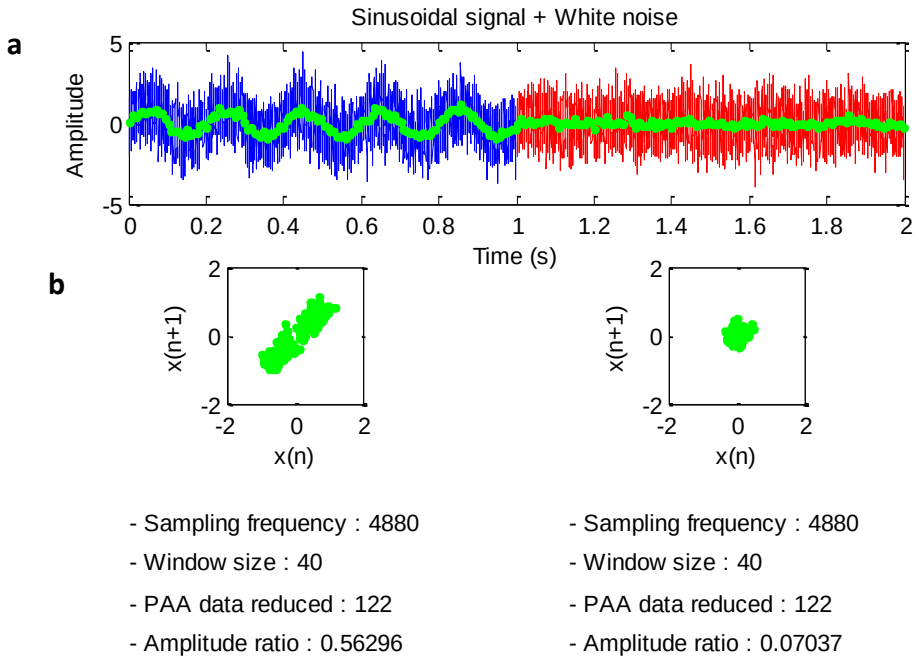

Figure 4.7 (a) Simulated 5Hz signal with added white noise for different amplitude ratio; (b) PAA result or data reduced representation plotted in neighborhood correlation plot.

Simulated defective bearing condition monitoring using PAA process

Simulated progressive deteriorating condition of the bearing can be viewed as composed of four stages shown in Figure 4.8. During stage I, the bearing is still in good condition and the amplitude of the background noise is larger than the amplitude of the bearing signal. In this stage, there is no fault in the bearing and the weak bearing signal is deeply buried in the background noise. Using a window size of 40, the neighborhood correlation plot shows centered or circle orientation. Stage II is defect inception stage. In this stage, the onset of damage starts to occur as signified by the increased amplitude of bearing signal. This stage usually does not last long. The neighborhood correlation plot of this stage has evolved from circle into a right ellipsoid orientation (45 degree). In stage III, the progressive fault occurs signified by the presence of unknown high frequency signal. The neighborhood correlation plot ellipsoid orientation is switched over from right to left. In the slew bearing case, this can occur when bearing defect frequency increases suddenly after faults initiation. As the defects strike another surface, they excite the resonance frequency of the sensor, bearing or test-rig itself [148] and produce the typical frequency signals which are

higher than bearing fault signals. These resonances would be higher than half the sampling frequency of 4880 Hz and therefore be aliased. In the last stage, the bearing is in a severely damaged condition signified by high bearing fault signal amplitude. At this stage, the ellipsoid has the right orientation again. The simulation demonstrates that any change of the bearing condition will be manifested in the change of ellipsoid orientation.

The question now is what if the orientation shift is an isolated instance. Can it still be a reliable parameter for monitoring the progressing fault? To get a definitive detection of bearing condition, the ellipsoid orientation is considered as a bearing signal feature and presented in the circular domain.

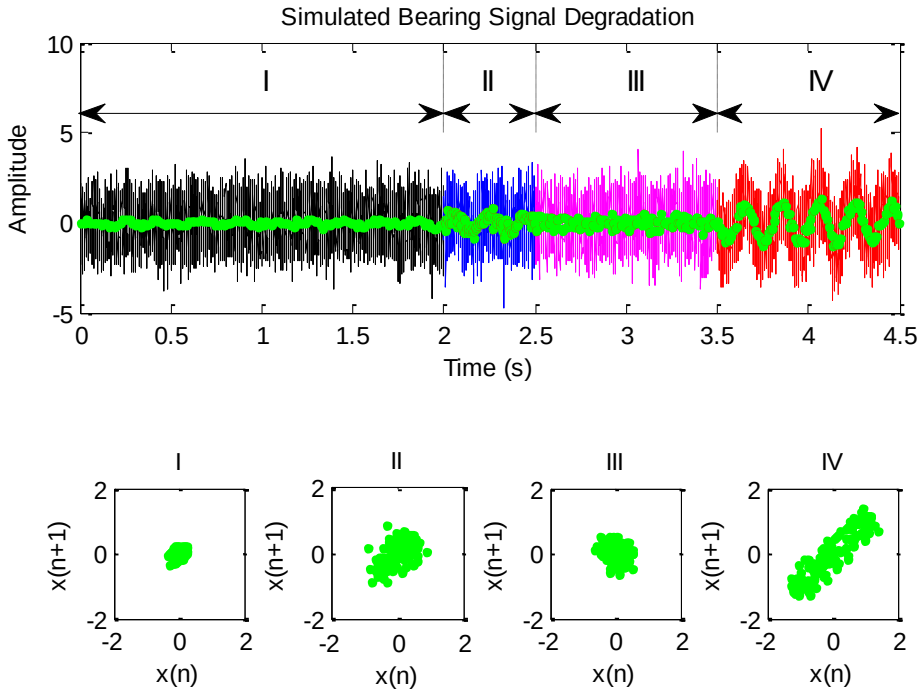

Figure 4.8 Progression of simulated bearing signal degradation and the detection of fault occurrence using PAA. This signal is simulated with sampling frequency of 4880 and PAA window size of 40. Stage I: 5Hz signal + white noise for amplitude ratio of 0.1. Stage II: 5Hz signal + white noise for amplitude ratio of 0.4. Stage III: 55Hz signal + white noise for amplitude ratio of 0.4. Stage IV: 5Hz signal + white noise for amplitude ratio of 1. The four neighborhood plots show the evolution of the ellipsoid and its orientation change.

Signal processing flow process from original slew vibration signal to ellipsoid pattern classification

Figure 4.9 shows the illustration of signal processing based on PAA and elliptical least-square fitting method for slew bearing signal acquired on May 25th. Each 1 second data set is examined instead of whole data set in 30 seconds to extract the high frequency component in short duration. Using the neighborhood correlation plot combined with elliptical fitting method, this high frequency component can be identified. It is well known that in one second, high frequency signal has more cycles than lower frequency signal. If the window size is constant, the mean value of samples in one window size will be different between the signals with more cycles and lower cycles. This result in the different neighborhood correlation plot, sample $x(n+1)$ against sample $x(n)$.

The three different data at 4 second, 14 second, and 23 second were selected for illustration. As shown in Figure 4.9, each second of data set which contains 4880 samples was reduced using PAA method with window size of 8. The 4880 samples were reduced into 610 samples. Then, the data reduced (610 samples) are plotted in neighborhood correlation plot, $x(n+1)$ against $x(n)$. Using elliptical least-square fitting method [145] explained previously, the shape of neighborhood correlation plot can be identified and classified into three different orientations: 'left shifted ellipsoid', 'right shifted ellipsoid', and 'centered'. The onset of bearing fault is signified by the presence of high frequency signal component and represented by the right shifted ellipsoid. Therefore, the right shifted ellipsoid is recorded as the term of 'occurrence' and is used in the next step of circular domain transformation (Figure 4.7) and circular domain features calculation (Figures 4.8 and 4.9).

The combined PAA and circular domain features is used to detect the defect inception stage. As mentioned earlier that the defect inception stage occurs in stage 2 (see Figure 4.8). The neighborhood correlation plot of stage 2 is right ellipsoid. Therefore, the right ellipsoid is recorded for further processing step as presented in Figure 4.9.

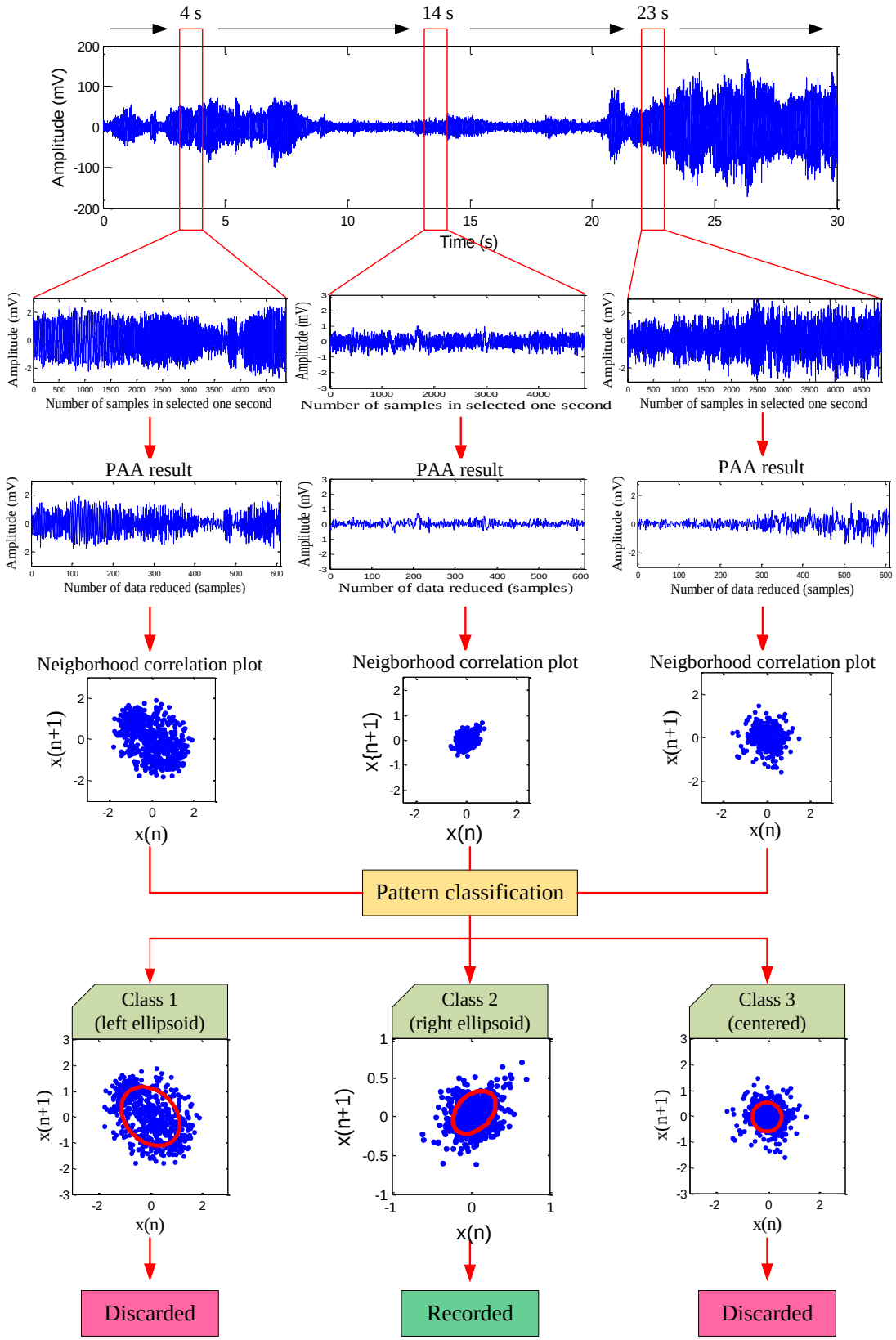

Figure 4.9 Illustration of signal processing based on PAA method and ellipse least-square fitting method using vibration data acquired on May 25th (the 90th day).

4.1.4 Circular feature analysis

Circular domain transformation

The working principle of circular features calculation is different from time domain features calculation. In time domain features calculation, the features are calculated directly from vibration signal. The time domain features calculated from normal bearing signal are different from faulty bearing signal. This condition has been recognized in typical speed bearing (>600 rpm). In slewing bearing case, the bearing fault signal is weak and background noise is dominant. Thus time domain features become undetectable to the change of bearing condition especially the onset of bearing fault. This is because features are calculated in noisy signal. This drawback is addressed in this thesis by introducing an alternative method called circular domain features calculation.

To calculate features in circular domain, the PAA processed data should be first transformed into angular domain. The purpose is to identify the changes of bearing condition, particularly to identify the presence of high frequency signal component. This component is due to the contact between rolling element and defect spot within a definite sampling period e.g. one second (≈ 6 degree of rotation) for bearing run at 1 rpm. In practice, the slewing bearing rotates in reversible mode at predefined span β e.g. 360°, 180°, 120° or 90°. Therefore the time domain when the vibration data is collected and is converted initially to an angular scale in degree by

$$\boldsymbol{\theta} = \left(\frac{\mathbf{t}}{t_{\max}} \right) \cdot \beta \tag{4.2}$$

where $\boldsymbol{\theta}$ is the angular scale vector in degree, $\mathbf{t} = (t_1, t_2, ..., t_N)$ is time occurrence (the member of vector $\mathbf{t}$ is depends on the time occurrence of each 1 second (≈ 6°) analysing using PAA method), and $t_{\max} = t_N$ is the total time the bearing rotate in one direction. If the bearing is run at 1 rpm with β = 180°, the duration of slewing bearing to complete one angular span, $t_{\max}$ is 30 second. It should be noted that the interval Δt corresponds to the sampling frequency, fs of the vibration data. Then from the angular scale in degree, it is converted to an angular scale in radians by

$$\boldsymbol{\alpha} = \left(\frac{\boldsymbol{\theta} \cdot \pi}{180} \right) \tag{4.3}$$

where $\boldsymbol{\alpha}$ is the angular scale in radians. Alternative straight forward equation to transform time vector, $\mathbf{t} = (t_1, t_2, ..., t_N)$ into angular quantity, $\boldsymbol{\alpha} = (\alpha_1, \alpha_2, ..., \alpha_N)$ is

$$\boldsymbol{\alpha} = \left(\frac{\mathbf{t}}{t_{\max}} \right) \cdot \left(\frac{\beta}{360} \right) \cdot 2\pi \tag{4.4}$$

Note that Eq. (4.4) computes the entire linear vector (time domain) and converts it into angular vector (circular domain). α is calculated according to PAA result (each sample of occurrence). Therefore, the new vector of α is $\boldsymbol{\alpha} = (\alpha_1, \alpha_2, ..., \alpha_N)$ where C is the number of occurrences and each data point of occurrence $\alpha_1, \alpha_2, ..., \alpha_i$ is denoted as i.

The PAA method as frequency alteration identification and circular domain transformation is illustrated in Figure 4.10. One second (≈ 6°) of time series vibration (May 25th 2007) containing 4880 sampled points is used as an input for PAA method. The occurrence and non-occurrence is identified as “1” and “0” respectively. The distribution of circular occurrence “1” in circular-domain is shown. Subsequently circular features such as circular mean, circular variance, circular skewness and circular kurtosis are calculated to obtain the statistical behaviour of scatter data in circular-domain. The detailed description about the application of circular features on the laboratory slew bearing data based PAA result is explained as following.

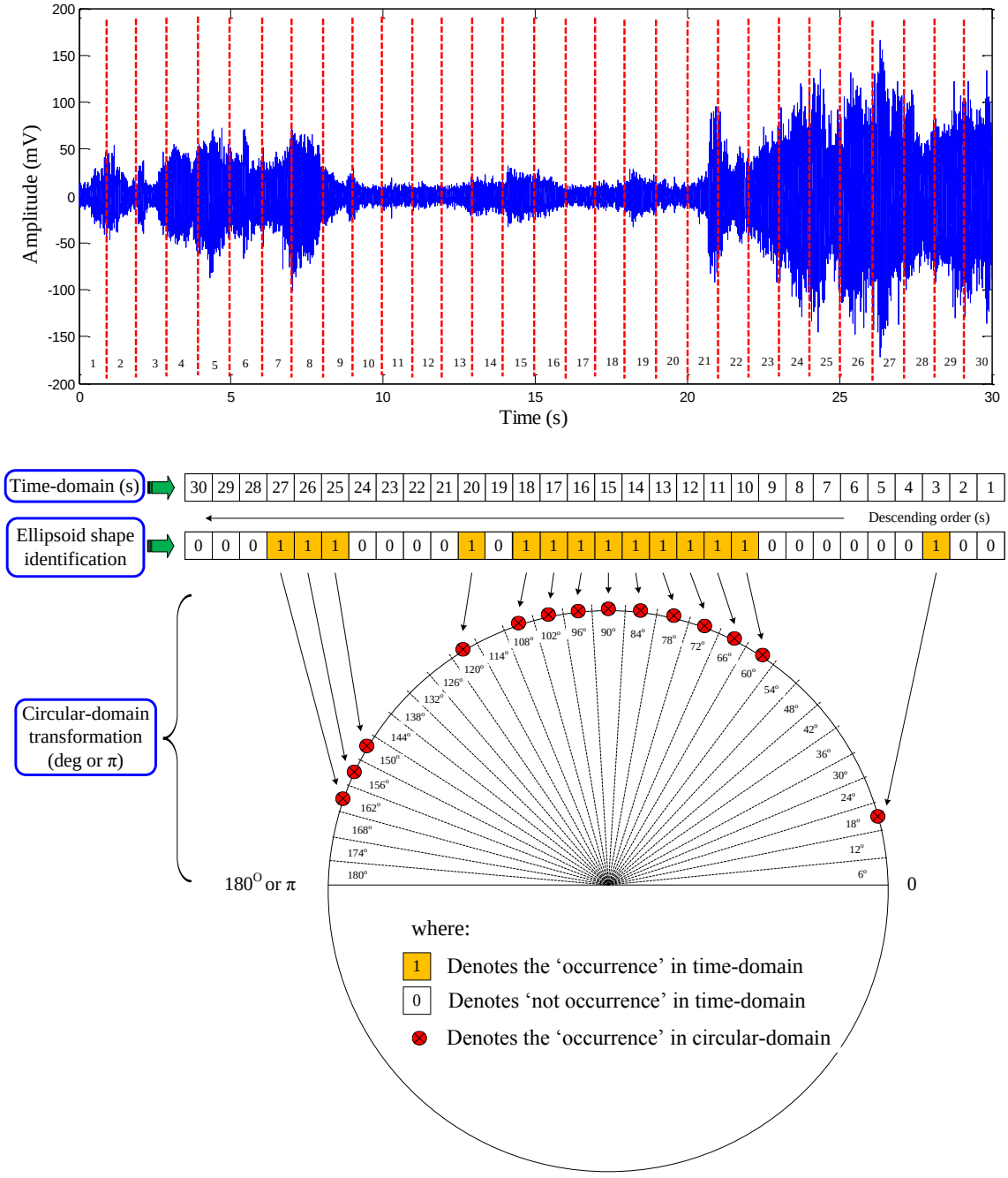

Figure 4.10 Illustration of PAA method as frequency alteration identification and time domain to circular domain transformation using the vibration data acquired on May 25th (the 90th day).

Circular features calculation

To apply circular features calculation, the second when class '1' orientation occurs is recorded. The time occurrence is transformed into angular dimension $\boldsymbol{\alpha}$ using Eq. (4.4).

Circular mean and mean resultant vector: The mean of vector $\boldsymbol{\alpha}$ cannot be estimated using simple linear averaging data points. Since $\boldsymbol{\alpha}$ is in angular directions, the members of vector $\boldsymbol{\alpha}$ are initially transformed to unit vectors in the two-dimensional plane by

$$Z_i = r\cos\alpha_i \quad \text{or} \quad Z_i = r\sin\alpha_i \tag{4.5}$$

where r is the radius of two-dimensional circular plane and $r=1$ is used in this thesis. This is illustrated in Figure 4.11(b), where all data points, α (occurrences) marked by blue circles lie on the unit circle. As indicated further in Figure 4.11(b), the *x*-coordinate of a point (α_i) corresponds to cosine of the angle and the *y*-coordinate to the sine. For the ease of implementation in MATLAB, this transformation is written in the following equation

$$Z_i = r(\cos\alpha_i + i\sin\alpha_i) = r\exp(i\alpha_i) \tag{4.6}$$

After this transformation, the mean of $\bar{Z}$ can be computed from the vectors Z_i by

$$\bar{Z} = \frac{1}{C}\sum_{i}^{C} Z_i \tag{4.7}$$

where C is the number of data points (occurrence). The vector $\bar{Z}$ is called mean resultant vector. To yield the circular mean $\bar{\alpha}$, the built-in function angle in MATLAB is used to transform $\bar{Z}$ into the circular mean $\bar{\alpha}$. Moreover, i indicates point in the circular domain where the correlation plot has the right orientation (45 degree) or class '1'.

Resultant vector length: The length of the mean resultant vector is a fundamental quantity for the measurement of circular spread in circular domain [130]. If the samples are concentrated, the resultant vector length is around the mean direction. The resultant vector length is estimated by

$$R = \left\|\bar{Z}\right\| \tag{4.8}$$

Circular variance: The circular variance is closely related to the length of the mean resultant vector. It is defined as

$$V = 1 - R \tag{4.9}$$

Moreover [130] mentioned the difference between the variance on a linear scale and the circular variance. The circular variance is bounded within the interval [0, 1]. It indicates the spread of a data set. If all sample points lie on the angular scale with the same direction, the resultant vector will have a length close to 1 and the circular variance will correspondingly be small. If the samples spread out evenly around the circle, the resultant vector will have length close to '0' and the circular variance will be close to maximum.

Circular skewness: As the third order statistical moment, circular skewness measures the symmetry of distribution data with respect to the circular mean. It can be calculated as follows [128]

$$m = \frac{1}{C}\sum_{i=1}^{C}\sin 2\left(\alpha_i - \overline{\alpha}\right) \tag{4.10}$$

Circular kurtosis: Similar to time domain kurtosis, circular kurtosis measures the degree of spread of the distribution around the peak. Kurtosis indicates the condition of bearing and provides potential damage detections at an earlier stage. When defects impact rolling element parts, they produce a response signal that has a probability density sharper than a normal condition [149]. Circular kurtosis can be estimated as [128]

$$k = \frac{1}{C}\sum_{i=1}^{C}\cos 2\left(\alpha_i - \overline{\alpha}\right) \tag{4.11}$$

A large positive sample value of k close to one indicates a sharp distribution. Circular kurtosis value will increase when the class '1' ellipsoid orientation occurs more frequently and data are distributed uniformly in circular domain. On the contrary, kurtosis value will decrease when the data is few and distributed randomly. This enables the onset of bearing fault to be identified using circular kurtosis coupled with PAA data reduction method in the slew bearing condition monitoring case.

Application of circular features on laboratory slew bearing data based PAA result

To obtain a clearer detection of bearing condition, the ellipsoid classification is considered as bearing signal feature and presented in circular domain. In order to determine whether a shift is an isolated instance or not, the ellipsoid orientation classification is conducted every second (≈ 6 degree) for one minute equivalent to reversible full rotation for 1rpm. The highlights of circular domain transformation and circular features calculation result are depicted in Figures 4.11 and 4.12. Figures 4.11 and 4.12 show the difference of circular features result based on PAA method obtained on day 9th and day 90th of the bearing running time. Day 9th is selected to represent the normal condition and day 90th is selected based on the observation result of circular domain features as shown in Figure 4.13. The time domain signal representation in circular domain is shown in part (a). The vibration signal plotted in circular domain is the slew bearing data in 30 seconds (≈ 180 degree). After the application of PAA process with the window size of 8 and the ellipse least-square fitting method, the ellipsoid shape classification based on the neighborhood correlation plot of PAA result is obtained. The classification result of every second is called 'occurrence'. The result of right ellipsoid occurrence '1' is shown in part (b) (shown in circle blue line). Finally, the four circular features based on the result plotted in part (b) are calculated to reflect the statistical behavior of the occurrences of the minute. The circular features calculation is presented in part (d). The process is then applied on the lab slew bearing data from February to August (139 days). The solid red line in Figures 4.11 and 4.12(b) and (c) is the resultant vector length, R. The R value decreases when the data is spread out to angular domain.

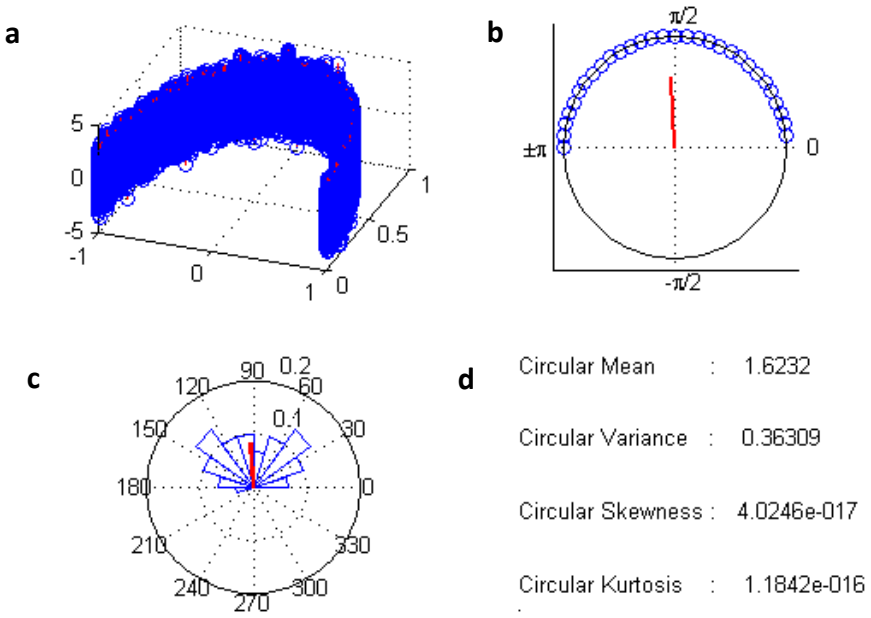

Figure 4.11 First laboratory slew bearing data acquired on March 1 (the 9th day): (a) vibration data in circular domain; (b) the 'occurrence' results plotted in circular domain (in radian); (c) circular histogram (in degree) (note: blue line and red line is circular histogram and resultant vector length (R), respectively); (d) circular feature extraction results.

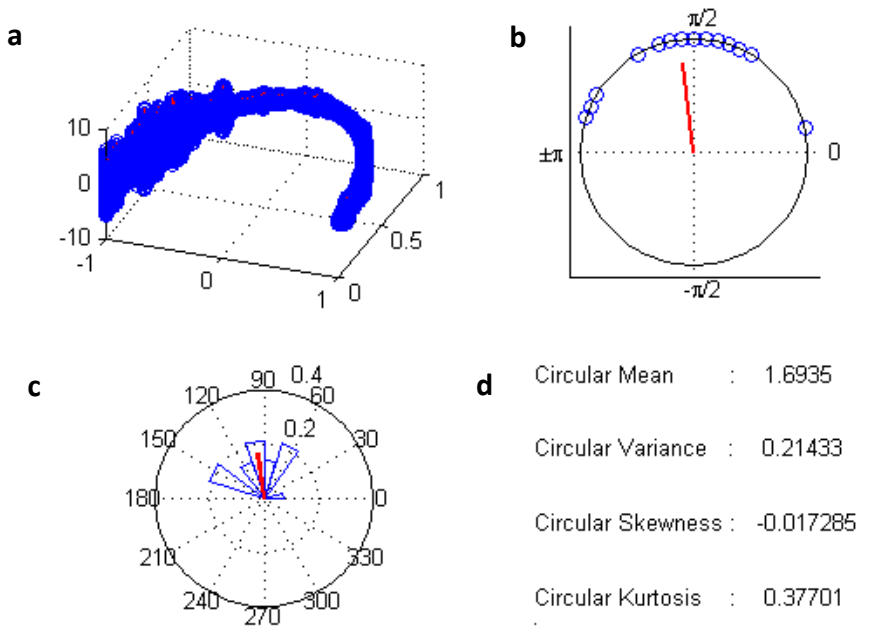

Figure 4.12 First Laboratory slew bearing data acquired on May 25 (the 90th day): (a) vibration data in circular domain; (b) the 'occurrence' results plotted in circular domain (in radian); (c) circular histogram (in degree) (note: blue line and red line is circular histogram and resultant vector length (R), respectively); (d) circular feature extraction results.

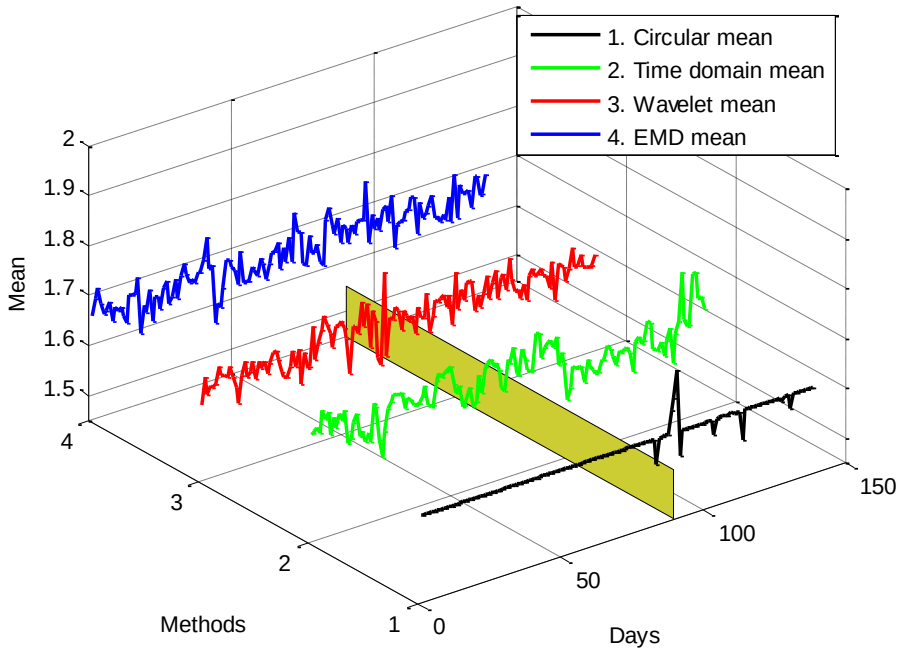

(a) Feature 1: Mean

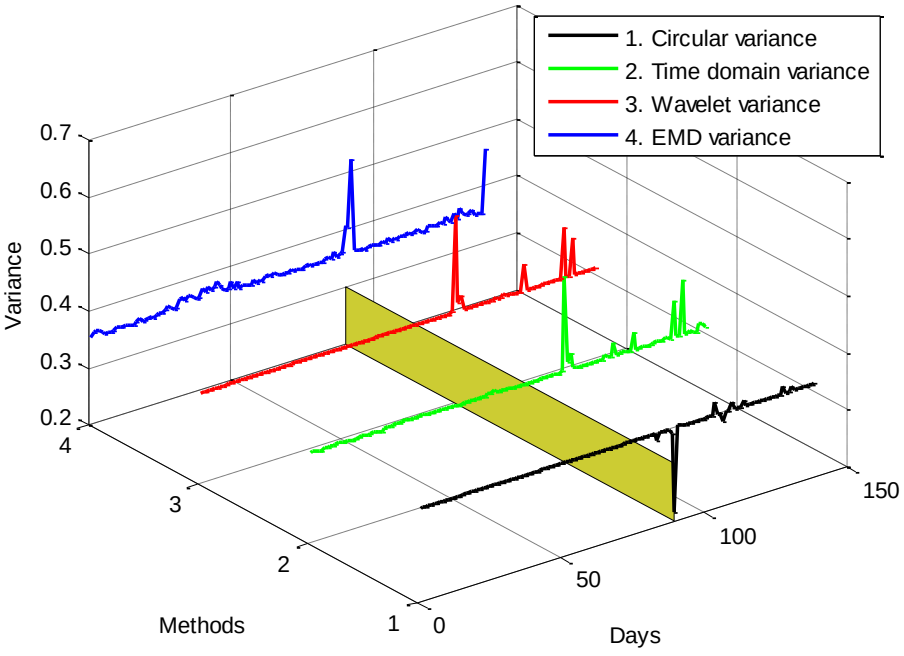

(b) Feature 2: Variance

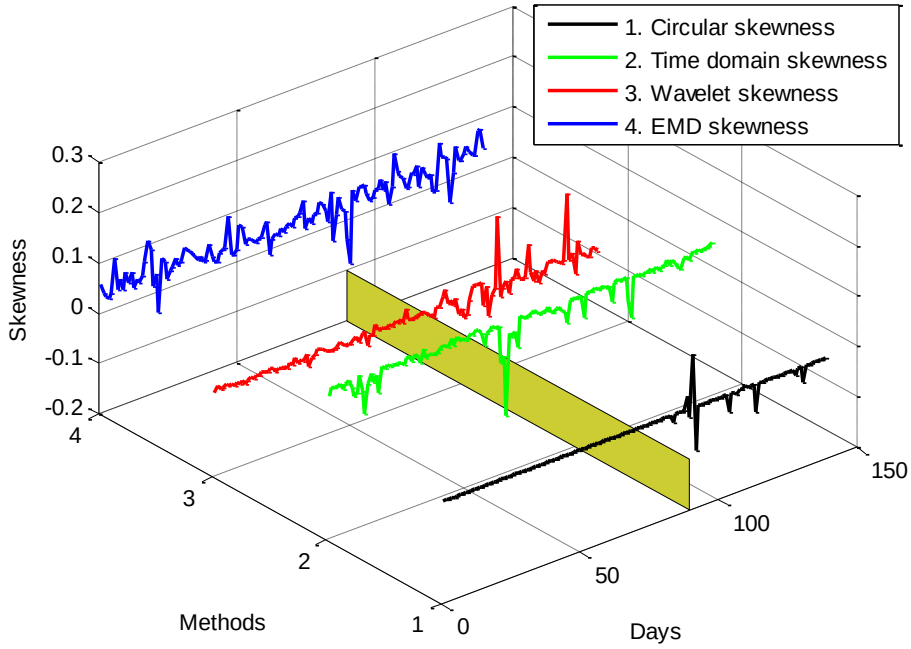

(c) Feature 3: Skewness

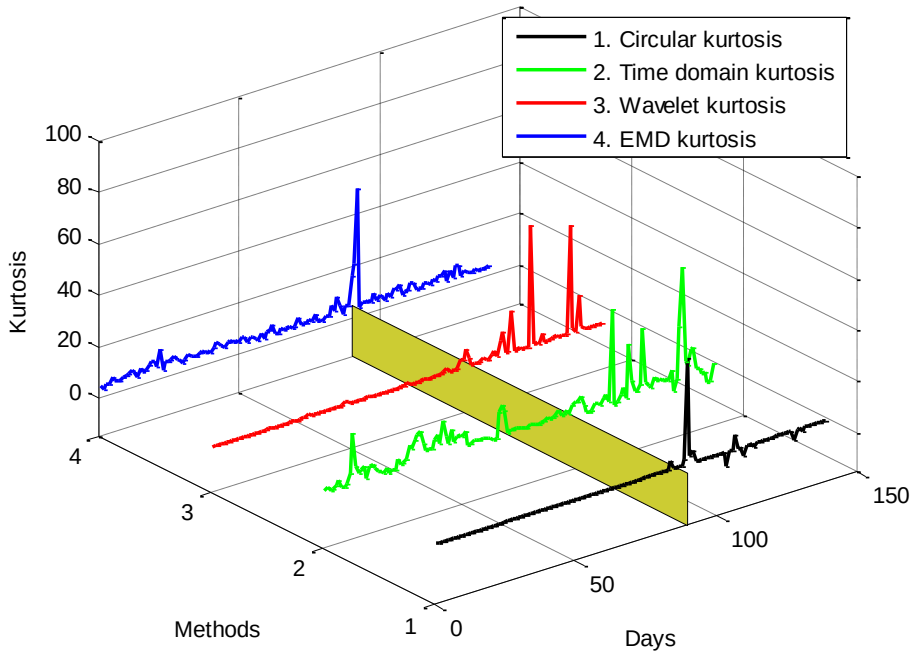

(d) Feature 4: Kurtosis

Figure 4.13 Circular-domain feature extraction results and comparable methods (time-domain features, wavelet decomposition and EMD) from February to August 2007 (139 days measurement).

The entire circular domain features calculation results from February to August (139 days period) are shown in Figure 4.13. The circular domain features are compared to time domain features, features calculated from detail coefficient (D3) of wavelet decomposition and features calculated from the summation of the low IMF frequencies (from IMF 9 to the lowest IMF) of the EMD results. Further discussion is presented in §4.1.5. It is shown that the onset of bearing fault can be detected in angular domain. This allows the engineer to make better scheduling of maintenance work. In detail, the circular features show steady condition in the early stage of the bearing operation indicating the bearing is still in normal condition as shown in Figures 4.13(a)-(d). When fault occurred, features show the peak value in the 90th day indicates the onset of bearing fault and fluctuates starting from the 90th until the 139th day (end of August 2007). The circular features can indicate the onset, however, a few tiny spikes from the day 90th to the day 139th hardly conclusive. Therefore, a more robust condition monitoring parameter is needed.

The effect of different window size is investigated in this study due to the importance of the proper window size in the detection of the frequency alteration. In order to obtain the same data points in one frame, the window size should be element of the factors of sampling rate. In this study, the sampling rate is 4880Hz and thus the window size should be the member of the factors of 4880. Five different window sizes which are the member of factors of 4880 were selected. The selected window sizes are 61, 40, 16, 8 and 4. In addition, eight different frequencies are also selected from 50Hz to 225Hz with the interval of 25Hz. Calculate the shift factor, ϕ as presented in Eq. (B3) using the predetermined window sizes and frequencies. The shift factor is used to identify the ellipsoid changes orientation from right to left or vice versa based on the threshold of ϕ = 2 (see Appendix B). The result of the calculated shift factors for different window sizes and different frequencies is presented in Table 4.1. It can be seen from Table 4.1 that for window size of 8, the shifting factor is greater than 2 for frequency less than 150Hz. On the contrary, the shifting factor is less than 2 for frequency greater than 150Hz. The clearer illustration is shown in Figure 4.14. This condition is confirmed by the FFT result of May 25 as shown in Figure 4.15, where the frequency of approximately 145 Hz is clearly shown. This frequency is much higher

than the bearing fault frequencies presented in Table 4.1. It is assumed that this frequency triggers the ellipsoid shifting orientation detected by PAA result.

Table 4.1 The effect of different window sizes on different unknown frequencies.

Window size, w	Shift factor, ϕ for different unknown frequency alteration and different window size (calculated using Eq. (B3))							
	50Hz	75Hz	100Hz	125Hz	150Hz	175Hz	200Hz	225Hz
$w = 61$	0.8	0.533	0.4	0.32	0.267	0.229	0.2	0.178
$w = 40$	1.22	0.813	0.61	0.488	0.407	0.349	0.305	0.271
$w = 16$	3.05	2.033	1.525	1.22	1.017	0.871	0.763	0.678
$w = 8$	6.1	4.067	3.05	2.44	**2.033**	1.743	1.525	1.356
$w = 4$	12.2	8.133	6.1	4.88	4.067	3.486	3.05	2.71

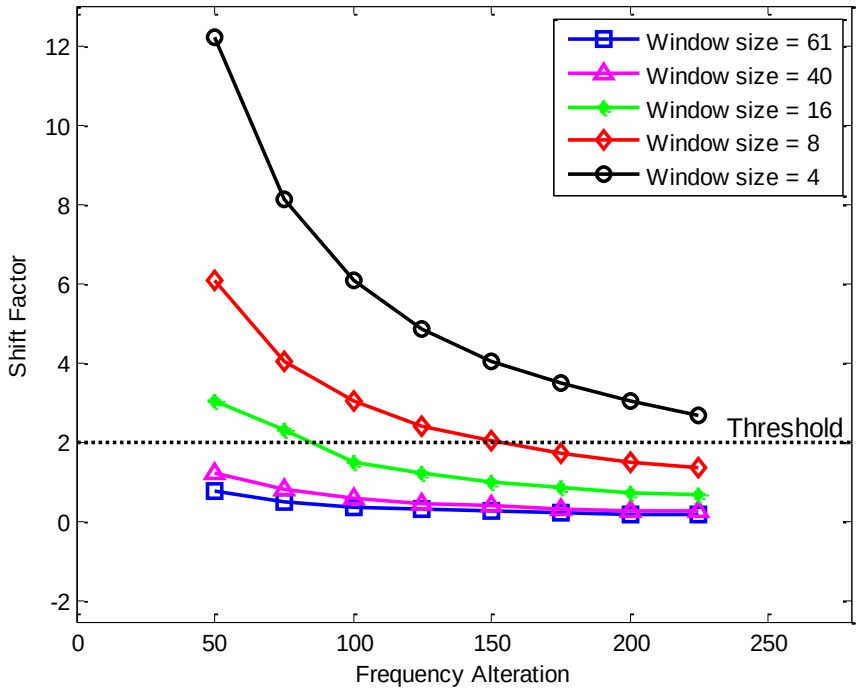

Figure 4.14 Shift factor value for different frequency alteration and different window size.

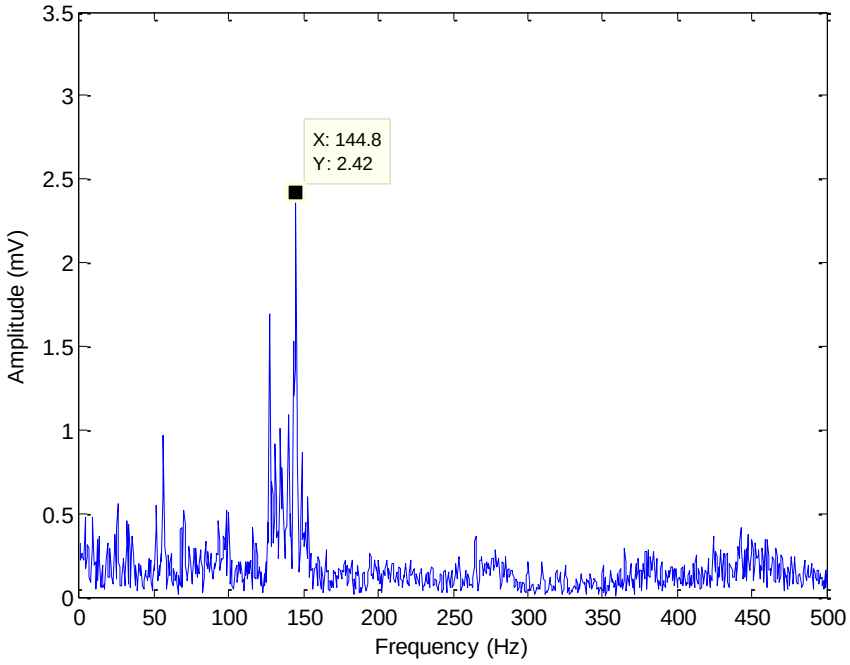

Figure 4.15 FFT of slew bearing data on May 25 data i.e. 90 days after the start.

4.1.5 Discussion

A new circular domain analysis for slew bearing condition monitoring based on PAA and circular domain features calculation has been introduced and presented. The method employed the different technique of calculation with previous and existing angular domain analysis as discussed in section 4.1.2. In order to present the unbiased performance comparison between the proposed method and other methods, the proposed method is compared to time domain features calculation directly from vibration signal and features. These were calculated from two advanced signal processing: wavelet transform and EMD. The performance comparison is summarized in Table 4.2 and Table 4.3. The performance comparison is based on two key questions with regard to advanced and effective condition monitoring method for slew bearing:

(1) Can the method identify the onset of bearing fault?

(2) Can the method present the progressive deterioration from the onset of bearing damage to the complete failure?

For question (1), it can be seen from Figure 4.13 that the features of the proposed method show the maximum feature value in the 90th day, while this is not observable

from time domain features calculation and wavelet transformation based features calculation. The maximum feature value in the 90th day is also identified in EMD based features calculation results especially in variance and kurtosis features. It is assumed that this phenomenon is the onset of slewing bearing fault. Therefore, for question (1), it is proved that the proposed method is able to identify the initial onset of bearing fault consistently as shown in four circular domain features compared to the other methods (see Figure 4.13 and Table 4.2). However, the proposed method is unable to determine the failure degradation trend or progressive deterioration from the identified onset of bearing fault to complete failure. The progressive deterioration is more visible in features calculated from wavelet decomposition particularly in variance, skewness and kurtosis features; and time domain features especially in variance and kurtosis. Therefore, for question (2), the wavelet transform is superior to the other methods (see Figure 4.13 and Table 4.3). During the slew bearing lab experiment, the complete failure is unpredictable. Sudden burst vibration signal on September 2nd 2007 occurred and the test-rig had to be shut down. To discover the severe damage of slew bearing and clarify the result of the features calculation, the slew bearing was dismantled for inspection after the test-rig was shut down which is after the 139th day. Some of the defective regions can be clearly seen in Figure 2.16.

Table 4.2 Comparison methods in identifying the initial onset of damage.

Feature	Methods comparison			
	Circular-domain	Time-domain	Wavelet decomposition	EMD
Mean	✓	✗	✗	✗
Variance	✓	✓	✓	✓
Skewness	✓	✗	✗	✗
Kurtosis	✓	✗	✗	✓

✓ Indicates clearly visible

✗ Indicates not visible

Table 4.3 Comparison methods in estimating the progressive deterioration.

Feature	Methods comparison			
	Circular-domain	Time-domain	Wavelet decomposition	EMD
Mean	✗	✗	✗	✗
Variance	✗	✓	✓	✗
Skewness	✗	✗	✓	✗
Kurtosis	✗	✓	✓	✗


Indicates clearly visible


Indicates not visible

4.2 Largest Lyapunov Exponent (LLE) feature

4.2.1 Introduction

To date, signal processing technique based on vibration has been the main technique used in the detection of change of bearing conditions and has been used as a warning of impending deterioration of rotating machinery. In the case of slew bearings, special signal processing is necessary to detect the changes in the condition of the bearing based on the vibration signal. With appropriate signal processing, the fault signal can be detected from the processed signal. It is well known that the vibration characteristic of rotating machinery is altered when a bearing has failed. As the change is identified by the non-linear trend, a non-linear dynamical analysis technique is necessary for fault detection and diagnosis [150]. Linear dynamic systems have constant natural frequencies and vibrate at the frequency of an externally applied harmonic excitation. However, in non-linear systems there are amplitude-dependant natural frequencies called 'internal resonances'. Furthermore, this kind of system may vibrate at a frequency different from an externally applied harmonic excitation [151].

In practice, a rolling element bearing has internal resonances due to the different parts of the system (e.g. interactions between shaft and bearing, between rolling element and raceway) vibrating at different frequencies. The combination of these internal resonances appears in the chaotic vibration signal. Certain methods to analyse the chaotic time series characteristic (in this paper referred to as the 'vibration signal characteristic') are phase-space dissimilarity measures [152, 153] including Kolmogorov entropy, fractal dimension, correlation dimension, approximate entropy, permutation entropy, and the largest Lyapunov exponent (LLE). These techniques use reconstruction vectors or phase-space as the input matrix to identify the existence and to measure the degree of non-linearity of the time series data. Most of these techniques have already been applied to vibration signal monitoring for machine health diagnostic such as the Kolmogorov-Smirnov test [154], fractal dimension [155], correlation dimension [156], approximate entropy [157], and permutation entropy [158].

This section presents an application of the LLE algorithm as a feature extraction method for low speed slew bearing vibration signals. Although the LLE algorithm has been widely used in some disciplines such as the bio-medical [159, 160] and finance [161] areas, this is the first time that it has been used in vibration-based condition monitoring. For instance, in biomedical applications [159, 160], the LLE algorithm is used to analyse the EEG signals to detect epileptic seizures; in finance [161], the LLE algorithm is used to analyse the stability of electricity prices. The LLE algorithm is usually used for non-linear time series analysis to quantify the appearance of signal non-linearity. Basically, the LLE algorithm measures the exponential divergence (positive or negative) of two initial neighbouring trajectories in the phase space based on the Euclidean distance. The LLE algorithm is presented in details in Section 4.2.2.

4.2.2 The LLE algorithm

To analyze the non-linearity or chaotic characteristic of the vibration signal, $\mathbf{x} = (x_1, x_2, ..., x_N)$ with N samples is first reconstructed. The reconstructed vector is done in phase-space [162]. The phase space reconstruction technique used is the method of delays (MOD) introduced by Takens [163]. The phase space has been used

in non-linear time series analyses [152-158] where the phase space matrix is defined as follows:

$$\mathbf{X}=\begin{bmatrix} x_1 & x_{1+J} & x_{1+2J} & \cdots & x_{1+(m-1)J} \\ x_2 & x_{2+J} & x_{2+2J} & \cdots & x_{2+(m-1)J} \\ x_3 & x_{3+J} & x_{3+2J} & \cdots & x_{3+(m-1)J} \\ \vdots & \vdots & \vdots & & \vdots \\ \vdots & \vdots & \vdots & & \vdots \\ \vdots & \vdots & \vdots & & \vdots \\ x_M & x_{M+J} & x_{M+2J} & \cdots & x_{M+(m-1)J} \end{bmatrix} \tag{4.12}$$

where J is the number of samples delay to construct the phase-space matrix $\mathbf{X}$, m represents the embedding dimension, M represents the number of reconstructed vectors and N is the number of samples of the vibration data. The parameter of J can be computed by time lag / Δt. By selected samples with predetermined time lag, the regularity of the signal can be measured. The relation between N, J, m and M can be defined in the following form: $N=M+(m\text{-}1)J$ or $M=N\text{-}(m\text{-}1)J$. The preparatory LLE algorithm flowchart including the phase-space and the initial Euclidean distance calculation is presented in Figure 4.16. A detailed discussion of the physical meaning of the reconstruction delay J is presented in Appendix C.

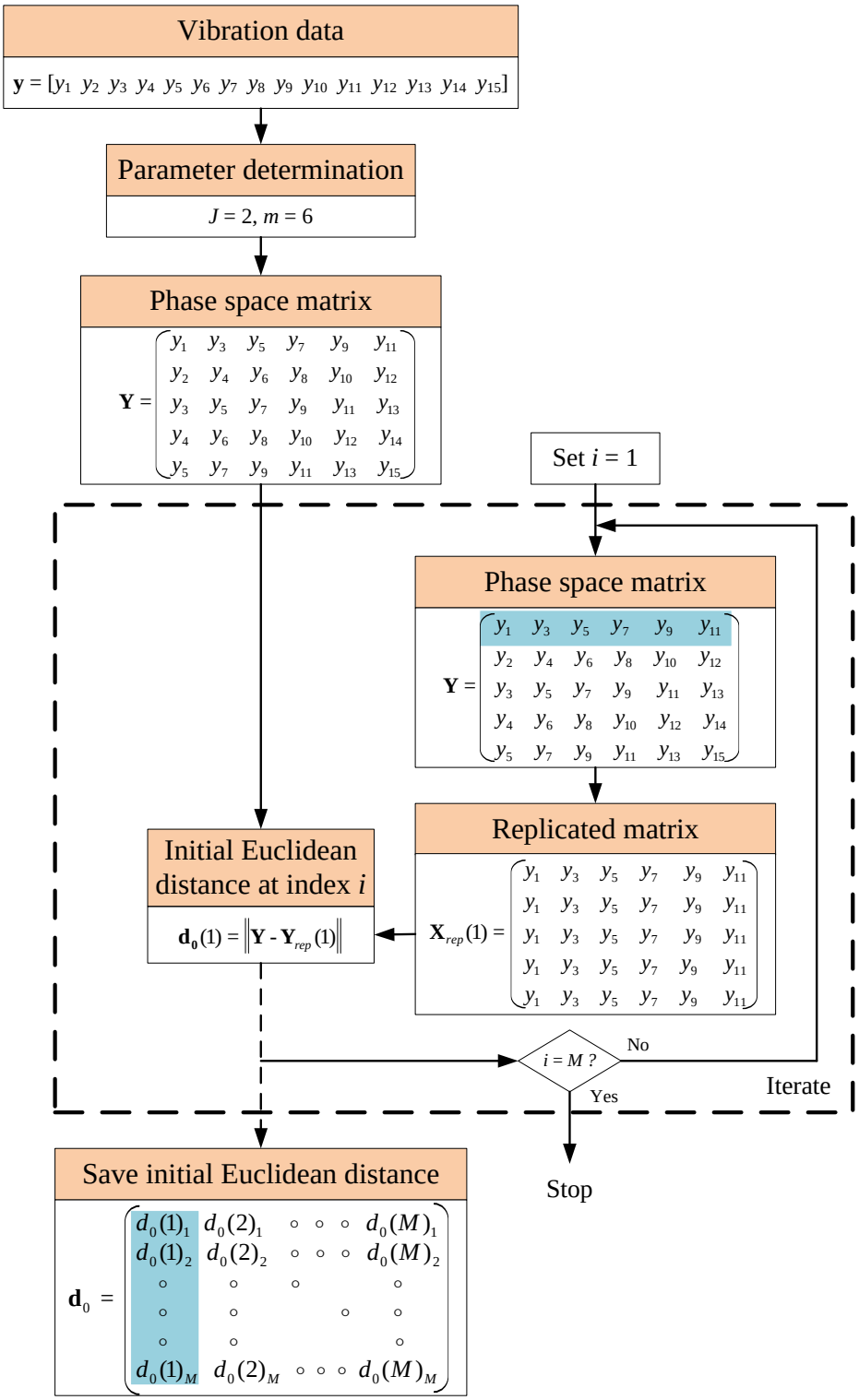

Figure 4.16 The flowchart of preparatory LLE algorithm (note: $N=15$, $J=2$ and $m=6$).

Further explanation of the LLE algorithm in this section is based on the actual slew bearing data. In the case of slew bearing data, the parameters *J* and *m* have been determined as $J=48$ and $m=100$. The parameter *J* is calculated from the dominant

frequency of FFT and *m* is determined empirically. A detailed discussion for the parameter selection is presented in section 4.2.3. The number of samples of slew bearing data N is 4880. Hence, the number of reconstructed vector M can be calculated, $M = 128$. The reason why these values were selected is explained in details in Section 4.2.3. Once the phase-space matrix $\mathbf{X}$ and the replicated matrix $\mathbf{X}_{rep}$ have been obtained, the initial Euclidean distance, vector $\mathbf{d}_0$, can be calculated as shown in Figure 4.16. It should be noted that the calculation of the Euclidean distance vector in the LLE algorithm plays an important role. The divergence of the LLE result (λ_1) can be analysed based on the Euclidean distance. The divergence represents the characteristic of the vibration signal being analysed. If the bearing vibration signal is linear, typically in normal condition, the calculated Euclidean distance between each row in the phase-space matrix is constant and divergence is not detected, and thus the λ_1 will be negative. On the other hand, if the vibration signal has non-linear characteristics, the Euclidean distance between each row in the phase-space matrix is no longer constant (it typically manifests exponentially), and thus the value of λ_1 will be positive. The physical reason for the LLE result (λ_1) mentioned above is discussed again in detail at the end of the LLE algorithm procedure in this section. However, the important Euclidean distance vector for the LLE result (λ_1) is not $\mathbf{d}_0$. To obtain the appropriate Euclidean distance vector for calculating λ_1, the initial Euclidean distance vector $\mathbf{d}_0$ described above needs to be processed by the two following steps:

Step 1: Calculate the new initial Euclidean distance value $\mathbf{d}_{0\_\text{new}}$

The first step to process the Euclidean distance vector $\mathbf{d}_0(i)$ is to determine the identifier of the minimum value of the Euclidean distance vector $\mathbf{d}_0(i)$ for each index i. The index i in the case of slew bearings is $i = 1, 2, ..., 128$. Prior to the calculation of the minimum identifier, it is necessary to calculate the minimum value of $\mathbf{d}_0(i)$ for each i, then the identifier of the minimum value of $\mathbf{d}_0(i)$ for each i can be obtained. If the minimum value is directly computed from $\mathbf{d}_0(i)$ as i progresses from $1, 2, ..., 128$, the minimum value will always be 'zero'. The reason for the 'zero' value is that at a particular index i, for instance at $i = 1$, the $\mathbf{d}_0(1)$ is computed from

$\left\|\mathbf{X}-\mathbf{X}_{rep}(1)\right\|$. As mentioned before, $\mathbf{X}_{rep}(1)$ is obtained by replicating the 1st row of the phase space matrix $\mathbf{X}$. If the Euclidean norm between $\mathbf{X}$ and $\mathbf{X}_{rep}(1)$ is calculated, the first row of the Euclidean distance vector $\mathbf{d}_0$ will be zero value. This is because the first row element of the phase space matrix $\mathbf{X}$ and the replicated matrix $\mathbf{X}_{rep}$ are identical. When i progresses up to, for example, $i=64$, the $\mathbf{d}_0(64)$ is computed from $\left\|\mathbf{X}-\mathbf{X}_{rep}(64)\right\|$. In a similar way, the matrix $\mathbf{X}_{rep}(64)$ is obtained by replicating the 64th row of the phase space matrix $\mathbf{X}$. If the Euclidean norm between $\mathbf{X}$ and $\mathbf{X}_{rep}(64)$ is applied, the 64th row of the Euclidean distance vector $\mathbf{d}_0$ will also be zero. The process, which produces the zero value of $\mathbf{d}_0$ as i progresses, is repeated up to the last i index, that is $i=128$. The illustration of the three calculation examples of $\mathbf{d}_0$ at three different i (at $i=1$, at $i=64$ and at $i=128$) are shown in Figures 4.17(a)–4.19(a).

To overcome the problem mentioned above, an additional constraint is employed in the LLE algorithm. The aims are to remove the 'zero' value as i progresses and to change the nearest zero value neighbours to a constant value (to provide a clearer illustration figure, a maximum value of $\mathbf{d}_0$ is used as a constant value). The reason why the nearest zero value neighbours need to be changed to a constant value is that the nearest zero value neighbours of $\mathbf{d}_0$ shows some transient behaviours as shown in Figures 4.17(a)–4.19(a). This is important to ensure an accurate measurement of the new initial distance value $\mathbf{d}_{0\_\text{new}}$. Once the transient part of $\mathbf{d}_0$ has been removed, the minimum value of the Euclidean distance vector $\mathbf{d}_0(i)$ will be calculated from the stationary part. To determine the constraint mentioned above, another index called j is used inside the sub-routine of index i in the LLE algorithm. The constraint is defined as follows:

$$\left| i - j \right| \le \mu \tag{4.13}$$

where $j=1, 2, ..., M$ and μ is the number of nearest zero value neighbours that need to be changed to a constant value. The μ in this paper is selected as 50 (the reason is given in Section 5.4). In addition, Eq. (4.13) means: if the absolute value of subtraction

i^{th} and j^{th} as i and j progressing from 1 to 128 is less than or equal to the μ, the element of $\mathbf{d}_0$ (with respect to current j) is replaced by the highest value of $\mathbf{d}_0(i)$. A more detailed explanation of Eq. (2) is presented in the LLE algorithm in Table 4.4. The updated Euclidean distance vector after the LLE algorithm is shown in Table 4.4 and is called the new Euclidean distance vector $\mathbf{d}_{0\_\text{new}}(j)$. It can be seen from Table 4.4 that the algorithm consists of two sub-routines based on the indices i and j. The results of $\mathbf{d}_{0\_\text{new}}$ are presented in Figures 4.17(b)–4.19(b). It can be seen in Figure 4.17(b) that when $i=1$, the fifty data points after the nearest neighbours of the zero value are replaced by the maximum value and became constant. Furthermore, when $i=64$, the nearest neighbours which need to be changed are 50 points before the zero value and 50 points after the zero value. Thus the result is shown in Figure 4.18(b). When i reaches the last number i.e. $i=128$, the fifty points before the nearest neighbours of the zero value are replaced by the maximum value and became constant as well, as shown in Figure 4.19(b). Note that the fifty points are the result of Eq. (4.13) or line 6 in the LLE algorithm for *j's* progression from $1, 2, \ldots, 128$.

Once the $\mathbf{d}_{0\_\text{new}}(j)$ is computed, the minimum value of $\mathbf{d}_{0\_\text{new}}(j)$ denoted by $\Delta_a(i)$ and the index of the minimum value denoted by $\Delta_b(i)$ are defined as follows:

$$[\,\Delta_a(i), \Delta_b(i)\,] = \min\left(\mathbf{d}_{0\_\text{new}}(j)\right) \tag{4.14}$$

Eq. (4.14) is incorporated in the LLE algorithm shown in Table 4.4 line 11 inside the sub-routine of index i. It should be noted that the minimum value $\Delta_a(i)$ is no longer used for further calculations. Only the identifier of the minimum distance value $\Delta_b(i)$ is used again in the next step. This index is necessary to create a new matrix, matrix $\mathbf{X}(\Delta_b(i))$. The element of the matrix $\mathbf{X}(\Delta_b(i))$ at a particular index i is based on the result of $\Delta_b(i)$. The use of matrix $\mathbf{X}(\Delta_b(i))$ is further illustrated in Eq. (4.15) and Table 4.5 line 19.

Table 4.4 The LLE algorithm showing the subroutines of i and j in order to calculate the new Euclidean distance $\mathbf{d}_{0\_new}$.

LLE Algorithm
1: $\mathbf{X}$, $\mathbf{X}_{rep}$ and $\mathbf{d}_0$ (are calculated from Figure 4.16)
2: μ is predetermined mean period (e.g. $\mu = 50$)
3: Create the new matrix $\mathbf{d}_{0\_new}$. Set $\mathbf{d}_{0\_new} = \mathbf{d}_0$ initially
4: **for** $i = 1$ **to** M **do**
5: **for** $j = 1$ **to** M **do**
6: **if** $\lvert j - i \rvert \le \mu$ **do**
7: $\mathbf{d}_{0\_new}(j) = \max(\mathbf{d}_0)$
8: **end if**
9: **end for** j
10: Vector $\mathbf{d}_{0\_new}$ obtained. This vector contain $1, 2, \ldots, M$ row
11: Find the minimum value of $\mathbf{d}_{0\_new}(j)$ and its identifier: $[\Delta_a(i), \Delta_b(i)] = \min(\mathbf{d}_{0\_new}(j))$
12: **end for** i

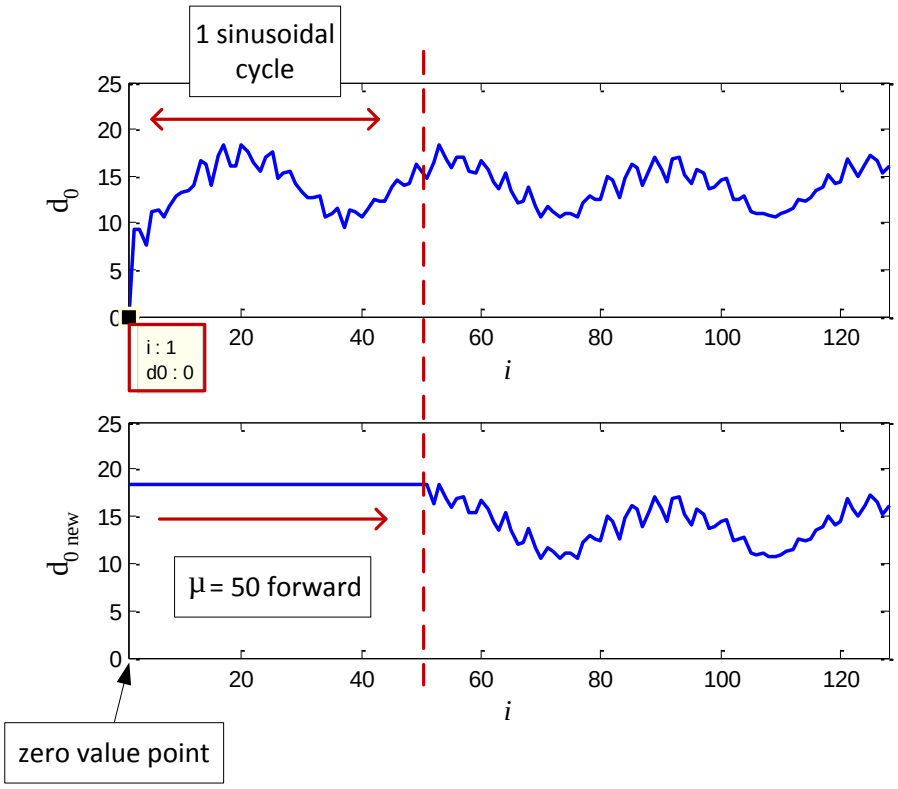

Figure 4.17 (a) The initial Euclidean distance $\mathbf{d}_0$ at $i = 1$; (b) The new initial Euclidean distance value $\mathbf{d}_{0\_new}$ at $i = 1$.

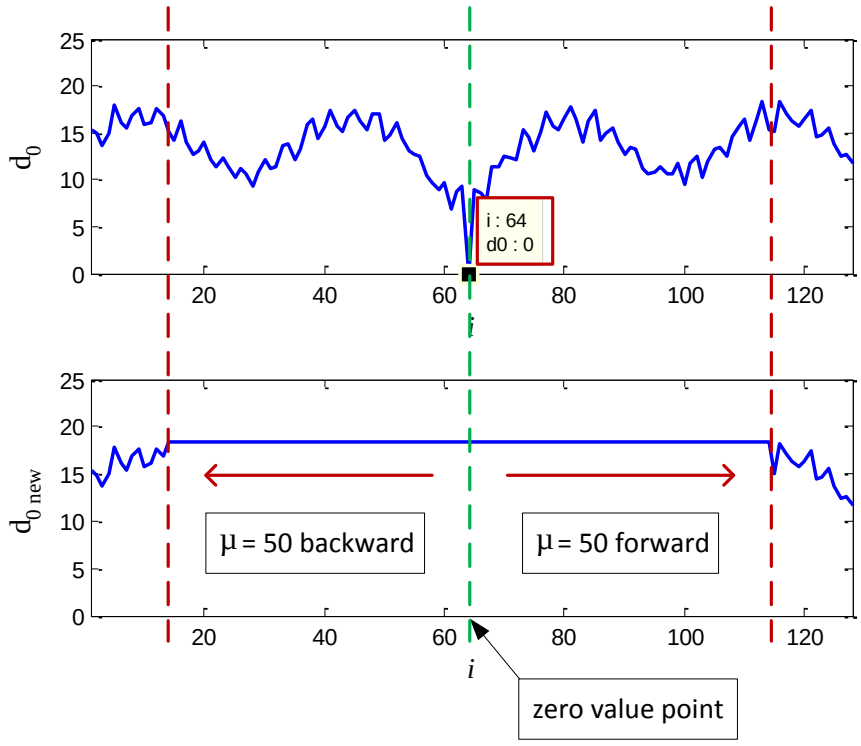

Figure 4.18 (a) The initial Euclidean distance $\mathbf{d}_0$ at $i = 64$; (b) The new initial Euclidean distance value $\mathbf{d}_{0\_new}$ at $i = 64$.

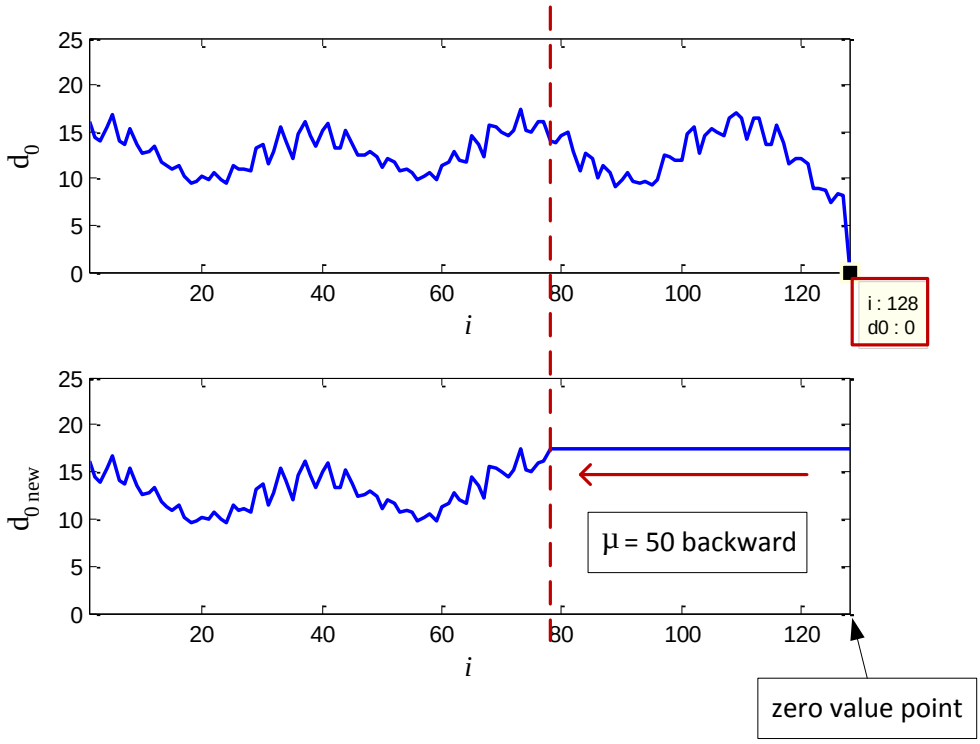

Figure 4.19 (a) The initial Euclidean distance $\mathbf{d}_0$ at $i = 128$; (b) The new initial Euclidean distance value $\mathbf{d}_{0\_new}$ at $i = 128$.

Step 2: Calculate measured distance $\mathbf{d}$ *and new measured distance* $\mathbf{d}_{\text{new}}$

The next step is the calculation of measured distance $\mathbf{d}(i)$ by estimating the distance between the phase space $\mathbf{X}(i)$ and the new matrix $\mathbf{X}(\Delta_b(i))$ (with respect to i). The elements of matrix $\mathbf{X}(\Delta_b(i))$ are the row vector data set of the phase space $\mathbf{X}$ based on the minimum index $\Delta_b(i)$.

$$\mathbf{d}(i) = \| \mathbf{X} - \mathbf{X}(\Delta_b(i)) \| \tag{4.15}$$

Even though the LLE result (λ_1) can be computed using the measured distance $\mathbf{d}(i)$, Sato et al. [164] used k iteration to improve the accuracy of the measured distance $\mathbf{d}(i)$. In this study, the iteration with $k = 1, 2, \ldots, 70$ is used. In order to show an adequate exponential graph of the measured distance, $\mathbf{d}$ and to decrease the computational time, it is recommended that k be any value greater than the mean period, μ and less than the embedding dimension, m. The algorithm used to improve the accuracy of the measured distance $\mathbf{d}(i)$ is presented in Table 4.5. The algorithm in Table 4.5 is an extension of the algorithm shown in Table 4.4. The result after the k iteration is called the new measured distance matrix, $\mathbf{d}_{\text{new}}(i)$.

The final step is the calculation of the LLE result (λ_1). Using the original largest Lyapunov exponent formula [165], the relation between $\mathbf{d}_{\text{new}}(i)$ and the LLE result $\lambda_1(i)$ is defined by the following:

$$\mathbf{d}_{\text{new}}(i) = S_i e^{\lambda_1(i,\Delta t)} \tag{4.16}$$

By taking the natural logarithm of both sides and removing the part '$\ln S_i$', the Largest Lyapunov Exponent can be computed using a least-square fit equation defined by

$$\lambda_1(i) = \frac{1}{\Delta t} \ln \mathbf{d}_{\text{new}}(i) \tag{4.17}$$

where $\lambda_1 < 0$ indicates normal condition and $\lambda_1 > 0$ indicates non-linear condition. The physical interpretation of negative LLE ($\lambda_1 < 0$) and positive LLE ($\lambda_1 > 0$) is shown in § 4.2.3 Figures 4.21(a) and (b).

Table 4.5 The algorithm to calculate $\mathbf{d}_{\text{new}}(i)$ based on k iteration and the index of minimum value, $\Delta_b(i)$.

LLE Algorithm (Cont.)
13: **for** $k = 1$ **to** 70 **do**
14: $\text{bound} = M - k$
15: $\text{evolve} = 0$
16: $\text{point} = 0$
17: **for** $i = 1$ **to** M **do**
18: **if** $i <= \text{bound}$ **and** $\Delta_b(i) <= \text{bound}$ **do**
19: $d = sqrt\left(sum\left((\mathbf{X}(i+(k-1),:) - \mathbf{X}(\Delta_b(i)+(k-1),:)\right).^{\wedge 2},\ 2\right)$
20: **if** $d \sim= 0$ **do**
21: $\text{evolve} = \text{evolve} + \log(d)$
22: $\text{point} = \text{point} + 1$
23: **end if**
24: **end if**
25: **end for** i
26: **if** $\text{point} > 0$
27: $\mathbf{d}_{\text{new}}(k) = \text{evolve} / \text{point}$
28: **else**
29: $\mathbf{d}_{\text{new}}(k) = 0$ $\mathbf{d_{new}}(k) = 0$
30: **end if**
31: **end for** k

Note: the algorithm written in Table 4.4 and 4.5 are in the form of MATLAB syntax.

4.2.3 LLE feature

LLE algorithm for one second vibration data (slew bearing data from Lab test 1)

The objective of using the LLE algorithm in this thesis is to identify the onset of the deterioration of the bearing. As the slew bearing rotates at very low rotational speed (≈ 1 rpm), the bearing signal generated from the contact between the rolling element and the defective point is very weak and buried in unwanted noise. Therefore, the onset of the deterioration in the condition of the bearing and the progression of the deterioration cannot be clearly identified. This has been as shown in the extracted

statistical moment features of the raw vibration data and the extracted features from wavelet decomposition and EMD as studied previously in [166].

The total data length for laboratory slew bearing data is calculated as follows: 60 seconds multiplied by the 4880 samples produced 292800 samples that were acquired at the same time each day. In the first application of the LLE algorithm for laboratory slew bearing data, the 30 second data containing 146400 samples was processed by the LLE algorithm. To identify non-linear characteristic of the vibration data, every one second containing 4880 samples ($N = 4880$) was inputted into the LLE algorithm. The illustration of the LLE algorithm applied at one second intervals is presented in Figure 4.21. The result is the LLE feature denoted by λ_1. As seen in the table in Figure 4.21, the result of the LLE feature (λ_1) can be positive or negative depending on the input data at a certain time (second). The detailed λ_1 result for each second during the 30 second vibration signal is depicted in Table 4.6. It can be seen from Figure 4.21 and Table 4.6 that during 30 seconds' measurement in one day, the majority of the LLE results are negative λ_1 ($-\lambda_1$) and only a few are positive λ_1 ($+\lambda_1$). The negative or positive $-\lambda_1$ is the computational result of Eq. (4.17), where, negative $-\lambda_1$ indicates the newly measured distance $\mathbf{d}_{\text{new}}(i)$ is unchanged or fixed.

The physical interpretation of negative λ_1 is given at the 9$^{\text{th}}$ second of the vibration data on April 26, as shown in Figure 4.21(a). If, the newly measured distance $\mathbf{d}_{\text{new}}(i)$ increases exponentially, the value of λ_1 is positive. The physical interpretation of positive λ_1 is given at the 16$^{\text{th}}$ second of the vibration data on April 26, as shown in Figure 4.21(b). In addition, the negative λ_1 means the processed vibration data at one particular second is in a stable or normal category, while positive λ_1 indicates the vibration data is chaotic. As time progresses and the condition of the slew bearing deteriorates or an unsustainable fault develops, the count of positive λ_1 is expected to increase. This is shown by the plotted count of positive λ_1 against 139 days' measurement as seen in Figure 4.22. It can be seen that in the last measurement period (i.e. August 2007), the count of positive λ_1 increases significantly. This indicates the vibration data in August 2007 is more chaotic than those in the previous months.

The LLE parameters to obtain the LLE features (λ_1), as shown in Figure 4.21, are determined as described below. It has been mentioned in section 4.2.2 that J is equal to 48. This value is determined based upon the dominant frequency of the vibration signal and the number of samples, N. From Figure 4.20(b), it can be seen that the dominant frequency of the vibration signal is 103.1 Hz. J is calculated as follows: (1/103.1 Hz) multiplied by 4880 samples = 47.33 (rounding it up to the nearest integer, thus $J = 48$). For selection of μ, it is recommended to remove the first sinusoidal cycle of $\mathbf{d}_0(i)$ which is the nearest neighbor of zero value at particular i, as shown, for example, in Figure 4.17 (at $i = 1$). This is because the first sinusoidal cycle that is close to zero value at a particular i typically demonstrates some transient behavior. Thus, μ is selected as 50. In addition, to achieve a faster computation time, m is determined empirically to get M as low as possible (note that it is possible to get a negative M value if the combination of the value m and J are inappropriate). If $J = 48$, the optimal $m = 100$, using the equation $M = N - (m-1)J$, $M = 128$. If $J = 48$ and m is changed to 110, M will be negative ($M = -352$). On the other hand, if J is still 48 and m is decreased ($m = 90$), the value of M is increased to about 608 (if M is higher, the computational time will be longer).

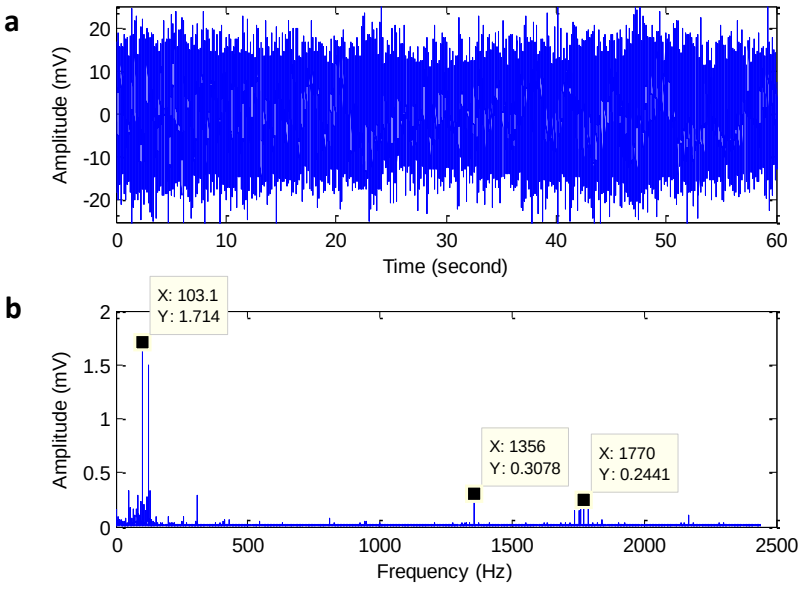

Figure 4.20 Vibration data acquired on 30 August: (a) raw vibration data and (b) FFT.

Table 4.6 The LLE result (λ_1) at one second intervals during the 30 second vibration signal (data April 26).

Time (sec)	LLE result (λ_1)	Time (sec)	LLE result (λ_1)
1	-7.3658	16	12.9481
2	-61.2420	17	-24.1665
3	-20.6105	18	-33.0387
4	-62.2330	19	-37.3419
5	-75.1535	20	-53.4996
6	11.2430	21	-9.4541
7	-52.0686	22	-63.5334
8	-49.3602	23	-10.2493
9	-10.1467	24	-65.9973
10	-60.8948	25	-24.5865
11	-2.9959	26	-36.1825
12	-74.9254	27	-7.0326
13	-52.4728	28	-50.9032
14	-49.9062	29	-6.5783
15	-101.4999	30	-21.7180

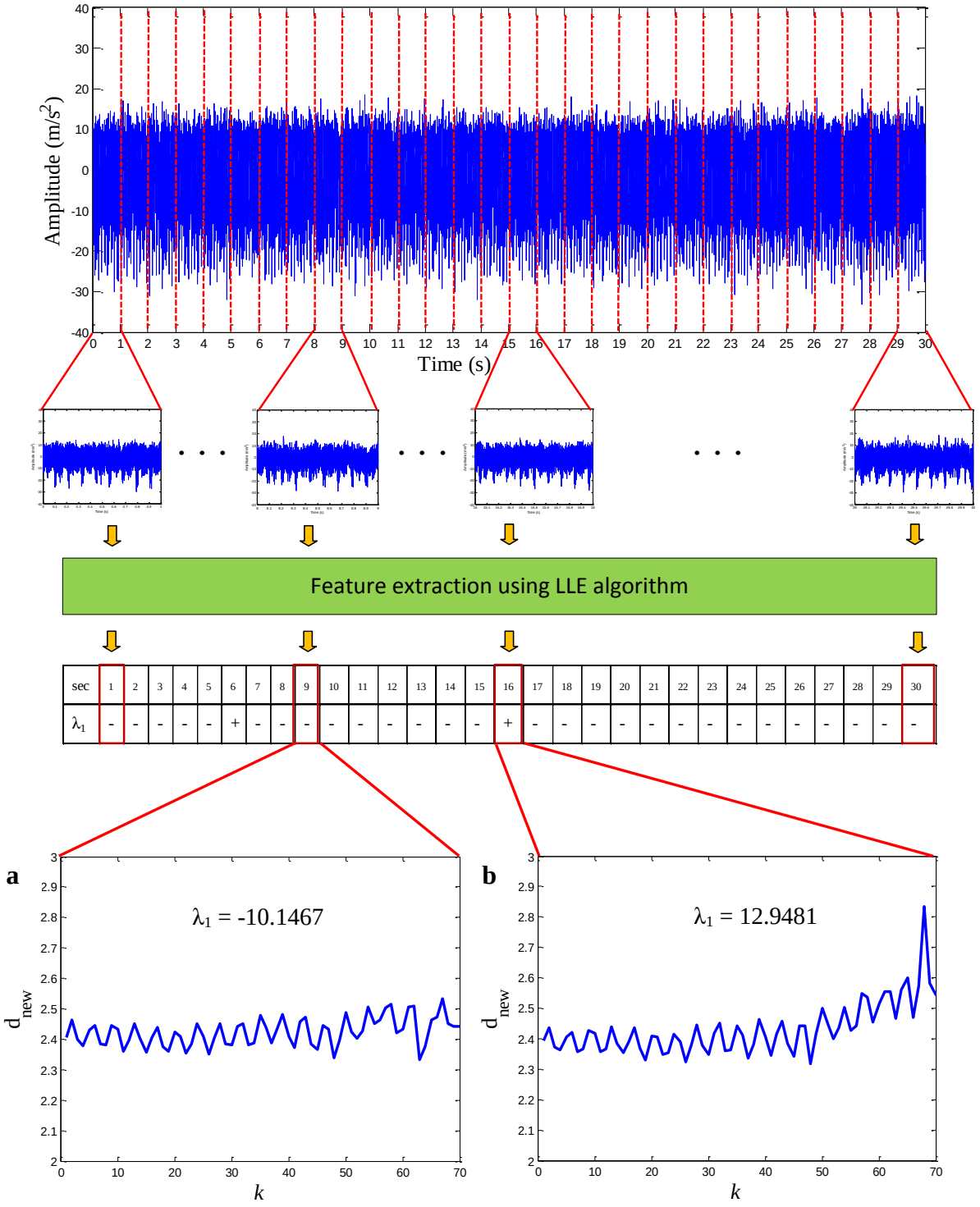

Figure 4.21 One day LLE result (data April 26): (a) at the 9th second (stable condition, negative λ_1); (b) at the 16th second (non-linear condition, positive λ_1).

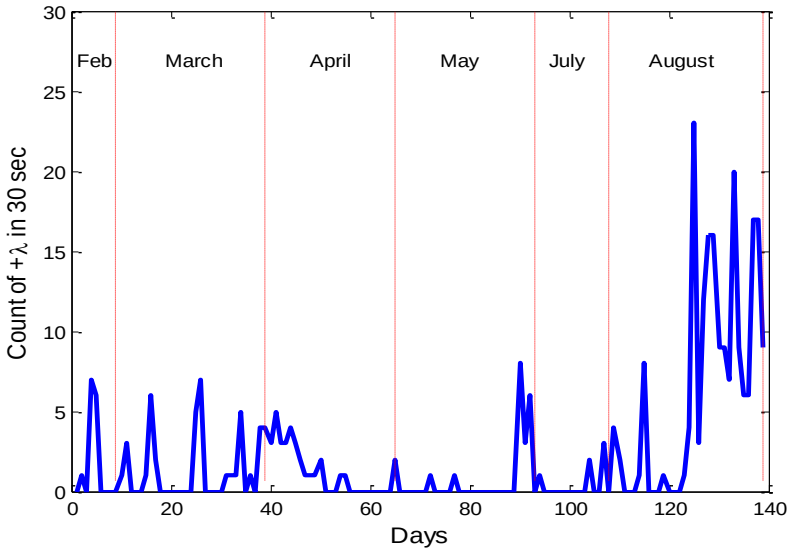

Figure 4.22 Number of positive λ_1 over the 139 measurement days from February to August 2007.

LLE algorithm for ten second vibration data

A practical challenge in monitoring low speed slew bearings is the large amount of data acquired over a long duration (e.g. 30 to 60 seconds). It is, therefore, necessary to have an efficient method to be applied for only short duration vibration. The method must also be able to provide rapid condition information for maintenance engineers to shorten the computational time. Instead of using the 30 second or 60 second vibration data, 10 second vibration data is used. The LLE algorithm is applied to every one second, as shown previously, but in this case, the duration of the vibration data used is only 10 seconds. The maximum (λ_1) is collected from 10 results for each day.

To explain the advantage of the proposed method, the LLE feature (largest λ_1) extracted from the 10 second vibration data each day during the 139 days measurement is plotted in the same figure with other comparable methods: kurtosis feature extracted from raw vibration data and kurtosis feature extracted from EMD, as shown in Figure 4.23(a). The LLE feature is normalized to the minimum and maximum values of the kurtosis feature extracted from raw vibration data before it is plotted in the same figure. Although the three comparable kurtosis features presented in Figure 4.23(a) show fluctuations in the last measurement days which indicates changes in the condition of the bearing, the LLE has an additional benefit. It can be seen that the LLE

feature also increases exponentially over the last measurement days (approximately from the 110th day to the 139th day) indicating the increased deterioration. Such an exponential trend cannot be extracted using time domain features extracted from raw vibration signals and features extracted from EMD. It should be noted that increasing deterioration is a warning of complete bearing failure. The LLE feature is supported by the inspection of the slew bearing damage after the 139th day as shown in Figure 2.16. Some defective regions in the roller element and the outer race can be clearly seen in Figure 2.16.

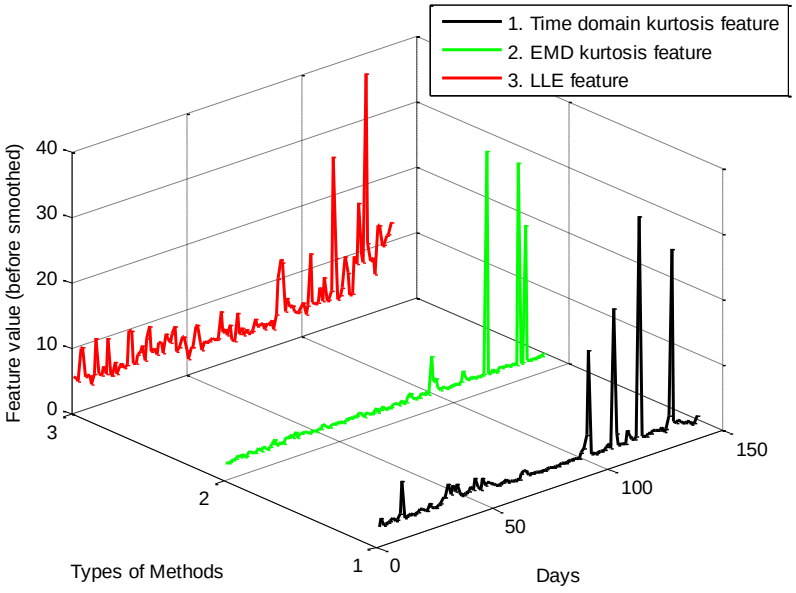

Figure 4.23 Comparison condition monitoring performance between the LLE feature and other features: time domain features of raw vibration data and features of EMD.

4.2.4 LLE feature applied in bridge reclaimer data

The RMS, skewness, kurtosis and LLE features extracted from 45 vibration data sets of the slew bearing coal bridge reclaimer are presented in Figure 4.25. Because the slew bearing is located in an open environment, the degradation of the bearing is expected to increase during the approximately 3.5 years' measurement from May 2003 to November 2006. However, the time domain RMS, skewness and kurtosis features did not show such a condition. It can be seen from Figures 4.25(a) to (c) that the RMS, skewness and kurtosis features did not show the progressive deterioration over 3.5 years. It can only be determined that the two high peaks appear in the

skewness and the kurtosis feature. The LLE algorithm was then applied to the similar data.

In contrast to the result of the time domain features, the LLE feature (λ_1) presented in Figure 4.25(d) shows a significant increase in the last measurement dates, especially in measurements 44 and 45. It is also clearly seen that the two high peaks on the skewness and the kurtosis feature were also seen in the LLE feature. The first peak indicates the onset of deteriorating bearing condition and the second peak shows the deterioration of the bearing will increase in the future. Additional information can also be found from the LLE feature that the second peak is greater than the first peak. This indicates that LLE feature can extract more information regarding to the development of bearing deterioration. In contrast, the second high peak of the time domain kurtosis remains in the same level as the first high peak, while it is difficult to evaluate the bearing deterioration for the first high peak. Unfortunately, the measurement had to be stopped at measurement 45 on the 30th November 2006, due to the commencement of preparation for the acquisition of vibration data from the laboratory slew bearing test rig. The LLE feature of the bridge reclaimer data shows that the actual vibration slew bearing data is more chaotic than the laboratory slew bearing vibration data. This is proven by the number of positive λ_1 is greater than the number of negative λ_1. At the beginning, λ_1 is negative, but as time progresses, λ_1 swiftly becomes positive. As wear develops, the value of the positive λ_1 will increase correspondently.

The parameters of LLE algorithm to calculate the LLE features (λ_1) as shown in Figure 4.25(d) are determined as follows: based on the known sampling rate of 240 samples per second acquired for 17.067 seconds, 4096 samples were produced. The first step for the LLE algorithm is to determine the variables J and m. Once J, m and N are known, M can be calculated. As shown in section 4.2.3, J can be calculated based upon the first dominant frequency of the vibration signal being analyzed. As shown in Figure 4.24, the first dominant frequency is 16.7 Hz. Thus J is calculated in the following way: (1/16.7 Hz) multiplied by 4096 Hz = 14.37. The numerical computation required the non-negative integer of J and also required that J should be the element of factorial 4096. Thus we round up 14.37 to a greater integer number

16. The integer 16 is selected because it is an element of factorial 4096. The reason why it needs to be an element of factorial 4096 is the phase-space requirement. If J is an element of factorial 4096, it will be easy to calculate the embedding dimension, m. Once J is known, the next variable which needed to be determined is m. As shown in section 4.2.3, m is selected to get the M as low as possible in order to speed up the computation time. The computation time of the feature extraction method is necessary in practice to provide a rapid condition monitoring result. Thus m in this paper for the coal bridge reclaimer data is 248. The variables μ and k are selected as 30 and 40, respectively.

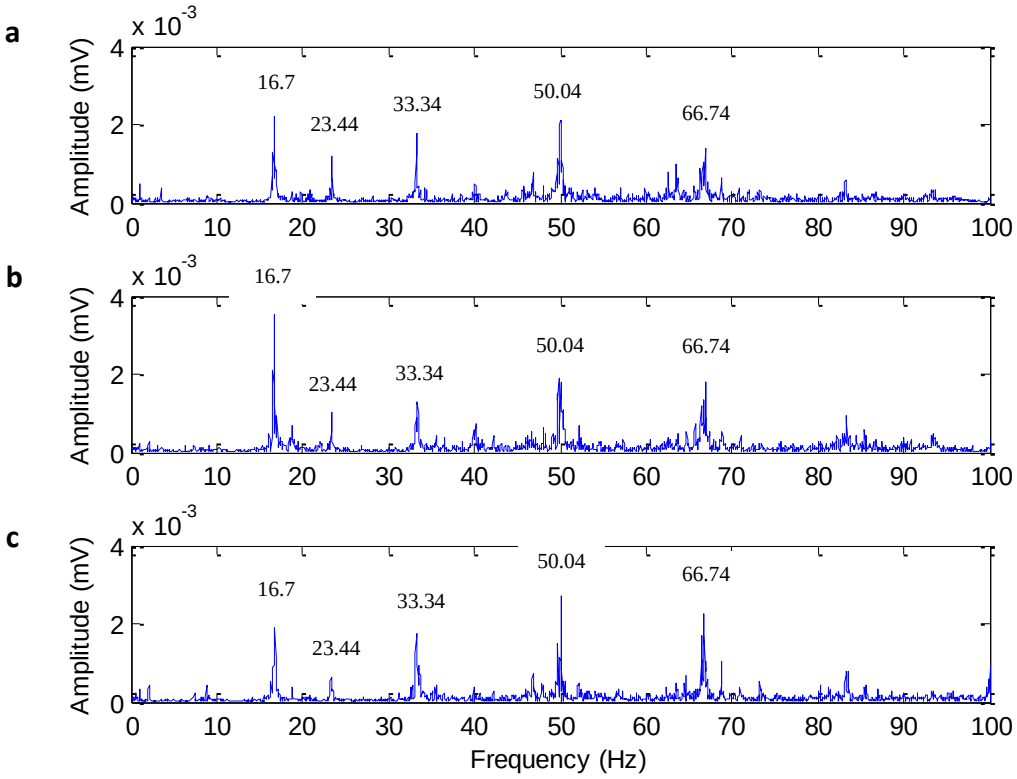

Figure 4.24 FFT of coal bridge reclaimer: (a) data 28 July 2003; (b) data 16 September 2004 and (c) data 14 September 2005.

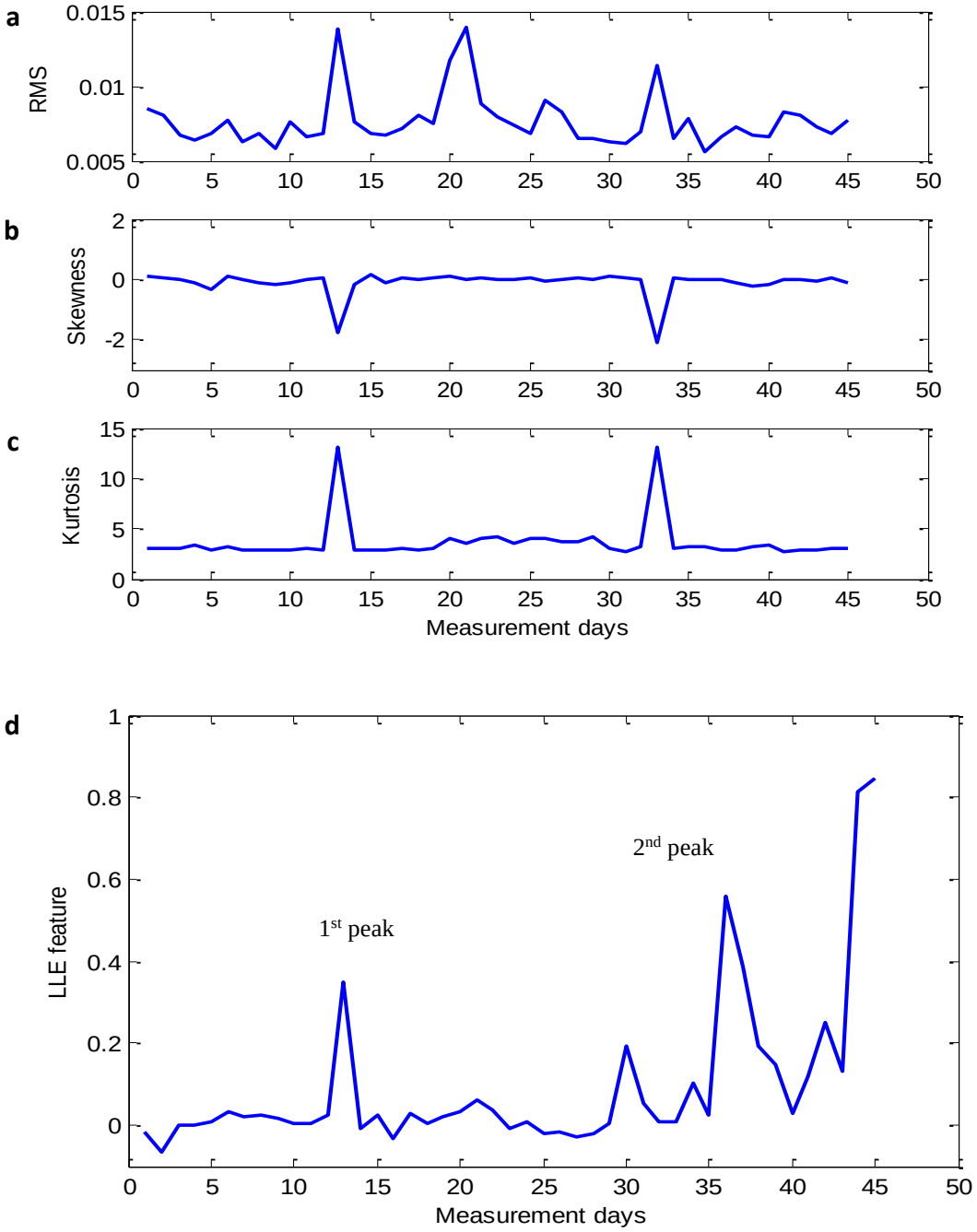

Figure 4.25 Comparison between time domain features and LLE feature extracted from the coal bridge reclaimer data: (a) RMS feature; (b) skewness feature; (c) kurtosis feature and (d) LLE feature. The measurement in the *x*-axis is related to Table 4.7.

Table 4.7 Details of LLE result (λ_1) related to the measurement dates.

Measurement day	λ_1	Measurement day	λ_1	Measurement day	λ_1
1	-0.01667	16	-0.031	31	0.05518
2	-0.06506	17	0.0296	32	0.01014
3	0.0003934	18	0.002878	33	0.007898
4	-0.0008573	19	0.02163	34	0.1046
5	0.0106	20	0.03241	35	0.02563
6	0.03377	21	0.06081	36	0.557
7	0.01959	22	0.03731	37	0.3844
8	0.02359	23	-0.007276	38	0.1947
9	0.01857	24	0.007093	39	0.1491
10	0.005054	25	-0.01873	40	0.0309
11	0.004379	26	-0.01511	41	0.1214
12	0.0271	27	-0.02856	42	0.2491
13	0.3485	28	-0.02158	43	0.1337
14	-0.008846	29	0.004501	44	0.8137
15	0.02722	30	0.1925	45	0.8475

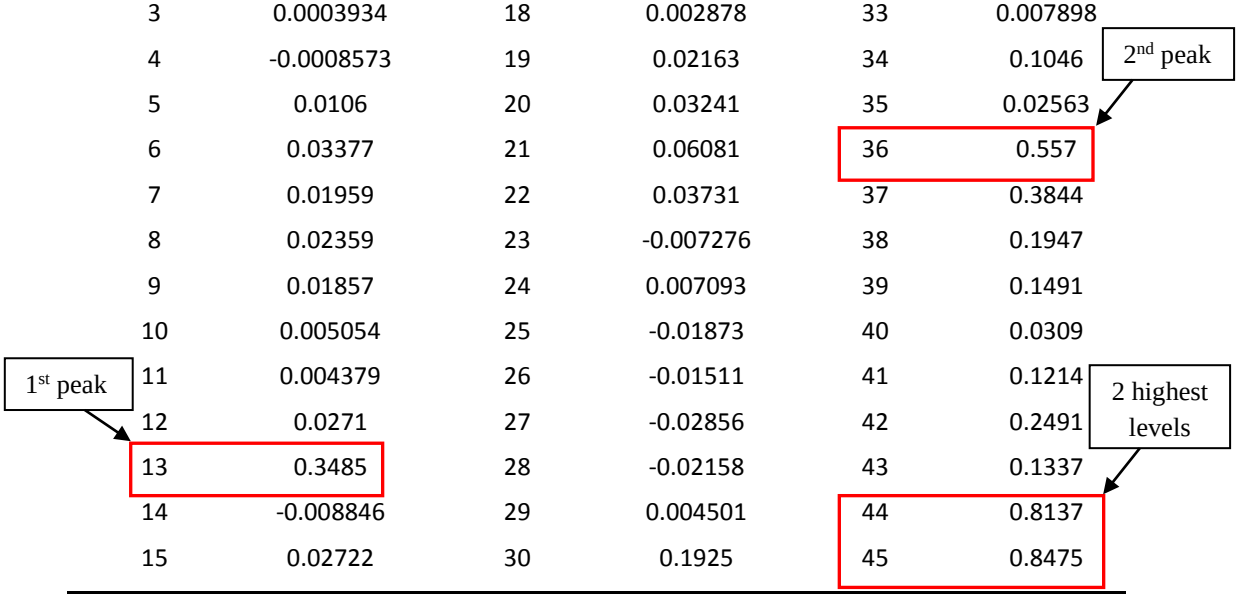

4.2.5 Evaluation criteria in tracking progressive slew bearing failure

In this study, four evaluation criteria for tracking the progressive failure of low speed slew bearings have been proposed. The criteria are:

1. Count of high peaks
2. High peak difference
3. Relative time from first peak detection
4. Interval between peaks

In order to substantiate the benefits of the LLE method, the four criteria above were applied to the time domain kurtosis feature, the EMD kurtosis feature and the LLE feature for laboratory slew bearing data. They were also applied to the kurtosis and the LLE feature of coal bridge reclaimer data. The result is presented in Tables 4.8 and 4.9. The definition of and the formula for each evaluation criterion are described below:

1. *Count of high peaks* (E_1): Since the deterioration of the slew bearing can be detected by the peaks in the monitored parameter or feature, this criterion counts the number of peaks which exceed the predetermined threshold level. The greater the number of such peaks detected, the more damaged the slew bearing. The formula for this calculation (E_1) is as follows:

$$E_1 = C \times c \tag{4.18}$$

where C is the number of peaks which exceed the predetermined threshold level (threshold = 12), and c is a normalization E_1 value of less than 1 ($c = 0.1$). It should be noted that each criterion value is expected to have a normalization value of less than 1 in order to be compared with other criterion value. The count of high peaks is illustrated in Figure 4.26. The threshold of 12 is arbitrarily determined according to the peaks fluctuation of the LLE feature. If the threshold of 10 is selected, a number of count of high peaks value will not be increase because it already detected from the beginning where the bearing is still in normal condition.

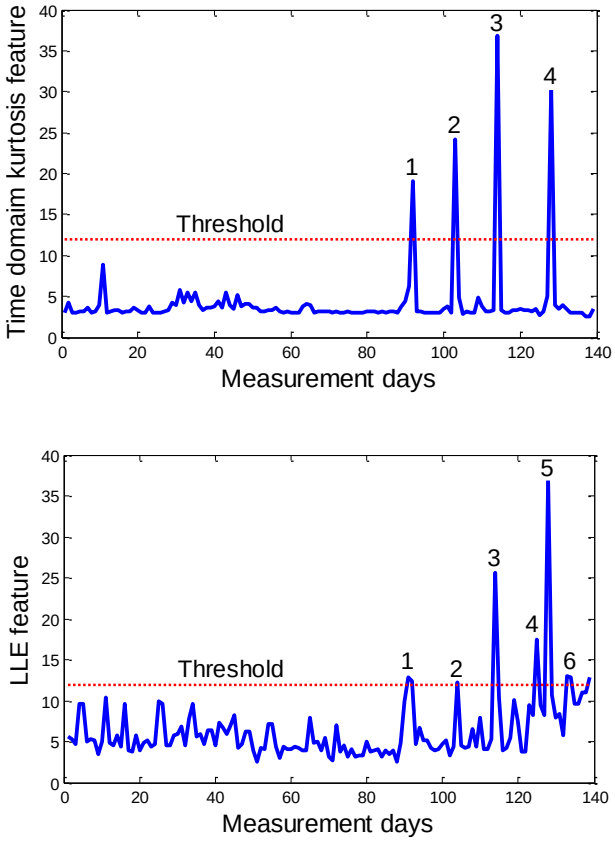

Figure 4.26 Count of peaks of features extracted from laboratory slew bearing data.

2. *High peak difference (E_2)*: This criterion calculates the difference in the high peaks between following peaks and the detection of the first peak (P_1). E_2 is given by:

$$E_2 = \frac{\frac{1}{C-1}\sum_{a=2}^{C}(P_a - P_1)}{\overline{P}} \tag{4.19}$$

where P_a is the following peaks and $\overline{P}$ is the average peak amplitude. If the most following peak levels P_a are lower than the detection of the first peak P_1, the result will be a negative value. This is illustrated in Figure 4.27.

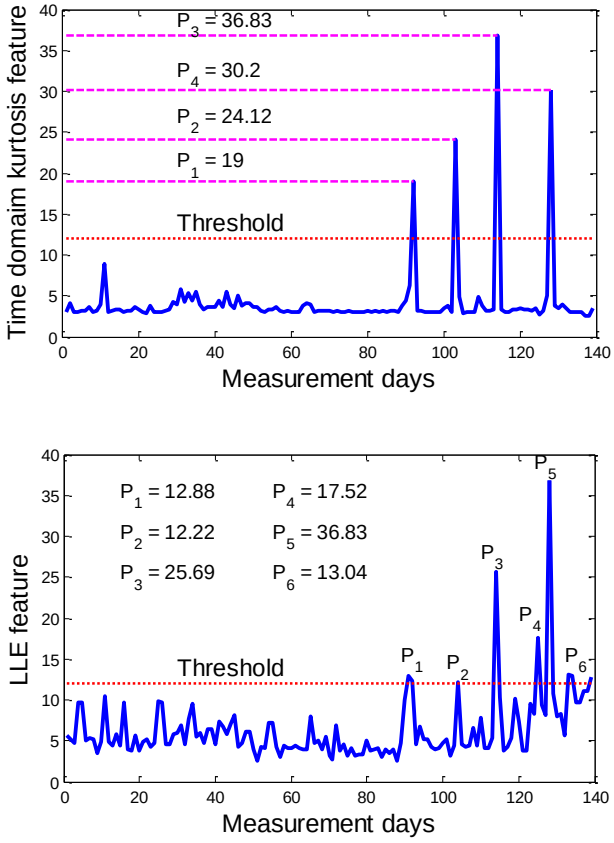

Figure 4.27 Peaks identification of features extracted from laboratory slew bearing data. These peaks were used further to calculate high peak difference (E_2).

3. *Relative time from first peak detection* (E_3): The initial failure of the slew bearing can be identified by the day of first peak detection, according to the monitored parameter or feature. The formula of the relative time from first peak detection

(E_3) is given as follows:

$$E_3 = \left[\frac{DL - DF}{DL} \right] \tag{4.20}$$

where DL is the last measurement day (i.e.139) and DF is the day of first peak detection, as shown in Figure 4.28.

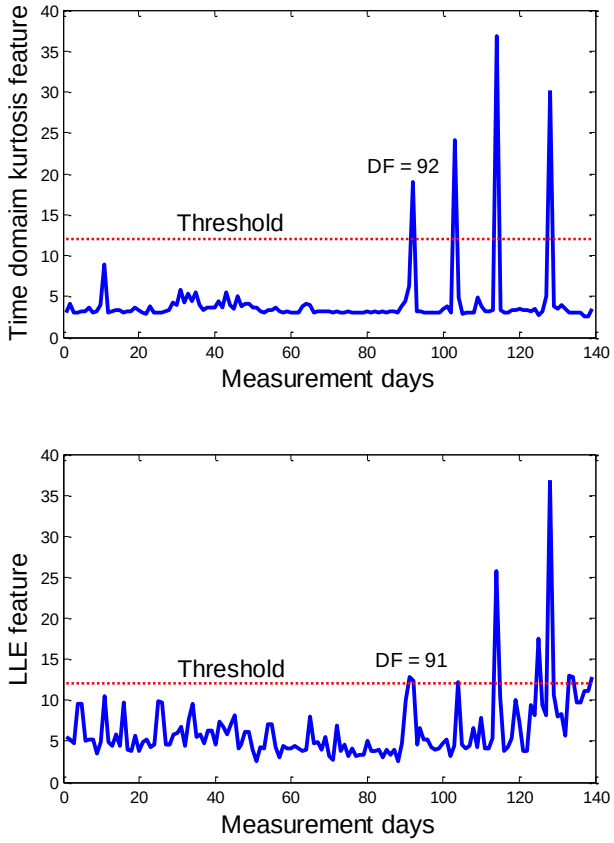

Figure 4.28 First peak detection of features extracted from laboratory slew bearing data.

4. *Interval between peaks* (E_4): This criterion measures the interval between two adjacent peaks. If the two adjacent peaks are close, it indicates the advance of the deterioration in the condition of the slew bearing. The interval between peaks (E_4) is calculated as follows:

$$\bar{I} = \frac{\sum_{a=2}^{C} (D_a - D_{a-1})}{C - 1} \tag{4.21}$$

$$E_4 = \frac{DL - \bar{I}}{DL} \tag{4.22}$$

where $\bar{I}$ is the average day interval, D_a and D_{a-1} are the anterior and the posterior day of two adjacent peaks, respectively, as shown in Figure 4.29.

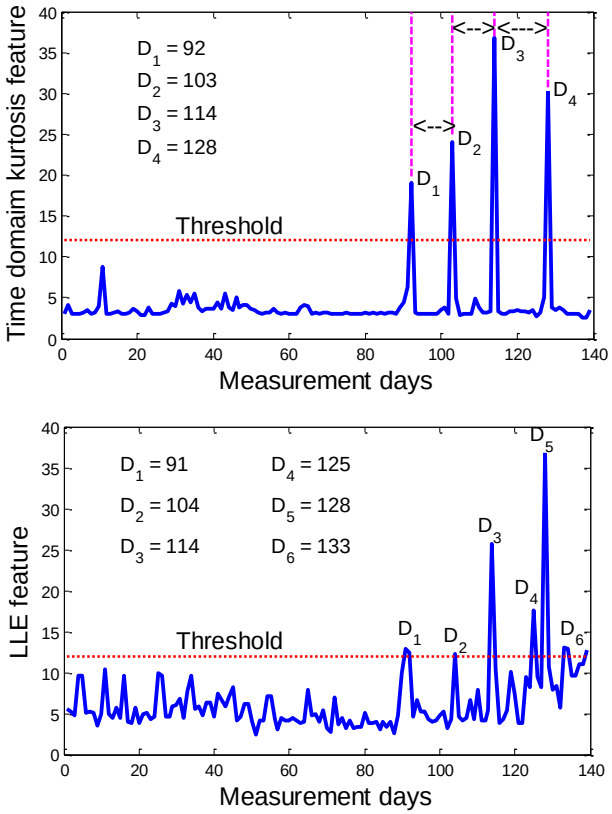

Figure 4.29 Interval between peaks of features extracted from laboratory slew bearing data.

In the case of laboratory slew bearing data, it can be seen that the overall evaluation score of the LLE feature in Table 4.8 was higher than the time domain kurtosis feature and the EMD feature. An overall evaluation score is the mean value of the evaluation criteria. A negative value of the E_2 criterion of EMD kurtosis feature is due to the fact that the next peaks are lower than the detection of the first peak. In the same way, the overall evaluation score of the LLE feature was greater than the kurtosis feature extracted from original vibration data for the case of coal bridge reclaimer data.

Table 4.8 Evaluation comparison result for laboratory slew bearing data.

		Time domain kurtosis feature	EMD kurtosis feature	LLE feature
		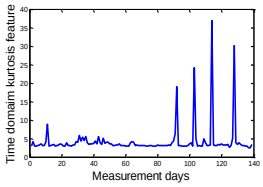	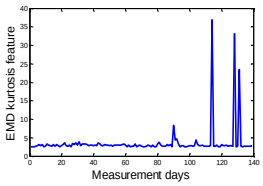	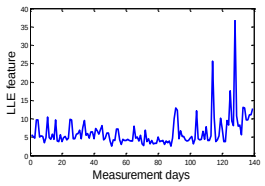
1	Count of high peaks (E_1)	0.4	0.3	0.6
2	High peak difference (E_2)	0.413	-0.264	0.416
3	Relative time from first peak detection (E_3)	0.338	0.179	0.345
4	Interval between peaks (E_4)	0.913	0.938	0.939
	Overall evaluation band score	**0.516**	**0.288**	**0.575**

Table 4.9 Evaluation comparison result for coal bridge reclaimer data.

		Time domain kurtosis feature	LLE feature
		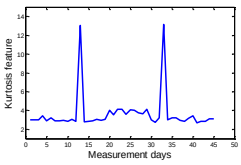	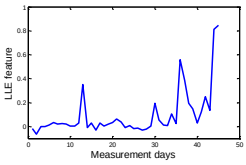
1	Count of high peaks (E_1)	0.2	0.5
2	High peak difference (E_2)	0.007	0.311
3	Relative time from first peak detection (E_3)	0.711	0.711
4	Interval between peaks (E_4)	0.555	0.822
	Overall evaluation band score	**0.368**	**0.586**

4.3 Conclusion

The circular domain feature extraction method has been developed. It is shown that the slight changes of bearing condition during operation can be identified more clearly in circular domain analysis compared to time-domain features, wavelet decomposition and EMD. This allows the maintenance engineers to better schedule the maintenance work. Four circular domain features were shown to consistently and clearly identify the onset (initiation) of fault from the peak feature value. This value, however, is not clearly observable in time-domain feature extraction, wavelet decomposition combine with time domain feature extraction and EMD combine with time-domain feature extraction. The application of the method is demonstrated with simulated data, laboratory slew bearing data and industrial bearing data from coal bridge reclaimer used in a local steel mill. The method has been published in the following title:

- W. Caesarendra, B. Kosasih, A.K. Tieu, C.A.S. Moodie, Circular domain features based condition monitoring for low speed slewing bearing, Mechanical Systems and Signal Processing 45 (2014) 114-138.

LLE algorithm, one of the phase-space dissimilarity measurements, has been employed as a feature extraction method for low speed slew bearing vibration data. The tested data are collected from the lab test condition monitoring and a coal bridge reclaimer that is used in a local steel mill industry. According to the result, this method can be used as an alternative method to deal with low energy chaotic vibration bearing signals in cases where the existing methods feature extraction are not suitable. Such existing methods have been applied for rolling element bearing condition monitoring such as vibration-based FFT, time domain feature extraction (e.g. RMS, skewness, kurtosis, etc) and advance fault diagnosis methods, e.g. EMD. The step-by-step computational algorithm has been presented in details. It must be noted that the most important LLE parameter is reconstruction delay, J. This parameter must be calculated before the other parameters m and M are determined. A simple and effective technique to select parameter J is has been proposed. Four evaluation criteria have also been proposed and introduced to substantiate the benefits of LLE method. The method has been published in the following title:

- W. Caesarendra, B. Kosasih, A.K. Tieu, C.A.S. Moodie, Application of the largest Lyapunov exponent algorithm for feature extraction in low speed slew bearing condition monitoring, Mechanical Systems and Signal Processing 50-51 (2015) 116-138.

Chapter 5 - Incipient defect detection method and damage analysis

"The real voyage of discovery consists not in seeking new landscape, but in having new eyes"
(Marcel Proust)

5.1 Introduction

This chapter presents an application of multivariate state estimation technique (MSET) and sequential probability ratio test (SPRT) to detect the incipient slew bearing defect. MSET was first introduced by Singer [167] and was further developed in the Argonne National Laboratory [168, 169]. Over the years, the technique has been applied successfully in many applications such as in the analysis of nuclear power reactor signals [167-170]. Recently, MSET has been used in condition monitoring studies such as the monitoring of lithium-ion battery performance [171], the detection of the onset of software aging [172] and early fault diagnosis of wind turbines [173]. However, the application of MSET as rolling element bearing condition monitoring and incipient defect detection method has not been explored. SPRT was introduced by Wald [174, 175] as a sequential statistical method. This method has been proven to work well either as a stand-alone decision-making method [176-180] or as an integrated method together with MSET [169, 172, 181]. When integrated with MSET, SPRT can be used to analyze the MSET result. SPRT can also be combined with auto-associative kernel regression algorithm [182].

5.2 Multivariate State Estimation Technique (MSET)

MSET is an effective technique for real-time signal monitoring. It is a method to analyse process behavior based on the sensor readings. MSET basically computes the correlation between the statistical characteristics of the past data and the monitored

signal. MSET numerically flags anomalous process behaviour as early as possible. This technique has been applied in process monitoring, signal validation and surveillance applications [167-173, 181]. However, the study on MSET for rolling element bearing condition monitoring, especially for low speed slew bearings, has not been explored. In the present study MSET combines multiple extracted features to provide information about the condition of the slew bearing. This is useful in practice because in this way, the site maintenance engineer only needs to monitor single reliable information extracted from multiple condition monitoring parameters or features.

The MSET algorithm is applied systematically in 5 steps [183] as shown in Figure 5.1 in the first and second blocks. First, data matrix $\mathbf{P}$ is created where the row elements of $\mathbf{P}$ are the extracted features and the columns are the measurement time i.e. days. Data matrix $\mathbf{P}$ of size m features × n days is defined in Eq. (5.1).

$$\mathbf{P} = \begin{array}{c} \begin{array}{cccccc} \text{day 1} & \text{day 2} & \text{day 3} & . & . & \text{day } n \end{array} \\ \begin{bmatrix} f_1(1) & f_1(2) & f_1(3) & . & . & f_1(n) \\ f_2(1) & f_2(2) & f_2(3) & . & . & f_2(n) \\ f_3(1) & f_3(2) & f_3(3) & . & . & f_3(n) \\ . & . & . & . & & . \\ . & . & . & & . & . \\ . & . & . & & . & . \\ f_m(1) & f_m(2) & f_m(3) & . & . & f_m(n) \end{bmatrix} \end{array} \begin{array}{l} \text{feature 1} \\ \text{feature 2} \\ \text{feature 3} \\ . \\ . \\ . \\ \text{feature } m \end{array} \tag{5.1}$$

Second, data matrix $\mathbf{P}$ is subdivided into two matrices: training matrix, $\mathbf{T}$ and observation matrix, $\mathbf{P}_{\text{obs}}$. $\mathbf{T}$ is further divided into memory matrix, $\mathbf{D}$ and remaining training matrix, $\mathbf{L}$. It should be noted that $\mathbf{T}$ holds data from the normal state while $\mathbf{P}_{\text{obs}}$ holds the monitored state, as shown in Eq. (5.2).

$$\mathbf{P} = \underbrace{\underbrace{\begin{bmatrix} f_1(1) & f_1(2) & \cdots & f_1(n_D) \\ f_2(1) & f_2(2) & \cdots & f_2(n_D) \\ f_3(1) & f_3(2) & \cdots & f_3(n_D) \\ \vdots & \vdots & \vdots & \vdots \\ f_m(1) & f_m(2) & \cdots & f_m(n_D) \end{bmatrix}}_{[\mathbf{D}]} \underbrace{\begin{bmatrix} f_1(n_D+1) & \cdots & f_1(n_L) \\ f_2(n_D+1) & \cdots & f_2(n_L) \\ f_3(n_D+1) & \cdots & f_3(n_L) \\ \vdots & \vdots & \vdots \\ f_m(n_D+1) & \cdots & f_m(n_L) \end{bmatrix}}_{[\mathbf{L}]}}_{[\mathbf{T}]} \underbrace{\begin{bmatrix} f_1(n_L+1) & f_1(n_L+2) & \cdots & f_1(n) \\ f_2(n_L+1) & f_2(n_L+2) & \cdots & f_2(n) \\ f_3(n_L+1) & f_3(n_L+2) & \cdots & f_3(n) \\ \vdots & \vdots & \vdots & \vdots \\ f_m(n_L+1) & f_m(n_L+2) & \cdots & f_m(n) \end{bmatrix}}_{[\mathbf{P}_{obs}]}$$

Normal state — Monitored state

(5.2)

where n_D is the number of days in $\mathbf{D}$ matrix and n_L is the number of days in $\mathbf{L}$ matrix.

Third, the weight vector for the normal state, $\mathbf{w}_1$ and the monitored state, $\mathbf{w}_2$ are calculated as follows [183]

$$\mathbf{w}_1 = (\mathbf{D}^{\mathrm{T}} \otimes \mathbf{D})^{-1} \bullet (\mathbf{D}^{\mathrm{T}} \otimes \mathbf{L}) \tag{5.3}$$

$$\mathbf{w}_2 = (\mathbf{D}^{\mathrm{T}} \otimes \mathbf{D})^{-1} \bullet (\mathbf{D}^{\mathrm{T}} \otimes \mathbf{P}_{\mathrm{obs}}) \tag{5.4}$$

Operator $\otimes$ is a non-linear operator. Several non-linear operators can be selected for MSET [184]. The most popular operator is the Euclidean distance, which is the one adopted in this thesis.

Fourth, the normal estimate matrix ($\mathbf{L}_{\mathrm{est}}$) is computed by Eq. (5.5)

$$\mathbf{L}_{\mathrm{est}} = \mathbf{D} \bullet \mathbf{w}_1 \tag{5.5}$$

and the monitored estimate matrix ($\mathbf{P}_{\mathrm{est}}$) is calculated by Eq. (5.6)

$$\mathbf{P}_{\mathrm{est}} = \mathbf{D} \bullet \mathbf{w}_2 \tag{5.6}$$

Fifth, the normal residual matrix ($\mathbf{R}_{\mathrm{N}}$) is the difference between $\mathbf{L}_{\mathrm{est}}$ and $\mathbf{L}$ and calculated by Eq. (5.7).

$$\mathbf{R}_{\mathrm{N}} = \mathbf{L}_{\mathrm{est}} - \mathbf{L} \tag{5.7}$$

And the monitored residual matrix ($\mathbf{R}_{\mathrm{M}}$) is the difference between $\mathbf{P}_{\mathrm{est}}$ and $\mathbf{P}_{\mathrm{obs}}$ and calculated by Eq. (5.8).

$$\mathbf{R}_{\mathrm{M}} = \mathbf{P}_{\mathrm{est}} - \mathbf{P}_{\mathrm{obs}} \tag{5.8}$$

5.3 Sequential Probability Ratio Test (SPRT)

SPRT, a sequential statistical binary hypothesis technique [174, 175], has been used as a simple and effective stand-alone decision-making technique for engineering systems. Such systems include the surveillance of nuclear power plant components [177], statistical damage classification of an automotive system [178], long-term radiation monitoring [179], and multiple fault recognition in gearboxes [180]. SPRT has been integrated with MSET to analyse the output of the MSET and to digitally assess the condition of the system being monitored [169, 181]. With this capability, SPRT is a potential early warning method embeddable in online monitoring systems. In this thesis, SPRT was used to analyse observations sequentially to determine whether the bearing is still in normal condition or already in defective condition.

To detect the incipient slew bearing defect, SPRT utilizes the outputs of MSET, the normal residual matrix ($\mathbf{R}_{\mathrm{N}}$) and the monitored residual matrix ($\mathbf{R}_{\mathrm{M}}$) as shown in Figure 5.1. Statistical features of the training data, such as mean and standard deviation, were extracted from normal residual matrix ($\mathbf{R}_{\mathrm{N}}$) to create a detection baseline. In the detection procedure, the similar features are also extracted from monitored data, namely the monitored residual matrix ($\mathbf{R}_{\mathrm{M}}$). The detection of the changes in bearing condition is conducted by comparing the baseline and the monitored data. The SPRT work is based on binary hypothesis tests. The binary hypothesis includes one null hypothesis and some alternative hypotheses. For a normal distribution, the null hypothesis H_0 represents the healthy state, with $\mathrm{mean} = 0$ and $\mathrm{standard\ deviation} = \sigma$. The alternative hypotheses H_{z} represent an abnormal state, with $\mathrm{mean} \neq 0$, or $\mathrm{standard\ deviation} \neq \sigma$, where z is the number of alternative hypothesis. Because the SPRT in this thesis was used to analyse the features matrix, the normal bearing condition denoted by a null hypothesis (H_0) is $\mathrm{mean} = \mathrm{M}$ and $\mathrm{standard\ deviation} = \sigma$. The defect condition was denoted by the

alternative hypotheses H_1, H_2, …, H_z that have a mean $\neq M$ and standard deviation $\neq \sigma$. And z is the number of the alternative hypothesis corresponding to the changes of bearing condition. A detailed application of these hypotheses for slew bearing damage detection is presented in Table 5.4.

In SPRT analysis (see Figure 5.1), the probability ratio, L was calculated by dividing the probability of statistical properties s_i that fall within the alternative hypotheses H_z and the probability of statistical properties s_i that fall within the null hypotheses H_0. The decision is then made based on the SPRT index calculated as follows [185]:

$$SPRT_{index} = \ln(L) = \sum_{i=1}^{n} \ln \frac{\Pr(s_i \mid H_z)}{\Pr(s_i \mid H_0)} \tag{5.9}$$

where L is given by

$$L = \prod_{i=1}^{n} \frac{\Pr(s_i \mid H_z)}{\Pr(s_i \mid H_0)} \tag{5.10}$$

where s_i are the statistical properties e.g. mean, M and standard deviation, σ of the observed features at the monitored measurement day.

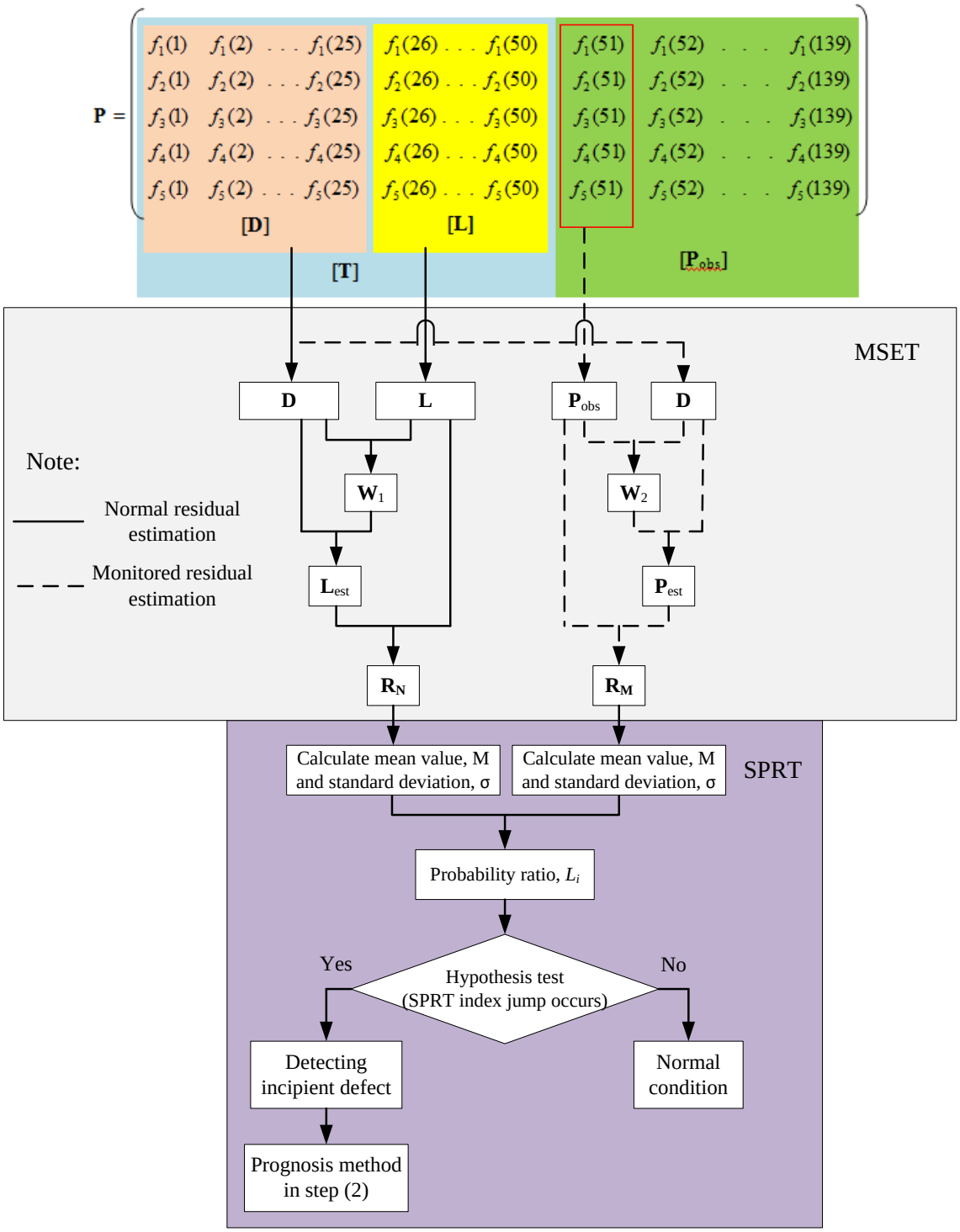

Figure 5.1 Flowchart of the proposed combined MSET and SPRT method in step (1).

5.4 Results and discussion

Twelve features have been extracted from four different methods [186]. Not all features are sensitive to the change of the bearing condition. Consequently, the

method only uses five of the most sensitive features as the input to the MSET. The five features are (1) kurtosis extracted from accelerometer signal, $f_1(t)$ [96]; (2) kurtosis extracted from the piecewise aggregate approximation (PAA) combined with circular analysis, $f_2(t)$ [96]; (3) kurtosis extracted from the wavelet decomposition, $f_3(t)$ [96]; (4) kurtosis extracted from the EMD, $f_4(t)$ [96]; and (5) LLE feature obtained from the largest Lyapunov exponent algorithm, $f_5(t)$ [186]. The five features were extracted over the 139 days test period. The plot of the aforementioned features is shown in Figure 5.2. These features are used to establish the data matrix $\mathbf{P}$. Thus, the dimension of data matrix $\mathbf{P}$ in Eq. (5.1) is 5 by 139, where 5 is the number of features and 139 is the number of days.

To detect the incipient slew bearing defect (Step 1), the MSET algorithm calculates the normal residual matrix ($\mathbf{R}_{\mathrm{N}}$) and the monitored residual matrix ($\mathbf{R}_{\mathrm{M}}$) (see Figure 5.1). In Step (1), the following inputs are required: training matrix $\mathbf{T}$, memory matrix $\mathbf{D}$, remaining training matrix $\mathbf{L}$ and observation matrix $\mathbf{P}_{\mathrm{obs}}$. In this paper, $\mathbf{T}$ of 50 days was used. In the computation, the sizes of matrices, $\mathbf{D}$ and $\mathbf{L}$ have to be half of $\mathbf{T}$ i.e. 25 days each. The reason why 50 days was used is that coal dust was not injected until the 58$^{\mathrm{th}}$ day. In other words, during the first 50 days, the vibration signal had been acquired when the condition of the bearing was still normal. In practice, matrix $\mathbf{P}_{\mathrm{obs}}$ is obtained from daily observation or measurement. The number of measurement days from normal to failure has been set as 139 days. $\mathbf{P}_{\mathrm{obs}}$ is the matrix from the 51$^{\mathrm{st}}$ to 139$^{\mathrm{th}}$ day.

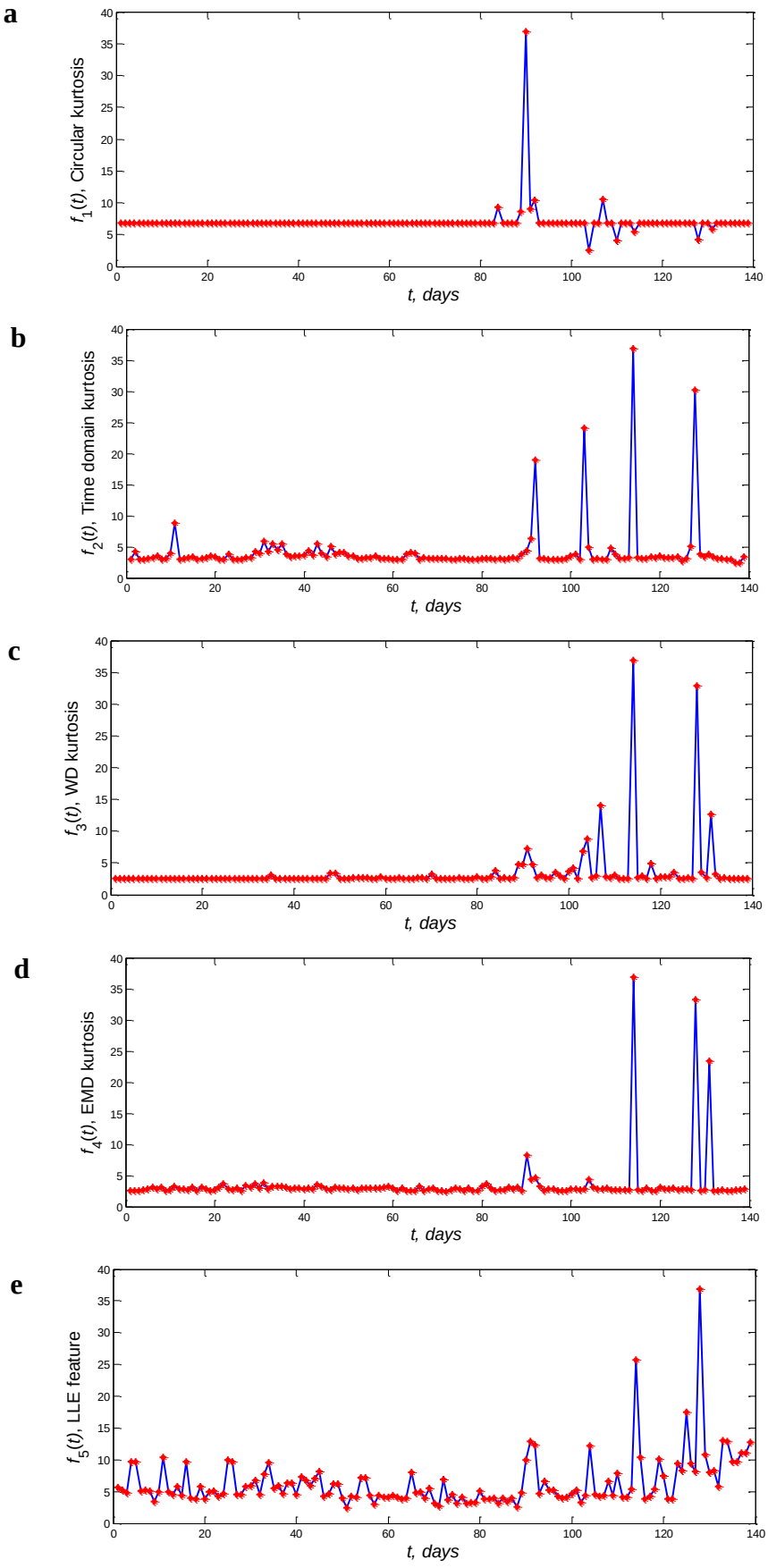

Figure 5.2 (a) Circular kurtosis; (b) Time-domain kurtosis; (c) Wavelet kurtosis; (d) EMD kurtosis; (e) The LLE feature. Note: t = dayth.

After $\mathbf{D}$ and $\mathbf{L}$ have been determined, the weight of normal state vector ($\mathbf{w}_1$) is then calculated using Eq. (5.3) by employing the Euclidean distance as the non-linear operator. Vector $\mathbf{w}_1$ represents the weight of normal data points in the training data. $\mathbf{w}_1$ is used to calculate the normal estimate matrix ($\mathbf{L}_{\text{est}}$) using Eq. (5.5). And the normal residual matrix ($\mathbf{R}_{\text{N}}$) is estimated by taking the difference between $\mathbf{L}_{\text{est}}$ and $\mathbf{L}$, as shown in Eq. (5.7). It should be noted that prior to the calculation of the statistical properties, matrix $\mathbf{R}_{\text{N}}$ is normalized with a mean of zero. This is necessary for the next process in the SPRT method because under normal bearing conditions the mean value of the normal residual matrix ($\mathbf{R}_{\text{N}}$) is expected to be ≈ 0. The result of normalized matrix ($\mathbf{R}_{\text{N}}$) is presented in Table 5.1. A similar procedure is also employed to obtain the monitored residual matrix ($\mathbf{R}_{\text{M}}$). Eq. (5.4) is used to calculate the weight of monitored state vector ($\mathbf{w}_2$), Eq. (5.6) is then used to calculate the monitored estimate matrix ($\mathbf{P}_{\text{est}}$) and Eq. (5.8) to calculate the monitored residual matrix ($\mathbf{R}_{\text{M}}$). Matrix $\mathbf{R}_{\text{M}}$ is then normalized within a range between maximum value and minimum value of the normalized normal residual matrix ($\mathbf{R}_{\text{N}}$). The calculation of $\mathbf{R}_{\text{N}}$ and $\mathbf{R}_{\text{M}}$ is the final step of MSET. Both results are then fed into the SPRT.

In SPRT, statistical characteristics such as mean value, standard deviation and the range between maximum and minimum values are calculated from each column of the normalized matrix, $\mathbf{R}_{\text{N}}$. These statistical properties belong to the normal condition of the bearing and are used as the reference normal data. These properties also form the set of hypotheses in SPRT. For the monitored state, prior to the calculation of the mean value and the standard deviation, the monitored residual matrix, $\mathbf{R}_{\text{M}}$ is normalized within the range between the maximum and minimum value of the normal state. The mean and standard deviation values of the normal state (up to days 25) are presented in Table 5.2 and Table 5.3, respectively. The detection of the incipient slew bearing defects is obtained by comparing the statistical characteristics, the mean value and the standard deviation) of the monitored state to the statistical characteristics of the normal state.

This comparison is repeated from the 51st to 139th columns of the $\mathbf{P}_{\text{obs}}$ matrix. If the mean value or the standard deviation in each day lies outside the range of the

reference mean values (Table 5.2) or standard deviation values (Table 5.3), then the incipient defect is considered to have occurred. This step is part of the SPRT procedure. To make a comparison, the list of hypotheses must be determined first including the normal condition (H_0) represented by mean value $= M_{normal}$ and the standard deviation $= \sigma_{normal}$. Alternative hypotheses, H_1 to H_4, indicate the abnormal conditions. The set of hypotheses is given in Table 5.4.

Table 5.1 Normalized $\mathbf{R}_N$ matrix.

day 1	day 2	day 3	day 4	day 5	day 6	day 7	day 8	day 9	day 10	day 11	day 12	day 13
0.044	0.042	0.042	0.042	0.042	0.043	0.042	0.043	0.044	0.042	0.042	0.042	0.043
0.025	0.021	0.021	0.022	0.022	0.023	0.021	0.024	0.025	0.022	0.022	0.021	0.022
0.016	0.015	0.015	0.015	0.015	0.016	0.015	0.016	0.016	0.015	0.015	0.015	0.015
0.018	0.017	0.017	0.017	0.017	0.018	0.017	0.018	0.018	0.017	0.017	0.017	0.018
-0.955	-0.957	-0.957	-0.957	-0.957	-0.956	-0.957	-0.956	-0.955	-0.957	-0.957	-0.957	-0.957

day 14	day 15	day 16	day 17	day 18	day 19	day 20	day 21	day 22	day 23	day 24	day 25
0.043	0.042	0.043	0.043	0.042	0.043	0.044	0.042	0.042	0.042	0.042	0.042
0.022	0.021	0.023	0.023	0.022	0.023	0.024	0.021	0.021	0.022	0.022	0.021
0.015	0.015	0.016	0.016	0.015	0.016	0.016	0.016	0.015	0.015	0.015	0.015
0.018	0.017	0.018	0.018	0.017	0.018	0.018	0.017	0.017	0.018	0.018	0.017
-0.957	-0.957	-0.956	-0.956	-0.957	-0.956	-0.955	-0.957	-0.957	-0.957	-0.957	-0.957

Table 5.2 Mean (M) values of normal state.

day 1	day 2	day 3	day 4	day 5	day 6	day 7	day 8	day 9	day 10	day 11	day 12	day 13
-0.169	-0.172	-0.171	-0.171	-0.171	-0.171	-0.172	-0.170	-0.170	-0.171	-0.171	-0.172	-0.171

day 14	day 15	day 16	day 17	day 18	day 19	day 20	day 21	day 22	day 23	day 24	day 25
-0.171	-0.172	-0.170	-0.171	-0.171	-0.171	-0.170	-0.172	-0.172	-0.171	-0.171	-0.172

Note: M_{min} = -0.172, M_{max} = -0.169

Table 5.3 Standard deviation (σ) values of normal state.

day 1	day 2	day 3	day 4	day 5	day 6	day 7	day 8	day 9	day 10	day 11	day 12	day 13
0.439	0.439	0.439	0.439	0.439	0.439	0.439	0.439	0.439	0.439	0.439	0.439	0.439

day 14	day 15	day 16	day 17	day 18	day 19	day 20	day 21	day 22	day 23	day 24	day 25
0.439	0.439	0.439	0.439	0.439	0.439	0.439	0.439	0.439	0.439	0.439	0.439

Note: $\sigma_{normal} = 0.439$

Table 5.4 Hypotheses for SPRT.

Hypothesis	Statistical properties	
	Mean (M)	Standard deviation (σ)
1. Normal condition (H_0)	$M_{min} < M < M_{max}$	$\sigma = \sigma_{normal}$
2. Abnormal condition 1 (H_1)	$M > M_{max}$	$\sigma = \sigma_{normal}$
3. Abnormal condition 2 (H_2)	$M < M_{min}$	$\sigma = \sigma_{normal}$
4. Abnormal condition 3 (H_3)	$M_{min} < M < M_{max}$	$\sigma > \sigma_{normal}$
5. Abnormal condition 4 (H_4)	$M_{min} < M < M_{max}$	$\sigma < \sigma_{normal}$

To mathematically measure the comparison, the ratio of the probability of alternative hypotheses (H_1 to H_4) and the probability of the null hypothesis (H_0) are calculated as in Eq. (5.10). Once probability ratio L_i is obtained, the SPRT index can be calculated by taking the natural logarithm of probability ratio L_i. The result of Step (1) is shown in Figure 5.3. It can be seen from the monitored data from the 51st to 89th day that the bearing is still in normal condition. The impending deterioration of the bearing is identified on the 90th day. Note that the impending deterioration is required in Step (2) to predict the future state and to estimate the RUL estimation. A sample calculation of L_i for one day (the 51st and 90th day) is presented in Table 5.5. When the condition of the bearing is still normal, the probability of statistical properties s_i that fall within the alternative hypotheses H_z, $\Pr(s_i \mid H_z)$ is much lower than the probability of statistical properties s_i of the null hypothesis H_0, $\Pr(s_i \mid H_0)$. To illustrate the normal condition (the 50th day), the natural logarithmic of L_i is given in Table 5.5 and shown in Figure 5.3. On the contrary, on the 90th day, the condition of the bearing started to deteriorate. When the bearing start to deteriorate, the probability of statistical properties s_i that fall within the hypotheses, H_z, $\Pr(s_i \mid H_z)$ will increase and the probability of statistical properties s_i that fall in the null hypothesis H_0, $\Pr(s_i \mid H_0)$ will decrease as shown in Table 5.5. The SPRT index is then given in Figure 5.3.

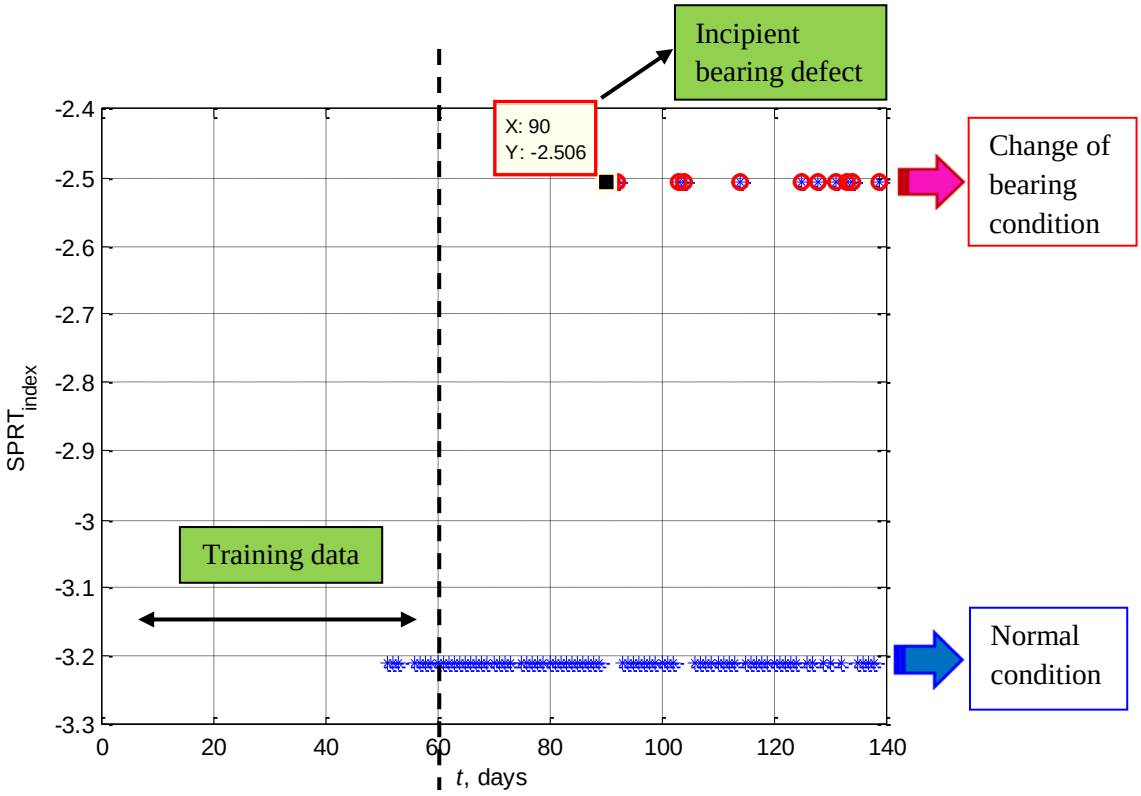

Figure 5.3 SPRT index result for detecting impending bearing deterioration.

Table 5.5 Example calculation of L_i in one day observation.

dayth observation	$\Pr(s_i \mid H_z)$	$\Pr(s_i \mid H_0)$	L_i (Eq. 5.10)
day 51	0.04	0.99	-3.209
day 90	0.08	0.98	-2.506

Note: $\Pr(s_i \mid H_z)$ is probability of statistical properties s_i given $\mathrm{H_z}$ is true and $\Pr(s_i \mid H_0)$ is probability of statistical properties s_i given $\mathrm{H_0}$ is true.

5.5 Damage analysis

The slew bearing damage photographs of the first laboratory test has been presented in Figure 2.16. It is shown the damages are caused by the contamination injected to the bearing in the middle of experiment. This section presented the damages of the slew bearing from the second laboratory test. Prior to the damage description, the selected time-domain features such as RMS, skewness, kurtosis and entropy are extracted first. The features are shown in Figure 5.4. From Figure 5.4 the

changes in the slew bearing condition can be seen from RMS, kurtosis and entropy feature on approximately December 2013 (red dashed line) and remained at a high level (up to red dotted line). These results are similar to the AE hit parameters of the AE signals in Chapter 6. The test rig was stopped on 30 January 2014 and the slew bearing was dismantled on 5 February 2014. The inner raceway, outer raceway and roller condition of the slew bearing were investigated. It was found that slew bearing parts such as the inner and the outer race were defective. The damage in the outer race was more severe than that in the inner race. The damage on the outer raceway is more than that on the inner raceway and the damage on the outer raceway is also denser than that on the inner raceway. According to Figure 5.5 and Figure 5.6 both outer race and inner race damages occurred on the right side due to the eccentric loading. This is shown in Figure 5.5 for the outer race damage and Figure 5.6 for the inner race damage. The damage clearly indicates a spalling which was initiated by subsurface cracking due to the fatigue caused by low frequency high loading and poor grease lubrication. Several similar wear scars can be seen in the dismantled rollers as presented in Figure 5.7.

In addition, it is shown in Figure 5.7 there is a rolling mark on the rollers. These rolling marks appeared partly on the rollers as there is a shinning part on the top side of the rollers. This is due to the poor grease lubrication and eccentric loading. The spalling damages were also shown in Figure 5.7. The SEM tests were conducted to identify the spalling damages. From the SEM tests, it is shown that the damages were probably due to the rolling fatigue between metal-to-metal contacts. Due to the eccentric loading, high load and reversible rotation, the crack was initiated from the part of roller surface with high stress contact points. This crack was developed into subsurface and finally make some amounts of material were chipped off and spall remained on the rollers.

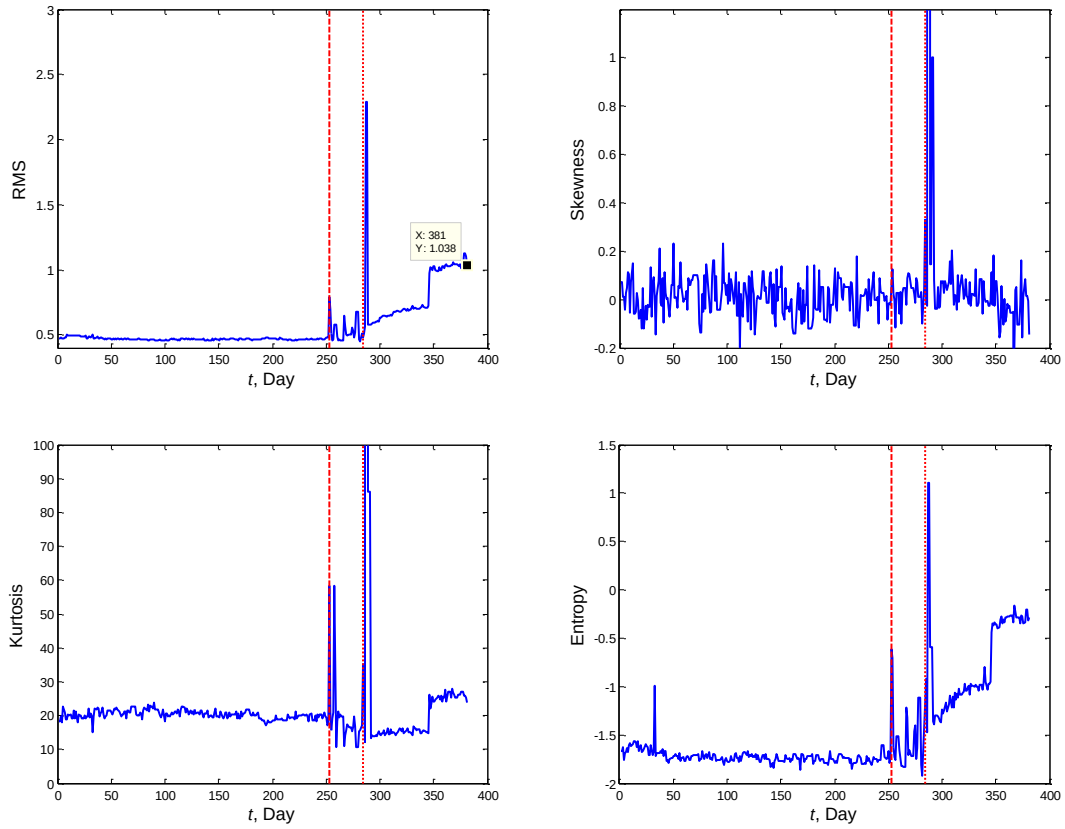

Figure 5.4 RMS, skewness, kurtosis and entropy features extracted from slew bearing data from the second laboratory test.

After cleaning, the bearing parts were assembled back to the test rig and the second measurement was restarted in 22 August 2014. The similar features are extracted and the results are shown in Figure 5.4 from the red dotted line to the last measurement day on day 381 (25 November 2014).

It noted that the circular domain and LLE feature extraction were not applied to the second laboratory test because the time domain features such as RMS, kurtosis and entropy have been shown to be effective in monitoring the bearing condition.

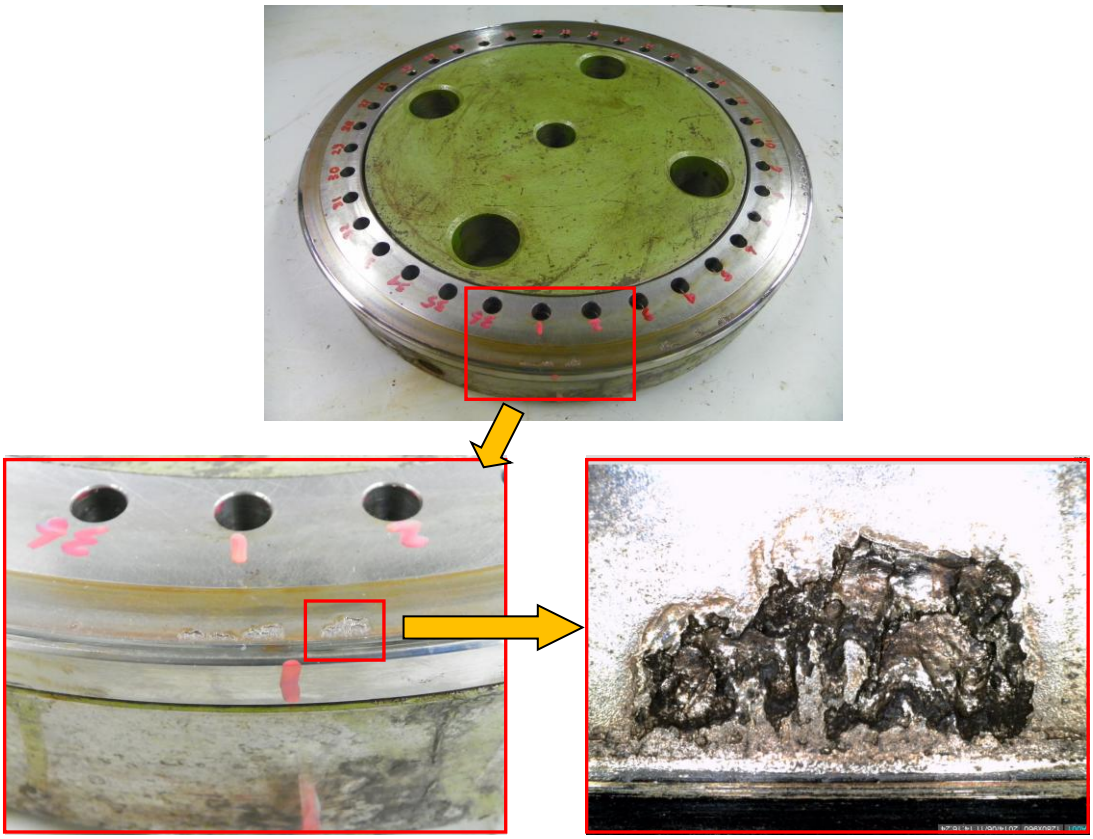

Figure 5.5 Naturally generated outer race damage photographs.

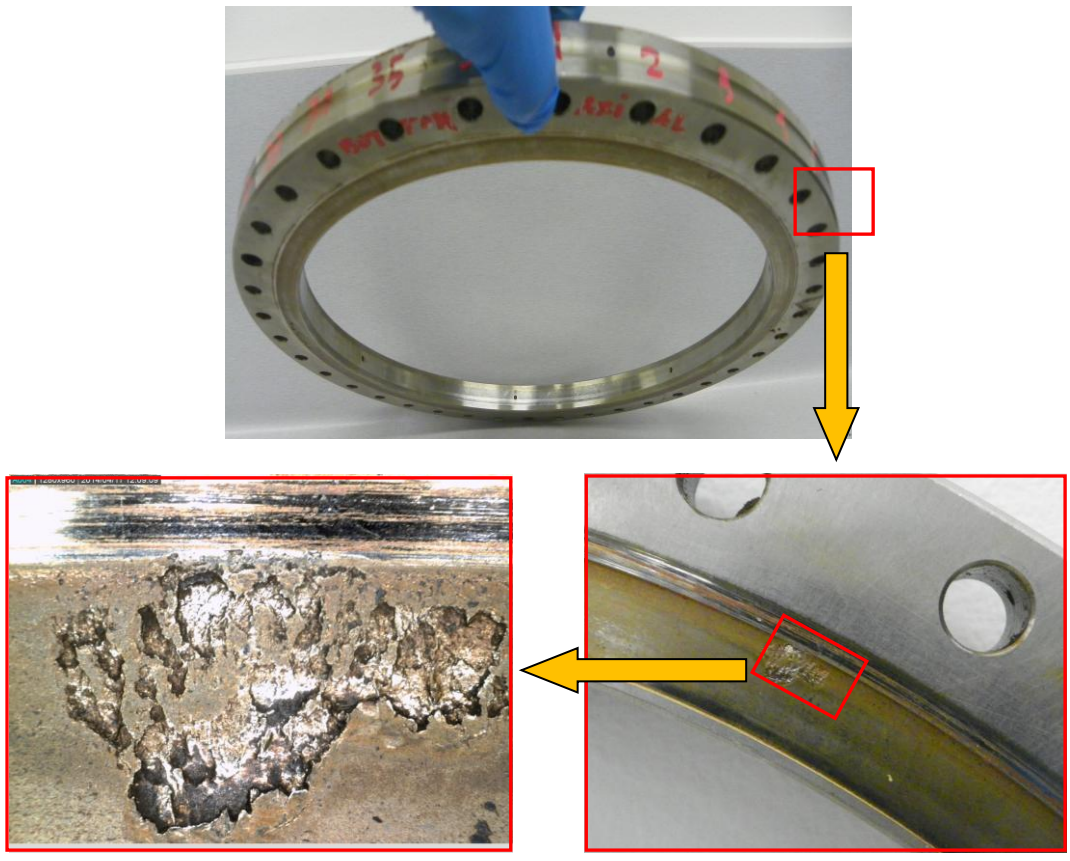

Figure 5.6 Naturally generated inner race damage photographs.

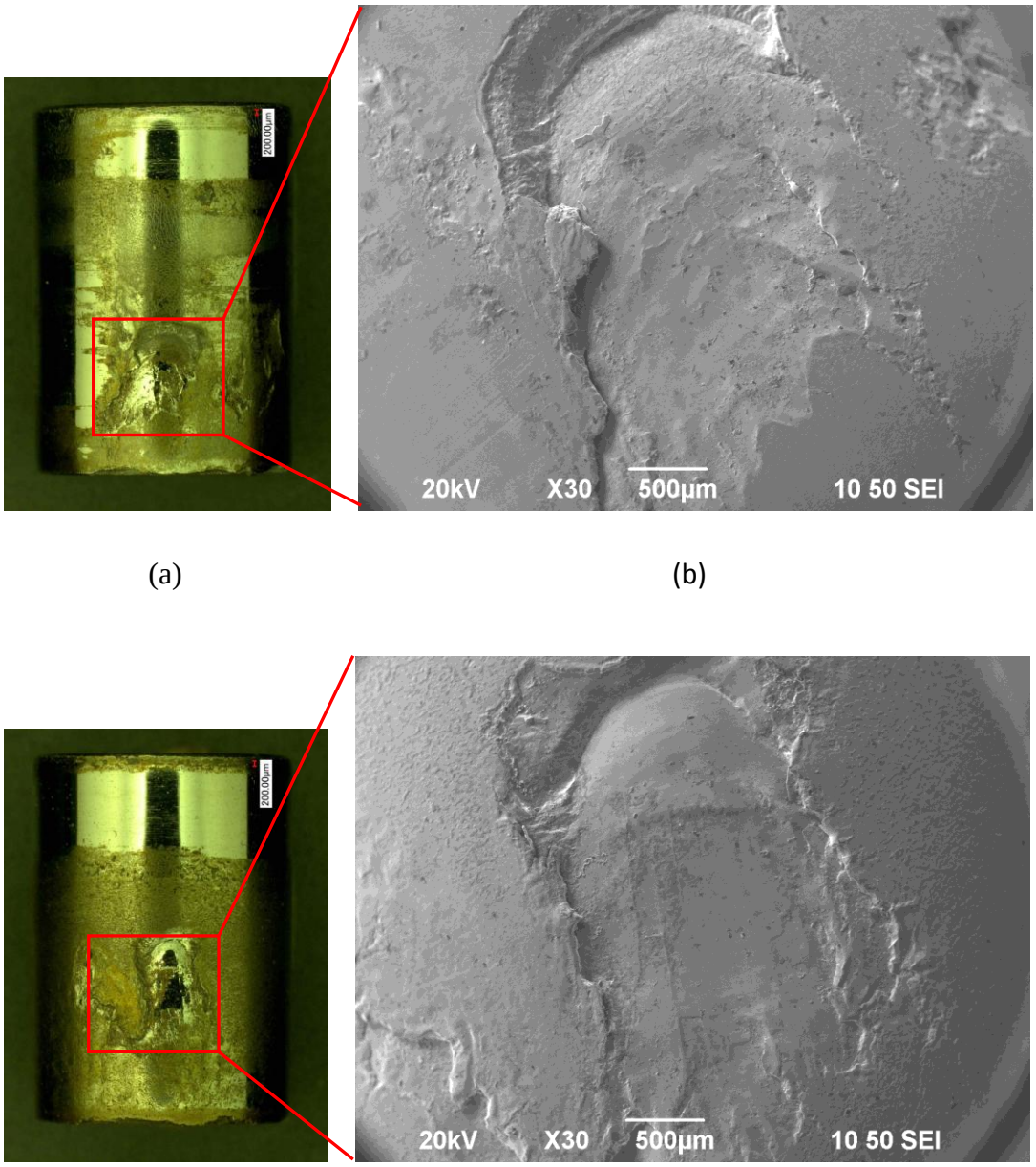

(a) (b)

(c) (d)

Figure 5.7 Naturally generated roller damage photographs and SEM images: (a) a photo of roller number 40; (b) a SEM of roller number 40; (c) a photo of roller number 81 and (d) a SEM of roller number 81. Note that the total number of roller is 82. The roller was marked in clockwise direction.

5.6 Conclusion

Manuscripts based on this chapter have been submitted to the Mechanical Systems and Signal Processing Journal with the following titles:

- W. Caesarendra, B. Kosasih, A.K. Tieu, C.A.S. Moodie, Integrated condition monitoring and prognosis method for incipient defect detection and remaining life prediction of low speed slew bearings, (under review in Mechanical Systems and Signal Processing Journal, Paper ID MSSP14-393).
- W. Caesarendra, B. Kosasih, A.K. Tieu, H. Zhu, C.A.S. Moodie, Acoustic emission-based condition monitoring methods: Review and Application for low speed slew bearing, (under review in Mechanical Systems and Signal Processing Journal, Paper ID MSSP14-741).

Chapter 6 - Acoustic emission-based condition monitoring

"Life is like riding a bicycle. To keep your balance, you must keep moving"
(Albert Einstein)

6.1 Introduction

Recently, there have been an increasing number of studies on slew bearing-based condition monitoring and early fault detection. The researches have employed a range of different methods such as vibration analysis [3, 4], finite element method (FEM) [5, 6, 8-10], oil analysis [11, 12] and acoustic emission (AE) [187-191]. AE has not been as largely used for slew bearings as it is in typical rolling element bearings. A pioneering study by Rodgers [2] used AE for monitoring slow rotating anti-friction slew bearings on cranes used in gas production.

In the present work, an experimental study on AE for condition monitoring and early fault detection of slew bearings was conducted. In the case of typical rolling element bearings, vibration analysis is more commonly used than AE. This is because it is simpler and has well developed data acquisition and analysis tools. In other scenarios, however, AE-based condition monitoring has been widely studied and has shown some advantages over vibration-based condition monitoring [80, 192-195]. One example is the comparison between AE and vibration analysis over a speed range of 600, 1000, 2000 and 3000 rpm and load range of 0.1, 4.43 and 8.86 kN [192]. AE achieved the early fault detection and provided an indication of the size of the artificially made defect. In another study [194] on the comparison of the used of vibration, AE and shock pulse methods (SPMs) on a bearing run at 1440 rpm with an artificial outer race defect. This study highlighted that the AE peak amplitude performed more reliable detection of the bearing defect than RMS of the vibration

signal. Another comparison study of AE and vibration analysis of naturally degraded roller bearings [80] applied a kurtogram for signal processing to both vibration and AE data from a defective bearing before root mean square (RMS) feature extraction. According to the overall trend of vibration and AE RMS, it was shown that AE is more sensitive in tracking the progression of the defect than the vibration-based method.

This chapter divides the previous studies into three categories: the AE method applied to rolling element bearings running at three different speed levels; the most widely used AE hit parameters for rolling element bearings; and the recent development of condition monitoring and fault detection methods using AE signals. The results of the first category are summarized in Table 6.1. It appears that there is no existing standard criterion for speed classification of rotating machinery, though some articles mentioned that rotating speed below 600 rpm is categorized as low [18, 19, 196] and speed greater than 600 rpm is considered as high [20, 21]. For this reason, three speed classifications: high-speed (> 600 rpm), low-speed (10 – 600 rpm) and very low-speed (< 10 rpm) have been adopted in this thesis. At low-speed, the AE signal is the transient elastic wave generated by the contact interaction of the rolling element and the raceway. At high speed, the AE signal is generated primarily by the impact between the rolling element and the raceway. At very low speed, the impact is lower than at high speed. This means that the transient wave generated by the interaction of the two metal surfaces is considered to be primarily due to friction and rubbing [127]. Several papers have indicated that for speeds below 100 rpm, and especially below 10 rpm, the signal is difficult to analyse [127, 197-202]. For example Jamaludin et al. [127] studied bearing condition monitoring at 1.12 rpm. Wu et al. [199] presented the characteristics of AE signals of the rolling bearing in a giant wheel rotating at 0.32 rpm. Miettinen et al. [202] conducted the AE measurements on the bearing when the rotational speed of the shaft was from 0.5 to 5 rpm. Each speed classification is further sub-divided into artificially and naturally induced damage.

It can be seen from Table. 6.1 that from more than 30 articles, even the most recent AE applications still focus on rolling element bearings rotating at speeds greater than 600 rpm and subject to artificial (seeded) damage. It can be concluded that condition monitoring at very low-speed (< 10 rpm) bearings has not yet been fully investigated.

The second category of the literature review identifies the most widely used AE hit parameters for bearing condition monitoring and fault detection of rolling element bearings. This is presented in Section 6.2.1.

Table 6.1 AE application in rolling element bearing for different speed levels and damage types.

	High speed (> 600 rpm)	Low speed (10 - 600 rpm)	Very low speed (< 10 rpm)
Artificially (seeded) damage	Refs. [187], [191], [2], [192], [194], [203], [204], [205], [206], [207], [208], [209], [210], [120], [211]	Refs. [190], [2], [19], [197], [208], [209], [120], [212], [213], [214]	Refs. [127], [197], [198], [199]
Naturally induced damage	Refs. [80], [215], [216], [217], [218], [219], [220]	Refs. [188], [189], [200], [122], [221]	Refs. [199], [200], [201], [202]

What makes slew bearings different from typical rolling element bearings? Slew bearings are large thrust bearings commonly used in heavy industrial machinery such as turntables, cranes, rotatable trolleys, excavators, reclaimers, swing shovels, and ladle cars founds in steel mills and mining. Recently, slew bearings have also been used in medical and military equipment [222, 223]. Slew bearings are usually attached at the base of the equipment or machine to enable rotation of the supported structure. The rotation of slew bearings is usually reversible and intermittent running at a very low speed (0.5–15 rpm). The inspection of slew bearings is challenging due to the difficulty in accessing them [224]. This often requires major disassembly of the larger system, resulting in productivity loss and higher maintenance cost. Therefore, this bearing tends to be poorly maintained and may increase the probability of sudden failure. These unexpected failures can be avoided if a condition monitoring system which is able to predict failure is integrated in the bearing condition monitoring system.

Because slew bearings have a typically long life, ranging from 5 to 10 years, an accelerated life test is required in the laboratory. Through this laboratory experiment, slew bearing condition monitoring data from brand new to impending failure was collected. In order to accelerate the failure, several defect accelerating methods such as: (1) irregular greasing; (2) application of continuous, heavy and excessive load; (3) presence of contamination; and (4) application of partial load, asymmetric or eccentric load acting, have been employed. The combination of continuous load and contamination has been studied [1] but did not include AE measurement during the period of bearing service life.

In the present study, a combination of irregular greasing, eccentric and continuous load were adopted. As the real faults would be hidden by lubricating the bearing and thus the AE signal is difficult to identify [225], irregular greasing is selected in this study. The objective is to identify which AE feature was the most appropriate and reliable one to indicate imminent failure. Due to low rotational speed, the signal generated from the metal-to-metal contact between the rolling element and defective spots is not as strong as that generated under similar conditions at high speed. The features commonly used for high speed bearings are not sensitive enough when applied to the slower slew bearing [120]. Features extracted from the low energy signal would not be clear because the weak signal is usually hidden behind the background noise.

6.2 AE-based condition monitoring in rolling element bearings

The study on AE condition monitoring in rolling element bearings can be classified into two main categories: (1) investigation of AE parameters and (2) development of AE-based signal processing, alternative feature extraction and pattern recognition.

6.2.1 AE hit parameters

The literature presents many studies on AE hit parameter-based methods associated with rolling element bearing defects. For example, AE hit parameters such as counts and peak amplitude have been used [187] to detect the changes

corresponding to the different sizes of simulated defects on the inner race and roller of radially loaded cylindrical roller bearings rotating at 1500 rpm. The study found that 'counts' is a good parameter for the detection of small defects. For larger defects, however, counts is unable to track the progression of the defect because it stops increasing after a certain defect size. In addition to counts, other AE hit parameters such as RMS, amplitude and energy were investigated by Morhain and Mba [206] for radially loaded bearings with artificially seeded defects in the inner race and the outer race. This study also investigated how well to determine the most appropriate threshold level for counts parameter. Another study [191] used the AE waveform of the rolling element bearings to correlate the AE parameters and the actual geometric size of the defect. Incremental seeded defect sizes were introduced on the four tested bearings. Energy, maximum amplitude and AE burst were extracted for each defect size. Two speeds were used: 1500 and 3000 rpm. 2.7, 5.3 and 8 kN forces were applied in sequence and AE data was acquired at each load condition. It was concluded that the geometric defect size of the outer race defect was easier to be determine from the AE waveform than that of the inner race defects. The AE burst at 3000 rpm was also clearer than that at 1500 rpm. The amplitude of the AE burst also became higher as the load increased.

In practice, multiple defects occurred naturally in rolling element slew bearing. This means that an artificial single defect is not appropriate for slew bearings. An attempt to correlate AE with natural defect generation and location in rolling element bearings was made by Elforjani and Mba [122]. The focus is to detect and monitor the natural growth propagation and locate natural defect initiation of high speed rolling element bearings using AE measurements. The accelerated natural degradation of a bearing raceway was generated from a special purpose test-rig. It is worth noting that the research discussed in [122] extended the work of Yoshioka [226] which attempted to identify the onset of natural degradation in bearings with AE. However, the tested bearing used in [226] only had three rollers and this is not representative of a typical operational bearing. In another study, Elforjani and Mba [188] studied the correlation between AE activity and natural defect generation in slow speed rotating shafts by

monitoring the mechanical integrity of rotating shafts. A special test-rig was designed in the study to generate the experimental data.

The summary of the extracted information about the use of certain AE hit parameters in the literature are presented in Table 6.2. It can be seen that amplitude and RMS are the AE hit parameters that are most often used in rolling element bearings rotating at greater than 10 rpm. For the case of rotational speeds of less than 10 rpm, counts and amplitude are most commonly applied.

AE hit parameters are shown in Figure 6.1. The definition of the AE hit parameters and their application on AE signals at two different speeds are summarized in Table 6.2.

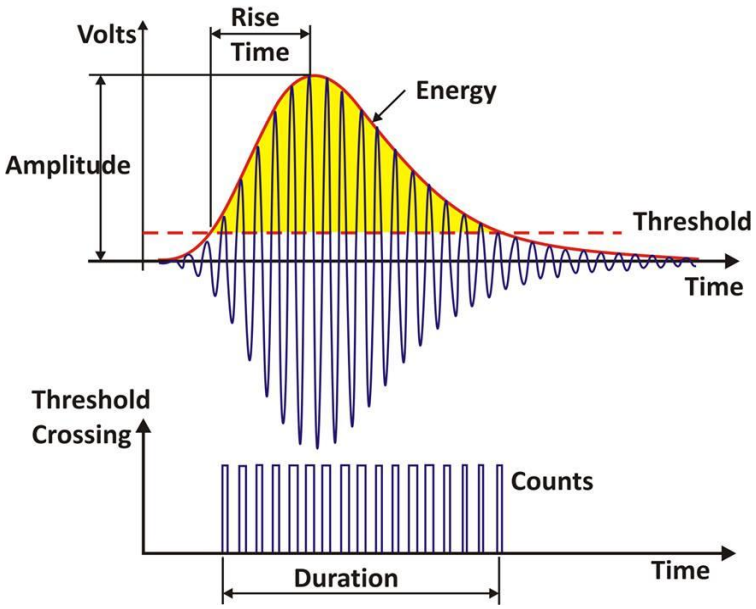

Figure 6.1 AE hit parameters on one event.

Table 6.2 Seven common AE hit parameters based on two speed classification.

AE parameters	Definition	Speed classification	
		< 10 rpm	> 10 rpm
Amplitude	The maximum (positive or negative) AE signal excursion during and AE hit [227]. The amplitude is expressed in dB using the relationship: $\mathrm{dB} = 20\log(\mathrm{V}_{\max}/1\mu - \mathrm{volt}) - (\mathrm{Preamp\,Gain})$	Refs. [190], [205], [228], [229], [230], [231], [232], [199]	Refs. [191], [192], [212], [207], [218], [221], [120], [233], [234], [214]
RMS	RMS is a measure of the continuously varying AE signal "voltage (V)" into the AE system [227]. The RMS of raw AE signal can be expressed as follows [235]: $AE_{RMS} = \sqrt{\frac{1}{T}\int_{t_0}^{t_0+T}\mathrm{V}^2(t)\,dt} = \sqrt{\frac{1}{N}\sum_{i=1}^{N}\mathrm{V}^2(i)}$ where V is the voltage signal from an AE sensor, t_0 denotes the initial time, T is the integration time of the signal, and N is the number of discrete AE data within the interval T.	Refs. [190], [206], [200], [228], [199]	Refs. [16], [38], [217], [200], [218], [221], [120], [233], [236], [237]
Energy	The integral of the square voltage signal over the duration of the AE hit [120], [227]. The numerical integration method within the time period (t_1, t_2) can be written as follows: $E \propto \int_{t_1}^{t_2}\mathrm{V}_{rms}^2\,dt = \int_{t_1}^{t_2}\mathrm{V}_{MS}\,dt$ $\mathrm{V}_{MS}(t) = \frac{1}{\Delta T}\int_{T}^{t+\Delta T}\mathrm{V}^2(\tau)\,d\tau$ where $V(t)$ is an AE signal and V_{MS} reflects the energy distribution of the AE signal [238].	Refs. [206], [228], [239], [199]	Refs. [188], [191], [122], [207], [221], [120], [233]
Counts	The number of detected AE signal excursion over the AE threshold. Also known as "ringdown counts".	Refs. [187], [190], [206], [199], [228],	Refs. [188], [219], [221], [120], [233],

		[229], [230], [231], [232], [239]	[214], [240]
Events	The phenomenon which releases elastic energy into the material, which then propagates as an elastic wave [23].	Refs. [190], [197], [228], [232]	Refs. [197], [220], [241], [240]
ASL	Average signal level (ASL) is a measure of the continuously varying and "averaged" amplitude of the AE signal [227]. ASL is defined as follows [242]: $ASL_{\mathrm{V}} = \frac{1}{T}\int_{t_0}^{t_0+T}\left\|\mathrm{V}(t)\,dt\right\| = \frac{1}{N}\sum_{i=1}^{N}\left\|\mathrm{V}(i)\right\|$ $ASL_{dB} = 20\log\frac{ASL_{\mathrm{V}}}{1\mu}$ where ASL_{V} is an average signal level in volts and ASL_{dB} is an average signal level in decibel (dB) .		Refs. [188], [221], [233]
AE Burst	A qualitative description of the discrete signal related to an individual emission event occurring within the material.		Refs. [191], [192], [234], [243], [216]

6.2.2 AE signal processing, feature extraction and pattern recognition

In very noisy environments, in order to extract the information to be used in fault detection of rolling element bearings, the AE signal needs to be further processed by AE signal processing, feature extraction or pattern recognition. Much research has been done to develop methods to process the raw AE signal. This research is summarised in Table 6.3. Some reviews can be summarised as follows:

AE signal processing methods

Cyclostationarity, a new method which has been used effectively for monitoring vibration signals [244], has been used for monitoring AE signals [203]. The construction

of cyclostationarity concepts is based on statistical moments. The latter are defined as mathematical expectations. The n^{th} order moment of a signal $x(t)$ is given by

$$m_n(t) = E\{x^n(t)\} \tag{6.1}$$

where E is the mathematical expectation. If this moment presents a periodicity T, the signal is considered to be cyclostationary at order n. Hence, one can write:

$$m_n(t) = m_n(t+T) \tag{6.2}$$

An interesting quantity deduced from the concept of statistical moments is the instantaneous autocorrelation defined by

$$R_{xx}(t,\tau) = E\{x(t-\tau/2)x^*(t+\tau/2)\} \tag{6.3}$$

where x^* denotes the conjugate of x. The autocorrelation function expresses the internal similarity of the signal at two instants taken with a lag τ.

The implementation of wavelet packet decomposition together with Hilbert Huang transform (WPD – HHT) for spindle bearings condition monitoring was presented by Law et al. [215]. This method is used to extract the crucial characteristics of AE data and correlate them with spindle running condition. The focus of the study is to detect the fault frequencies of the bearings under different load and running times. Other established methods for AE such as Wigner-Ville distribution (WVD), wavelet scalogram and adaptive line enhancer (ALE) have been presented by Bin et al. [245], He et al. [246] and Shiroshi et al. [247], respectively. The time-frequency method, WVD, is considered by He et al. [245] because the AE signals exhibit a multi-frequency, multi-mode and multi-modal spectrum. Hence, WVD can be used to extract the characteristic signals acquired from the multi-frequency AE signal [245]. Eftekharnejad et al. [80] presents the applicability of AE and vibration technology in monitoring naturally degraded rolling bearings. They also investigate the comparative effectiveness of applying the kurtogram to both vibration and AE data from a defective bearing. Spectral kurtosis (SK) is applied in the paper. It is based on the transformation of the signal into the time-frequency domain using short-time Fourier transform (STFT). SK is also used as a de-noising technique to improve the signal-to-noise ratio of AE and the vibration signal. To date, the most comprehensive calculations of SK have been developed by Antoni [248] as the fourth order cumulant of the spectral moment (*K*):

$$K_y(f) = \frac{S_{4Y}(f)}{S_{2Y}^2(f)} - 2, \quad f \neq 0 \tag{6.4}$$

and

$$S_{nY}(f) \overset{\Delta}{=} \left\langle |Y_W(t,f)|^n \right\rangle \tag{6.5}$$

$Y_W(t,f)$ is estimated using the STFT:

$$Y_W(t,f) \overset{\Delta}{=} \sum_{-\infty}^{\infty} Y(n)W(n-t)e^{-j2\pi nf} \tag{6.6}$$

where $Y(n)$ is the sampled version of the signal, $Y(t)$, and $W(n)$ is the window function having zero value outside a chosen interval. For the above calculations to be valid, the size of window $N(w)$ must be smaller than the length between two consecutive impulses [80].

A new signal processing method for low speed bearings, the peak-hold-down-sample (PHDS) algorithm, was developed by Lin et al. [209]. The method is useful to overcome the problem of large data size acquired from AE measurement with high sampling rates in low speed machine applications. The PHDS algorithm is an improvement on the traditional down-sample process in signal processing which selects the n^{th} sample at equal intervals. Besides, it discards the rest of the samples from the original data to reduce the data size. The PHDS method is effectively the same as the Piecewise Aggregate Approximation (PAA) method presented in Chapter 4. The difference is that the PHDS method takes the peak value between samples rather than the mean value. A mathematical description of the down-sampled data series of an original discrete data series [209], $s(t) = [s(t_0), s(t_1), s(t_2), \ldots, s(t_i), \ldots]$, $0 \le i \le N-1$, can be written as:

$$S(T) = [S(T_0), S(T_1), S(T_2), \ldots, S(T_j), \ldots], \; 0 \le j \le M-1, \tag{6.7}$$

where $M = \text{int}(N/r)$ and $r = f_o / f_d$ is the down-sample ratio. $f_o = 1/(t_{i+1} - t_i)$ is the sampling frequency of the original data and $f_d = 1/(T_{j+1} - T_j)$ is the sampling frequency of the down-sampled data series.

PHDS algorithm comprises of data segmentation step and enveloping method. The data segment described in [209] is given by

$$X(T_j) = [s(t_i), s(t_{i+1}), s(t_{i+2}), \ldots, s(t_{i+r})], \tag{6.8}$$

where $t_i \geq T_j$ and $t_{i+r} < T_{j+1}$.

The enveloping method consists of three steps: (1) data rectification, (2) Hilbert transformation to obtain the imaginary component to form the envelope and (3) fast Fourier transform (FFT) to obtain the power spectra of the envelope signals.

The main parameter of the PHDS algorithm is the down-sample ratio, *r*, which is the ratio between the sampling frequency of the original data and the sampling frequency of the down-sampled data series. The results show that the PHDS algorithm can reduce the size of data while retaining the critical bearing defect information such as ball pass frequency outer race (BPFO), ball pass frequency inner race (BPFI) and fundamental train frequency (FTF). However, there is no further explanation for how the down-sample ratio is determined.

AE feature extraction methods

A number of methods have been used for feature extraction of rolling element bearing AE signals. Some of them adopt established methods such as auto-regression (AR) coefficients [198, 201], complex Morlet wavelet [249], Mahalanobis distance [250] and zero-inflated Poisson (ZIP) regression [214], approximate entropy (ApEn) [251]. Others have proposed new methods such as energy index (EI) technique [211], short-time energy function [252], peak ratio (PR) [253] and ratio of AE mean and AE standard deviation [254]. The present study does not include discussion on the first four of these methods.

ApEn is one of the phase-space dissimilarity measures [155] that can be used to compute the value of the regularity in the vibration signal. A smaller value indicates more regularity and a higher value indicates less regularity in the vibration data set [155]. ApEn is based on phase-space or reconstruction vectors. Suppose $\mathbf{Y} = (y_1, y_2, ..., y_N)$ is the original time series or vibration signal in one second with sampling rate, N, then the phase-space of the original time series can be defined as follows:

$$\mathbf{X}=\begin{bmatrix} y_1 & y_{1+J} & y_{1+2J} & \cdots & y_{1+(m\ 1)J} \\ y_2 & y_{2+J} & y_{2+2J} & \cdots & y_{2+(m\ 1)J} \\ y_3 & y_{3+J} & y_{3+2J} & \cdots & y_{3+(m\ 1)J} \\ . & . & . & & . \\ . & . & . & & . \\ . & . & . & & . \\ y_M & y_{M+J} & y_{M+2J} & \cdots & y_{M+(m\ 1)J} \end{bmatrix} \tag{6.9}$$

where J represents reconstruction delay and can be computed by time lag $/\Delta t$, m represents the embedding dimension and M represents the number of reconstructed vectors. The relation between N, J, m and M can be defined in the following form: $N=M+(m\text{-}1)J$ or $M=N\text{-}(m\text{-}1)J$. The dimension of phase-space is a $M\times m$ matrix. According to [251], the initial step of approximate entropy is to measure the distance between two vectors $X(i)$ and $X(j)$ which can be defined as the maximum difference in their respective corresponding elements:

$$d[X(i),X(j)]=\max_{k=0,1,2,\ldots,m-1}(|x(i+k)-x(j+k)|) \tag{6.10}$$

where $i=1,2,\ldots,N-m+1$, $j=1,2,\ldots,N-m+1$ and N is the number of data points that are contained in the time series. For each vector $X(i)$, a measure that describes the similarity between the vector $X(i)$ and all other vectors $X(j)$, where $j\neq 1$ can be constructed as

$$C_i^m(r)=\frac{1}{N-(m+1)}\sum_{j\neq i}\Theta\{r-d[X(i),X(j)]\} \tag{6.11}$$

where $j=1,2,\ldots,N-m+1$ and the Heaviside step function, $\Theta(x)$ is similar to the symbol in correlation dimension where $\Theta(x)=0$ if $X\leq 0$ and $\Theta(x)=1$ if $X>0$.

The symbol r in (K) denotes a predetermined tolerance value, defined as

$$r=k.std(\mathbf{Y}) \tag{6.12}$$

where $std(\mathbf{Y})$ is the standard deviation of original time series or AE signal, $\mathbf{Y}$, and k is a constant $(k>0)$. By defining

$$\phi^m(r)=\frac{1}{N-m+1}\sum_i \ln\left[C_i^m(r)\right],\quad i=1,2,\ldots,N-m+1 \tag{6.13}$$

the ApEn value of time series can be calculated as

$$ApEn(m,r)=\lim_{N\to\infty}[\phi^m(r)\text{-}\phi^{m+1}(r)] \tag{6.14}$$

For practical applications, a finite time series consisting of N data points is used to estimate the ApEn value of the time series, which is defined as

$$ApEn(m,r,N) = \phi^m(r) - \phi^{m+1}(r) . \quad (6.15)$$

An alternative feature extraction method, the energy index (EI) technique, was introduced by Al-Balushi et al. [211]. This method is used to detect the early symptoms of defects from the masked AE signatures. The identification of the earliest signs of damage can be achieved by improving the signal-to-noise ratio. However, the high sampling rates of the AE signal is a significant problem. Thus, the EI technique overcomes the problem by conducting subsequent signal processing. In addition, the EI technique is defined as a square of the RMS ratio of a part of a signal to the RMS of the entire signal. It was found that the EI technique works successfully in detecting the AE bursts associated with seeded bearing defects. The EI is expressed by the following equation:

$$\text{Energy Index (EI)} = \left(\frac{\text{RMS}_{\text{segment}}}{\text{RMS}_{\text{total}}} \right)^N \quad (6.16)$$

where N is the power of EI. In case of bearing signal, N is selected of 10 [211].

The EI value for a stationary signal is expected to be 1.0. For a signal with transient or non-stationary activities, the EI value will be higher than 1.0. The higher the value of the EI, the higher the energy activity is in a specific segment. However, there is no further discussion on how to determine the segment for calculating the $\text{RMS}_{\text{segment}}$. Future study on the EI technique for the low speed bearings is required as this method has been employed for bearings running at speeds greater than 1000 rpm. This method is also suitable for the AE signal with one periodic impulse generated by a single defect. For multiple defects, the method needs to be tested.

Because the bearing AE signal has significant fluctuations in the peak amplitude of the signal and there is also considerable frequency variation content, the short-time energy function method was proposed by Li and Li [252]. The source of these time-dependent variations is the periodic impulses generated by a damaged bearing. To extract these meaningful impulses which change relatively slowly over time, short

segments of the bearing signal are used and processed. Such processes produce a new time-dependent sequence which can serve as a representation of the signal [252]. The formula for the short-time energy function is:

$$E(n) = \sum_{m=-\infty}^{\infty} x^2(m)\, w(n-m) \tag{6.17}$$

where $x(n)$ is the sampled signal and $w(n)=1$ if $0 \le n \le N-1$, $w(n)=0$ otherwise (N is the width of window). This method has been tested for AE signals with obvious periodic impulses generated by a seeded defect bearing running at high speed i.e. 2200 rpm. However, the selection criteria for N must be explained and the application of this method for low speed bearings also requires further study.

A peak ratio (PR) feature was proposed by Kim et.al. [253]. PR is the formula derived from the average of the defect frequency and the peak harmonic value. The PR is given in terms of dB and can be expressed as follows:

$$PR = 20\log_{10} \frac{\sum_{j=1}^{n} (P_j - A_s)}{A_s} \tag{6.18}$$

A simple AE parameter defined by the ratio of AE mean, μ and AE standard deviation, σ formulated as μ/σ has been proposed by Niknam et al. [254]. The parameter was tested in dry and lubricated bearings. Radial loads were varied for 2268, 4537, 6805 and 9073 N. Each test on one load, the rotational speed was increased incrementally from 10, 20 to 100 Hz. The results show that the calculated parameters of lubricated bearing case were higher in most tests than the parameters of dry bearing.

AE pattern recognition methods

Compared to the previous two categories, there has not been research conducted in this category. Fuzzy *c*-mean for bearing condition monitoring using AE has been studied [213]. The application of the relevance vector machine (RVM) and the support vector machine have been studied [19, 212]. Recent AE-based fault diagnosis and clustering methods have also been studied [238, 255]. An AE-based fault diagnosis method using asymmetric proximity function combined with *K*-nearest neighbour (APF-KNN) has been presented [238]. The AE signal was processed initially using HHT to estimate the intrinsic mode functions (IMFs). A number of statistical and acoustic

features were also calculated from the IMF signal. The sensitive features are selected using KNN. A number of classifiers were compared to APF-KNN. The result showed that the APF-KNN is the most efficient supervised learning classifier compared to seven supervised classifiers. In [255], the adaptive sequential *k*-means (ASK) clustering algorithm was presented.

Table 6.3 Classification of AE-based condition monitoring and fault diagnosis methods.

Category 1: Signal processing methods	Category 2: Feature extraction methods	Category 3: Pattern recognition methods
Cyclostationary [203].	Auto-regression (AR) coefficients [198], [201].	Fuzzy *c*-mean clustering [213].
Wavelet packet decomposition – Hilbert Huang transform (WPD-HHT) [215].	Approximate entropy [251].	Relevance vector machine (RVM) and support vector machine (SVM) [19].
Kurtogram-based short-time Fourier transform (STFT) [80].	Energy index (EI) technique [211].	Multi-class RVM [212].
Peak-hold-down-sample (PHDS) algorithm [209].	Complex Morlet wavelet [249].	Asymmetric proximity function combined with *k*-nearest neighbour (APF-KNN) [238].
Self-adaptive noise cancellation (SANC), spectral subtraction and wavelet denoising [210].	Short-time energy function, short-time average zero crossing rate and median smoothing [252].	Adaptive sequential *k*-means (ASK) clustering algorithm [255].
Spectral kurtosis [256].	Peak ratio (PR) [253].	
Wigner-Ville distribution [245].	Zero-inflated Poisson (ZIP) regression [214].	
Wavelet scalogram [246].	Mahalanobis distance [250].	
Adaptive line enhancer (ALE) and high-frequency resonance technique (HFRT) [247].	Ratio of AE mean and AE standard deviation [254].	

6.3 Results and discussion

6.3.1 AE hit parameters

Detailed AE experiment has been presented in Chapter 3. During the experiment from April 2013 to January 2014 (285 days), AE hit parameters: counts, energy, duration, amplitude, ASL and RMS were extracted from AE signals acquired from clockwise and anti-clockwise measurement. The user selection of these parameters is available in the AEwin software set-up prior to the experiment. The results produce minimum, maximum and average values. The average values were collected and are presented in this chapter. The illustration and the definition of the AE hit parameters used here have been presented in Figure 6.1 and Table 6.2, respectively. The additional parameter used in this study is defined as follows:

- Duration – the time from the first threshold crossing to the end of the last threshold crossing, such as the parameter duration which was used by [214] and [199].

Six AE hit parameters are presented in Figure 6.2. It can be seen that all parameters detected significant changes on the 254th day. After the first significant changes, the parameters show fluctuation and some remain at a level far above the normal average level. This indicates that the condition of the slew bearing had deteriorated. Although the selected AE hit parameters can detect the incipient fault of the slew bearing, the change is too sudden for a maintenance engineer to prepare for the maintenance work. This demonstrates the necessity for the present study. Furthermore, the levels of all AE hit parameters between channel 1 and 2 are different. The parameters levels produced from channel 2 are higher than that of channel 1. This could be due to the eccentric load applied on the slew bearing. It should be noted that eccentric load is the typical loading condition in practice. The maximum differences between channel 1 and 2 were shown in energy and RMS parameters. Moreover, the amplitude parameter was the noisiest parameter.

According to the review of AE hit parameters presented in Table 6.2, counts and amplitude are the most commonly used parameters for rolling element bearings rotating at less than 10 rpm. To observe the damage, the daily AE measurement of the

slew bearing was shut off on 1 February 2014 and the slew bearing was dismantled after that. The wear condition of the inner raceway, outer raceway and roller are presented in Chapter 5.

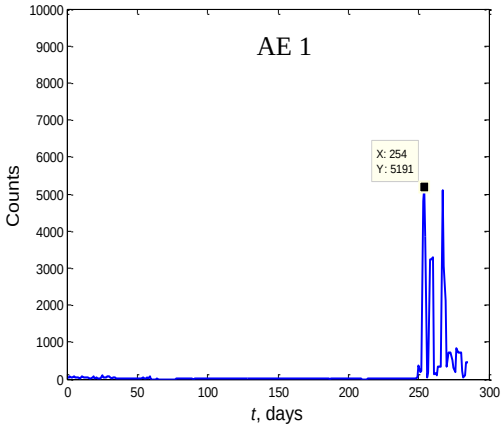

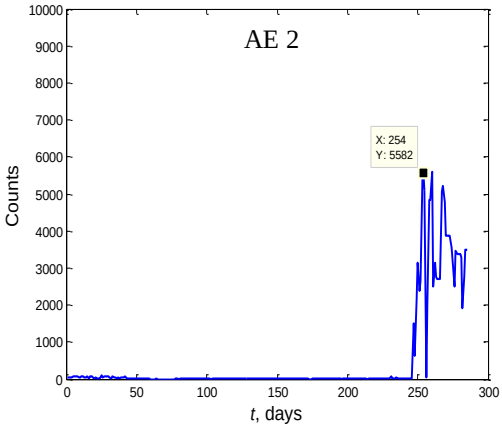

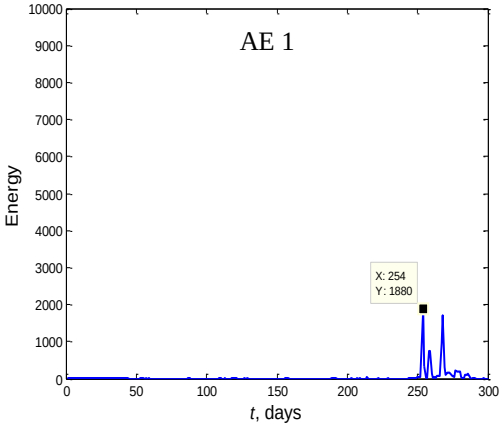

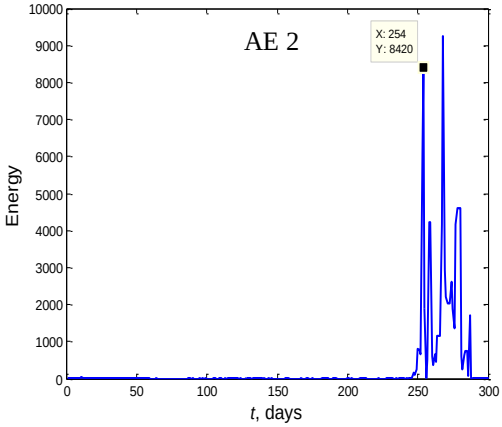

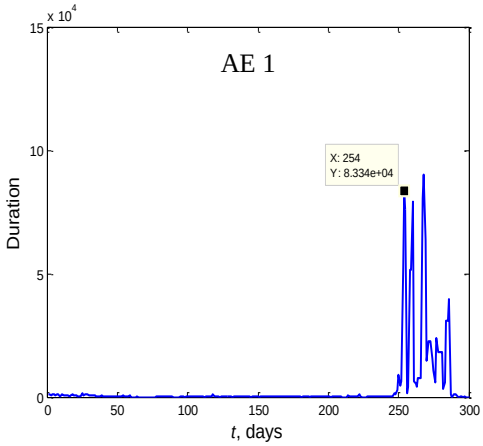

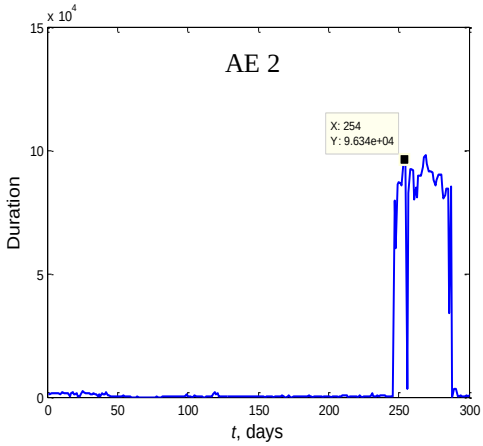

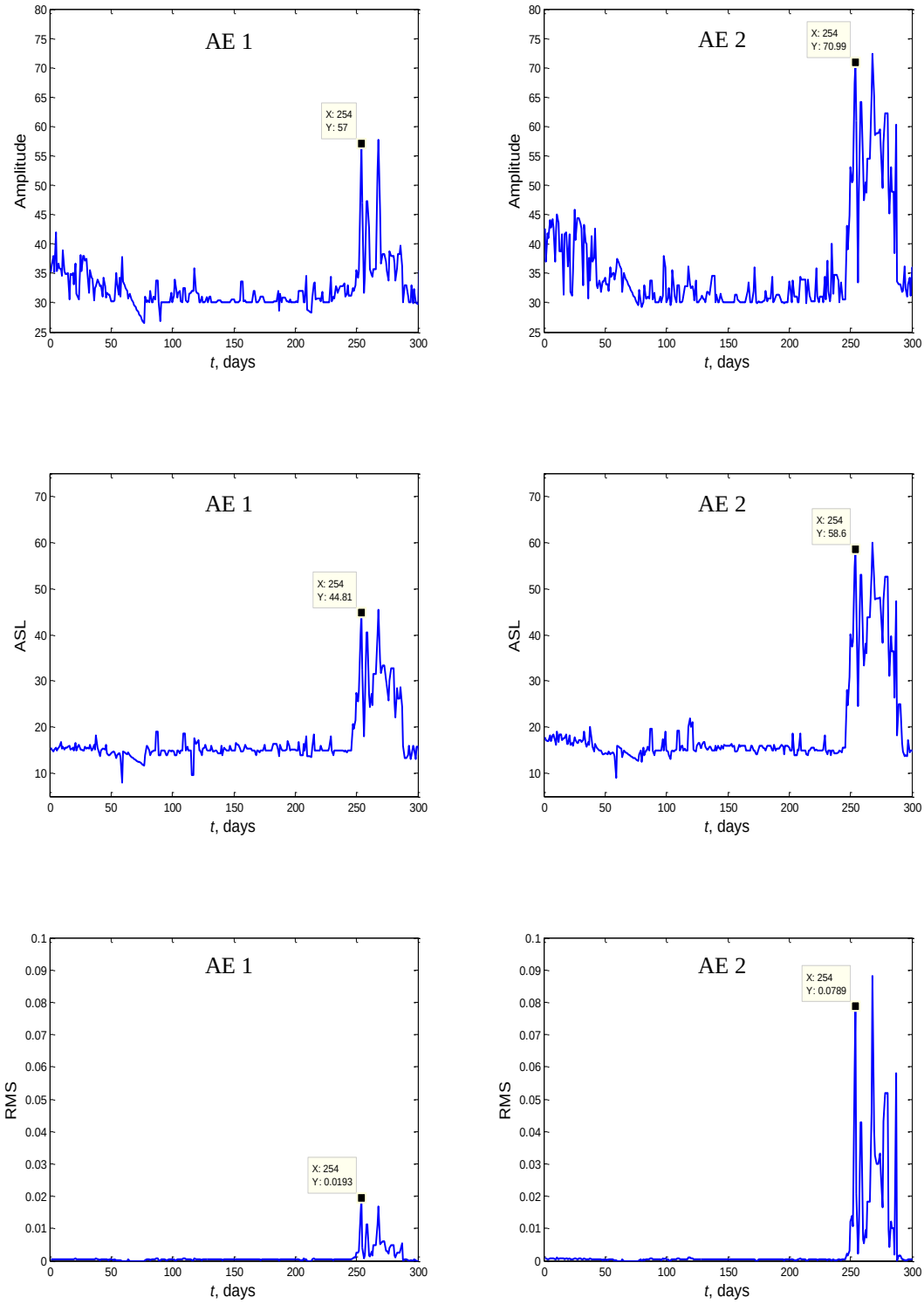

Figure 6.2 AE hit parameters extracted from AE data at clockwise rotational direction.

6.3.2 Complexity analysis of AE signals

In most applications, AE hit parameters are the most commonly used to detect the incipient damage and to evaluate the damage progression [251]. However, AE hit

parameters are related to the absolute energy level of the measured waveform which relies on a pre-set amplitude threshold [257]. The threshold set for the AE signal relies on the operator's experience. AE hit parameters also produce a rough evaluation and approximate description of the AE signal, and thus cannot be used to analyse more detailed AE characteristics. The AE signals generated by the elastic impulse and strain due to the contact mechanism between rolling elements are paroxysmal and non-linear [251]. Therefore, nonlinear parameter estimation methods can be used to extract defect-related features hidden in such an AE signal [251]. Due to the limitation of the AE hit parameters, it is required to have an alternative feature independent of absolute energy levels and sensitive to chaotic data emanating from a nonlinear system. A number of related studies have been conducted. These studies have applied several methods such as correlation dimension [105, 258-261], approximate entropy (ApEn) [251], Kolmogorov entropy [105], Kolmogorov-Smirnov (KS) test [113, 257, 262] and largest Lyapunov exponent (LLE) [105, 260, 261].

Complexity analysis of AE signals in civil engineering, tool machining and steel rubbing

The use of the correlation dimension for AE signals in the field of civil engineering, especially in construction materials, has been presented by Kacimi and Laurens [258]. In another study, the combination of wavelet multi-resolution and correlation dimension for AE signals from machine tools is proposed by Song et al. [259]. The study shows the correlation dimension of worn tools is greater than that of sharp tools. The larger values of the correlation dimension indicate that the AE signal from worn tools is more chaotic or complex than that from sharp tools. A similar study which used the correlation dimension for the AE signal from tool wear is presented by Xi et al. [260]. The AE signal has been acquired from different periods during the cutting process. The authors also use the LLE. The trend of correlation dimension and the LLE qualitatively describe the chaotic characteristic of the AE signal. Li and Chu [263] proposed the use of ApEn to analyze the AE signal from the cracks in the steel tube and to identify the cracked state. The first known attempt to apply the KS test for an AE signal was presented by Hall et al. [257]. The KS statistic for the examination of the AE signal has been generated by partial rubbing between a rotating central shaft and the surrounding stationary components in a gas turbine. This demonstrated that

the KS feature is able to identify different classes of shaft-seal rubbing. The KS feature results are compared to statistical moment features such as RMS, median and kurtosis, and AR coefficients.

Complexity analysis of AE signals in rolling element bearing application

Recent research discusses the use of the correlation dimension, the LLE and Kolmogorov entropy in the vibration signals of rolling bearing [105]. In other studies, Ghafari et al. [261] investigated the effect of localized faults on chaotic vibration of rolling element bearings based on the correlation dimension and the LLE. The use of a KS test based on the AR model to estimate the performance degradation of rolling bearings is proposed by Cong et al. [113]. The method is applied to vibration data over a whole bearing service life (normal-fault-failure) collected from a bearing accelerated life test. Yan and Gao [264] have investigated the use of ApEn in vibration rolling element bearings with different defect severities, under different rotational speeds and loading conditions. The effect of ApEn parameters such as data length and dimension on the ApEn values has also been investigated.

As indicated in the above literature review, chaos and/or complexity analysis has been effectively conducted for the vibration signal of rolling element bearings. However, the chaos analysis in rolling element bearing AE signals has not been widely studied. Only one study has been found on the use of ApEn in the AE signal of rolling element bearings [251]. The authors introduce the ApEn to analyze the AE signal generated by the rolling element bearing defects. The sensitivity of ApEn to the different running conditions of the bearings such as different rotational speeds and different loads was investigated. The selection of ApEn parameters i.e. embedded dimension m and tolerance r, is also investigated. The bearings under test are artificially seeded with defect sizes of 3 mm and 5 mm diameters. This work shows that ApEn is also effective for the AE signal of rolling element bearings. Wavelet transform (WT), a pre-processing method, was employed for de-noising. The combined ApEn and WT is applied to identify the differences between the normal bearing and the artificially damaged bearing. Further study on bearing with a natural defect, especially the study on the transition period from normal to damage condition, is required.

Complexity analysis of AE signals based on LLE feature extraction

In a previous study by the writer [186], LLE has been applied to the vibration signal of low-speed slew bearings. It has been shown that the LLE can extract the key feature related to the degradation. LLE also demonstrates better tracking of the progressive deterioration of the bearing during the 139-day measurement than comparable methods such as statistical moment feature extraction from the raw vibration signal and empirical mode decomposition (EMD). The theoretical background and the procedure of LLE feature extraction can be found in [186]. In this paper, the LLE feature is used in the AE signal of reversible slew bearings. The AE signal measurement consists of clockwise and anti-clockwise rotation. Each measurement consists of three stages: (1) the deceleration to acceleration stage; (2) the stationary stage; and (3) the second deceleration to acceleration stage. Each whole measurement, from stage (1) to (3), is acquired over approximately 30 seconds. This process is presented in Figure 6.3 which shows one example of the AE signal when the bearing was still in the normal state on 11 April 2013. Electronic noise as seen in the last figure of Figure 6.3 is difficult to be avoided in practice. In case of low speed slew bearing, the noise signal amplitude is higher than the bearing signal amplitude when the bearing is in normal condition (e.g. 30 May 2013). However, when the bearing starts to deteriorate or already in defect condition (e.g. 24 December 2013), the bearing signal amplitude is higher than the noise signal amplitude. This is illustrated in Figures 6.4 – 6.5.

The present study conducted a complexity analysis in the acceleration stage. Prior to the LLE feature extraction, a simple method is developed and used to identify the transition position of a certain point between deceleration and acceleration (stage 1). The method consists of finding the samples above the zero mean, setting up minimum and maximum levels based on the RMS level, differentiating the samples and the matrix rotation. This calculation is necessary for identifying the starting point of the accelerate stage from the AE waveform as can be seen in Figure 6.3. When the bearing starts to deteriorate, the identification of the starting point of the accelerate stage will be more difficult because the impact due to the contact between the rolling element and the defect generates high amplitude and high frequency signal as shown in Figure 6.5. The other reason is that the robust condition monitoring method requires less

operator involvement in the data processing step. For this reason, 10,000 AE waveform samples were separated and fed into the LLE feature extraction. The number of samples chosen, i.e. 10 000, was determined based on the selection of one LLE parameter and this will be discussed later. The plot of 10 000 samples for LLE input can be seen in Figure 6.3 prior to LLE feature extraction.

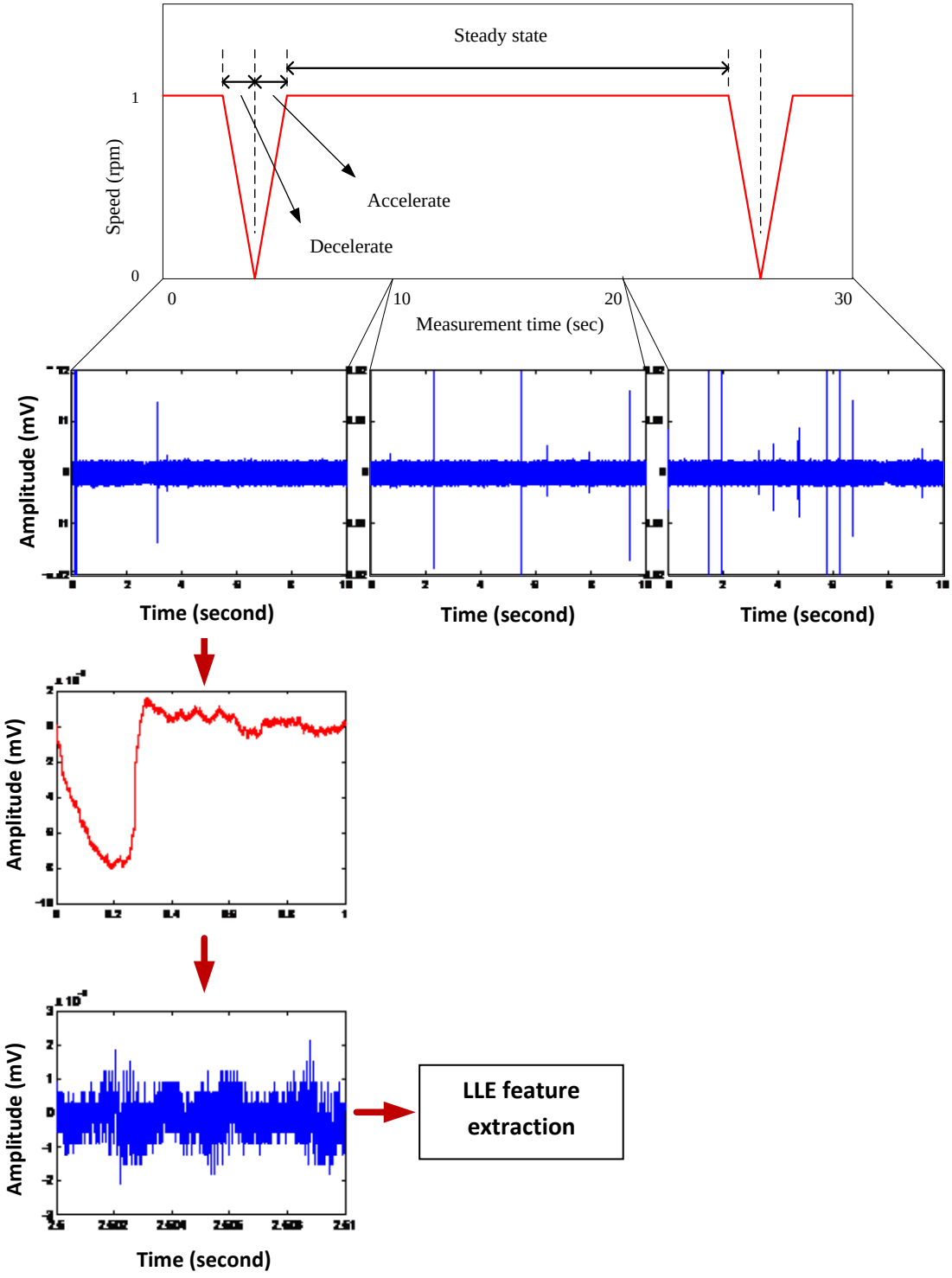

Figure 6.3 Illustration of one AE measurement in a clockwise rotation.

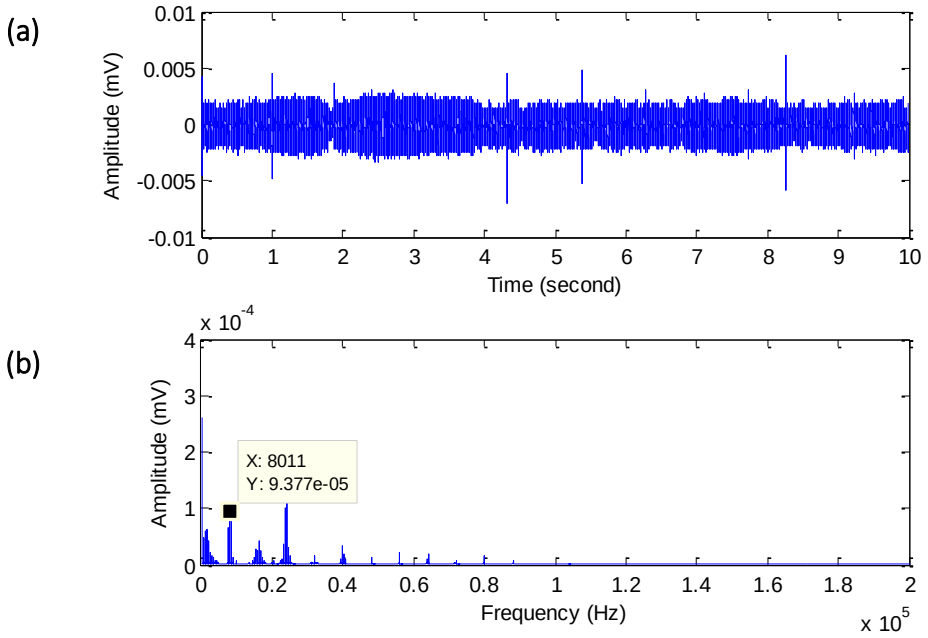

Figure 6.4 (a) AE signal on 30 May 2013; (b) FFT.

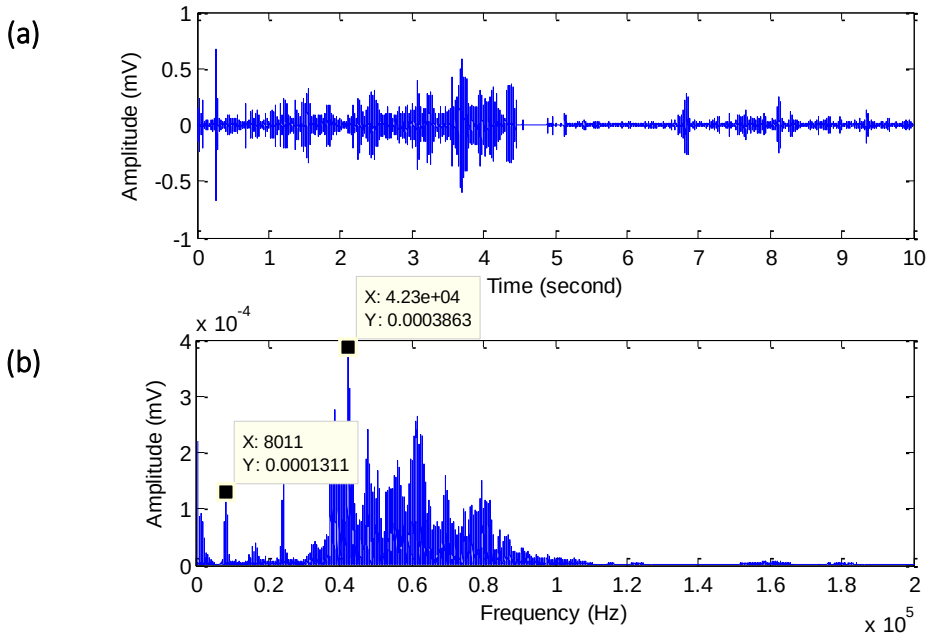

Figure 6.5 (a) AE signal on 24 December 2013; (b) FFT.

Because LLE feature extraction is based on the phase-space matrix, the most important phase-space parameter is the reconstruction delay, J. According to the previous study of the writer [186], J is determined based on the dominant frequency of the FFT of the vibration signal. It can be seen from Figure 6.4 that the dominant frequency is 8011 Hz, thus J is estimated according to the following formula [186]:

$$J = \frac{1}{f_1} sf \tag{6.19}$$

where f_1 is the dominant frequency of the FFT result ($f_1 = 8011$) and sf is the sampling frequency ($sf = 1\text{MHz}$). Then, J is computed to be 125. Other parameters such as N are calculated using 0.01 times sf equal to 10000, $m = 50$ and $\mu = 25$. The 0.01 second is selected according to the computational time. Because of the large AE signal sampled at 1MHz, minimum samples for LLE input are necessary to reduce the computation time. To overcome this problem, this paper employs the LLE algorithm proposed by Rosenstein et al. [265] which is suitable for small samples of data sets. LLE feature extraction is used for 285-day measurement. The LLE feature is presented in Figure 6.6. Because most damage occurs on the side where eccentric loading is applied, this paper only presents the LLE feature of AE channel 2. From the LLE feature result, it can be seen that the incipient fault can be identified on the 247th day, which is on 16 December 2013. The LLE feature can identify the incipient fault 7 days earlier that the AE hit parameters which detect the incipient fault on day 254. The progression trend of the LLE feature is also shown to increase gradually rather than jump significantly as illustrated in the AE hit parameters.

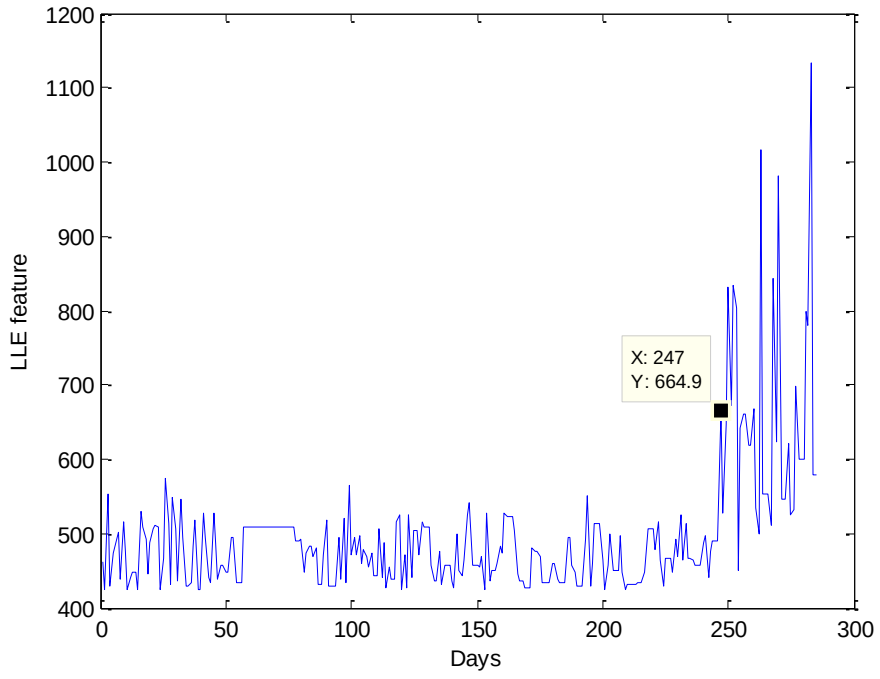

Figure 6.6 LLE feature of AE channel 2.

In case of AE signal, the frequency of 8011 Hz is identified in the FFT spectra of all signals. Two representative data from 285-day measurement are presented in Figure 6.4 and Figure 6.5 which clearly display the frequency 8011 Hz. It noted that the rest data are similar which also display the frequency 8011 Hz. When the bearing condition is changed, the frequency of 8011 Hz in no longer dominant as shown in December 24, 2013 (Figure 6.5). The spectra in December 24, 2013 shown that the frequency of 8011 Hz is changed to 42300 Hz. It should be noted that both frequencies are below the nominal lower limiting frequency (200 kHz) of the transducer. These frequencies presumed to be the resonance frequency excited by the contact between rolling elements. When surface material of the bearing deform due to high applied load and high friction, it actually excite the high frequency content. However, this high frequency content has short period, and thus it is not appear dominantly in FFT. This can be seen in the FFT in December 24, 2013 that frequency of approximately 160000 Hz and 180000 Hz can be seen even in low energy. This also prove by the result of AE hit parameter presented in Figure 6.2 where all AE-hit parameters jumped significantly after December 24, 2013. The AE hit parameters are usually used to captured the high frequency content due to the deformation and crack. In addition, although the frequency of 8011 Hz and 42300 Hz are below the frequency range of the transducer, the transducer still can pick this frequency as indicated in the Appendix E.

6.4 Conclusion

The application of AE for low speed reversible slew bearings has been proposed in this chapter. The study focuses on investigation of AE features as condition monitoring parameters for slew bearing with a natural defect. Review of previous research indicated that there has not been much work done on the application of AE for very low-speed bearings with naturally occurring damage.

From the experimental study of low speed slew bearing with accelerated defect, two primary conclusions can be drawn:

1. The investigation of AE hit parameter results shows that the counts, energy, duration, amplitude, ASL and RMS effectively identify significant change in the slew bearing condition. These changes, however, are too sudden and this means

that they cannot provide the maintenance engineers with adequate information in practice.

2. Due to the limitation of the AE hit parameters in certain cases, some researchers have considered alternative feature extraction methods e.g. approximate entropy and energy index. For AE signal origination from low speed bearing, approximate entropy as a complexity measure has been considered as a reliable feature in the literature review. However, this method needs further study on its application at very low speed with naturally defective bearings.
3. The analysis of rolling element bearing AE signals revealed that the LLE feature can be considered as an alternative feature extraction method. However, the time computation of the LLE feature extraction has an undesirable side-effect. The more samples used for the LLE input, the more accurate the result, but the more computation time will be required.

Manuscript based on this chapter has been submitted to the Mechanical Systems and Signal Processing Journal with the following title:

- W. Caesarendra, B. Kosasih, A.K. Tieu, H. Zhu, C.A.S. Moodie, Acoustic emission-based condition monitoring methods: Review and Application for low speed slew bearing, (under review in Mechanical Systems and Signal Processing Journal, Paper ID MSSP14-741).

Chapter 7 - Prognostic method for slew bearing

"If you can't explain it simply, you don't understand it well enough"
(Albert Einstein)

7.1 Review on prognostic methods

Literature reviews presented in Chapter 2, 4 and 6 indicate that current research still focuses on the slew bearing condition monitoring and fault diagnostics. There has not been much work done on the low speed slew bearings prognostics, especially on the study of the entire life cycle of slew bearings. Prognosis is a composite word consisting of Greek words pro and gnosis, literally translated into the ability to acquire knowledge (gnosis) about events before (pro) they actually occur. Prognosis (also called prognostics) can be defined as the ability to assess current conditions of part or system, observe future conditions of the part or system and predict the time left before catastrophic failure occurs. As in diagnostics, most prognostic methods focus on the degradation models and performance assessment based on feature extraction [266]. The feature extraction of slew bearing review and study has been presented in Chapter 2 and Chapter 4. The degradation models as a prediction object of prognostic method are based on these appropriate and reliable features.

In addition, prognostic methods are usually applied to predict the lifetime of rotating components, which generally can be divided into two stages. The first stage referred to normal zone where no significant deviation from the normal operating state observed. The second stage is abnormal zone; this stage is initiated by potential failure and progressively develops into actual failure [7]. It is on the second stage that prognostic methods are usually applied to predict unexpected failure in time basis from the incipient or impending damage using either event data or condition monitoring (CM) data.

In order to select an appropriate prognostic method for slew bearing, a review of existing prognostic methods is first presented in this chapter. The review consists of two parts: (1) a brief review on classification of prognostic approaches and (2) a review on prognostic methods for rolling element bearings.

7.1.1 Classification of prognostic approaches

There have been many papers that reviewed the prognostic approaches for rotating machineries [266-273]. For example, Lee et al. [266] reviewed prognostic methods for critical components such as bearing, gear, shaft, pump and alternator. The authors classified the prognostic approaches into three, namely model-based, data-driven and hybrid prognostic approaches. However, the classification does not include complete methods on each prognostic approach. In their work, two methods were classified into model-based approaches i.e. alpha-beta-gamma tracking filter and Kalman filter, while neural network (NN), fuzzy logic and decision tree are included in data-driven approach.

Another review paper by Jardine et al. [267] presented clearer classification in prognostic approaches, but the discussion on rotating machinery diagnostics was more dominant than the discussion on machinery prognostics. The authors classified the prognostic approaches into three groups: statistical approaches, artificial intelligent (AI) approaches and model-based approaches. The statistical approaches include statistical process control (SPC), logistic regression, autoregressive and moving average (ARMA), proportional hazard model (PHM), proportional intensity model (PIM) and hidden Markov model (HMM). In AI techniques, e.g. artificial neural network (ANN) and its sub-classes such as self-organising neural networks, dynamic wavelet neural networks and recurrent neural networks, back propagation neural network and neural-fuzzy inference systems are still commonly used in AI prognostics. Among model-based approaches, defect propagation models via mechanistic modelling and crack growth rate model are the commonly used methods.

A popular review paper on prognostic methods was presented by Heng et al. [271] . The authors broke down the methods for predicting rotating machinery failure into two categories: physics-based and data-driven prognostic models. A number of papers

focusing on physics-based prognostics which used Paris' formula are still found to be dominant [271]. Other methods such as finite element analysis (FEA) to calculate stress and strain field, and Forman law of linear elastic fracture mechanics are also classified in physics-based approaches. Similar to the result from two review papers mentioned previously, ANN and its variants is currently the most commonly used method classified in the data-driven prognostic. Other methods such as fuzzy logic, regression analysis, particle filtering, recursive Bayesian technique and HMM are also included in data-driven prognostic methods. However, a number of methods classified in data-driven methods as presented in [271] need more sub-classification e.g. artificial intelligence or statistical approaches.

A list of literatures which reviewed the prognostic approaches is presented in Table 7.1. The table provides the year of publication and the classification groups of prognostic approaches.

Although the merits and the demerits of prognostic approaches have also been presented in Lee et al. [266] and Heng et al. [271], to date there have been scientific gaps of prognostics reviews. They are (1) *the classification of prognostics approaches that remain unclear*: many review papers presented different classifications as seen in Table 7.1 and sometimes the classified methods in each approach are overlapping depending on the authors; and (2) *in what applications can certain prognostic approach be used*: the prognosis literature provides few information to help typical industry users in selecting an appropriate approach or method for their specific needs. This chapter aims to bridge the gap by providing another classification of prognostic approaches. Such approaches include the basic prognostic method selection for specific needs (shown in Figure 7.1) and the classified methods of each prognostic approach as presented in Section 7.2.2.

Table 7.1 Classification of prognostic approaches extracted from literatures.

No	Author	Refs.	Year	Classification groups
1	Lee et al.	[266]	2014	- Model-based - Data-driven - Hybrid prognostics approaches
2	Jardine et al.	[267]	2006	- Statistical approaches - Artificial intelligence approaches - Model-based approaches
3	Kothamasu et al.	[268]	2006	- Reliability-based - Model-based - Signal-based - Statistical
4	Goh et al.	[269]	2005	- Data-driven - Model-based
5	Vachtsevanos et al.	[270]	2006	- Data-driven - Experience-based - Model-based (Physics of failure)
6	Heng et al.	[271]	2009	- Physics-based prognostics models - Data-driven prognostics models
7	Peng et al.	[272]	2010	- Physical model-based methodology - Knowledge-based methodology - Data-driven methodology - Combination model
8	Dragomir et al.	[273]	2009	- Model-based approaches - Data-driven approaches
9	Hines et al.	[274]	2008	- Time-to-failure data-based prognostics - Stress-based prognostics - Effect-based prognostics
10	Kim	[275]	2010	- Data-driven approaches - Model-based approaches - Reliability-based approaches

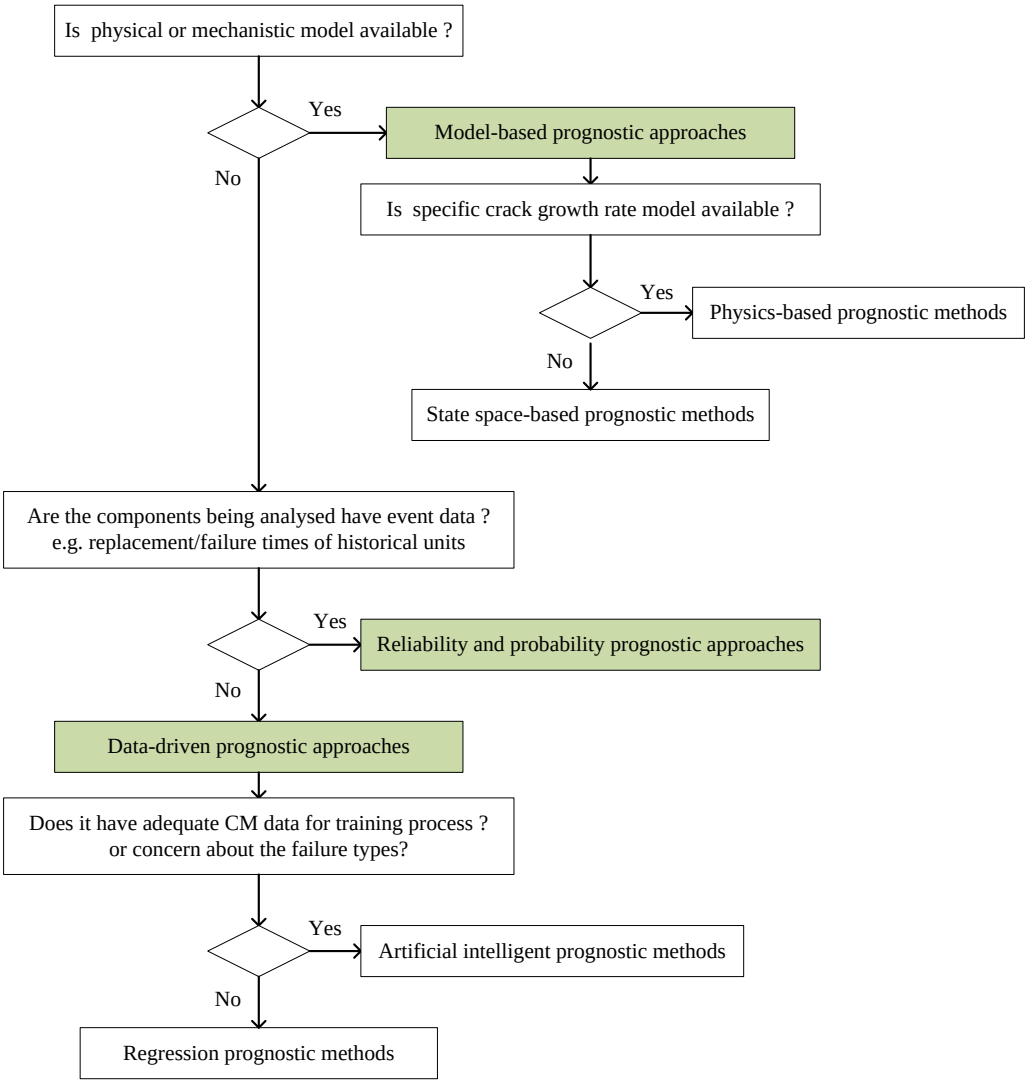

Figure 7.1 A general prognostic approach or method selection for specific needs.

7.1.2 Prognostic methods for rolling element bearings

According to the literature review presented in Table 7.1, four prognostic approaches have been adopted in this thesis. The prognostic methods of each approach are reviewed and presented in Table 7.2. Table 7.2 also presented the degradation parameters or feature extractions which were applied in a particular method or algorithm. It can be seen that RMS and kurtosis are the most commonly used features in prognostic methods. It is worth noting that the reviewed methods in this thesis only focused on rolling element bearings prognostics. The approaches are: (1) model-based approaches; (2) reliability-based methods and probability models; (3) data-driven approaches; and (4) combined data-driven approaches and reliability-based methods.

Table 7.2 Prognostic methods for rolling element bearing.

No	Classification	Method or algorithm	Features used
1	Model-based approaches		
	- Physics-based prognostic models	- Paris' formula [276, 277]	
		- Stiffness-based prognostic model [278]	
	- State space-based Methods	- Kalman filter [279]	
		- Particle filter [280]	RMS and envelope acceleration
2	Reliability-based methods and probability models	- Gaussian process models [281]	Rényi entropy
		- PIM [282]	Kurtosis
		- PCM [283]	Principal features
		- Stochastic model [284]	
		- PHM [285, 286]	
		- Weibull distribution [[287]]	
		- HMM [288]	RMS
		- WPD and HMM [289]	Peak-to-peak, energy and kurtosis
3	Data-driven approaches		
	- Artificial intelligence (AI) methods	- ANN [290, 291]	
		- Fuzzy logic [292]	
		- Genetic algorithm (GA) [293]	Monitoring index
	- Regression methods	- ALE and ARIMA [294]	RMS, skewness, kurtosis
		- Recursive least square (RLS) [277]	RMS
		- Dempster-Shafer regression [295]	RMS and envelope acceleration
		- ARMA/GARCH model [296]	RMS and envelope acceleration
	- Combined AI and regression methods	- RVM and logistic regression [47]	Kurtosis
		- RVM and exponential regression [297]	RMS
4	Combined data-driven and reliability-based methods	- Cox-proportional hazard (CPH) model and SVM [285]	Kurtosis
		- ARMA, PHM and SVM [286]	Peak acceleration and RMS
		- SVM and survival probability [126]	Kurtosis
		- RVM and survival probability [298]	Kurtosis
		- ANN and Weibull distribution [299]	RMS, kurtosis and entropy estimation

Review on model-based approaches

Methods included in model-based approaches require an accurate mathematical model to be developed. They also use residuals as features, where residuals are the outcomes of consistency checks between the measurements of a real system and the

outputs of a mathematical model [275]. Model-based prognostic approaches in this thesis are divided into two classifications: physic-based prognostic models and state space-based methods.

Physics-based prognostic models

The physic-based approaches assume that accurate mathematical or physical models of the monitored system or machine are available and provide a technically comprehensive approach that has been used traditionally to understand failure mode progression. A common model used in physic-based prognostic model is Paris's law equation. The physic-based methods can predict the failure progression accurately if the appropriate model is used. However, a limitation of physic-based approaches is inflexibility which means that the particular model can only be applied to specific types of components [300].

Some literatures applied model-based prognostic methods are presented as follows:

Li et al. [276] present a defect propagation model by mechanistic modelling approach for bearing prognostic to estimate RUL of rolling element bearing.

In slew bearing prognostic study, several works has been conducted. Potočnik et al. [301] calculate the maximal contact force by means of analytical expression of the Hertzian contact theory, and then used a strain-life model to calculate the fatigue life on the basis of the subsurface stresses. Glodez et al. [9] compare the two methods for calculating the fatigue life of a slewing bearing: strain-life approach and stress-life approach based on ISO 281 [302]. Results show that the stress-life approach is the most precise method for calculating bearing fatigue lifetime.

State space-based methods

Besides physic-based methods, the state space-based methods such as Kalman filter and particle filter are also considered as a part of model-based prognostic methods because it builds a dynamic model of system being analysed to predict a future point in time.

Kalman filtering (KF) incorporates the signal embedded with noise and forms that can be considered as a sequential minimum mean square error estimator (MMSE) of the signal [275].

Particle filter or Monte Carlo methods for nonlinear filtering are based on sequential versions of the importance sampling paradigm. This is a technique that amounts to simulating samples under an instrumental distribution and then approximates the target distributions by weighting these samples using appropriately defined importance weight. Particle filter offers the great advantage of not being subject to the assumption of linearity, Gaussianity and stationarity [280]. Particle filter for rolling element bearing prognostics is presented in [280].

Review on reliability-based methods and probability models for prognostic

As aforementioned, prognostics is used to predict how much time left before a failure occurs given the current machine condition and past operation profile which is commonly called as remaining useful life (RUL). In some situation, especially when a fault is catastrophic (e.g., nuclear power plant), it would be desirable to predict the chance that a machine operates without a fault or a failure up to some future time given the current machine condition and past operation profile [267]. This issue can be addressed using failure-based reliability or probability prognostic models. Failure-based reliability is used to estimate the lifetime distribution and its parameters when sufficient, complete and/or censored failure time data exist. If prior knowledge of the lifetime distribution exists for similar components, then often the lifetime distribution is assumed to follow the same distribution of a similar component [275]. For example, Goode et al. [303] separate two intervals of whole machine life: the I-P (Installation-Potential failure) interval in which the machine is running normally and the P-F (Potential failure-Functional failure) in which the machine condition has a problem. Based on two Weibull distributions assumed for the I-P and P-F intervals, failure prediction has been derived in the two intervals and the RUL is estimated.

Proportional hazards models (PHMs) are commonly used in failure prediction and reliability analysis. The method was proposed by Cox in 1972 [304] and was first introduced in the clinical studies to characterise the disease progression in existing cases by revealing the importance of covariates [285]. It is the most popular model for survival analysis due to its simplicity. The reason is that it is not based on any assumptions concerning the nature or shape of the survival distribution [285]. PHMs assume that hazard changes proportionately with covariates and that the

proportionality constant remains the same at all time [271]. The method has been used in bearing prognostics [285, 286]. A review of the existing literature on the PHM is presented in [305]. Usually PHM cannot be used as a stand-alone prognostic method. PHM is usually used together with AI method. PHM is used to build the degradation model, based on this model, AI method e.g. SVM is used to predict the degradation model [285, 286].

A proportional covariates model (PCM) is proposed by Sun et al. [283]. PCM can be used to estimate the hazard functions of mechanical components in cases of sparse or no historical failure data provided that the covariates are proportional to the hazard.

Heng et al. [306] introduce an intelligent reliability model called the intelligent product limit estimator, which was able to include suspended CM data in machinery fault prognostic. The accurate data modelling of suspended data has been found to be of great importance, since in practice machines are rarely allowed to run to failure and data are commonly suspended. The model consists of a feed-forward neural network (FFNN) whose training targets are asset survival probabilities estimated using a variation of the Kaplan-Meier estimator and the true survival status of historical units.

Vlok et al. [282] utilise statistical residual life estimate (RLE) on roller bearings to study changes in diagnostics measurements of vibration and lubrication levels which can influence bearing life. RLEs are based on PIMs and mainly used for non-repairable systems utilising historic failure data and the corresponding diagnostic measurements.

A prediction method for residual life of rolling element bearing based on stochastic process called gamma process is presented in [284].

In slew bearing cases, several reliability methods for prediction have also been studied. Yang et al. [287] present the reliability prediction approach for slew bearing based on the Weibull distribution. Hai et al. [307] develop a method for evaluating rolling contact fatigue (RCF) reliability of slew bearings, which replaced the reliability factor a_1 from ISO 281 with the Lundberg-Palmgren theory.

The use of hidden Markov models (HMMs) in bearing fault prognostic is investigated by Zhang et al. [288]. In a HMM, a system is modelled to be a stochastic process in which the subsequent states have no causal connection with previous states

[271]. It is assumed that the state transition time of estimated vectors follows some multivariate distribution. Once the distribution is addressed, the conditional probability distribution of a distinct state transition can be estimated [272].

Ocak et al. [289] develop a new robust scheme based on wavelet decomposition and hidden Markov model for tracking the severity of bearing faults, and reached the conclusion that the probabilities of the normal bearing's hidden Markov model keep decreasing as the bearing damage progresses toward bearing failure.

Tallian [308] presents a rolling bearing life prediction model using statistical lifetime determination.

Review on data-driven prognostic approaches

Data-driven approaches are derived directly from routine condition monitoring (CM) data of the monitored system (e.g. temperature, vibration, oil debris, current, etc). Data-driven approaches can be regarded as degradation-based methods because they focus on using measures of component degradation, not on failure data, to assess the remaining of a component. In other words data-driven approaches rely on the availability of run-to-failure data and require performing suitable extrapolation to the damage progression to estimate RUL. One major advantage of these techniques is the simplicity of their calculations [271] because these methods do not require mechanistic or physical knowledge of the system or component being analysed. Data-driven approaches may often produce more available solution in many practical cases. The reason is probably that the data-driven models calculated from data-driven methods are easier to obtain compared to an accurate model from a system or component. A main drawback of data-driven approaches is their dependency on the equality of the monitored data. In data-driven approaches, the proper selection of a trending parameter or feature is the key issue in implementing the prognosis. The selection criteria for such parameter should include the diagnosis ability, sensitivity, consistency and the amount of calculation required [290]. In this thesis, data-driven approaches are divided into three sub-categories: (i) artificial intelligence (AI) methods; (ii) regression methods; and (iii) combined AI and regression methods.

AI methods

The first data-driven approaches sub-class (AI methods) are based on machine-learning techniques for prognostics. AI methods predict the selected features that correlate with the failure progression based on the learning or training process. The methods rely on past patterns of degradation to project future degradation. The features used in AI methods are extracted from CM data e.g. vibration signals. More CM data are used in the training process, and more accurate model is obtained, but computational time increases. As AI methods use experimental data to train the methods in order to build a prediction model, thus, AI methods are highly-dependent on the quantity and quality of the measured data. In general, AI methods adopt a one-step or multi-step ahead prediction technique in order to predict the future state. A review of AI methods for prognostics can be found in [309]. Several AI methods have been developed for decades. Artificial neural network (ANN) and its variants such as self-organizing map (SOM) and back propagation neural network (BPNN) methods are most commonly used [63, 77, 290, 291, 310]. Although ANN is the most commonly used method and it has worked successfully in bearing prognosis application, it has fundamental drawbacks in model development. Such drawbacks include how many hidden layers should be included and what is the number of processing nodes that should be used for each layer. These are the major questions for users.

Another popular AI technique that is used for prognostics is the fuzzy logic technique. Fuzzy logic provides a language (with syntax and local semantics) into which one can translate qualitative knowledge about the problem to be solved. In particular, fuzzy logic allows the use of linguistic variables to model dynamic systems. These variables take fuzzy values that are characterized by a sentence and a membership function. The meaning of a linguistic variable may be interpreted as an elastic constraint on its value. These constraints are propagated by fuzzy inference operations. The resulting reasoning mechanism has powerful interpolation properties that in turn give fuzzy logic a remarkable robustness with respect to variations in the system's parameters and disturbances.

Other AI prognostics methods for bearing have been applied e.g. LVQ is used by Zhang et al. [311] to generate a sequence of codes for representing fault signatures in the model.

Regression methods

The second data-driven sub-class (regression methods) are based on time series analysis techniques for prognostics. The regression methods are useful if a reliable or accurate system model is not available. The data-driven prognostic approaches through regression methods are used to determine the RUL. This is achieved by trending the trajectory of a developing fault and predicting the amount of time before it reaches a predetermined threshold level [266].

Niu and Yang [312] introduce the Dempster-Shafer regression for multi-step-ahead prediction of a methane compressor in a petrochemical plant. Using the similar vibration data, Pham et al. [296] develop a forecasting method based on ARMA/GARCH model.

Kosasih et al. [294] present the adaptive line enhancer (ALE) and auto-regressive integrated moving average (ARIMA). Jantunen [292] uses high-order regression functions to mimic bearing fault development and also to save trending data in a compact form.

Combined AI and regression methods

In combination of AI and regression methods, Caesarendra et al. [47] develop a combined prognostics method based on regression and AI method. Logistic regression (LR) is used to estimate failure degradation of bearing based on run-to-failure datasets and the results are then regarded as target vectors of failure probability. Relevance vector machine (RVM) is then used to train the run-to-failure bearing data and target vectors of failure probability. After the training process, RVM is employed to predict failure probability of individual bearing. The performance of the proposed method is validated using experimental and simulated data. The result shows the plausibility and effectiveness of the method which can be considered as the machine degradation assessment model. In another work, Caesarendra et al. [124] present a combined Cox-proportional hazard model and SVM. The failure rate is calculated using the Cox-PHM.

The Kurtosis is extracted as a bearing condition parameter under specified operating conditions. SVM is trained using the kurtosis and the failure rate as a target vector to build the prediction model. The trained SVM is then used to predict the final failure time of individual bearing.

Tran et al. [313] employ a multi-step-ahead regression technique and ANFIS to predict the trending data.

Review on combined data-driven method and reliability-based methods

In this method, the statistical methods are used when the AI prognostics methods require quantitative data measurements.

Widodo and Yang [126] develop an intelligent machine prognostics method using survival probability method namely survival analysis (SA) and SVM. The method has the benefit that it employed censored data which is commonsensical in practice. SA utilizes censored and uncensored data collected from CM routine and then estimates the survival probability of failure time of machine components. SVM is trained by data input from CM history data that correspond to target vectors of estimated survival probability. After validation process, SVM is employed to predict failure time of individual unit of machine component. Still dealing with censored data and survival probability analysis, Widodo and Yang [298] develop a combined survival probability analysis and RVM. In this study, Kaplan-Meier (KM) estimator is used to build a survival probability model. The RVM is then used to train the model and predict the final failure of individual unit of machine component.

7.2 Integrated condition monitoring and prognostic method

To date, prognostic methods have been applied mainly in typical rolling element bearings with rotational speed greater than 1000 rpm [22, 66, 314]. The prognosis of very low speed bearings with naturally generated damage has not been explored. Moreover, most of bearing condition monitoring [3, 209, 315] and bearing prognostic methods [22, 66, 314] usually have been applied and studied separately. In typical rolling element bearing, an integrated fault diagnosis and prognostic method for

bearing health monitoring and CBM has been presented in [311]. The proposed method consists of PCA, HMM and an adaptive stochastic fault prediction model. Another integrated diagnostics and prognostics method which employs SVM and HMM is proposed in [316]. Other studies which proposes integrated frameworks for diagnostics and prognostics are presented in literature [315, 317]. None of them have been applied for very low speed bearing. The integrated condition monitoring and prognostic method reported in this chapter is the first method to be applied for slow speed slew bearings.

The proposed integrated condition-monitoring and prognostic method is implemented as follows. Step (1) is the detection of the incipient slew bearing defect where combined MSET and SPRT is used to process circular-domain kurtosis [96], time-domain kurtosis [96], WD kurtosis [96], EMD kurtosis [96] and LLE feature [186]. Step (2) predicts the trends of the selected features and estimates the RUL of the slew bearing. In this step, kernel regression is used to predict the trend of the time-domain kurtosis, WD kurtosis and the LLE features. Step (2) is initiated when the incipient bearing defect from Step (1) is registered. Figure 7.2 illustrates the computational implementation of the method.

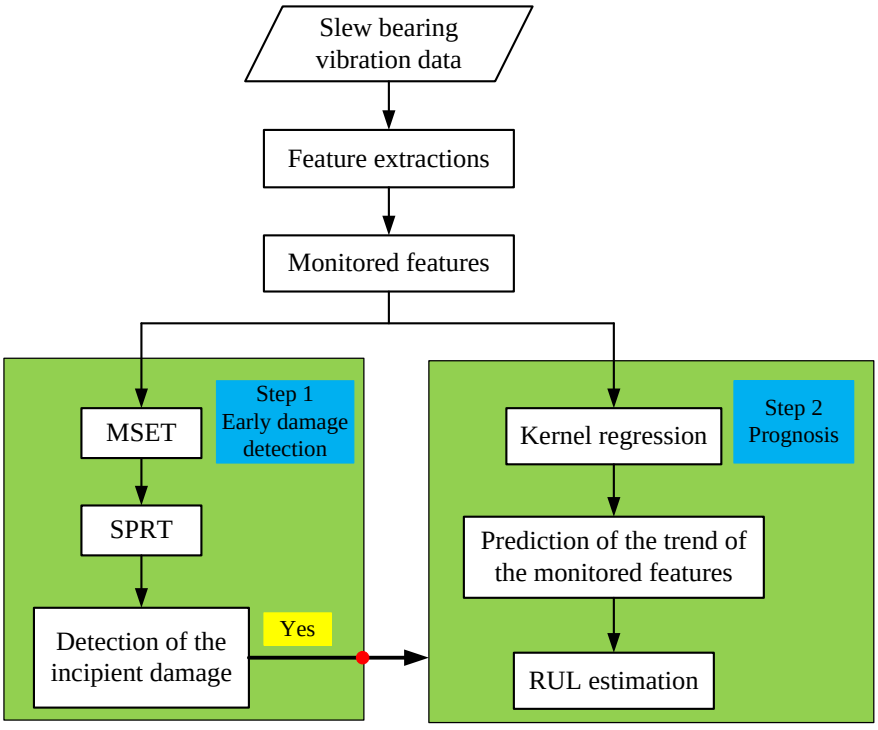

Figure 7.2 Integrated condition monitoring and prognostic method for low speed slew bearing.

7.2.1 Kernel regression

Traditionally, kernel regression is applied in image processing studies such as image de-noising and enhancement [318] and image reconstruction [319]. It is an appropriate prediction method [320]. Kernel regression [321-323] is a non-parametric and non-linear regression technique used to estimate regression function $f(x,y)$ that best fit data set (X_j,Y_j). X_j refers to the measurement day and Y_j is the value of the extracted feature. Unlike linear regression or polynomial regression, kernel regression does not assume any underlying distribution to estimate the regression function [324]. The kernel regression uses a set of identically weighted function called local *kernels* to each observation data point. The kernel basis function only depends on the kernel width from local data point X to a set of neighboring locations, x. The procedures of the proposed kernel regression-based prognostic are implemented in three systematic steps.

Firstly, three of the five features presented in Figure 7.2 are selected based on the evaluation criteria (described in Section 4.2). Once Step (1) has triggered the incipient defect, initial threshold is established. The initial threshold is set at four times the kurtosis value of the normal bearing condition. In Step (2), the data point that exceeds the predetermined initial threshold of each selected feature is saved and used for prediction. From the laboratory slew bearing data, it was found that the minimum number of data points used for prediction is 3. Time-domain kurtosis is used as an illustration in Figure 7.3. The measurement day and the kurtosis level of the first three data points which exceed the threshold are presented in Table 7.3. We refer these points as ‘data with non-uniform interval’ because the interval between one point and the next is unequal and the level of kurtosis does not always increase linearly.

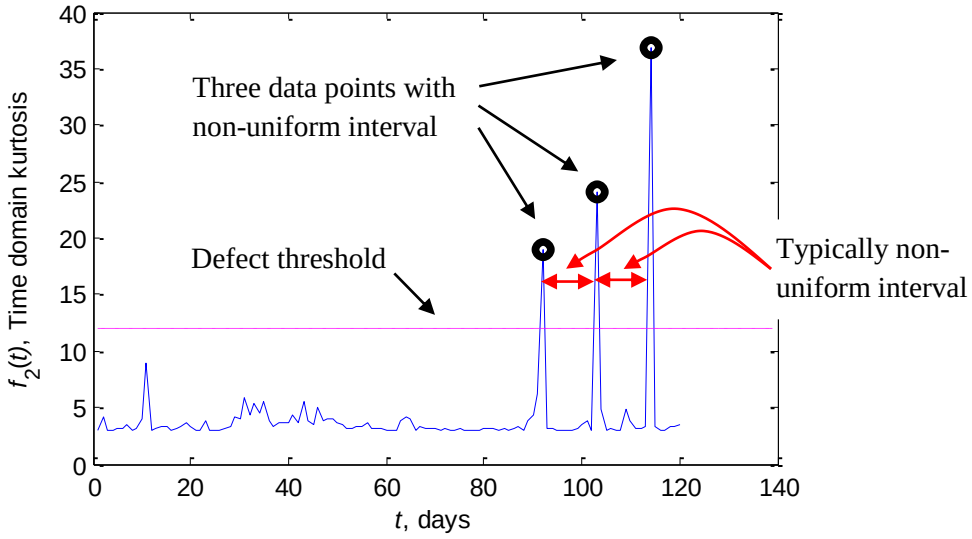

Figure 7.3 Kurtosis extracted from the original vibration signal. The well-known kurtosis value for normal bearing is 3 [47]. The alarm threshold is set at 4 x 3 = 12.

Table 7.3 Data points with non-uniform interval

Data point	Measurement day, X_j	Feature level
A	92	19
B	103	24.12
C	114	36.83

where j represents points A, B or C

Secondly, the non-linear regression model is built in the following four steps. (1) Calculate data point x_j with small step dx. dx equal to 0.2 (days) is used throughout this paper. The result is the vector $\mathbf{x}$. (2) Set the kernel width α. α for time-domain kurtosis prediction is 6. dx and α are selected by trial and error to get the optimum regression model. (3) Apply the Gaussian kernel to each data point X_j using the following equation

$$\mathbf{K}_j(\mathbf{x}, X_j) = \exp\left(\frac{(\mathbf{x} - X_j)^2}{2\alpha^2}\right) \tag{7.1}$$

where subscript j denotes data point with non-uniform interval. According to the example given in Table 7.3, X_j are X_A, X_B and X_C. (4) Compute the weight vector

$\mathbf{w} = (w_1, w_2, ..., w_p)$ using the least square method by minimizing the sum square error between predicted $\hat{Y}_j$ and monitored Y_j as follows:

$$\varepsilon = \sum_{j=1}^{p} (\hat{Y}_j - Y_j) \tag{7.2}$$

where p is the number of data points to be regressed and predicted. In this example, $p = 3$. *lsqcurvefit* MATLAB function is used to obtain the weight vector $\mathbf{w}$. The result of the non-linear regression model is presented in Table 7.4 and shown in Figure 7.4.

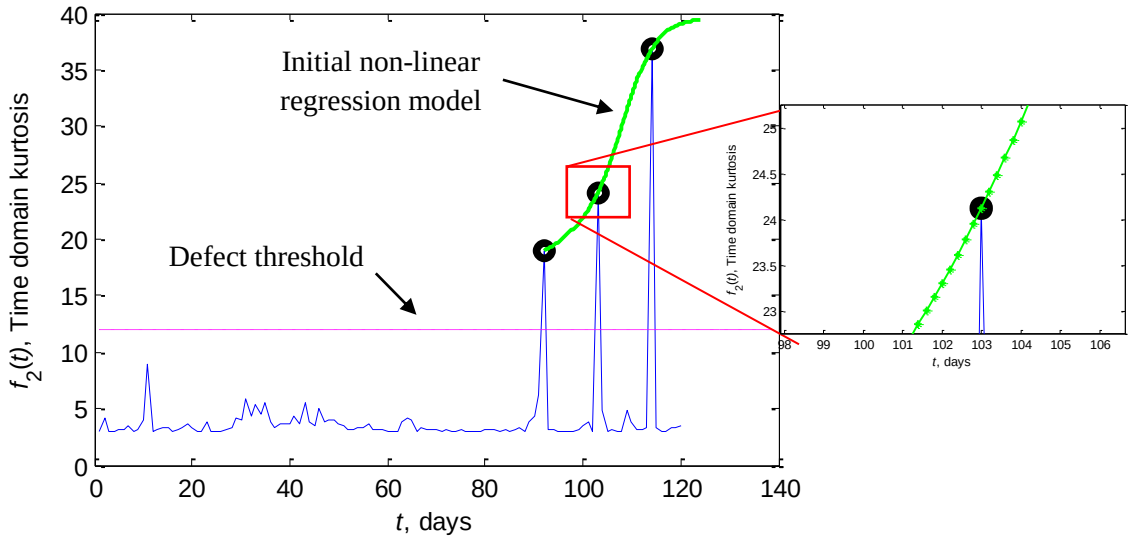

Figure 7.4 Regression model of three data points and one-step-ahead prediction.

Thirdly, the future value of the feature is predicted. The predicted value of Y_j at future X_j is given by the kernel regression formula (also called Nadaraya-Watson kernel weighted average) [324] as follows:

$$\hat{Y}_j = \frac{\sum_{j=1}^{p} w_j \mathbf{K}_j}{\sum_{j=1}^{p} \mathbf{K}_j} \tag{7.3}$$

The one-step-ahead prediction of time-domain kurtosis is presented in Figure 7.5. The result is based on modified kernel regression, not from the original kernel regression.

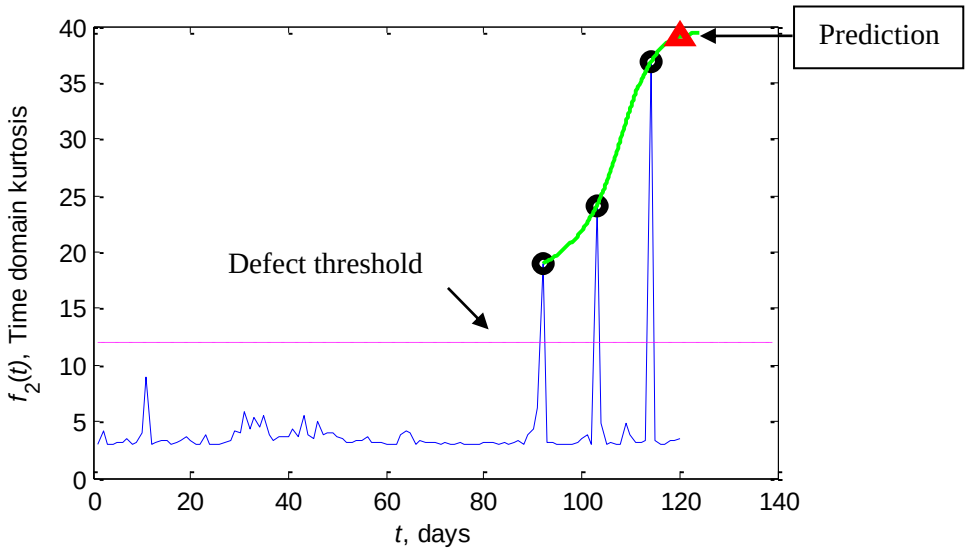

Figure 7.5 One-step-ahead prediction based in modified kernel regression.

Table 7.4 Kernel regression model for 1 step-ahead prediction of time-domain kurtosis.

Data point (*x*-axis)	**x**	$\mathbf{K}_1(\mathbf{x}, X_A)$	$\mathbf{K}_2(\mathbf{x}, X_B)$	$\mathbf{K}_3(\mathbf{x}, X_C)$	$w_1\mathbf{K}_1$	$w_2\mathbf{K}_2$	$w_3\mathbf{K}_3$	$\sum_{j=1}^{p} w_j\mathbf{K}_j$	$\sum_{j=1}^{p}\mathbf{K}_j$	Data point (*y*-axis)
X_A = 92	**92**	1	0.186	0.0012	18.354	4.158	0.047	22.560	1.187	Y_A = **18.998**
	92.2	0.999	0.197	0.0014	18.344	4.417	0.053	22.815	1.198	19.033
	92.4	0.997	0.210	0.0015	18.313	4.688	0.060	23.062	1.209	19.070
	.	.	.	.	.	.	.	.	.	.
	.	.	.	.	.	.	.	.	.	.
	.	.	.	.	.	.	.	.	.	.
	102.6	0.210	0.997	0.164	3.854	22.273	6.505	32.633	1.372	23.780
	102.8	0.197	0.999	0.175	3.632	22.310	6.927	32.869	1.372	23.949
X_B = 103	**103**	0.186	1	0.186	3.418	22.322	7.367	33.109	1.372	Y_B = **24.122**
	103.2	0.175	0.999	0.197	3.214	22.310	7.827	33.352	1.372	24.301
	103.4	0.164	0.997	0.210	3.018	22.273	8.307	33.599	1.372	24.484
	.	.	.	.	.	.	.	.	.	.
	.	.	.	.	.	.	.	.	.	.
	.	.	.	.	.	.	.	.	.	.
	113.6	0.0015	0.210	0.997	0.0282	4.688	39.466	44.183	1.209	36.535
	113.8	0.0014	0.197	0.999	0.0250	4.417	39.532	43.975	1.198	36.685
X_C = 114	**114**	0.0012	0.186	1	0.0221	4.158	39.554	43.734	1.187	Y_C = **36.830**
	114.2	0.0011	0.175	0.999	0.0195	3.909	39.532	43.461	1.175	36.968
	114.4	0.0009	0.164	0.997	0.0173	3.671	39.466	43.155	1.163	37.100
	.	.	.	.	.	.	.	.	.	.
	.	.	.	.	.	.	.	.	.	.
	.	.	.	.	.	.	.	.	.	.
	119.6	0.000025	0.021	0.646	0.00046	0.486	25.588	26.074	0.668	38.992
	119.8	0.000021	0.019	0.626	0.0004	0.442	24.790	25.233	0.646	39.025
$\hat{X}_D$ = 120	**120**	0.000018	0.018	0.606	0.00034	0.403	23.991	24.394	0.624	$\hat{Y}_D$ = **39.055**

Note: $w = [w_1; w_2; w_3] = [18.35; 22.32; 39.55]$

7.2.2 Results and discussion

Features extracted from slew bearing vibration signals have different characteristics from those extracted from accelerometers signals of typical rolling element bearings. In typical rolling element bearings, when the bearing condition deteriorates, the features values gradually increase. In slew bearings, the changes of the slew bearing condition can be detected from a sharp increase of feature value. However, this value does not increase steadily as it does in typical high speed roller bearings. The extracted features of the slew bearing signal usually revert to the normal level and rise again as the condition has significantly deteriorated. This condition is referred as 'self-healing' characteristic [1]. This is one of the difficulties in defect prediction especially for data-driven prognostic methods [124, 285, 295]. In this chapter, the problem has been solved using kernel regression. Prior to the use of kernel regression, all features have to be evaluated.

Caesarendra et al. [96] presented four evaluation criteria to track the progressive bearing defect. In the present study, another evaluation criterion based on exponential function is proposed. It is well known that as bearing deteriorates, certain features will increase exponentially. Hence, an evaluation criterion, E obtained from the coefficient of the exponential curve fitting of the feature being evaluated is used as illustrated below. Suppose $f(t)$ is the monitored evaluation function.

$$f(t) = a e^{(Et)} \tag{7.4}$$

where a and E are the curve fitting exponential coefficients, and t is the measurement days. The calculation of E for the time-domain kurtosis feature and the LLE feature is presented in Figure 7.6. The two figures clearly show that the LLE feature demonstrates a greater exponential increasing trend than the time-domain kurtosis feature. The dotted line in Figures 7.6(a) and (b) is the exponential curve fitted from the 80th day to the 139th day.

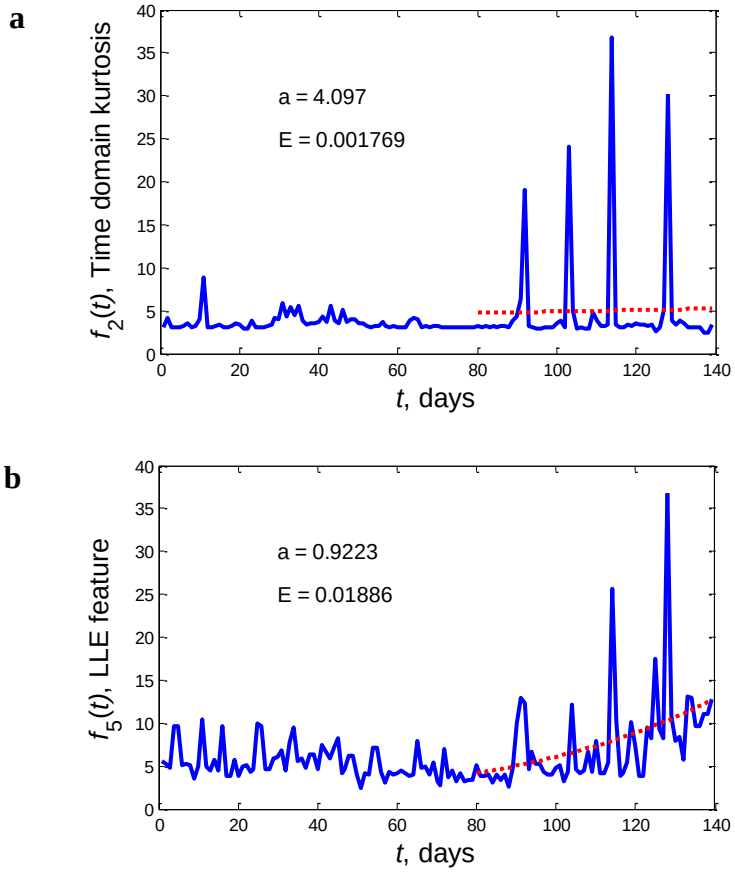

Figure 7.6 Calculation of evaluation criterion, E : (a) time domain kurtosis feature; (b) LLE feature.

In Step (2), kernel regression is employed to predict the future bearing condition and to estimate the RUL of the slew bearing. This prediction starts when there is warning of impending deterioration of the bearing condition. The basic kernel regression algorithm is improved by adding a *k*-step-ahead subroutine. At each *k*-step, non-linear regression model and posterior (predicted) point are estimated and updated. The purpose of this process is to estimate a one-step-ahead prediction of the kernel regression model based on the past data points.

Kernel regression is an effective method to build a model from data with non-uniform interval. The process is done by taking the highest data point of the current kernel regression model and then using it as the next data point (e.g. predict the 4th data point if the initial model is built from three data points). The new data point is then used to build a new kernel regression model and estimate the next data point. The process is repeated until the specified *k*-step-ahead prediction is reached. To illustrate the process, a time domain kurtosis feature is used as the monitored

parameter is predicted. The prediction result is presented in Figure 7.7. Differ to other regression techniques, where the prediction data is based on a polynomial or exponential curve fit equation, the kernel regression is based on previous data samples. In this thesis, three previous chaotic data were utilised to predict one next data. The second predicted data also based on three previous data. The predicted data is presented in Figure 7.7.

Kurtosis is selected as an input of kernel regression because it has a certain value for normal bearing condition and it also has the kurtosis value for defect condition. This is necessary for the detection of incipient defect in Step (1), which is set as the predetermined warning threshold, and for the prediction in Step (2), which is set as the damage bearing threshold. The kurtosis value for normal bearing signals is approximately 3 [47] for the definition based on moment. The increase of this value indicates that the bearing condition has changed. For example, one literature mentioned that the kurtosis value will reach about 50 when high impact occurs [325]. In addition, some severity can give very different kurtosis values, depending primarily on the speed of a machine. For a given severity, represented by the strength of a single impulse response (IR) to a fault, the kurtosis is very much affected by the ratio of the spacing of these IRs compared with the length of an individual one. It tends therefore to be much higher for low speed machines where they are far apart, and may not be different from the normal condition for very high speed machines. Some research mentioned that the kurtosis value of a fault on a low speed radar tower bearing rotating at 5 RPM is 541 [13]. Another literature, Aye [326] studied the kurtosis of normal and faulty tapered bearings running at speed 409 RPM. It has been found that the kurtosis value for normal bearings is 2.89. The kurtosis value for faulty bearings with 409 RPM significantly increases to about 30.26. The same author [326] demonstrated that the kurtosis value of bearing damage with low rotational speed (low RPM) can be much higher than the normal value. In case of kurtosis based on the definition of cumulant, Guo et al. [327] presented a method for recovering the bearing signal from large noisy signal. This was achieved by using a hybrid method based on spectral kurtosis and ensemble EMD (EEMD). It was found that the kurtosis value of each bearing fault condition was recovered and identified more easily. For instance,

the kurtosis value of a bearing with an inner race defect and a ball defect is 18.35 and 41.20, respectively.

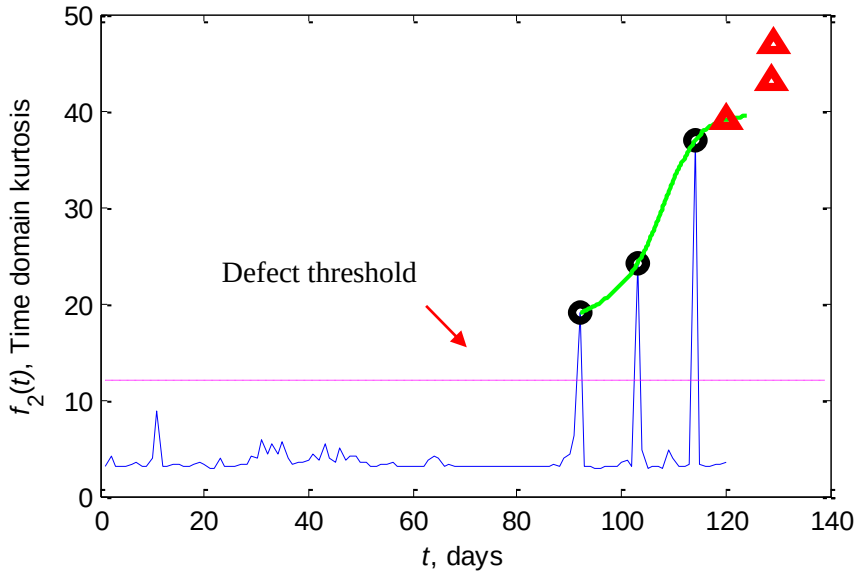

Figure 7.7 Kernel regression model and three-step-ahead prediction.

The final failure threshold has been studied in the past studies [325-327]. However, different case has different final failure threshold. Therefore it is difficult to justify and determine an appropriate threshold level. In this thesis, the third predicted data was selected to be the final failure. From the third predicted data, it is set that the threshold kurtosis value of 45 for the time-domain kurtosis and the WD feature, while the threshold for the LLE feature is set at 35. Noted that, different feature may have different threshold value.

The proposed kernel regression method was applied up to 120 days. This is because by the 120th day the kurtosis value has exceeded four times the normal value, and three data points that are greater than the alarm threshold level have been detected. It should be noted that three data points are the minimum requirement in the initial kernel regression model. Note that the levels of the three selected features up to the 120th day are still below the bearing damage threshold of 45. The predictions of the kernel regression of the three features mentioned above are presented in Figures 7.8(a) to (c). The four step-ahead of kernel regression is used (k = 4). Thus, the 4 step-ahead predicted data points are shown with 'Δ' symbol, while 'o' represents the actual value. It can be seen that the predicted future values have increased. When the data

point exceeds the damage threshold level, the last predicted day is noted and used to estimate the histogram of final failure. Once the histogram of final failure is obtained, the RUL can be easily estimated by taking the difference between the predicted final failure time and the last measurement day (the 120th day).

Based on this analysis, the predicted failure day of the bearing is shown to be dependent on the features and is summarized in Table 7.5. Detailed information of the three data used to build the initial model and the predicted data point of the modified kernel regression method for each feature is shown in Tables 7.6-7.8 (point A - D). Points D – G are the predicted features values. These points are estimated based on the 4-step-ahead prediction of the kernel regression. According to the results in Tables 7.6-7.8, the *y*-axis values of the fourth predicted points exceed the bearing damage threshold. The day of each fourth predicted point (point G) is noted as the final failure of the slew bearing. Three predicted days (point G) are then inputted to the histogram. The result of this is presented in Figure 7.8(d). It should be noted that with more features used, the more accurate the distribution fit of the histogram will be. It can be seen from Figure 7.8(d) that the predicted final failure is the 135th day. Furthermore, the RUL of the bearing can be estimated by taking the difference between the predicted failure day and the last measurement day i.e. 135-120 = 15 day.

During the slew bearing lab experiment, complete failure is unpredictable. When a burst vibration signal on the 141th day was detected, the test-rig had to be shut down. To inspect the damage and verify the result of the proposed prognostic method, the slew bearing was dismantled and inspected. Some of the defective rollers and outer race can be clearly seen in Figure 2.16. The actual final failure day of lab slew bearing is considered one day before the severe burst vibration signal i.e. the 140th day. The accuracy of prediction is estimated as follows:

$$A_p = \left(1 - \frac{\left|t_a - t_p\right|}{t_a}\right) \times 100\% = \left(1 - \frac{\left|140 - 135\right|}{140}\right) \times 100\% = 96.43\ \% \qquad (7.5)$$

where the predicted day of 135 is calculated from the PDF of the predicted failure day of the slew bearing as presented in Figure 7.8 (d).

Table 7.5 The prediction of failure day.

Feature	n^{th} Day failure (x-axis)	Feature level (y-axis)	Threshold
Time-domain	137.6	55	45
WD kurtosis	130.8	46	45
LLE feature	137	39	35

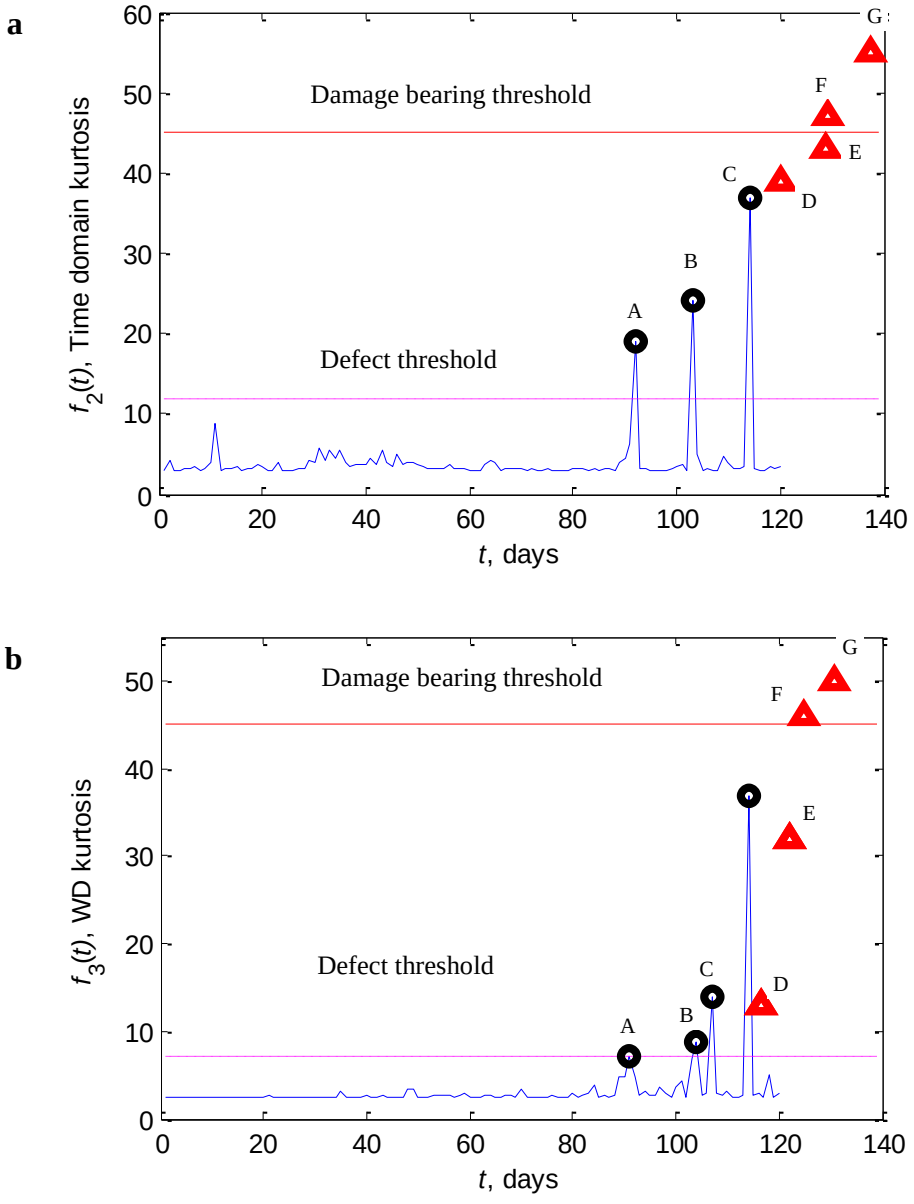

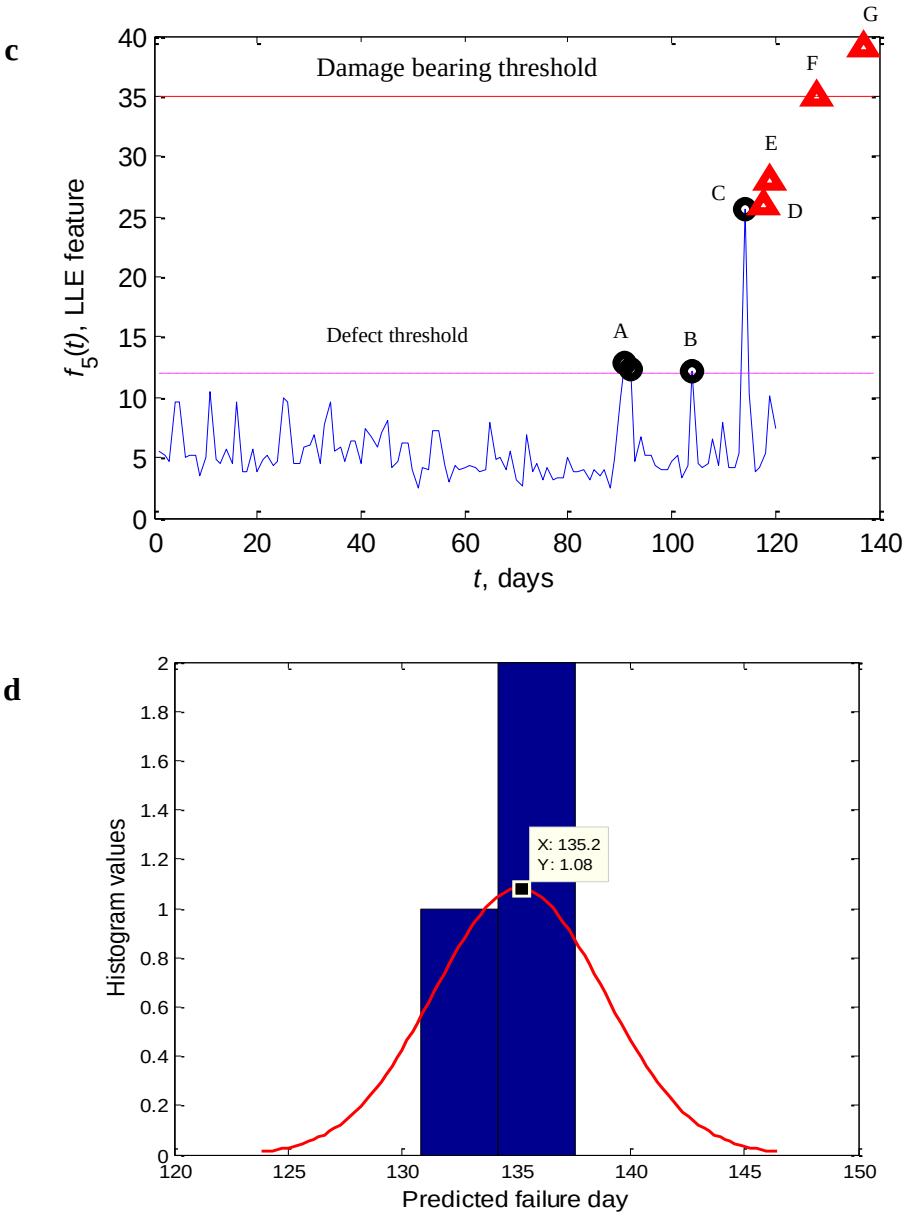

Figure 7.8 Prediction of modified Kernel regression: (a) Time-domain kurtosis; (b) Wavelet kurtosis; (c) LLE feature; (d) PDF of the predicted failure day of the slew bearing. 135.2 is the peak value of the normal distribution. (Note: the defect threshold is set differently to capture the abnormal peak of a particular feature; different feature may have different defect threshold value).

Table 7.6 Original and predicted data points of time-domain kurtosis.

Data point	Measurement day	Feature value	
A	92	19	
B	103	24.12	
C	114	36.83	
D	120	39	Prediction
E	128.6	43	
F	129.2	47	
G	137.6	55	

Table 7.7 Original and predicted data points of WD kurtosis.

Data point	Measurement day	Feature value	
A	91	7.24	
B	104	8.84	
C	107	14	
D	116.4	13	Prediction
E	122.2	32	
F	125	46	
G	130.8	50	

Table 7.8 Original and predicted data points of LLE feature.

Data point	Measurement day	Feature value	
A	92	12.36	
B	104	12.22	
C	114	25.69	
D	117.8	26	Prediction
E	118.8	28	
F	128	35	
G	137	39	

Table 7.6 to 7.8 present the prediction of the three selected features from three previous data (A - C). Kernel regression is applied to predict up to four next data. It is shown that the prediction of time-domain kurtosis feature and LLE feature show close to the actual final failure. In practice, more features are needed. From those features, the average of final failure prediction is calculated.

7.3 Conclusion

A prognostic review and an integrated condition monitoring and prognostic method for low speed slew bearing have been presented. The method employs combined MSET and SPRT to detect the incipient bearing defect and kernel regression to predict the future state and to estimate the RUL. The method has been implemented in the monitoring and prediction of laboratory slew bearing condition. The test was run with new bearing condition until failure. Combined MSET and SPRT method has been used to analyse the vibration features calculated from the accelerometer data of 139 measurement days. Based on the set of hypotheses in SPRT method, it is found that the incipient defect of slew bearing occurred on the 90^{th} day. After the incipient defect was detected, the kernel regression calculation started to predict the future state. To validate the method, 120 measurement days were analysed. The predicted failure days were constructed and the final failure day (the 135^{th} day) was predicted based on the peak of the normal distribution fit of the histogram from the three prognosis, time-domain, WD kurtosis and LLE. The RUL was estimated to be 15 days (from the 135^{th} to the 120^{th}).

Manuscript based on this chapter has been submitted to the Mechanical Systems and Signal Processing Journal with the following title:

- W. Caesarendra, B. Kosasih, A.K. Tieu, H. Zhu, C.A.S. Moodie, Integrated condition monitoring and prognosis method for incipient defect detection and remaining life prediction of low speed slew bearings, (under review in Mechanical Systems and Signal Processing Journal, Paper ID MSSP14-393).

Chapter 8 – Conclusions and recommendations for future work

"If you can resist and focus on a particular hard thing, it will end up with something amazing"
(Wahyu Caesarendra)

8.1 Conclusions

Detailed conclusions for each chapter have been described in the corresponding chapters. The general conclusions are outlined below.

8.1.1 Vibration-based condition monitoring

- The research in vibration analysis of rolling element bearing has mainly focused on high speed bearings with artificially damaged bearings so far. In the past five years, a number of studies on bearing speed greater than 600 rpm are still more dominant than those below 600 rpm.
- Recent slew bearing studies mainly focus on finite element analysis. The vibration analysis based on slew bearing condition monitoring is still being studied.
- In practice, FFT and envelope spectral analysis are the commonly used methods for bearing vibration analysis and fault diagnosis. However, these methods cannot extract the pertinent bearing signal when they are applied in very low speed slew bearing. It is because the slew bearing signal has low energy and is non-stationary and chaotic. This thesis presents an alternative condition monitoring method for very low speed slew bearing.

8.1.2 Vibration feature extraction

- Slew bearing condition monitoring method required reliable features. In this thesis, feature extraction methods have been investigated. The methods are classified into six categories, namely, (1) time-domain feature extraction; (2) frequency-domain feature extraction; (3) time-frequency representation; (4) phase-space dissimilarity measurement, (5) complexity measurement; and (6) other features. Most of methods for each category have been tested using slew bearing vibration data. The results show that most of methods are less suited to detect changes in the bearing condition.
- When the commonly accepted features are less appropriate, alternative methods such as circular domain analysis and LLE algorithm can be used. In circular domain analysis, PAA is an important pre-processing step to detect the frequency alteration. First, the slew bearing vibration signal was processed to determine an ellipsoid orientation. From the ellipsoid orientation, the frequency alteration was detected. The frequency alteration is related to changes of bearing condition. In addition, the ellipsoid orientation called shifting factor was empirically derived. From the processed signal, circular features are applied to detect the changes of bearing condition and incipient bearing damage. However, this proposed method has a limitation that is unable to identify the bearing damage progression obviously.
- Since slew bearing operating at very low speed with highly applied load, the vibration signals exhibit non-linear, non-stationary and chaotic behaviour. The phase-space dissimilarity measurement such as approximate entropy and LLE algorithm can be used to extract pertinent bearing signal corresponding to the bearing damage progression. This thesis conducted study on LLE algorithm for slew bearing vibration signals. The parameter selection to construct phase-space matrix, **X** such as number of samples delay, J and embedding dimension, m are important to obtain an optimum result. This thesis proposes the selection of J based on the dominant frequency of slew bearing vibration signal. The LLE algorithm has a limitation whereby the computational time is longer

than the commonly accepted features such as RMS and kurtosis. This is due to the LLE algorithm consist of looping algorithm to analyse the phase-space. The computational time of LLE algorithm can takes couple minutes for calculating one LLE feature value in one measurement day, where the common time domain feature e.g. kurtosis only takes less than one minute.

8.1.3 AE-based condition monitoring

- AE is a preferable condition monitoring method for low speed bearing rather than vibration measurement. This thesis presented a review of AE in rolling element bearings. The review show that AE have been used for high speed (> 600 rpm) and low speed (10 – 600 rpm) rolling element bearings. The application of AE for very low speed slew bearing (1 rpm) is presented in this thesis.
- In this thesis, vibration and AE-based condition monitoring have been presented. The vibration and AE measurements can monitor changes in the slew bearing condition. However, there are two main issues in the vibration measurement: (1) appropriate vibration features have to be selected and investigated carefully; and (2) the appropriate vibration features are noisier compared to AE hit parameters.

8.1.4 AE feature extraction

- AE hit parameters such as counts, energy, duration, amplitude, ASL and RMS are the commonly used AE features to detect changes in the bearing condition. In this thesis, these features were used to monitor the slew bearing condition from new to failure. In the experiment, significant changes in the slew bearing condition were detected by these features after the new bearing had run continuously for approximately 15 months. However, these changes are drastic and therefore it is difficult to estimate the degradation model for prognostic purpose.
- Due to the limitations of AE hit parameters in certain cases, alternative feature extraction methods such as AR coefficients, approximate entropy, energy

index, short-time energy function and peak ratio have been presented in literatures. Similar to vibration analysis studies, most of the proposed methods are applied to artificially defective bearings rather than naturally defective bearings.

- This thesis presents the LLE algorithm for feature extraction method of slew bearing AE signals. The LLE algorithm was applied to the slew bearing with reversible rotation where the short transition period between acceleration and deceleration is the main part being analysed. Compared to AE hit parameters where the changes are too drastic, LLE feature can detect signs of failure earlier and demonstrate a better damage progression trend of the defect.

8.1.5 Integrated condition monitoring and prognostic method

- A number of studies to correlate the bearing damage sizes and the vibration or AE signals in typical rolling element bearings have been presented in literatures. Different to the previous studies presented in literatures, the installation and the assembly work of the slew bearing is more difficult than typical rolling element bearings. Thus in this thesis, the identification of bearing damage is conducted at the last measurement days after the bearing have already been in the failure condition. The failure condition is alarmed by the feature extraction.
- Combined data-driven and statistic prognostic methods based on MSET, SPRT and kernel regression have been presented in this thesis. This prognostic method is suitable for the condition where the trend of bearing damage progression was not monitored clearly as shown in feature extraction of the first Laboratory test.

8.2 Recommendations for future work

- The vibration condition monitoring and feature extraction methods have been presented in this thesis. First, speed classification review was presented to show that a study of very low speed bearing is still being studied. Second, a number of feature extraction methods have been reviewed. Most of feature

extraction methods are tested using laboratory slew bearing data. However, some features were not tested due to time limitation. Those features are zero-crossing, Shannon entropy, spectral skewness, spectral kurtosis, PMM, WVD, *S* transform and SVD. It is necessary to conduct a further study in order to investigate the benefit of these features for slew bearing data.

- The circular domain and LLE features have been employed in the first laboratory test. The application of these features to the second laboratory test will be conducted in a further study.
- Vibration and AE measurements for low speed slew bearing have been conducted. Four accelerometers and two AE sensors were used. In the future, due to the large dimension of slew bearing, more sensors are necessary. At least, eight accelerometers and four AE sensors are needed. Four accelerometers will be attached on axial row and the other four accelerometers will be attached on radial row at 90 degree to each other. In addition, four AE sensors are enough to be attached on axial row. Based on these sensors' configuration, the damage location of slew bearing can be identified.
- This thesis presented online monitoring system based on FTP. Time-domain features such as RMS, skewness, kurtosis, crest factor, shape factor and entropy were embedded in the online monitoring system. In the future, potential features such as circular domain features, LLE feature, impulse factor and margin factor can be embedded in the online monitoring system to provide accurate information related to the changes in the bearing condition.
- This thesis developed combined data-driven statistical prognostic method. In the future, model-based prognostic approach could be useful for slew bearing failure prediction. As slew bearing operated in different conditions such as high load, contamination, dynamic load and reversible rotation, a failure prediction model can be derived based on the above mentioned conditions. Once the model is obtained, the failure can be predicted. However, this model-based prognostic approach requires more than one slew bearing being tested for the experimental work in order to derive the model empirically.

References

[1] C.A.S. Moodie, An investigation into the condition monitoring of large slow speed slew bearings, Faculty of Engineering, University of Wollongong, Wollongong, 2009.
[2] L.M. Rodgers, The application of vibration analysis and acoustic emission source location to on-line condition monitoring of anti-friction bearings, Tribology International (1979) 51-59.
[3] M. Žvokelj, S. Zupan, I. Prebil, Multivariate and multiscale monitoring of large-size low-speed bearings using ensemble empirical mode decomposition method combined with principal component analysis, Mechanical Systems and Signal Processing 24 (2010) 1049-1067.
[4] M. Žvokelj, S. Zupan, I. Prebil, Non-linear multivariate and multiscale monitoring and signal denoising strategy using kernel principal component analysis combined with ensemble empirical mode decomposition method, Mechanical Systems and Signal Processing 24 (2011) 2631-2653.
[5] L. Kania, Modeling of rollers in calculation of slewing bearing with the use of finite elements, Mechanism and Machine Theory 41 (2006) 1359-1376.
[6] P. Göncz, R. Potočnik, S. Glodež, Load capacity of a three-row roller slewing bearing raceway, Procedia Engineering 10 (2011) 1196-1201.
[7] W. Wang, A two-stage prognosis model in condition based maintenance, European Journal of Operational Research 182 (2007) 1177-1187.
[8] Z. Gang, Z. Xue, J. Dede, L. Mingyan, Z. Jian, FEA of large-scale cross roller slewing bearing used in special propeller, Applied Mechanics and Materials 150 (2012) 165-169.
[9] S. Glodež, R. Potočnik, J. Flašker, Computational model for calculation of static capacity and lifetime of large slewing bearing's raceway, Mechanism and Machine Theory 47 (2012) 16-30.
[10] J. Aguirrebeitia, M. Abasolo, R. Avilés, I.F.d. Bustos, Theoretical calculation of general static load-carrying capacity for the design and selection of three row roller slewing bearings, Mechanism and Machine Theory 48 (2012) 52-61.
[11] R. Liu, Condition monitoring of low-speed and heavily loaded rolling element bearing, Industrial Lubrication and Tribology 59 (2007) 297-300.
[12] X. Bai, H. Xiao, L. Zhang, The condition monitoring of large slewing bearing based on oil analysis method, Key Engineering Materials 474-476 (2011) 716-719.
[13] R.B. Randall, Vibration-based Condition Monitoring: Industrial, Aerospace, and Automotive Applications, John Wiley and Sons, UK, 2011.
[14] S. Braun, Mechanical Signature Analysis, Academic Press, London, 1986.
[15] B.S. Yang, A. Widodo, Introduction of Intelligent Machine Fault Diagnosis and Prognosis, Nova Science Publishers, New York, 2009.
[16] Ultra low speed bearing monitoring, http://www.spmhd.com/low-speed-bearing-monitoring
[17] D. Mba, R.H. Bannister, G.E. Findlay, Condition monitoring of low-speed rotating machinery using stress waves, Proceedings of the Institution of Mechanical Engineers, Part E: Journal of Process Mechanical Engineering 213 (1999) 153-170.
[18] A.C.C. Tan, Y.H. Kim, V. Kosse, Condition monitoring of low-speed bearing – a review, Australian Journal of Mechanical Engineering 6 (2008) 61-68.
[19] A. Widodo, E.Y. Kim, J.D. Son, B.S. Yang, A.C.C. Tan, D.S. Gu, B.K. Choi, J. Mathew, Fault diagnosis of low speed bearing based on relevance vector machine and support vector machine, Expert Systems with Applications 36 (2009) 7252-7261.
[20] Y.H. Kim, A.C.C. Tan, J. Mathew, B.S. Yang, Condition monitoring of low speed bearings: A comparative study of the ultrasound technique versus vibration measurements, 1st World Congress on Engineering Asset Management (WCEAM), Australia, 2006.
[21] ISO2372.

[22] X. Zhu, Y. Zhang, Y. Zhu, Bearing performance degradation assessment based on the rough support vector data description, Mechanical Systems and Signal Processing 34 (2013) 203-217.

[23] L. Renaudin, F. Bonnardot, O. Musy, J.B. Doray, D. Rémond, Natural roller bearing fault detection by angular measurement of true instantaneous angular speed, Mechanical Systems and Signal Processing 24 (2010) 1998-2011.

[24] F. Cong, Kolmogorov–Smirnov test for rolling bearing performance degradation assessment and prognosis, Journal of Vibration and Control 17 (2010) 1337-1347.

[25] F. Cong, J. Chen, G. Dong, F. Zhao, Short-time matrix series based singular value decomposition for rolling bearing fault diagnosis, Mechanical Systems and Signal Processing 34 (2013) 218-230.

[26] Y. Pan, J. Chen, The changes of complexity in the performance degradation process of rolling element bearing, Journal of Vibration and Control (2014) 1-14.

[27] P. Shakya, M.S. Kulkarni, A.K. Darpe, A novel methodology for online detection of bearing health status for naturally progressing defect, Journal of Sound and Vibration 333 (2014) 5614-5629.

[28] L.F. Villa, A. Reñones, J.R. Perán, L.J.d. Miguel, Angular resampling for vibration analysis in wind turbines under non-linear speed fluctuation, Mechanical Systems and Signal Processing 25 (2011) 2157-2168.

[29] C.T. Yiakopoulos, K.C. Gryllias, I.A. Antoniadis, Rolling element bearing fault detection in industrial environments based on a K-means clustering approach, Expert Systems with Applications 38 (2011) 2888-2911.

[30] Y. Dong, M. Liao, X. Zhang, F. Wang, Faults diagnosis of rolling element bearings based on modified morphological method, Mechanical Systems and Signal Processing 25 (2011) 1276-1286.

[31] B.J.v. Wyk, M.A.v. Wyk, G. Qi, Difference histograms: A new tool for time series analysis applied to bearing fault diagnosis, Pattern Recognition Letters 30 (2009) 595-599.

[32] T. Wang, M. Liang, J. Li, W. Cheng, Rolling element bearing fault diagnosis via fault characteristic order (FCO) analysis, Mechanical Systems and Signal Processing 45 (2014) 139-153.

[33] K. Feng, Z. Jiang, W. He, Q. Qin, Rolling element bearing fault detection based on optimal antisymmetric real Laplace wavelet, Measurement 44 (2011) 1582-1591.

[34] S. Wang, W. Huang, Z.K. Zhu, Transient modeling and parameter identification based on wavelet and correlation filtering for rotating machine fault diagnosis, Mechanical Systems and Signal Processing 25 (2011) 1299-1320.

[35] T.I. Patargias, C.T. Yiakopoulos, I.A. Antoniadis, Performance assessment of morphological index in fault prediction and trending of defective rolling element bearing, Nondestructive Testing and Evaluation 22 (2006) 39-60.

[36] N. Päivinen, S. Lammi, A. Pitkanen, J. Nissinen, M. Penttonen, T. Grönfors, Epileptic seizure detection: A nonlinear viewpoint, Computer Methods and Programs in Biomedicine 79 (2005) 151-159.

[37] E.D. Ubeyli, Adaptive neuro-fuzzy inference system for classification of EEG signals using Lyapunov exponents, Computer Methods and Programs in Biomedicine 93 (2009) 313-321.

[38] E. Keogh, K. Chakrabarti, M. Pazzani, S. Mehrotra, Dimensionality reduction for fast similarity search in large time series databases, Knowledge and Information Systems 3 (2001) 263-286.

[39] S. Seker, E. Ayaz, Feature extraction related to bearing damage in electric motors by wavelet analysis, Journal of The Franklin Institute 340 (2003) 125-134.

[40] V. Sugumaran, V. Muralidharan, K.I. Ramachandran, Feature selection using decision tree and classification through proximal support vector machine for fault diagnostics of roller bearing, Mechanical Systems and Signal Processing 21 (2007) 930-942.

[41] G. Niu, B.S. Yang, M. Pecht, Development of an optimized condition-based maintenance system by data fusion and reliability-centered maintenance, Reliability Engineering and System Safety 95 (2010) 786-796.

[42] J. Yu, Bearing performance degradation assessment using locality preserving projections and Gaussian mixture models, Mechanical Systems and Signal Processing 25 (2011) 2573-2588.

[43] Z. Xia, S. Xia, L. Wan, S. Cai, Spectral regression based fault feature extraction for bearing accelerometer sensor signals, Sensors 12 (2012) 13694-13719.

[44] Y. Li, S. Billingtong, C. Zhang, T. Kurfess, S. Danyluk, S. Liang, Dynamic prognostic prediction of defect propagation on rolling element bearings, Tribology Transactions 42 (1999) 385-392.

[45] K. Shen, Z. He, X. Chen, C. Sun, Z. Liu, A monotonic degradation assessment index of rolling bearings using fuzzy support vector data description and running time, Sensors 12 (2012) 10109-10135.

[46] D. Siegel, H. Al-Atat, V. Shauche, L. Liao, J. Snyder, J. Lee, Novel method for rolling element bearing health assessment – A tachometer-less synchronously average envelope feature extraction technique, Mechanical Systems and Signal Processing 29 (2012) 362-376.

[47] W. Caesarendra, A. Widodo, B.S. Yang, Application of relevance vector machine and logistic regression for machine degradation assessment, Mechanical Systems and Signal Processing 24 (2010) 1161-1171.

[48] A. Widodo, B.S. Yang, Wavelet support vector machine for induction machine fault diagnosis based on transient current signal, Expert Systems with Applications 35 (2008) 307-316.

[49] F. Cong, J. Chen, G. Dong, Research on the Order Selection of the Autoregressive Modelling for Rolling Bearing Diagnosis, Proceedings of the Institution of Mechanical Engineers, Part C: Journal of Mechanical Engineering Science 224 (2010) 2289-2297.

[50] I.A. Rezek, S.J. Roberts, Stochastic complexity measures for physiological signal analysis, IEEE Transactions on Biomedical Engineering 45 (1998) 1186-1191.

[51] L. Zhang, J. Xu, J. Yang, D. Yang, D. Wang, Multiscale morphology analysis and its application to fault diagnosis, Mechanical Systems and Signal Processing 22 (2008) 597-610.

[52] N.G. Nikolaou, I.A. Antoniadis, Application of morphological operators as envelope extractors for impulsive-type periodic signals, Mechanical Systems and Signal Processing 17 (2003) 1147-1162.

[53] P.E. William, M.W. Hoffman, Identification of bearing faults using time domain zero-crossing, Mechanical Systems and Signal Processing 25 (2011) 3078-3088.

[54] C. Faloutsos, M. Ranganathan, Y. Manolopoulos, Fast subsequence matching in time-series databases, SIGMOD '94 Proceedings of the 1994 ACM SIGMOD international conference on Management of data, ACM New York, NY, USA, 1994, pp. 419-429.

[55] D. Wang, S. Sun, P.W. Tse, A general sequential Monte Carlo method based optimal wavelet filter: A Bayesian approach for extracting bearing fault features, Mechanical Systems and Signal Processing.

[56] Y.N. Pan, J. Chen, X.L. Li, Spectral entropy: A complementary index for rolling element bearing performance degradation assessment, Proceedings of the Institution of Mechanical Engineers, Part C: Journal of Mechanical Engineering Science 223 (2009) 1223-1231.

[57] C.E. Shannon, A mathematical theory of communication, Bell Systems and Technology Journal 27 (1948) 379-423.

[58] R.M. Rangayyan, Biomedical Signal Analysis: A Case-Study Approach, IEEE Press Series on Biomedical Engineering, Wiley, New York, 2002.

[59] J. Antoni, Fast computation of the kurtogram for the detection of transient faults, Mechanical Systems and Signal Processing 21 (2007) 108-124.

[60] J. Antoni, R.B. Randall, The spectral kurtosis: application to the vibratory surveillance and diagnostics of rotating machines, Mechanical Systems and Signal Processing 20 (2006) 308-331.

[61] N. Sawalhi, R.B. Randall, H. Endo, The enhancement of fault detection and diagnosis in rolling element bearings using minimum entropy deconvolution combined with spectral kurtosis, Mechanical Systems and Signal Processing 21 (2007) 2616-2633.

[62] R.G.T.d. Almeida, S.A.d.S. Vicente, L.R. Padovese, New technique for evaluation of global vibration levels in rolling bearings, Shock and Vibration 9 (2002) 225-234.

[63] R. Huang, L. Xi, X. Li, C.R. Liu, H. Qiu, J. Lee, Residual life predictions for ball bearings based on self-organizing map and back propagation neural network methods, Mechanical Systems and Signal Processing 21 (2007) 193-207.

[64] G. Dong, J. Chen, Noise resistant time frequency analysis and application in fault diagnosis of rolling element bearings, Mechanical Systems and Signal Processing 33 (2012) 212-236.

[65] J. Urbanek, T. Barszcz, R. Zimroz, J. Antoni, Application of averaged instantaneous power spectrum for diagnostics of machinery operating under non-stationary operational conditions, Measurement 45 (2012) 1782-1791.

[66] H. Qiu, J. Lee, J. Lin, G. Yu, Wavelet filter-based weak signature detection method and its application on rolling element bearing prognostics, Journal of Sound and Vibration 289 (2006) 1066-1090.

[67] K. Chan, A.W. Fu, Efficient time series matching by wavelets, In proceedings of the 15th IEEE International Conference on Data Engineering, Sydney, Australia, 1999, pp. 126-133.

[68] S. Braun, M. Feldman, Decomposition of non-stationary signals into varying time scales: Some aspects of the EMD and HVD methods, Mechanical Systems and Signal Processing 25 (2011) 2608-2630.

[69] G. Rilling, P. Flandrin, P. Gonçalves, On empirical mode decomposition and its algorithms, IEEE-EURASiP Workshop on Nonlinear Signal and Image Processing, Grado, June 2003.

[70] H. Wang, J. Chen, G. Dong, Feature extraction of rolling bearing's early weak fault based on EEMD and tunable Q-factor wavelet transform, Mechanical Systems and Signal Processing 48 (2014) 103-119.

[71] B. Li, P.L. Zhang, D.S. Liu, S.S. Mi, G.Q. Ren, H. Tian, Feature extraction for rolling element bearing fault diagnosis utilizing generalized S transform and two-dimensional non-negative matrix factorization, Journal of Sound and Vibration 330 (2011) 2388-2399.

[72] A. Accardo, M. Affinito, M. Carrozi, F. Bouquet, Use of the fractal dimension for the analysis of electroencephalographic time series, Biological Cybernetics 77 (1997) 339-350.

[73] J. Yang, Y. Zhang, Y. Zhu, Intelligent fault diagnosis of rolling element bearing based on SVMs and fractal dimension, Mechanical Systems and Signal Processing 21 (2007) 2012-2024.

[74] D. Logan, J. Mathew, Using the correlation dimension for vibration fault diagnosis of rolling element bearings-I. Basics concepts, Mechanical Systems and Signal Processing 10 (1996) 241-250.

[75] R. Yan, R.X. Gao, Approximate entropy as a diagnostic tool for machine health monitoring, Mechanical Systems and Signal Processing 21 (2007) 824-839.

[76] R. Yan, Y. Liu, R.X. Gao, Permutation entropy: A nonlinear statistical measure for status characterization of rotary machines, Mechanical Systems and Signal Processing 29 (2012) 474-484.

[77] S. Zhang, R. Ganesan, Multivariable trend analysis using neural networks for intelligent diagnotics of rotating machinery, Journal of Enginering for Gas Turbines and Power 119 (1997) 378-384.

[78] E. Keogh, K. Chakrabarti, M. Pazzani, S. Mehrotra, Locally adaptive dimensionality reduction for indexing large time series databases, In proceedings of ACM SIGMOD Conference on Management of Data, Santa Barbara, Canada, 2001, pp. 151-162.

[79] B.K. Yi, C. Faloutsos, Fast time sequence indexing for arbitrary Lp norms, VLDB '00 Proceedings of the 26th International Conference on Very Large Data Bases Cairo, Egypt, 2000, pp. 385-394

[80] B. Eftekharnejad, M.R. Carrasco, B. Charnley, D. Mba, The application of spectral kurtosis on Acoustic Emission and vibrations from a defective bearing, Mechanical Systems and Signal Processing 25 (2011) 266-284.

[81] W. Caesarendra, B. Kosasih, K. Tieu, C.A.S. Moodie, An Application of Nonlinear Feature Extraction – A Case Study for Low Speed Slewing Bearing Condition Monitoring and Prognosis, 2013 IEEE/ASME International Conference on Advanced Intelligent Mechatronics (AIM), Wollongong, Australia, July 9-12, 2013.

[82] J. Serra, Image analysis and mathematical morphology, Academic Press, New York, USA, 1982.

[83] S. Nishida, M. Nakamura, M. Miyazaki, S. Suwazono, M. Honda, T. Nagamine, H. Shibazaki, Construction of a morphological filter for detecting an event related potential P300 in single sweep EEG record in children, Medical Engineering Physics 17 (1995) 425-430.

[84] S. Nishida, M. Nakamura, K. Shindo, M. Kanda, H. Shibazaki, A morphological filter for extracting waveform characteristics of single sweep evoked potentials, Automatica 35 (1997) 937-943.

[85] S. Nishida, M. Nakamura, A. Ikeda, H. Shibazaki, Signal separation of background EEG and spike by using morphological filter, Medical Engineering Physics 21 (1999) 601-608.

[86] M.H. Sedaaghi, ECG wave detection using morphological filters, Applied Signal Processing 5 (1998) 182-194.

[87] J. Wang, G. Xu, Q. Zhang, L. Liang, Application of improved morphological filter to the extraction of impulsive attenuation signals, Mechanical Systems and Signal Processing 23 (2009) 236-245.

[88] R. Santhana, N. Murali, Early classification of bearing faults using morphological operators and fuzzy inference, IEEE Transactions on Industrial Electronics 60 (2013) 567-574.

[89] C.F. Drummond, D. Sutanto, Classification of power quality disturbances using the Iterative Hilbert Huang Transform, 14th International Conference on Harmonics and Quality of Power, IEEE, 2010, pp. 107.

[90] A. Lerch, An Introduction to Audio Content Analysis: Applications in Signal Processing and Music Informatics, Wiley-IEEE Press, 2012.

[91] Z. Feng, M. Liang, F. Chu, Recent advances in time-frequency analysis methods for machinery fault diagnosis: A review with application examples, Mechanical Systems and Signal Processing 38 (2013) 165-205.

[92] F. Al-Badour, M. Sunar, L. Cheded, Vibration analysis of rotating machinery using time-frequency analysis and wavelet techniques, Mechanical Systems and Signal Processing 25 (2011) 2083-2101.

[93] J.B. Allen, Short term spectral analysis, synthesis, and modification by discrete Fourier transform, IEEE Transactions on Acoustics, Speech, and Signal Processing 25 (1977) 235-238.

[94] Z.K. Peng, F.L. Chu, Application of the wavelet transform in machine condition monitoring and fault diagnostics: a review with bibliography, Mechanical Systems and Signal Processing 18 (2004) 199-221.

[95] C.I. Daubechies, Ten Lectures on Wavelet, SIAM, Pennsylvania, USA, 1992.

[96] W. Caesarendra, B. Kosasih, A.K. Tieu, C.A.S. Moodie, Circular domain features based condition monitoring for low speed slewing bearing, Mechanical Systems and Signal Processing 45 (2014) 114-138.

[97] G. Niu, A. Widodo, J.D. Son, B.S. Yang, D.H. Hwang, D.S. Kang, Decision-level fusion based on wavelet decomposition for induction motor fault diagnosis using transient current signal, Expert Systems with Applications 35 (2008) 918-928.

[98] B. Liu, S.F. Ling, Q. Meng, Machinery diagnosis based on wavelets packets, Journal of Vibration and Control 3 (1997) 5-17.

[99] N.E. Huang, Z. Shen, S.R. Long, M.C. Wu, H.H. Shih, Q. Zheng, N.C. Yen, C.C. Tung, H.H. Liu, The empirical mode decomposition and the Hilbert spectrum for nonlinear and non-stationary time series analysis, Proceedings of the Royal Society London A 454 (1998) 903-995.

[100] Y. Lei, J. Lin, Z. He, M.J. Zuo, A review on empirical mode decomposition in fault diagnosis of rotating machinery, (2013) 108-126.

[101] W. Caesarendra, P.B. Kosasih, A.K. Tieu, C.A.S. Moodie, B.K. Choi, Condition monitoring of naturally damaged slow speed slewing bearing based on ensemble empirical mode decomposition, Journal of Mechanical Science and Technology 27 (2013) 1-10.

[102] W.J. Staszewski, K. Worden, G.R. Tomlinson, Time-frequency analysis in gearbox fault detection using the Wigner-Ville distribution and pattern recognition, Mechanical Systems and Signal Processing 11 (1997) 673-692.

[103] S.J. Loutridis, Instantaneous energy density as a feature for gear fault detection, Mechanical Systems and Signal Processing 20 (2006) 1239-1253.

[104] T.A.M. Claasen, W.F.G. Mecklenbrauker, The Wigner distribution—a tool for time-frequency analysis. Part 1: continuous time signals, Philips Journal of Research 35 (1980) 217-250.

[105] C. Lu, Q. Sun, L. Tao, H. Liu, C. Lu, Bearing health assessment based on chaotic characteristics, Shock and Vibration 20 (2013) 519-530.

[106] T. Higuchi, Relationship between the fractal dimension and the power law index for a time series: A numerical investigation, Physica D: Nonlinear Phenomena 46 (1990) 254–264.

[107] M. N'Diaye, C. Degeratu, J.M. Bouler, D. Chappard, Biomaterial porosity determined by fractal dimensions, succolarity and lacunarity on microcomputed tomographic images, Materials Science and Engineering C 33 (2013) 2025-2030.

[108] R.D. King, A.T. George, T. Jeon, L.S. Hynan, T.S. Youn, D.N. Kennedy, B. Dickerson, t.A.s.D.N. Initiative, Characterization of atrophic changes in the cerebral cortex using fractal dimensional analysis, Brain Imaging and Behaviour 3 (2009) 154-166.

[109] J.Z. Liu, L.D. Zhang, G.H. Yue, Fractal dimension in human Cerebellum measured by magnetic resonance imaging, Biophysical Journal 85 (2003) 4041-4046.

[110] A.J. Roberts, A. Cronin, Unbiased estimation of multi-fractal dimensions of finite data sets, Physica A: Statistical Mechanics and its Applications 233 (1996) 867-878.

[111] P. Maragos, A. Potamianos, Fractal dimensions of speech sounds: Computation and application to automatic speech recognition, The Journal of the Acoustical Society of America 105 (1999) 1925-1932.

[112] P. Grassberger, I. Procaccia, Estimation of the Kolmogorov entropy from a chaotic signal, Physical Review A 28 (1983) 2591-2593.

[113] F. Cong, J. Chen, Y. Pan, Kolmogorov-Smirnov test for rolling bearing performance degradation assessment and prognosis, Journal of Vibration and Control 17 (2011) 1337-1347.

[114] J.S. Richman, J.R. Moorman, Physiological time-series analysis using approximate entropy and sample entropy, American Journal of Physiology - Heart and Circulatory Physiology 278 (2000) H2039-H2049.

[115] X. Chen, C. Yin, W. He, Feature extraction of gearbox vibration signals based on EEMD and sample entropy, 10th International Conference on Fuzzy Systems and Knowledge Discovery (FSKD), Shenyang, China, 23-25 July 2013, pp. 811-815.

[116] M.L.D. Wong, C. Liu, A.K. Nandi, Classification of ball bearing faults using entropic measures, Surveillance 7, France, 29-30 October 2013, pp. 1-8.

[117] P.P. Kanjilal, S. Palit, On multiple pattern extraction using singular value decomposition, IEEE Transactions on Signal Processing 43 (1995) 1536-1540.

[118] P.P. Kanjilal, J. Bhattacharya, G. Saha, Robust method for periodicity detection and characterization of irregular cyclical series in term of embedded periodic components, Physical Review E 59 (1999) 4013-4025.

[119] K. Chakrabarti, E. Keogh, S. Mehrotra, M. Pazzani, Locally adaptive dimensionality reduction for indexing large time series databases, ACM Transactions on Database Systems 27 (2002) 188-228.

[120] Y.H. Kim, A.C.C. Tan, B.S. Yang, Parameters comparison of acoustic emission signals for condition monitoring of low-speed bearings, Australian Journal of Mechanical Engineering 6 (2008) 45-52.

[121] M. Kang, J. Kim, J.M. Kim, Reliable fault diagnosis for incipient low-speed bearings using fault feature analysis based on a binary bat algorithm, Information Sciences 294 (2015) 423-438.

[122] M. Elforjani, D. Mba, Natural mechanical degradation measurements in slow speed bearings, Engineering Failure Analysis 16 (2009) 521-532.

[123] C.T. Yiakopoulos, K.C. Gryllias, I.A. Antoniadis, Rolling element bearing fault detection in industrial environments based on a k-means clustering Approach, Expert System with Application 38 (2011) 2888-2911.

[124] W. Caesarendra, A. Widodo, P.H. Thom, B.S. Yang, J.D. Setiawan, Combined probability approach and indirect data-driven method for bearing degradation prognostics, IEEE Transactions on Reliability 60 (2011) 14-20.

[125] Y. Lei, Z. He, Y. Zi, A combination of WKNN to fault diagnosis of rolling element bearings, ASME Journal of Vibration and Acoustics 31 (2009) 1-6.

[126] A. Widodo, B.S. Yang, Machine health prognostics using survival probability and support vector machine, Expert Systems with Applications 38 (2011) 8430-8437.

[127] N. Jamaludin, D. Mba, R.H. Bannister, Condition monitoring of slow-speed rolling element bearings using stress waves, Proceedings of the Institution of Mechanical Engineers, Part E: Journal of Process Mechanical Engineering 215 (2001) 245-271.

[128] A. Pewsey, The Large-Sample Joint Distribution of Key Circular Statistics, Metrika 60 (2004) 25-32.

[129] N.I. Fisher, Statistical Analysis of Circular Data, Revised ed., Cambridge University Press, 1995.

[130] P. Berens, CircStat: A MATLAB Toolbox for Circular Statistics, Journal of Statistics Software 31 (2009) 1-21.

[131] M.F. Luo, J. Mathew, Angle domain analysis technique for monitoring machinery with varying speed, Centre for Machine Condition Monitoring Research Bulletin, Monash University, 1993, pp. 4.1-4.10.

[132] K.R. Fyfe, E.D.S. Munck, Analysis of computed order tracking, Mechanical Systems and Signal Processing 11 (1997) 187-205.

[133] K.M. Bossley, R.J. McKendrick, C.J. Harris, C. Mercer, Hybrid computed order tracking, Mechanical Systems and Signal Processing 13 (1999) 627-641.

[134] F. Bonnardot, R.B. Randall, J. Antoni, Enhanced unsupervised noise cancellation using angular resampling for planetary bearing fault diagnosis, International Journal of Acoustics and Vibration 9 (2004) 51-60.

[135] L. Renaudin, F. Bonnardot, O. Musy, J.B. Doray, D. Réymond, Natural roller bearing fault detection by angular measurement of true instantaneous angular speed, Mechanical Systems and Signal Processing 24 (2010) 1998-2011.

[136] F. Bonnardot, M.E. Badaoui, R.B. Randall, J. Danière, F. Guillet, Use of the acceleration signal of a gearbox in order to perform angular resampling (with limited speed fluctuation), Mechanical Systems and Signal Processing 19 (2005) 766-785.

[137] F. Combet, L. Gelman, An automated methodology for performing time synchronous averaging of a gearbox signal without speed sensor, Mechanical Systems and Signal Processing 21 (2007) 2590-2606.

[138] F. Combet, R. Zimrov, A new method for the estimation of the instantaneous speed relative fluctuation in a vibration signal based on the short time scale transform, Mechanical Systems and Signal Processing 23 (2009) 1382-1397.
[139] L.F. Villa, A. Renones, J.R. Perán, L.J. de Miguel, Angular resampling for vibration analysis in wind turbines under non-linear speed fluctuation, Mechanical Systems and Signal Processing 25 (2011) 2157-2168.
[140] L.F. Villa, A. Renones, J.R. Perán, L.J.d. Miguel, Statistical fault diagnosis based on vibration analysis for gear test-bench under non-stationary conditions of speed and load, Mechanical Systems and Signal Processing 29 (2012) 436-446.
[141] M. Akar, Detection of a static eccentricity fault in a closed loop driven induction motor by using the angular domain order tracking analysis method, Mechanical Systems and Signal Processing 34 (2013) 173-182.
[142] C. Kovacs, Condition monitoring of low speed systems, Maintenance Management Conference, 1990, pp. 1-20.
[143] B.K. Yi, C. Faloutsos, Fast Time Sequence Indexing for Arbitrary Lp Norms, 26th VLBD Conference, Cairo, Egypt, 2000, pp. 385-394.
[144] E. Keogh, K. Chakrabarti, M. Pazzani, S. Mehrotra, Dimensionality reduction for fast similarity search in large time series databases, Knowledge and Information Systems 3 (2000) 263-286.
[145] A. Fitzgibbon, M. Pilu, R.B. Fisher, Direct least square fitting of ellipses, IEEE Transactions on Pattern Analysis and Machine Intelligence 21 (1999) 476-480.
[146] P.L. Rosin, A note on the least squares fitting of ellipses, Pattern Recognition Letters 14 (1993) 799-809.
[147] W. Gander, G.H. Golub, R. Strebel, Least-Square Fitting of Circles and Ellipses, BIT Numerical Mathematics 34 (1994) 558-578.
[148] S. Hou, Y. Li, Z. Wang, M. Liang, A new low-frequency resonance sensor for low speed roller bearing monitoring, ASME Journal of Vibrations and Acoustics 132 (2010) 1-8.
[149] W. Caesarendra, A. Widodo, B.S. Yang, Application of relevance vector machine and logistic regression for machine degradation assessment, Mechanical Systems and Signal Processing 24 (2010) 1161-1171.
[150] S. Janjarasjitt, H. Ocak, K.A. Loparo, Bearing condition diagnosis and prognosis using applied nonlinear dynamical analysis of machine vibration analysis, Journal of Sound and Vibration 317 (2008) 112-126.
[151] P.F. Pai, Nonlinear vibration characterization by signal decomposition, Journal of Sound and Vibration 307 (2007) 527-544.
[152] V. Protopopescu, L.M. Hively, Phase-space dissimilarity measures of nonlinear dynamics: industrial and biomedical applications, Recent Research Developments in Physics 6 (2005) 1-40.
[153] G.F. Wang, Y.B. Li, Z.G. Luo, Fault classification of rolling bearing based on reconstructed phase space and Gaussian mixture model, Journal of Sound and Vibration 323 (2009) 1077-1089.
[154] X. Wang, V. Makis, Autoregressive model-based gear shaft fault diagnosis using the Kolmogorov-Smirnov test, Mechanical Systems and Signal Processing 327 (2009) 413-423.
[155] W. Caesarendra, B. Kosasih, K. Tieu, C.A.S. Moodie, An application of nonlinear feature extraction – A case study for low speed slewing bearing condition monitoring and prognosis, 12th IEEE/ASME International Conference on Advanced Intelligent Mechatronics (AIM), Wollongong, Australia, 9-12 July 2013, pp. 1713-1718.
[156] A. Rolo-Naranjo, M.E. Montesino-Otero, A method for the correlation dimension estimation for on-line condition monitoring of large rotating machinery, Mechanical Systems and Signal Processing 19 (2005) 939-954.
[157] Y. Ruqiang, R.X. Gao, Approximate entropy as a diagnostic tool for machine health monitoring, Mechanical Systems and Signal Processing 21 (2007) 824-839.

[158] R. Yan, Y. Liu, R.X. Gao, Permutation entropy: A nonlinear statistical measure for status characterization of rotary machines, Mechanical Systems and Signal Processing 29 (2011) 474-484.
[159] N. Paivinen, S. Lammi, A. Pitkannen, J. Nissinen, M. Penttonen, T. Gronfors, Epileptic seizure detection: A nonlinear viewpoint, Computer Methods and Programs in Biomedicine 79 (2005) 151-159.
[160] F. Shayegh, S. Sadri, R. Amirfattahi, K.A. Ansari-Asl, Model-based method for computation of correlation dimension, Lyapunov exponents and synchronization from depth-EEG signals, Computer Methods and Programs in Biomedicine 113 (2014) 323-337.
[161] M. Bask, T. Liu, A. Widerberg, The stability of electricity prices: Estimation and inference of the Lyapunov exponents, Physica A 376 (2007) 565-572.
[162] J. Wang, Q. He, Automatic fault diagnosis of rotating machines by time-scale manifold ridge analysis, Mechanical Systems and Signal Processing 40 (2013) 237-256.
[163] F. Takens, Detecting strange attractors in turbulence, Lecture Notes in Mathematics, Springer, New York, 1981.
[164] S. Sato, M. Sano, Y. Sawada, Practical methods of measuring the generalized dimension and the largest Lyapunov exponent in high dimensional chaotic systems, Progress of Theoretical Physics 77 (1987) 1-5.
[165] M.T. Rosenstein, J.J. Collins, C.J.D. Luca, A practical method for calculating largest Lyapunov exponents from small data sets, Physica D 65 (1993) 117-134.
[166] W. Caesarendra, B. Kosasih, A.K. Tieu, C.A.S. Moodie, Circular domain features based condition monitoring for low speed slewing bearing, Mechanical Systems and Signal Processing 45 (2015) 114-138.
[167] R.M. Singer, K.C. Gross, J.P. Herzog, R.W. King, S.W. Wegerich, Model-based nuclear power plant monitoring and fault diagnosis: theoretical foundations, 9th International Conference on Intelligent Systems Applications to Power Systems (ISAP), Seoul, South Korea, July 6-10, 1997.
[168] K.C. Gross, R.M. Singer, S.W. Wegerich, J.P. Herzog, Application of a model-based fault detection system to nuclear plant signals, 9th International Conference on Intelligent Systems Applications to Power Systems (ISAP), Seoul, South Korea, July 6-10, 1997.
[169] N. Zavaljevski, K.C. Gross, Sensor fault detection in nuclear power plants using multivariate state estimation technique and support vector machine, 3rd International Conference of the Yugoslav Nuclear Society YUNSC, Belgrade, Yugoslavia, October 2-5, 2000.
[170] A.V. Gribok, A.M. Urmanov, J.W. Hines, Uncertainty analysis of memory based sensor validation techniques, Real-Time Systems 27 (2004) 7-26.
[171] J. Peng, W.D. Xiao, X.P. Huang, A health monitoring method based on multivariate state estimation technique, Applied Mechanics and Materials 281 (2013) 80-85.
[172] K. Vaidyanathan, K. Gross, MSET performance optimization for detection of software aging, 14th IEEE International Symposium in Software Reliability Engineering (ISSRE), Denver, USA, November 2003.
[173] Z. Yongjie, W. Dongfeng, Z. Junying, H. Yuejiao, Research on early fault diagnostic method of wind turbines, Telkomnika 11 (2013) 2330-2341.
[174] A. Wald, Sequential test of statistical hypotheses, The Annals of Mathematical Statistics 16 (1945) 117-186.
[175] A. Wald, Sequential Analysis, John Wiley and Sons, New York, 1947.
[176] M. Pecht, R. Jaai, A prognostics and health management roadmap for information and electronics-rich-systems, Microelectronics Reliability 50 (2010) 317-323.
[177] K.C. Gross, K.E. Humerik, Sequential probability ratio tests for nuclear plant component surveillance, Nuclear Technology 93 (1991) 131-137.
[178] H. Sohn, D.W. Allen, K. Worden, C.R. Farrar, Statistical damage classification using sequential probability ratio tests, Structural Health Monitoring 2 (2003) 57-74.

[179] K.D. Jarman, L.E. Smith, D.K. Carlson, Sequential probability ratio test for long-term radiation monitoring, IEEE Transactions on Nuclear Science 50 (2004) 1662-1666.
[180] H. Chen, Y. Shang, K. Sun, Multiple fault condition recognition of gearbox with sequential hypothesis test, Mechanical Systems and Signal Processing 40 (2013) 469-482.
[181] K.C. Gross, W. Lu, Early detection of signal and process anomalies in enterprise computing systems, IEEE International Conference on Machine Learning and Applications (ICMLA), Las Vegas, USA, 2002.
[182] G. Niu, Y. Zhao, M. Defoort, M. Pecht, Fault diagnosis of locomotive electro-pneumatic brake through uncertain bond graph modeling and robust online monitoring, Mechanical Systems and Signal Processing 50-51 (2015) 676-691.
[183] S. Cheng, M. Pecht, Multivariate state estimation technique for remaining useful life prediction of electronic product, Association for the Advancement of Artificial Intelligence (2007) 26-32.
[184] C.L. Black, R.E. Uhrig, J.W. Hines, System modelling and instrument calibration verification with a nonlinear state estimation technique, Maintenance and Reliability Conference (MARCON), Knoxville, USA, 1998.
[185] S. Cheng, K. Tom, L. Thomas, M. Pecht, A wireless sensor system for prognostics and health management, IEEE Sensors Journal 10 (2010) 856-862.
[186] W. Caesarendra, B. Kosasih, A.K. Tieu, C.A.S. Moodie, Application of the largest Lyapunov exponent algorithm for feature extraction in low speed slew bearing condition monitoring, Mechanical Systems and Signal Processing 50-51 (2015) 116-138.
[187] A. Choundhury, N. Tandon, Application of acoustic emission technique for the detection of defects in rolling element bearings, Tribology International 33 (2000) 39-45.
[188] M. Elforjani, D. Mba, Detecting natural crack initiation and growth in slow speed shafts with the acoustic emission technology, Engineering Failure Analysis 16 (2009) 2121-2129.
[189] M. Elforjani, D. Mba, Accelerated natural fault diagnosis in slow speed bearings with acoustic emission, Engineering Fracture Mechanics 77 (2010) 112-127.
[190] Y. He, X. Zhang, M.I. Friswell, Defect diagnosis for rolling element bearings using acoustic emission, Journal of Vibration and Acoustics 131 (2009) 1-10.
[191] S. Al-Dossary, R.I.R. Hamzah, D. Mba, Observations of changes in acoustic emission waveform for varying seeded defect sizes in a rolling element bearing, Applied Acoustics 70 (2009) 58-81.
[192] A.M. Al-Ghamd, D. Mba, A comparative experimental study on the use of acoustic emission and vibration analysis for bearing defect identification and estimation of defect size, Mechanical Systems and Signal Processing 20 (2006) 1537-1571.
[193] X. Liu, X. Wu, C. Liu, A comparison of acoustic emission and vibration on bearing fault detection, International Conference on Transportation, Mechanical, and Electrical Engineering (TMEE), China, December 16-18, 2011, pp. 922-926.
[194] N. Tandon, G.S. Yadava, K.M. Ramakrishna, A comparison of some condition monitoring techniques for the detection of defect in induction motor ball bearings, Mechanical Systems and Signal Processing 21 (2007) 244-256.
[195] N. Tandon, A. Choudhury, A review of vibration and acoustic measurement methods for the detection in rolling element bearings, Tribology International 32 (1999) 469-480.
[196] D. Mba, R.H. Bannister, G.E. Findlay, Condition monitoring of low-speed rotating machinery using stress waves, Part 1, Proceedings of the Institution of Mechanical Engineers, Part E: Journal of Process Mechanical Engineering 213 (1999) 153-170.
[197] T. Sako, O. Yoshie, Diagnostic method of low speed rolling element bearing using AE envelope waveform, IEEE Region 10 Annual International Conference TENCON, Fukuoka, Japan, November 21-24, 2010, pp. 724.
[198] N. Jamaludin, D. Mba, Monitoring extremely slow rolling element bearings: part I, Nondestructive Test and Evaluation International 35 (2002) 349-358.

[199] Z. Wu, G. Shen, J. Zhang, Characteristics of acoustic emission signals in the rolling bearing on giant wheel, 30th European Conference on Acoustic Emission Testing & 7th International Conference on Acoustic Emission, University of Granada, September 12-15, 2012.

[200] M. Nagata, M. Fujita, M. Yamada, T. Kitahara, Evaluation of tribological properties of bearing materials for marine diesel engines utilizing acoustic emission technique, Tribology International 46 (2012) 183-189.

[201] N. Jamaludin, D. Mba, Monitoring extremely slow rolling element bearings: part II, Nondestructive Test and Evaluation International 35 (2002) 359-366.

[202] J. Miettinen, P. Pataniitty, Acoustic emission in monitoring extremely slowly rotating rolling bearing, International Congress of Condition Monitoring and Diagnostic Engineering Management (COMADEM), Oxford, Coxmoor Publishing Company, 1999, pp. 289-297.

[203] B. Kilundu, X. Chiementin, J. Duez, D. Mba, Cyclostationarity of acoustic emissions (AE) for monitoring bearing defects, Mechanical Systems and Signal Processing 25 (2011) 2061-2072.

[204] D. Mba, Acoustic emission and monitoring bearing health, Tribology Transactions 46 (2003) 447-451.

[205] M.W. Hawman, W.S. Galinaitis, Acoustic emission monitoring or rolling element bearings, IEEE Ultrasonics Symposium, 1988, pp. 885-889.

[206] A. Morhain, D. Mba, Bearing defect diagnosis and acoustic emission, Proceeding of the Institute of Mechanical Engineers, Part J, Journal of Engineering Tribology 217 (2003) 257-272.

[207] D.S. Gu, B.K. Choi, Machinery Faults Detection Using Acoustic Emission Signal, in: M.G. Beghi (Ed.) Acoustic Waves - From Microdevices to Helioseismology, InTech, 2011.

[208] W. Wei, L. Qiang, Research on feature extraction of acoustic emission signals in time-domain, Advanced Materials Research 819 (2013) 171-175.

[209] T.R. Lin, E. Kim, A.C.C. Tan, A practical signal processing approach for condition monitoring of low speed machinery using Peak-Hold-Down-Sample algorithm, Mechanical Systems and Signal Processing 36 (2013) 256-270.

[210] X. Chiementin, D. Mba, B. Charnley, S. Lignon, J.P. Dron, Effect of the denoising on acoustic emission signals, Journal of Vibration and Acoustics 132 (2010) 1-7.

[211] K.R. Al-Balushi, A. Addali, B. Charnley, D. Mba, Energy index technique for detection of acoustic emissions associated with incipient bearing failures, Applied Acoustics 71 (2010) 812-821.

[212] A. Widodo, B.S. Yang, E.Y. Kim, A.C.C. Tan, J. Mathew, Fault diagnosis of low-speed bearing based on acoustic emission signal and multi-class relevance vector machine, Nondestructive Testing and Evaluation 24 (2009) 313-328.

[213] T. Kaewkongka, Y.H.J. Au, R.T. Rakowski, B.E. Jones, Fuzzy c-mean for bearing lubrication condition monitoring using acoustic emission, Instrumentation to Innovation - Application and Developments in Metal Production and Use, London, February 2002.

[214] S.A. Niknam, T. Thomas, J.W. Hines, R. Sawhney, Analysis of acoustic emission data for bearings subject to unbalance, International Journal of Prognostics and Health Management 4 (2013) 1-10.

[215] L.S. Law, J.H. Kim, W.Y.H. Liew, S.K. Lee, An approach based on wavelet packet decomposition and Hilbert-Huang transform (WPD-HHT) for spindle bearings condition monitoring, Mechanical Systems and Signal Processing 33 (2012) 197-211.

[216] A.W. Lees, Z. Quiney, The use of acoustic emission for bearing condition monitoring, Journal of Physics: Conference Series 305 (2011) 1-10.

[217] S.A. Mirhadizadeh, E.P. Moncholi, D. Mba, Influence of operational variables in a hydrodynamic bearing on the generation of acoustic emission, Tribology International 43 (2010) 1760-1767.

[218] N. Tandon, K.M. Ramakrishna, G.S. Yadava, Condition monitoring of electric motor ball bearings for the detection of grease contaminations, Tribology International 40 (2007) 29-36.
[219] Z. Rahman, H. Ohba, T. Yoshioka, T. Yamamoto, Incipient damage detection and its propagation monitoring of rolling contact fatigue by acoustic emission, Tribology International 42 (2009) 807-815.
[220] T. Yoshioka, S. Shimizu, Monitoring of ball bearing operation under grease lubrication using a new compound diagnostic system detecting vibration and acoustic emission, Tribology Transactions 52 (2009) 725-730.
[221] M. Lin, J. Yang, J. Xu, Trend analysis of the slow-speed and heavy-load equipment with acoustic emission, Advanced Materials Research 201-203 (2011) 2578-2582.
[222] ROLLIX, Slew Bearing Application >> Medical.
[223] ROLLIX, Slew Bearing Application >> Radar Military.
[224] J. Craig, J. Blankenship, C. Mecham, R.J. Mcneil, SLEW BEARING SYSTEM, NUCOR CORPORATION, USA, 2012.
[225] S.A. Niknam, V. Songmene, Y.H.J. Au, The use of acoustic emission information to distinguish between dry and lubricated rolling element bearings in low-speed rotating machines, International Journal of Advanced Manufacturing Technology 69 (2013) 2679-2689.
[226] T. Yoshioka, Detection of rolling contact sub-surface fatigue cracks using acoustic emission technique, Lubrication Engineering 49 (1993) 303-308.
[227] PCI-2 Based AE System User's Manual, Rev 2, PAC, Princetown Junction, New York, October 2004.
[228] J.R. Mathew, Acoustic Emission, Gordon and Break Science Publishers Inc., New York, 1983.
[229] N. Tandon, B.C. Nakra, Defect detection of rolling element bearings by acoustic emission method, Journal of Acoustic Emission 9 (1990) 25-28.
[230] A.C.C. Tan, Application of acoustic emission to the detection of bearing failures, The Institution of Engineers Australia, Tribology Conference, Brisbane, Australia, December 3-5, 1990, pp. 110-114.
[231] N. Tandon, B.C. Nakra, The application of the sound-intensity technique to defect detection in rolling-element bearings, Applied Acoustics 29 (1990) 207-217.
[232] V. Bansel, B.C. Gupta, A. Prakash, V.A. Eshwar, Quality inspection of rolling element bearing using acoustic emission technique, Journal of Acoustic Emission 9 (1990) 142-146.
[233] M. Li, J. Yang, Feature selection of acoustic emission signal for the slow-speed and heavy-load equipment, Applied Mechanics and Materials 110-116 (2012) 3199-3203.
[234] D. Mba, The use of acoustic emission for estimation of bearing defect size, Journal of Failure Analysis and Prevention 8 (2008) 188-192.
[235] P.R. Aguiar, C.H.R. Martins, M. Marchi, E.C. Bianchi, Digital Signal Processing for Acoustic Emission, Data Acquisition Applications, in: P.Z. Karakehayov (Ed.), InTech, 2012.
[236] D.W. Schwach, Y.B. Guo, A fundamental study on the impact of surface integrity by hard turning on rolling contact fatigue, International Journal of Fatigue 28 (2006) 1838-1844.
[237] E.D. Price, A.W. Lees, M.I. Friswell, B.J. Roylance, Online detection of subsurface by acoustic emissions, Key Engineering Materials 245-246 (2003) 451-460.
[238] D.H. Pandya, S.H. Upadhyay, S.P. Harsha, Fault diagnosis of rolling element bearing with intrinsic mode function of acoustic emission data using APF-KNN, Expert Systems with Applications 40 (2013) 4137-4145.
[239] R.K. Sreenilayam-Raveendran, M.H. Azarian, C. Morillo, M.G. Pecht, K. Kida, E.C. Santos, T. Honda, H. Koike, Comparative evaluation of metal and polymer ball bearings, Wear 302 (2013) 1499-1505.
[240] F. Hort, P. Mazal, Application of acoustic emission for measuring of contact fatigue of axial bearing, Engineering Mechanics 18 (2011) 117-125.

[241] T. Yoshioka, H. Mano, T. Yamamoto, A. Korenaga, Diagnosis of rolling bearing by measuring time interval of AE generation, Journal of Tribology 121 (1999) 468-472.
[242] W. Kaewwaewnoi, A. Prateepasen, P. Kaewtrakulpong, Measurement of valve leakage rate using acoustic emission, ECTI, Pattaya, Thailand, May 12-13, 2005.
[243] Z. Zhi-qiang, L. Guo-lu, W. Hai-dou, X. Bin-shi, P. Zhong-yu, Z. Li-na, Investigation of rolling contact fatigue damage process of the coating by acoustics emission and vibration signals, Tribology International 47 (2012) 25-31.
[244] J. Antoni, Cyclostationarity by examples, Mechanical Systems and Signal Processing 23 (2009) 987-1036.
[245] G.F. Bin, C.J. Liao, X.J. Li, The method of fault feature extraction from acoustic emission signals using Wigner-Ville distribution, Advanced Materials Research 216 (2011) 732-737.
[246] Y. He, X. Zhang, M.I. Friswell, Observation of time-frequency characteristics of the acoustic emission from defects in rolling element bearings, Non-Destructive Testing and Condition Monitoring 52 (2010) 412-419.
[247] J. Shiroshi, Y. Li, S. Liang, T. Kurfess, S. Danyluk, Bearing condition diagnostics via vibration and acoustic emission measurements, Mechanical Systems and Signal Processing 11 (1997) 693-705.
[248] J. Antoni, The spectral kurtosis: A useful tool for characterising non-stationary signals, Mechanical Systems and Signal Processing 20 (2006) 282–307.
[249] P. He, P. Li, H. Sun, Feature extraction of acoustic signals based on complex Morlet wavelet, Procedia Engineering 15 (2011) 464-468.
[250] H. Oh, M.H. Azarian, M. Pecht, Estimation of fan bearing degradation using acoustic emission analysis and mahalanobis distance, In Technical Program for MFPT: The Applied Systems Health Management Conference 2011: Enabling Sustainable Systems.
[251] Y. He, X. Zhang, Approximate entropy analysis of the acoustic emission from defects in rolling element bearings, Journal of Vibration and Acoustics 134 (2012) 1-8.
[252] C.J. Li, S.Y. Li, Acoustic emission analysis for bearing condition monitoring, Wear 185 (1995) 67-74.
[253] B.S. Kim, D.S. Gu, J.G. Kim, Y.C. Kim, B.K. Choi, Rolling element bearing fault detection using acoustic emission signal analysed by envelope analysis with discrete wavelet transform, 4th World Conference on Engineering Asset Management (WCEAM), Athens, Greece, September 28-30, 2009.
[254] S.A. Niknam, V. Songmene, Y.H.J. Au, Proposing a new acoustic emission parameter for bearing condition monitoring in rotating machines, Transactions of the Canadian Society for Mechanical Engineering 37 (2013) 1105-1114.
[255] E. Pomponi, A. Vinogradov, A real-time approach to acoustic emission clustering, Mechanical Systems and Signal Processing 40 (2013) 791-804.
[256] C. Ruis-Cárcel, E. Hernani-Ros, Y. Cao, D. Mba, Use of spectral kurtosis for improving signal to noise ratio of acoustic emission signal from defective bearings, Journal of Failure Analysis and Prevention 14 (2014) 363-371.
[257] L.D. Hall, D. Mba, R.H. Bannister, Acoustic emission signal classification in condition monitoring using the Kolmogorov-Smirnov statistic, Journal of Acoustic Emission 19 (2001) 209-228.
[258] S. Kacimi, S. Laurens, The correlation dimension: A robust chaotic feature for classifying acoustic emission signals generated in construction materials, Journal of Applied Physics 106 (2009) 024909-024901-024908.
[259] W. Song, J. Yang, C. Qiang, Tool condition monitoring based on fractal and wavelet analysis by acoustic emission, in: O. Gervasi, M.L. Gavrilova (Eds.) The International Conference on Computational Science and Its Applications (ICCSA), Kuala Lumpur, Malaysia, 2007, pp. 469-479.

[260] J. Xi, W. Han, Y. Liu, Relationship analysis between chaotic characteristic of acoustic emission signal and tool wear condition, Third International Workshop on Advanced Computational Intelligence, Suzhou, Jiangsu, China, August 25-27, 2010, pp. 612-617.
[261] S.H. Ghafari, F. Golnaraghi, F. Ismail, Effect of localized faults on chaotic vibration of rolling element bearings, Nonlinear Dynamics 53 (2008) 287-301.
[262] L.D. Hall, D. Mba, Acoustic emission diagnosis of rotor-stator rubs using the KS statistic, Mechanical Systems and Signal Processing 18 (2004) 849-868.
[263] L. Lin, F. Chu, Approximate entropy as acoustic emission feature parametric data for crack detection, Nondestructive Testing and Evaluation 26 (2011) 119-128.
[264] R. Yan, R.X. Gao, Approximate Entropy as a diagnostic tool for machine
health monitoring, Mechanical Systems and Signal Processing 21 (2007) 824-839.
[265] M.T. Rosenstein, J. Collins, C.J.D. Luca, A practical method for calculating largest Lyapunov exponents from small data sets, Physica D 65 (1993) 117-134.
[266] J. Lee, F. Wu, W. Zhao, M. Ghaffari, L. Liao, D. Siegel, Prognostics and health management design for rotary machinery systems – Reviews, methodology and applications, Mechanical Systems and Signal Processing 42 (2014) 314-334.
[267] A.K.S. Jardine, D. Lin, D. Banjevic, A review on machinery diagnostics and prognostics implementing condition-based maintenance, Mechanical Systems and Signal Processing 20 (2006) 1483–1510.
[268] R. Kothamasu, S.H. Huang, W.H. VerDuin, System health monitoring and prognostics – a review of current paradigms and practices, International Journal of Advanced Manufacturing Technology 28 (2006) 1012-1024.
[269] K.M. Goh, B. Tjahjono, T. Bainers, S.A. Subramaniam, Review of research in manufacturing prognostics, IEEE International Conference on Industrial Informatics, Singapore, Aug 16-18, 2006, pp. 417 - 422.
[270] G. Vachtsevanos, F.L. Lewis, M. Roemer, A. Hess, B. Wu, Intelligent Fault Diagnosis and Prognosis for Engineering Systems, John Wiley and Sons, New Jersey, 2006.
[271] A. Heng, S. Zhang, A.C.C. Tan, J. Mathew, Rotating machinery prognostics: State of the art, challenges and opportunities, Mechanical Systems and Signal Processing 23 (2009) 724-739.
[272] Y. Peng, M. Dong, M.J. Zuo, Current status of machine prognostics in condition-based maintenance: a review, The International Journal of Advanced Manufacturing Technology 50 (2010) 297-313.
[273] O.E. Dragomir, R. Gouriveau, F. Dragomir, E. Minca, N. Zerhouni, Review of Prognostic Problem in Condition-Based Maintenance, European Control Conferece (ECC), Budapest, Hungary, 2009.
[274] J.W. Hines, A. Usynin, Current computational trends in equipment prognostics, International Journal of Computational Intelligence Systems 1 (2008) 94-102.
[275] H.E. Kim, Machine Prognostics based on Health State Probability Estimation, School of Engineering Systems Faculty of Built Environmental Engineering, Queensland University of Technology, Brisbane, 2010.
[276] Y. Li, S. Billington, C. Zhang, T. Kurfess, S. Danyluk, S. Liang, Adaptive prognostics for rolling element bearing condition, Mechanical Systems and Signal Processing 13 (1999) 103-113.
[277] Y. Li, T.R. Kurfess, S.Y. Liang, Stochastic prognostics for rolling element bearings, Mechanical Systems and Signal Processing 14 (2000) 747-762.
[278] J. Qiu, C. Zhang, B.B. Seth, S.Y. Liang, Damage mechanics approach for bearing lifetime prognostics, Mechanical Systems and Signal Processing 16 (2002) 817-829.
[279] C.K.R. Lim, D. Mba, SwitchingKalmanfilterforfailureprognostic, Mechanical Systems and Signal Processing.
[280] W. Caesarendra, G. Niu, B.S. Yang, Machine condition prognosis based on sequential Monte Carlo method, Expert Systems with Applications 37 (2010) 2412-2420.

[281] P. Boškoski, M. Gašperin, D. Petelin, Đ. Juričić, Bearing fault prognostics using Rényi entropy based features and Gaussian process models, Mechanical Systems and Signal Processing.

[282] P.-J. Vlok, M. Wnek, M. Zygmunt, Utilising statistical residual life estimates of bearings to quantify the influence of preventive maintenance actions, Mechanical Systems and Signal Processing 18 (2004) 833-847.

[283] Y. Sun, L. Ma, J. Mathew, W. Wang, S. Zhang, Mechanical systems hazard estimation using condition monitoring, Mechanical Systems and Signal Processing 20 (2006) 1189-1201.

[284] W. Wang, A model to predict the residual life of rolling element bearings given monitored condition information to date, IMA Journal of Management Mathematics 13 (2002) 3-16.

[285] W. Caesarendra, A. Widodo, B.S. Yang, Combination of probability approach and support vector machine towards machine health prognostics, Probabilistic Engineering Mechanics 26 (2011) 165-173.

[286] V.T. Tran, H.T. Pham, B.S. Yang, T.T. Nguyen, Machine performance degradation assessment and remaining useful life prediction using proportional hazard model and support vector machine, Mechanical Systems and Signal Processing 32 (2012) 320-330.

[287] F. Yang, H. Xiaodiao, C. Jie, W. Hua, H. Rongjing, Reliability-based residual life prediction of large-size low-speed slewing bearings, Mechanism and Machine Theory 81 (2014) 94-106.

[288] X. Zhang, R. Xu, C. Kwan, S.Y. Liang, Q. Xie, L. Haynes, An integrated approach to bearing fault diagnostics and prognostics, American Control Conference, Portland, OR, USA, 2005, pp. 2750–2755.

[289] H. Ocak, K.A. Loparo, F.M. Discenzo, Online tracking of bearing wear using wavelet packet decomposition and probabilistic modeling: A method for bearing prognostics, Journal of Sound and Vibration 302 (2007) 951-961.

[290] Y. Shao, K. Nezu, Prognosis of remaining bearing life using neural networks, Proceedings of the Institution of Mechanical Engineers, Part I: Journal of Systems and Control Engineering 214 (2000) 217-230.

[291] N. Gebraeel, M. Lawley, R. Liu, V. Parmeshwaran, Residual life predictions from vibration-based degradation signals: A neural network approach, IEEE Transactions on Industrial Electronics 51 (2004) 694-700.

[292] E. Jantunen, Prognosis of rolling bearing failure based on regression analysis and fuzzy Logic, Journal of Vibration Engineering and Technologies 5 (2006) 97-108.

[293] D.Z. Li, W. Wang, An enhanced GA technique for system training and prognostics, Advances in Engineering Software 42 (2011) 452-462.

[294] B. Kosasih, W. Caesarendra, K. Tieu, A. Widodo, C.A.S. Moodie, Degradation trend estimation and prognosis of large low speed slewing bearing lifetime, Applied Mechanics and Materials 493 (2014) 343-348.

[295] G. Niu, B.S. Yang, Dempster-Shafer regression for multi-step-ahead time-series prediction towards data-driven machinery prognosis, Mechanical Systems and Signal Processing 23 (2009) 740-751.

[296] H.T. Pham, B.S. Yang, Estimation and forecasting of machine health condition using ARMA/GARCH model, Mechanical Systems and Signal Processing 24 (2010) 546-558.

[297] F.D. Maio, K.L. Tsui, E. Zio, Combining relevance vector machines and exponential regression for bearing residual life estimation, Mechanical Systems and Signal Processing 31 (2012) 405-427.

[298] A. Widodo, B.S. Yang, Application of relevance vector machine and survival probability to machine degradation assessment, Expert Systems with Applications 38 (2011) 2592-2599.

[299] J.B. Ali, B. Chebel-Morello, L. Saidi, S. Malinowski, Accurate bearing remaining useful life prediction based on Weibull distribution and artificial neural network, Mechanical Systems and Signal Processing 56-57 (2015) 150-172.
[300] W. Caesarendra, Model-based and data-driven approach for machine prognostics, Department of Mechanical Design Engineering, Pukyong National University, Busan, 2010.
[301] R. Potočnik, P. Göncz, J. Flašker, S. Glodež, Fatigue life of double row slewing ball bearing with irregular geometry, Procedia Engineering 2 (2010) 1877-1886.
[302] ISO281, Dynamic load ratings and rating life, 2007.
[303] K.B. Goode, J. Moore, B.J. Roylance, Plant machinery working life prediction method utilizing reliability and condition-monitoring data, Proceeding of the Institute of Mechanical Engineers, Part J, Journal of Process Mechanical Engineering 214 (2000) 109-122.
[304] D.R. Cox, Regression models and life-tables, Royal Statistical Society 34 (1972) 187-220.
[305] D. Kumar, B. Klefsjö, Proportional hazards model: a review, Reliability Engineering and System Safety 44 (1994) 177-188.
[306] A. Heng, A. Tan, J. Mathew, B.S. Yang, Machine prognosis with full utilization of truncated lifetime data, Proceedings of the Second World Congress on Engineering Asset Management, Harrogate, UK, 2007, pp. 775-784.
[307] G.X. Hai, H.X. Diao, H.R. Jing, W. Hua, C. Jie, A rolling contact fatigue reliability evaluation method and its application to a slewing bearing, Journal of Tribology 134 (2012) 1-7.
[308] T.E. Tallian, Data fitted bearing life prediction model for variable operating conditions, Tribology International 42 (1999) 241-249.
[309] M. Schwabacher, K. Goebel, A survey of artificial intelligence for prognostics, AAAI Fall Symposium, Arlington VA, 2007.
[310] P. Wang, G. Vachtsevanos, Fault prognostics using dynamic wavelet neural networks, Artificial Intelligence for Engineering Design, Analysis and Manufacturing 15 (2001) 349-365.
[311] X.D. Zhang, R. Xu, K. Chiman, S.Y. Liang, Q.L. Xie, L. Haynes, An integrated approach to bearing fault diagnostics and prognostics, Proceedings of the 2005 American Control Conference, Portland, OR (USA), 8 - 10 Jun 2005, pp. 2750 - 2755.
[312] G. Niu, B.S. Yang, Dempster–Shafer regression for multi-step-ahead timeseries prediction towards data-driven machinery prognosis, Mechanical Systems and Signal Processing 23 (2009) 740-751.
[313] V.T. Tran, B.S. Yang, A.C.C. Tan, Multi-step ahead direct prediction for the machine condition prognosis using regression trees and neuro-fuzzy systems, Expert Systems with Applications 36 (2009) 9378-9387.
[314] C. Lu, L. Tao, H. Fan, An intelligent approach to machine component health prognostics by utilizing only truncated histories, Mechanical Systems and Signal Processing 42 (2014) 300-313.
[315] C.S. Byington, M.J. Roemer, M.J. Watson, Prognostic enhancements to diagnostic systems (PEDS) applied to shipboard power generation systems, in Proceedings of ASME Turbo Expo 2004 Power for Land, Sea and Air, Vienna, Austria, 2004.
[316] F. Camci, Process monitoring, diagnostics and prognostics using support vector machines and hidden Markov models, Wayne State University, 2005.
[317] J. Lee, J. Ni, D. Djurdjanovic, H. Qiu, H. Liao, Intelligent prognostics tools and e-maintenance, Computers in Industry 57 (2006) 476-489.
[318] E. López-Rubio, M.N. Florentín-Núnez, Kernel regression based feature extraction for 3D MR image denoising, Medical Image Analysis 15 (2011) 498-513.
[319] H. Takeda, S. Farsiu, P. Milanfar, Kernel regression for image processing and reconstruction, IEEE Transactions on Image Processing 16 (2007) 349-366.
[320] M.C. Jones, H. Park, K.I. Shin, S.K. Vines, S.O. Jeong, Relative error prediction via kernel regression smoothers, Journal of Statistical Planning and Inference 138 (2008) 2887-2898.

[321] C.G. Atkeson, A.W. Moore, S. Schaal, Locally weighted learning, Artificial Intelligence Review 11 (1997) 11-73.
[322] E.A. Nadaraya, On estimating regression, Theory of Probability and its Applications 9 (1964) 141-142.
[323] G.S. Watson, Smooth regression analysis, The Indian Journal of Statistics, Series A 26 (1964) 359-472.
[324] Kernel Regression, http://people.revoledu.com/kardi/tutorial/Regression/KernelRegression/
[325] F.d. Lorenzo, M. Calabro, Kurtosis: a statistical approach to identify defect in rolling bearing, The 2nd International Conference on Marine Research and Transportation, Ischia Naples, Italy, June 28-30, 2007, pp. 17-24.
[326] S.A. Aye, Statistical approach for tapered bearing fault detection using different methods, World Congress on Engineering (WCE), London, UK, July 6-8, 2011.
[327] W. Guo, P.W. Tse, A. Djordjevich, Faulty bearing signal recovery from large noise using a hybrid method based on spectral kurtosis and ensemble empirical mode decomposition, Measurement 45 (2012) 1308-1322.
[328] Die Wälzlagerpraxis: Handbuch für die Berechnung und Gestaltung von Lagerungen,
[329] http://www.physicalacoustics.com/by-product/sensors/WD-100-900-kHz-Wideband-Differential-AE-Sensor?page_context=category&faceted_search=0

Appendices

Appendix A: The formula for calculating bearing fault frequencies [328]

- Fault frequency of outer ring:

$$F_{OR} = \left| \frac{\left| IR_{rpm} - OR_{rpm} \right|}{2} \cdot \left[1 - \frac{\left(\cos(\alpha) \right) \cdot d_r}{d_m} \right] \right| \cdot z \tag{A1}$$

- Fault frequency of inner ring:

$$F_{IR} = \left| \frac{\left| IR_{rpm} - OR_{rpm} \right|}{2} \cdot \left[1 + \frac{\left(\cos(\alpha) \right) \cdot d_r}{d_m} \right] \right| \cdot z \tag{A2}$$

- Fault frequency of rolling element:

$$F_R = \left| \frac{\left| IR_{rpm} - OR_{rpm} \right|}{2} \cdot \left[\frac{d_m}{d_r} - \frac{\left(\cos(\alpha) \right)^2 \cdot d_r}{d_m} \right] \right| \tag{A3}$$

where IR_{rpm} and OR_{rpm} are the rotational speeds of the inner ring and outer ring. For 1 rpm the value of IR_{rpm} is 1 and the value of OR_{rpm} is 0. d_m denotes the mean bearing diameter, d_r is diameter of the rolling element and z is number of rolling elements.

Appendix B: Circular domain feature analysis

B.1 The effect of window size to neighborhood correlation plot

The physical explanation why the right ellipsoid of neighborhood correlation plot will change and switch over is that the number of new data-reduced for a half sinusoidal signal is equal or less than 2. Through this appendix the answer is empirically conducted which also explain the phenomenon in Figure 4.2, Figure 4.3 and Figure 4.4. Then the selection of window size of 8 in Laboratory slew bearing data will be explained.

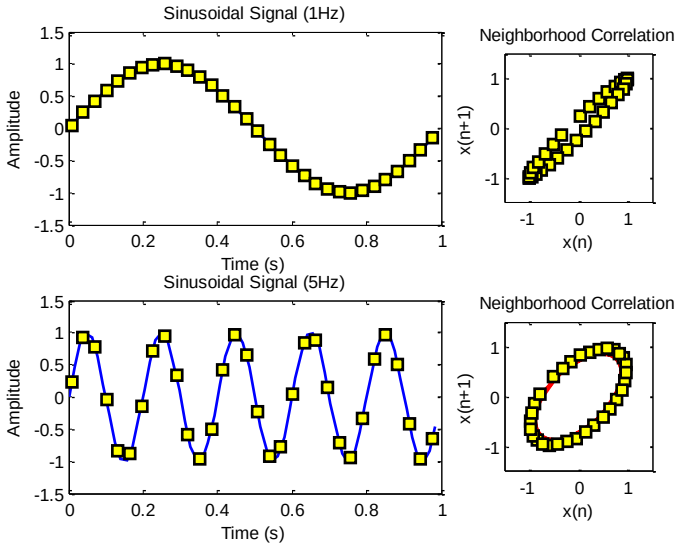

Figure 4.2 ($w = 2$):

(a) In 1Hz signal with sampling frequency of 64 for 1 second, the number of samples for one cycle sinusoidal signal is 64/1 = 64 samples. The number of samples for a half sinusoidal signal is 64 samples/2 = 32 samples. If the window size is 2, thus in a half sinusoidal signal there are: 32 samples/2 window size = 16 samples. (Note: right ellipsoid orientation)

(b) In 5Hz signal with sampling frequency of 64 for 1 second, the number of samples for one cycle sinusoidal is 64/5 = 12.8 samples. The number of samples for a half sinusoidal signal is 12.8 samples/2 = 6.4 samples. If the window size is 2, thus in a half sinusoidal signal there are: 6.4 samples/2 window size = 3.2 samples. (Note: still right ellipsoid orientation)

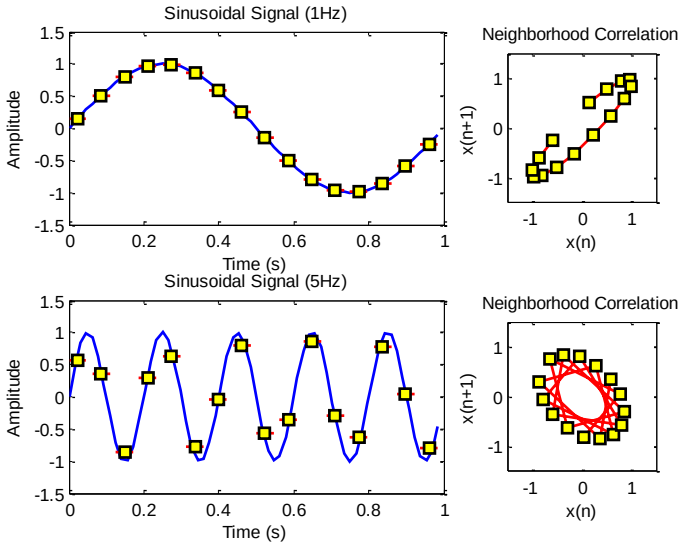

Figure 4.3 ($w = 4$):

(c) In 1Hz signal with sampling frequency of 64 for 1 second, the number of samples for one cycle sinusoidal signal is 64/1 = 64 samples. The number of samples for a half sinusoidal signal is 64 samples/2 = 32 samples. If the window size is 4, thus in a half sinusoidal signal there are: 32 samples/4 window size = 8 samples. (Note: still right ellipsoid orientation)

(d) In 5Hz signal with sampling frequency of 64 for 1 second, the number of samples for one cycle sinusoidal is 64/5 = 12.8 samples. The number of samples for a half sinusoidal signal is 12.8 samples/2 = 6.4 samples. If the window size is 4, thus in a half sinusoidal signal there are: 6.4 samples/4 window size = 1.6 samples. (Note: switch over to left ellipsoid orientation)

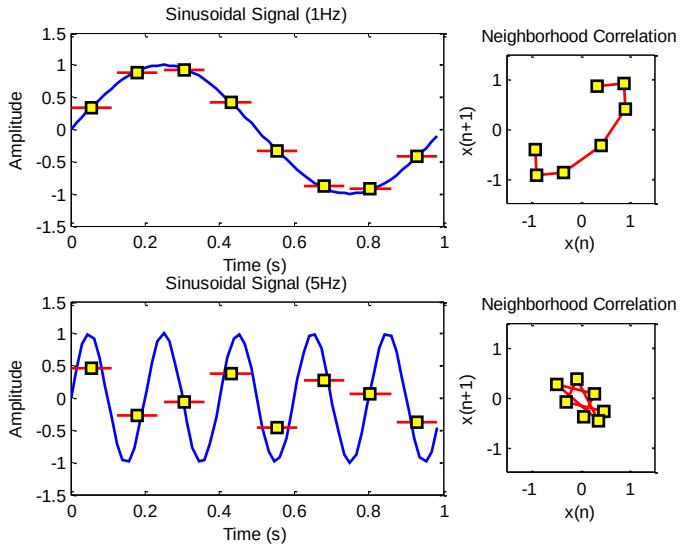

Figure 4.4 ($w = 8$):

(e) In 1Hz signal with sampling frequency of 64 for 1 second, the number of samples for one cycle sinusoidal signal is 64/1 = 64 samples. The number of samples for a half sinusoidal signal is 64 samples/2 = 32 samples. If the window size is 8, thus in a half sinusoidal signal there are: 32 samples/8 window size = 4 samples. (Note: still right ellipsoid orientation)

(f) In 5Hz signal with sampling frequency of 64 for 1 second, the number of samples for one cycle sinusoidal is 64/5 = 12.8 samples. The number of samples for a half sinusoidal signal is 12.8 samples/2 = 6.4 samples. If the window size is 8, thus in a half sinusoidal signal there are: 6.4 samples/8 window size = 0.8 samples. (Note: change to left ellipsoid orientation)

B.2 The formula to calculate shifting factor

According to the empirical calculation above, the number of samples for a half sinusoidal signal, S can be calculated by:

$$S = 0.5\frac{fs}{\lambda} \tag{B1}$$

where, *fs* is sampling frequency and λ is frequency that trigger the change of ellipsoid orientation. Introducing an important dimensionless parameter called shifting factor, ϕ:

$$\phi = \frac{S}{w} \tag{B2}$$

where w is the window size. The different pattern of ellipsoid can be identified based on the value of, ϕ:

if ϕ > 2, the neighborhood correlation plot will be the right ellipsoid.

If ϕ ≤ 2, the neighborhood correlation plot will be the left ellipsoid

Substitute Eq. (B1) to Eq. (B2) to calculate the shifting factor, ϕ:

$$\phi = \frac{0.5 * \frac{fs}{\lambda}}{w} \tag{B3}$$

Appendix C: Physical meaning of the reconstruction delay, *J*

The illustration of the samples delay J is presented as follows. Suppose $\mathbf{Y}$ is the vibration data with number of samples $N = 15$ is given as follows.

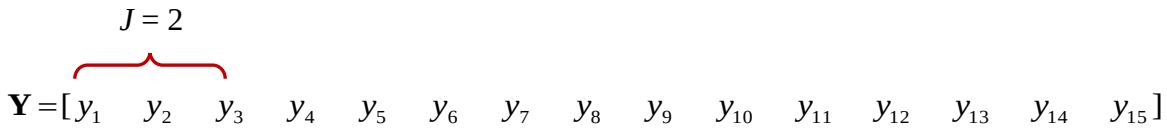

With the reconstruction delay $J = 2$ and the embedding dimension $m = 6$, using the equation $M = N - (m - 1)J$, the number of reconstructed vector is $M = 5$. Consequently, the dimension of the phase-space matrix $\mathbf{X}$ is an M-by-m matrix or 5-by-6 matrix. The detailed process to obtain the reconstructed vectors for vibration data with 15 samples is shown as follows:

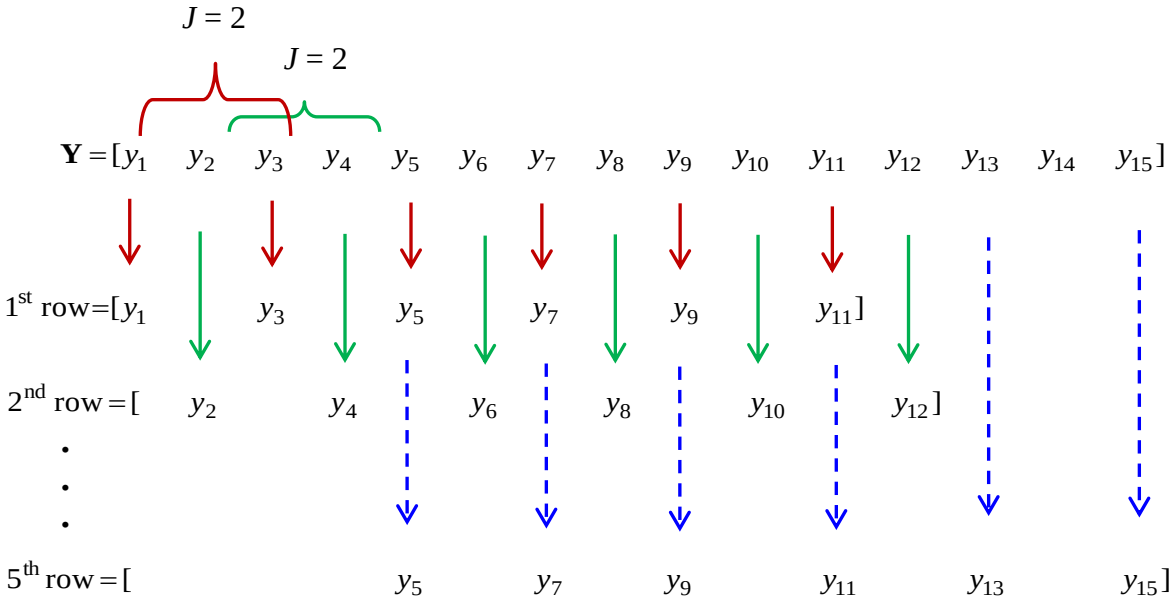

The reconstruction vectors process of example vibration data, shown above, can be represented in the phase-space matrix $\mathbf{X}$:

$$\mathbf{X} = \begin{bmatrix} y_1 & y_3 & y_5 & y_7 & y_9 & y_{11} \\ y_2 & y_4 & y_6 & y_8 & y_{10} & y_{12} \\ y_3 & y_5 & y_7 & y_9 & y_{11} & y_{13} \\ y_4 & y_6 & y_8 & y_{10} & y_{12} & y_{14} \\ y_5 & y_7 & y_9 & y_{11} & y_{13} & y_{15} \end{bmatrix} \tag{C1}$$

Appendix D: MATLAB codes

D.1 Time-domain feature extraction: RMS, variance, skewness, kurtosis, shape factor, crest factor, entropy, histogram upper bound and histogram lower bound.

```
% Time-domain feature extraction for vibration slew bearing signal
% 30/03/2013
% by Wahyu Caesarendra

function n = parameter()
disp('1. February')
disp('2. March')
disp('3. April')
disp('4. May')
disp('5. July')
disp('6. August')
bulan = input('which month you want to select: \n')

if bulan == 1
    start_day = 21;
    end_day = 28;
elseif bulan == 2
    start_day = 1;
    end_day = 31;
elseif bulan == 3
    start_day = 1;
    end_day = 26;
elseif bulan == 4
    start_day = 1;
    end_day = 28;
elseif bulan == 5
    start_day = 17;
    end_day = 31;
else bulan == 6
    start_day = 1;
    end_day = 31;
end

baris = 1;
% ====================== Loading data ==================
for day = start_day:end_day              % Number of data

    if bulan == 1
        bln = ['february' num2str(day) '.txt']
    elseif bulan == 2
        bln = ['march' num2str(day) '.txt']
    elseif bulan == 3
        bln = ['april' num2str(day) '.txt']
    elseif bulan == 4
        bln = ['may' num2str(day) '.txt']
    elseif bulan == 5
        bln = ['july' num2str(day) '.txt']
    else bulan = 6
        bln = ['august' num2str(day) '.txt']
    end
```

```
    data_load = load(bln);

        feat_counter = 1;
        % =============== Time domain feature extraction ==========
        for i = 2:5 % channel 1 to 4

            data = data_load(:,i);

            m = mean(data);
            rms = sqrt(sum(data.^2)/size(data,1));% RMS(F1)
            variance = var(data);                 % variance(F2)
            skew = skewness(data,0);              % skewness(F3)
            kur = kurtosis(data);                 % kurtosis(F4)
            sf = rms/m;                           % shape factor(F5)
            peak = sum(data);
            cf = peak/rms;                        % crest factor(F6)
            data_inverse = data';
            [ESTIMATE,NBIAS,SIGMA,DESCRIPTOR]=ENTROPY(data_inverse);
            entropy = ESTIMATE;                   % entropy(F7)
            histupper = DESCRIPTOR(1); % Histogram upper bound(F8)
            histlower = DESCRIPTOR(2); % Histogram lower bound(F9)

            feature.rms = rms;
            feature.variance = variance;
            feature.skew = skew;
            feature.kur = kur;
            feature.sf = sf;
            feature.cf = cf;
            feature.entropy = entropy;
            feature.histupper = histupper;
            feature.histlower = histlower;

                % ************** features data saving **************
                nfile = 1;
                features(nfile,1) = feature.rms;
                features(nfile,2) = feature.variance;
                features(nfile,3) = feature.skew;
                features(nfile,4) = feature.kur;
                features(nfile,5) = feature.sf;
                features(nfile,6) = feature.cf;
                features(nfile,7) = feature.entropy;
                features(nfile,8) = feature.histupper;
                features(nfile,9) = feature.histlower;

                [ndata, nfeat] = size(features);

                 total_features(baris,nfeat*(feat_counter-
                 1)+1:feat_counter*nfeat) = features;
                feat_counter = feat_counter+1;
        end
        baris = baris + 1;
end

cd TimeDomainFeatures_Thesis

% Saving features
if bulan == 1
    save TotFeat_Feb.dat total_features -ascii
elseif bulan == 2
    save TotFeat_Mar.dat total_features -ascii
```

```
elseif bulan == 3
    save TotFeat_Apr.dat total_features -ascii
elseif bulan == 4
    save TotFeat_May.dat total_features -ascii
elseif bulan == 5
    save TotFeat_Jul.dat total_features -ascii
else bulan == 6
    save TotFeat_Aug.dat total_features -ascii
end
```

D.2 Other time-domain feature extraction: AR coefficients, impulse factor, margin factor, activity, mobility and complexity.

```
% Other time-domain feature extraction for vibration slew bearing
signal
% 20/10/2014
% by Wahyu Caesarendra

function n = parameter()

disp('1. February')
disp('2. March')
disp('3. April')
disp('4. May')
disp('5. July')
disp('6. August')
bulan = input('which month you want to select: \n')

if bulan == 1
    start_day = 21;
    end_day = 28;
elseif bulan == 2
    start_day = 1;
    end_day = 31;
elseif bulan == 3
    start_day = 1;
    end_day = 26;
elseif bulan == 4
    start_day = 1;
    end_day = 28;
elseif bulan == 5
    start_day = 17;
    end_day = 31;
else bulan == 6
    start_day = 1;
    end_day = 31;
end

baris = 1;
% ====================== Loading data ==================
for day = start_day:end_day              % Number of data

    if bulan == 1
        bln = ['february' num2str(day) '.txt']
    elseif bulan == 2
        bln = ['march' num2str(day) '.txt']
    elseif bulan == 3
        bln = ['april' num2str(day) '.txt']
    elseif bulan == 4
        bln = ['may' num2str(day) '.txt']
    elseif bulan == 5
        bln = ['july' num2str(day) '.txt']
    else bulan = 6
        bln = ['august' num2str(day) '.txt']
    end

    data_load = load(bln);
```

```
        feat_counter = 1;
        % =============== time domain feature extraction ==========
        for i = 2:5 % channel 1 to 4

            data = data_load(:,i);

            feature.ar = armcov(data,8);          % AR features (F1-F8)
            IF = max(abs(data))/mean(abs(data)); % Impulse factor (F9)
            MF = max(abs(data))/mean(sqrt(abs(data)))^2; % MF(F10)

            h1 = var(data);   % Hjorth parameter1 (activity) (F11)
            diff1 = diff(data);
            h2 = std(diff1)/std(data); % Hjorth param2 (mobility)(F12)
            diff2 = diff(diff1);
            h3 = (std(diff2)/std(diff1))/(std(diff1)/std(data)); %
            Hjorth parameter3 (complexity) (F13)

            feature.ar1 = ar(2);     % (F1)
            feature.ar2 = ar(3);     % (F2)
            feature.ar3 = ar(4);     % (F3)
            feature.ar4 = ar(5);     % (F4)
            feature.ar5 = ar(6);     % (F5)
            feature.ar6 = ar(7);     % (F6)
            feature.ar7 = ar(8);     % (F7)
            feature.ar8 = ar(9);     % (F8)
            feature.IF = IF;         % (F9)
            feature.MF = MF;         % (F10)
            feature.h1 = h1;         % (F11)
            feature.h2 = h2;         % (F12)
            feature.h3 = h3;         % (F13)

            % *************** features data saving ***************
            nfile = 1;
            features(nfile,1) = feature.ar(2);
            features(nfile,2) = feature.ar(3);
            features(nfile,3) = feature.ar(4);
            features(nfile,4) = feature.ar(5);
            features(nfile,5) = feature.ar(6);
            features(nfile,6) = feature.ar(7);
            features(nfile,7) = feature.ar(8);
            features(nfile,8) = feature.ar(9);
            features(nfile,9) = feature.IF;
            features(nfile,10) = feature.MF;
            features(nfile,11) = feature.h1;
            features(nfile,12) = feature.h2;
            features(nfile,13) = feature.h3;

            [ndata, nfeat] = size(features);
            total_features(baris,nfeat*(feat_counter-
            1)+1:feat_counter*nfeat) = features;
            feat_counter = feat_counter+1;
        end
        baris = baris + 1;
end

cd TimeDomainFeatures_Thesis_lainnya

% saving features
if bulan == 1
    save TotFeat_Feb.dat total_features -ascii
```

```
elseif bulan == 2
    save TotFeat_Mar.dat total_features -ascii
elseif bulan == 3
    save TotFeat_Apr.dat total_features -ascii
elseif bulan == 4
    save TotFeat_May.dat total_features -ascii
elseif bulan == 5
    save TotFeat_Jul.dat total_features -ascii
else bulan == 6
    save TotFeat_Aug.dat total_features -ascii
end
```

D.3 Frequency-domain feature extraction: frequency centre, root mean square frequency, root variance frequency.

```
% Frequency-domain feature extraction for vibration slew bearing
signal
% 30/03/2013
% by Wahyu Caesarendra

function n = parameter()
disp('1. February')
disp('2. March')
disp('3. April')
disp('4. May')
disp('5. July')
disp('6. August')
bulan = input('which month you want to select: \n')

if bulan == 1
    start_day = 21;
    end_day = 28;
elseif bulan == 2
    start_day = 1;
    end_day = 31;
elseif bulan == 3
    start_day = 1;
    end_day = 26;
elseif bulan == 4
    start_day = 1;
    end_day = 28;
elseif bulan == 5
    start_day = 17;
    end_day = 31;
else bulan == 6
    start_day = 1;
    end_day = 31;
end
baris = 1;
% ====================== Loading data ==================
for day = start_day:end_day             % Number of data
    if bulan == 1
        bln = ['february' num2str(day) '.txt']
    elseif bulan == 2
        bln = ['march' num2str(day) '.txt']
    elseif bulan == 3
        bln = ['april' num2str(day) '.txt']
    elseif bulan == 4
        bln = ['may' num2str(day) '.txt']
    elseif bulan == 5
        bln = ['july' num2str(day) '.txt']
    else bulan = 6
        bln = ['august' num2str(day) '.txt']
    end

    data_load = load(bln);

        feat_counter = 1;
        % ============ frequency domain feature extraction ==========
        for i = 2:5 % channel 1 to 4
```

```
            data = data_load(:,i);

            data_dif = diff(data);
            max_freq = 2000;
            fre_max = max_freq * 2.56;
            l = length(data);

            FC=fre_max*sum(data_dif.*data(2:l))/(2*pi*sum(data.^2));%
            FC(F1)
            MSF = fre_max^2*sum(data_dif.^2)/(4*(pi^2)*sum(data.^2));
            RMSF = sqrt(MSF);       % RMSF (F2)
            RVF = sqrt(MSF-FC^2):   % RVF (F3)

            feature.FC = FC;
            feature.RMSF = RMSF;
            feature.RVF = RVF;

            % **************features data saving ****************
            nfile = 1;
            features(nfile,1) = feature.FC;
            features(nfile,2) = feature.RMSF;
            features(nfile,3) = feature.RVF;

            [ndata, nfeat] = size(features);
            total_features(baris,nfeat*(feat_counter-
            1)+1:feat_counter*nfeat) = features;
            feat_counter = feat_counter+1;
        end
        baris = baris + 1;
end

cd FreqDomainFeatures_Thesis

% features saving
if bulan == 1
    save TotFeat_Feb.dat total_features -ascii
elseif bulan == 2
    save TotFeat_Mar.dat total_features -ascii
elseif bulan == 3
    save TotFeat_Apr.dat total_features -ascii
elseif bulan == 4
    save TotFeat_May.dat total_features -ascii
elseif bulan == 5
    save TotFeat_Jul.dat total_features -ascii
else bulan == 6
    save TotFeat_Aug.dat total_features -ascii
end
```

D.4 Combined time-domain feature extraction and wavelet decomposition.

```
% Combined time-domain feature extraction and wavelet decomposition
for vibration slew bearing signal
% 04/08/2013
% created by Wahyu Caesarendra

function n = parameter()
disp('1. February')
disp('2. March')
disp('3. April')
disp('4. May')
disp('5. July')
disp('6. August')
bulan = input('which month you want to select: \n')

if bulan == 1
    start_day = 21;
    end_day = 28;
elseif bulan == 2
    start_day = 1;
    end_day = 31;
elseif bulan == 3
    start_day = 1;
    end_day = 26;
elseif bulan == 4
    start_day = 1;
    end_day = 28;
elseif bulan == 5
    start_day = 17;
    end_day = 31;
else bulan == 6
    start_day = 1;
    end_day = 31;
end

baris = 1;
% ====================== Loading data ==================
for day = start_day:end_day              % Number of data

    if bulan == 1
        bln = ['february' num2str(day) '.txt']
    elseif bulan == 2
        bln = ['march' num2str(day) '.txt']
    elseif bulan == 3
        bln = ['april' num2str(day) '.txt']
    elseif bulan == 4
        bln = ['may' num2str(day) '.txt']
    elseif bulan == 5
        bln = ['july' num2str(day) '.txt']
    else bulan = 6
        bln = ['august' num2str(day) '.txt']
    end

    raw_data = load(bln);

    feat_counter = 1;
```

```
% ============== Data loading based selected channel ==========
    for i = 2 % channel 1
        data = raw_data(:,i);
        rpm = 1;
        dt = 60/(rpm*60);
        deg = 180;                  % reversible rotation angle
        maxTime = dt*(deg/360)*60;  % total time for 180 deg
        time = 1:dt:maxTime;

        sf = 4880;
        x = data(1:sf*maxTime)';
        [C,L] = wavedec(x,3,'db9'); % wavelet decomposition db9

        % Reconstruct approximation / detail at level 1-3
        A1 = wrcoef('a', C, L, 'db9',1); % A: approximation
        D1 = wrcoef('d', C, L, 'db9',1); % D1: decomposition 1
        D2 = wrcoef('d', C, L, 'db9',2); % D2: decomposition 2
        D3 = wrcoef('d', C, L, 'db9',3); % D3: decomposition 3

        rata2_A1 = mean(A1);
        sigma2_A1 = var(A1);
        skew_A1 = skewness(A1);
        kur_A1 = kurtosis(A1);

        rata2_D1 = mean(D1);
        sigma2_D1 = var(D1);
        skew_D1 = skewness(D1);
        kur_D1 = kurtosis(D1);

        rata2_D2 = mean(D2);
        sigma2_D2 = var(D2);
        skew_D2 = skewness(D2);
        kur_D2 = kurtosis(D2);

        rata2_D3 = mean(D3);
        sigma2_D3 = var(D3);
        skew_D3 = skewness(D3);
        kur_D3 = kurtosis(D3);

            % ************ features saving ***************
            feature.rata2_A1 = rata2_A1;
            feature.sigma2_A1 = sigma2_A1;
            feature.skew_A1 = skew_A1;
            feature.kur_A1 = kur_A1;

            features_A1(1,1) = feature.rata2_A1;
            features_A1(1,2) = feature.sigma2_A1;
            features_A1(1,3) = feature.skew_A1;
            features_A1(1,4) = feature.kur_A1;

            [ndata, nfeat] = size(features_A1);
            total_features_A1(baris,nfeat*(feat_counter-
             1)+1:feat_counter*nfeat) = features_A1;

            % ----------------------------------------
            feature.rata2_D1 = rata2_D1;
            feature.sigma2_D1 = sigma2_D1;
            feature.skew_D1 = skew_D1;
            feature.kur_D1 = kur_D1;
```

```
                features_D1(1,1) = feature.rata2_D1;
                features_D1(1,2) = feature.sigma2_D1;
                features_D1(1,3) = feature.skew_D1;
                features_D1(1,4) = feature.kur_D1;

                [ndata, nfeat] = size(features_D1);

                total_features_D1(baris,nfeat*(feat_counter-
                1)+1:feat_counter*nfeat) = features_D1;

                % ----------------------------------------
                feature.rata2_D2 = rata2_D2;
                feature.sigma2_D2 = sigma2_D2;
                feature.skew_D2 = skew_D2;
                feature.kur_D2 = kur_D2;

                features_D2(1,1) = feature.rata2_D2;
                features_D2(1,2) = feature.sigma2_D2;
                features_D2(1,3) = feature.skew_D2;
                features_D2(1,4) = feature.kur_D2;

                [ndata, nfeat] = size(features_D2);

                total_features_D2(baris,nfeat*(feat_counter-
                1)+1:feat_counter*nfeat) = features_D2;

                % ----------------------------------------
                feature.rata2_D3 = rata2_D3;
                feature.sigma2_D3 = sigma2_D3;
                feature.skew_D3 = skew_D3;
                feature.kur_D3 = kur_D3;

                features_D3(1,1) = feature.rata2_D3;
                features_D3(1,2) = feature.sigma2_D3;
                features_D3(1,3) = feature.skew_D3;
                features_D3(1,4) = feature.kur_D3;

                [ndata, nfeat] = size(features_D3);
                total_features_D3(baris,nfeat*(feat_counter-
                1)+1:feat_counter*nfeat) = features_D3;
                feat_counter = feat_counter+1;
        end
        baris = baris + 1

    end

cd total_wavedec_features

if bulan == 1
    save TotFeat_Feb_A1.dat total_features_A1 -ascii
    save TotFeat_Feb_D1.dat total_features_D1 -ascii
    save TotFeat_Feb_D2.dat total_features_D2 -ascii
    save TotFeat_Feb_D3.dat total_features_D3 -ascii
elseif bulan == 2
    save TotFeat_Mar_A1.dat total_features_A1 -ascii
    save TotFeat_Mar_D1.dat total_features_D1 -ascii
    save TotFeat_Mar_D2.dat total_features_D2 -ascii
    save TotFeat_Mar_D3.dat total_features_D3 -ascii
```

```
elseif bulan == 3
    save TotFeat_Apr_A1.dat total_features_A1 -ascii
    save TotFeat_Apr_D1.dat total_features_D1 -ascii
    save TotFeat_Apr_D2.dat total_features_D2 -ascii
    save TotFeat_Apr_D3.dat total_features_D3 -ascii
elseif bulan == 4
    save TotFeat_May_A1.dat total_features_A1 -ascii
    save TotFeat_May_D1.dat total_features_D1 -ascii
    save TotFeat_May_D2.dat total_features_D2 -ascii
    save TotFeat_May_D3.dat total_features_D3 -ascii
elseif bulan == 5
    save TotFeat_Jul_A1.dat total_features_A1 -ascii
    save TotFeat_Jul_D1.dat total_features_D1 -ascii
    save TotFeat_Jul_D2.dat total_features_D2 -ascii
    save TotFeat_Jul_D3.dat total_features_D3 -ascii
else bulan == 6
    save TotFeat_Aug_A1.dat total_features_A1 -ascii
    save TotFeat_Aug_D1.dat total_features_D1 -ascii
    save TotFeat_Aug_D2.dat total_features_D2 -ascii
    save TotFeat_Aug_D3.dat total_features_D3 -ascii
end
```

D.5 STFT feature extraction.

```
% STFT feature extraction for vibration slew bearing signal
% 23/09/2014
% created by Wahyu Caesarendra

x = load('may3.txt');
x = x(1:48800,2);
fs = 4880;
xmax = max(abs(x));          % find the maximum absolute value
x = x/xmax;                              % scalling the signal

% define analysis parameters
xlen = length(x); % length of the signal
wlen = 2048;      % window length (recommended to be power of 2)
h = wlen/8;       % hop size (recommended to be power of 2)
nfft = 16384;     % number of FFT points

% define the coherent amplification of the window
K = sum(hamming(wlen, 'periodic'))/wlen;

% perform STFT
[stft, f, t] = stft(x, wlen, h, nfft, fs);

% take the amplitude of fft(x) and scale it, so not to be a function
of the length of the window and its coherent amplification
s = abs(stft)/wlen/K;

% correction of the DC & Nyquist component
if rem(nfft, 2)          % odd nfft excludes Nyquist point
    s(2:end, :) = s(2:end, :).*2;
else                     % even nfft includes Nyquist point
    s(2:end-1, :) = s(2:end-1, :).*2;
end

% plot the STFT result
figure(1)
t = fliplr(t);
mesh(t,f,s)
xlabel('Time (s)')
ylabel('Frequency (Hz)')
zlabel('Amplitude (mV)')
```

D.6 Fractal dimension, correlation dimension and approximate entropy feature extraction.

```
% Phase-space dissimilarity measurements feature extraction for
vibration slew bearing signal
% 22/10/2012
% created by Wahyu Caesarendra


function n = parameter()
disp('1. February')
disp('2. March')
disp('3. April')
disp('4. May')
disp('5. July')
disp('6. August')
bulan = input('which month you want to select:')

if bulan == 1
    start_day = 21;
    end_day = 28;
elseif bulan == 2
    start_day = 1;
    end_day = 31;
elseif bulan == 3
    start_day = 1;
    end_day = 26;
elseif bulan == 4
    start_day = 1;
    end_day = 28;
elseif bulan == 5
    start_day = 18;
    end_day = 31;
else bulan == 6
    start_day = 1;
    end_day = 31;
end

baris = 1;
% ====================== Loading data ==================
for day = start_day:end_day             % Number of data

    if bulan == 1
        bln = ['february' num2str(day) '.txt']
    elseif bulan == 2
        bln = ['march' num2str(day) '.txt']
    elseif bulan == 3
        bln = ['april' num2str(day) '.txt']
    elseif bulan == 4
        bln = ['may' num2str(day) '.txt']
    elseif bulan == 5
        bln = ['july' num2str(day) '.txt']
    else bulan == 6
        bln = ['august' num2str(day) '.txt']
    end

    raw_data = load(bln);
```

```
        feat_counter = 1;
        % ========== Data Loading based selected channel ==========
        for i = 2 % channel 1
            raw_data = raw_data(:,i);
            data = raw_data(48801:97600);
            x = (data-mean(data))/std(data);

            % Fractal Dimension
            N = length(x);
            c = 48; % 50
            FD = FractalDimension(x,N,c);
            feat(baris,1) = FD;

            % Correlation dimension
            T = 48; % 50
            D2 = CorrelationDimension(x,N,T);
            feat(baris,1) = D2;

            % ApproximatEntropy
            dim = 8;
            r = 0.2 * std(x);
            tau = 1;
            apen = ApEn(dim,r,x,tau);
            feat(baris,3) = apen;
         end
        baris = baris + 1
end

cd PhaseSpaceFeatures_Thesis
if bulan == 1
    save feat_feb2.dat feat -ascii
elseif bulan == 2
    save feat_mar2.dat feat -ascii
elseif bulan == 3
    save feat_apr2.dat feat -ascii
elseif bulan == 4
    save feat_may2.dat feat -ascii
elseif bulan == 5
    save feat_jul2.dat feat -ascii
else bulan == 6
    save feat_aug2.dat feat -ascii
end
```

```
function D = FractalDimension(s,N,k)
% fractal dimension function
% ==========================
% created by Wahyu Caesarendra
% 6-Sept-2012

% References:
% Niina Paivinen et.al.
% Epileptic seizure detection: A nonlinear viewpoint
% Computer Methods and Programs in Biomedicine (2005) 79, 151-159


% input:
% ======
% s is original time series
% N is dimension of original time series
% k is lag time or interval time

% output:
% =======
% D is fractal dimension

m = N/k;     % dimension of phase space (m could not be > N/k)
    for i = 1:k;
        for j = 1:m;
            X(i,j) = s(i+k*(j-1));    % Eq. 7
        end
    end

    L2 = 0;
    for i = 1:k
        for j = 2:m;
            L1(i,j-1) = abs(X(i,j)-X(i,j-1)); % Eq. 8
            L2 = L2 + L1(i,j-1);
            Lm(i,j-1) = (1/k)*L2;
        end
    end
    L(1:k,1) = mean(Lm');

    for i = 1:k
        S(i,1) = log(i);
        S(i,2) = log(L(i));
    end

    P = polyfit(S(:,1),S(:,2),1);
    f = polyval(P,S(:,1));
    % plot(S(:,1),S(:,2),'o',S(:,1),f,'-')
    D = P(1);
end
```

```
function D2 = CorrelationDimension(data,N,T)

% correlation sum and correlation dimension
% ========================================
% created by Wahyu Caesarendra
% 7-Sept-2012

% References:
% Xiaoyun Zang and John Howell
% Correlation dimension and Lyapunov exponent based isolation of
plant-wide
% oscillations


% input:
% ======
% data is original time series or vibration data
% N is dimension of original time series
% T is lag time or interval time

% output:
% =======
% D is fractal dimension

x = data;
m = N/T;        % dimension of phase space (m could not be > N/T)
epsilon = 5;

    % creating phase space data from original time series
    for i = 1:T;
        for j = 1:m;
            X(i,j) = x(i+T*(j-1));    % Eq. 7
        end
    end

    % calculate the correlation sum in some phase space
    for k = 2:T
        Xi = X(k-1,:);
        Xj = X(k,:);
        step1 = epsilon - abs(Xi-Xj);
        H = find(step1>0); % Heaviside step function (Theta).if x<=0
        Theta=0, else x>0 Theta=1
        step2(k-1,1) = sum(step1(H));
    end
    C = (2/((N-m)*(N-m-1)))*sum(step2); % Eq. 2

    % correlation dimension
    D2 = log(C)/log(epsilon);           % Eq. 3
end
```

```
function apen = ApEn( dim, r, data, tau ) %ApEn
%   dim : embedded dimension
%   r : tolerance (typically 0.2 * std)
%   data : time-series data
%   tau : delay time for downsampling

%   Changes in version 1
%       Ver 0 had a minor error in the final step of calculating ApEn
%       because it took logarithm after summation of phi's.
%       In Ver 1, I restored the definition according to original
paper's
%       definition, to be consistent with most of the work in the
%       literature. Note that this definition won't work for Sample
%       Entropy which doesn't count self-matching case, because the
count
%       can be zero and logarithm can fail.
%
%       A new parameter tau is added in the input argument list, so
the users
%       can apply ApEn on downsampled data by skipping by tau.
%---------------------------------------------------------------------
% coded by Kijoon Lee,  kjlee@ntu.edu.sg
% Ver 0 : Aug 4th, 2011
% Ver 1 : Mar 21st, 2012
%---------------------------------------------------------------------
if nargin < 4, tau = 1; end
if tau > 1, data = downsample(data, tau); end

N = length(data);
result = zeros(1,2);

for j = 1:2
    m = dim+j-1;
    phi = zeros(1,N-m+1);
    dataMat = zeros(m,N-m+1);

    % setting up data matrix
    for i = 1:m
        dataMat(i,:) = data(i:N-m+i);
    end

    % counting similar patterns using distance calculation
    for i = 1:N-m+1
        tempMat = abs(dataMat - repmat(dataMat(:,i),1,N-m+1));
        boolMat = any( (tempMat > r),1);
        phi(i) = sum(~boolMat)/(N-m+1);
    end

    % summing over the counts
    result(j) = sum(log(phi))/(N-m+1);
end

apen = result(1)-result(2);


end
```

D.7 KS test feature extraction.

```
% KS test feature extraction for vibration   slew bearing signal
% 22/10/2012
% created by Wahyu Caesarendra

function n = parameter()

for bulan = 1:6

if bulan == 1
    start_day = 21;
    end_day = 28;
elseif bulan == 2
    start_day = 1;
    end_day = 31;
elseif bulan == 3
    start_day = 1;
    end_day = 26;
elseif bulan == 4
    start_day = 1;
    end_day = 28;
elseif bulan == 5
    start_day = 17;
    end_day = 31;
else bulan == 6
    start_day = 1;
    end_day = 31;
end

baris = 1;
% ====================== Loading data ==================
for day = start_day:end_day              % Number of data

    if bulan == 1
        bln = ['february' num2str(day) '.txt']
    elseif bulan == 2
        bln = ['march' num2str(day) '.txt']
    elseif bulan == 3
        bln = ['april' num2str(day) '.txt']
    elseif bulan == 4
        bln = ['may' num2str(day) '.txt']
    elseif bulan == 5
        bln = ['july' num2str(day) '.txt']
    else bulan = 6
        bln = ['august' num2str(day) '.txt']
    end

    data_load = load(bln);

        feat_counter = 1;
        % ============= KS test feature extraction ==========
        for i = 2 % channel 1

            data = data_load(:,i);

            normal_data = load('february22.txt'); % february23
            ND_ch1 = normal_data(:,i);
```

```
            data = abs(data);
            ND_ch1 = abs(ND_ch1);
            [KS,p]=kstest2(ND_ch1,data,'Alpha',0.01,'tail','larger');
            feature.KS = KS;     % (F1)
            feature.p = p;       % (F2)

            % *************** Saving data features ***************
            nfile = 1;
            features(nfile,1) = feature.KS;
            features(nfile,2) = feature.p;

            [ndata, nfeat] = size(features);
            total_features(baris,nfeat*(feat_counter-
            1)+1:feat_counter*nfeat) = features;
            feat_counter = feat_counter+1;
        end
        baris = baris + 1;

end

cd KolmogorovSmirnovFeatures_Thesis

total_features_double = double(total_features);

if bulan == 1
    save TotFeat_Feb.dat total_features_double -ascii
elseif bulan == 2
    save TotFeat_Mar.dat total_features_double -ascii
elseif bulan == 3
    save TotFeat_Apr.dat total_features_double -ascii
elseif bulan == 4
    save TotFeat_May.dat total_features_double -ascii
elseif bulan == 5
    save TotFeat_Jul.dat total_features_double -ascii
else bulan == 6
    save TotFeat_Aug.dat total_features_double -ascii
end

clear KS
clear p
clear total_features
clear total_features_double

cd ..
end
cd KolmogorovSmirnovFeatures_Thesis
```

D.8 Circular domain feature extraction.

```
% Circular domain feature extraction for vibration slew bearing signal
% 25/10/2012
% created by Wahyu Caesarendra

function n = parameter()

disp('1. February')
disp('2. March')
disp('3. April')
disp('4. May')
disp('5. July')
disp('6. August')
bulan = input('which month you want to select: \n')

if bulan == 1
    start_day = 21;
    end_day = 28;
elseif bulan == 2
    start_day = 1;
    end_day = 31;
elseif bulan == 3
    start_day = 1;
    end_day = 26;
elseif bulan == 4
    start_day = 1;
    end_day = 28;
elseif bulan == 5
    start_day = 17;
    end_day = 31;
else bulan == 6
    start_day = 1;
    end_day = 31;
end

baris = 1;
% ====================== Loading data ==================
for day = start_day:end_day              % Number of data

    if bulan == 1
        bln = ['february' num2str(day) '.txt']
    elseif bulan == 2
        bln = ['march' num2str(day) '.txt']
    elseif bulan == 3
        bln = ['april' num2str(day) '.txt']
    elseif bulan == 4
        bln = ['may' num2str(day) '.txt']
    elseif bulan == 5
        bln = ['july' num2str(day) '.txt']
    else bulan = 6
        bln = ['august' num2str(day) '.txt']
    end

    raw_data = load(bln);

        feat_counter = 1;

        % ============ Data Loading based selected channel ==========
```

```
for i = 2 % channel 1
    data = raw_data(:,i);
    rpm = 1;
    dt = 60/(rpm*60);
    deg = 180;
    maxTime = dt*(deg/360)*60;
    time = 1:dt:maxTime;

    sf = 4880;
    x = data(1:sf*maxTime)';
    % normalize to zero mean
    xx = (x-mean(x))/std(x);
    new_data = reshape(xx,sf,maxTime); % 1 second data

    % PAA method
    [r c]=size(new_data);
    for j = 1:c
        data = new_data(:,j);
        win_size = 8;
        L = length(data);
        nseg = L/win_size; % win_size*nseg = length of data
        PAA = mean(reshape(data,win_size,nseg)); % PAA
        N = length(PAA);
        a = PAA(1:N-1); % x(n)
        b = PAA(2:N);   % x(n+1)

        % Ellipse fit
        XY(:,1) = a;
        XY(:,2) = b;
        [A, posisi] = EllipseDirectFit(XY);
        syms x y
        % ax^2 + bxy + cy^2 +dx + ey + f = 0 (ellipse formula)
        Z = A(1)*x^2 + A(2)*x*y + A(3)*y^2 + A(4)*x + A(5)*y +
       A(6);
        bentuk(1,j) = posisi;
    end

    nol = find(bentuk==0);  % center (0)
    satu = find(bentuk==1); % right shifted (1)
    dua = find(bentuk==2);  % left shifted (2)

    ang_deg0 = time2ang(nol,maxTime,deg)';% time to angle
    conversion
    rad0 = ang2rad(ang_deg0);  % angle to radian conversion
    ang_deg1 = time2ang(satu,maxTime,deg)';
    rad1 = ang2rad(ang_deg1);
    ang_deg2 = time2ang(dua,maxTime,deg)';
    rad2 = ang2rad(ang_deg2);

    % Plot raw data in circular shape
    f = figure(day);
    set(f,'color',[1 1 1]);
    subplot(2,2,1)
    time2 = 1/4880:1/4880:maxTime;
    tRad = time2rad(time2,maxTime,deg); % time to radian
    conversion
    circ_plot4(tRad,xx,'Color','r')


    subplot(2,2,2)
```

```
circ_plot1(rad1,'LineWidth',2,'Color','r'),
subplot(2,2,3)
circ_plot2(rad1,'-',20,'LineWidth',2,'Color','r'),

[alpha_bar0 R0] = Resultant(rad0);
[alpha_bar1 R1] = Resultant(rad1);
[alpha_bar2 R2] = Resultant(rad2);

var0 = circ_var(rad0);
var1 = circ_var(rad1);
var2 = circ_var(rad2);

[skewPewsey0 skewFisher0] = circ_skewness(rad0);
[skewPewsey1 skewFisher1] = circ_skewness(rad1);
[skewPewsey2 skewFisher2] = circ_skewness(rad2);

[kurPewsey0 kurFisher0] = circ_kurtosis(rad0);
[kurPewsey1 kurFisher1] = circ_kurtosis(rad1);
[kurPewsey2 kurFisher2] = circ_kurtosis(rad2);

subplotHandle = subplot(2,2,4);
text(0,1,['Circular Mean :', num2str(alpha_bar1)]);
text(0,0.7,['Circular Variance :', num2str(var1)]);
text(0,0.4,['Circular Skewness :', num2str(skewPewsey1)]);
text(0,0.1,['Circular Kurtosis :', num2str(kurPewsey1)]);

    % setting the axes invisible
    set(subplotHandle,'Xcolor',[1 1 1]);
    set(subplotHandle,'Ycolor',[1 1 1]);


    % ************** Saving the features *****************
    feature0.mean = alpha_bar0;
    feature1.mean = alpha_bar1;
    feature2.mean = alpha_bar2;

    feature0.var = var0;
    feature1.var = var1;
    feature2.var = var2;

    feature0.skewA = skewPewsey0;
    feature0.skewB = skewFisher0;
    feature1.skewA = skewPewsey1;
    feature1.skewB = skewFisher1;
    feature2.skewA = skewPewsey2;
    feature2.skewB = skewFisher2;

    feature0.kurA = kurPewsey0;
    feature0.kurB = kurFisher0;
    feature1.kurA = kurPewsey1;
    feature1.kurB = kurFisher1;
    feature2.kurA = kurPewsey2;
    feature2.kurB = kurFisher2;

    nfile = 1;
    features0(nfile,1) = feature0.mean;
    features1(nfile,1) = feature1.mean;
    features2(nfile,1) = feature2.mean;
```

```
                features0(nfile,2) = feature0.var;
                features1(nfile,2) = feature1.var;
                features2(nfile,2) = feature2.var;

                features0(nfile,3) = feature0.skewA;
                features1(nfile,3) = feature1.skewA;
                features2(nfile,3) = feature2.skewA;

                features0(nfile,4) = feature0.skewB;
                features1(nfile,4) = feature1.skewB;
                features2(nfile,4) = feature2.skewB;

                features0(nfile,5) = feature0.kurA;
                features1(nfile,5) = feature1.kurA;
                features2(nfile,5) = feature2.kurA;

                features0(nfile,6) = feature0.kurB;
                features1(nfile,6) = feature1.kurB;
                features2(nfile,6) = feature2.kurB;

                [ndata, nfeat] = size(features1);

                total_features0(baris,nfeat*(feat_counter-
                 1)+1:feat_counter*nfeat) = features0;
                total_features1(baris,nfeat*(feat_counter-
                 1)+1:feat_counter*nfeat) = features1;
                total_features2(baris,nfeat*(feat_counter-
                 1)+1:feat_counter*nfeat) = features2;

                feat_counter = feat_counter+1;
        end
        baris = baris + 1
    end

cd TotalCircularFeatures

if bulan == 1
    save CircFeat1_Feb.dat total_features1 -ascii
elseif bulan == 2
    save CircFeat1_Mar.dat total_features1 -ascii
elseif bulan == 3
    save CircFeat1_Apr.dat total_features1 -ascii
elseif bulan == 4
    save CircFeat1_May.dat total_features1 -ascii
elseif bulan == 5
    save CircFeat1_Jul.dat total_features1 -ascii
else bulan == 6
    save CircFeat1_Aug.dat total_features1 -ascii
end
```

```
function [A, posisi] = EllipseDirectFit(XY)

%  Direct ellipse fit, proposed in article
%    A. W. Fitzgibbon, M. Pilu, R. B. Fisher
%     "Direct Least Squares Fitting of Ellipses"
%     IEEE Trans. PAMI, Vol. 21, pages 476-480 (1999)
%
%  Our code is based on a numerically stable version
%  of this fit published by R. Halir and J. Flusser
%
%     Input:  XY(n,2) is the array of coordinates of n points
x(i)=XY(i,1), y(i)=XY(i,2)
%
%     Output: A = [a b c d e f]' is the vector of algebraic
%             parameters of the fitting ellipse:
%             ax^2 + bxy + cy^2 +dx + ey + f = 0
%             the vector A is normed, so that ||A||=1
%
%  This is a fast non-iterative ellipse fit.
%
%  It returns ellipses only, even if points are
%  better approximated by a hyperbola.
%  It is somewhat biased toward smaller ellipses.

centroid = mean(XY);   % the centroid of the data set

D1 = [(XY(:,1)-centroid(1)).^2, (XY(:,1)-centroid(1)).*(XY(:,2)-
centroid(2)),...
      (XY(:,2)-centroid(2)).^2];
D2 = [XY(:,1)-centroid(1), XY(:,2)-centroid(2), ones(size(XY,1),1)];
S1 = D1'*D1;
S2 = D1'*D2;
S3 = D2'*D2;
T = -inv(S3)*S2';
M = S1 + S2*T;
M = [M(3,:)./2; -M(2,:); M(1,:)./2];
[evec,eval] = eig(M);
cond = 4*evec(1,:).*evec(3,:)-evec(2,:).^2;
A1 = evec(:,find(cond>0));
A = [A1; T*A1];
A4 = A(4)-2*A(1)*centroid(1)-A(2)*centroid(2);
A5 = A(5)-2*A(3)*centroid(2)-A(2)*centroid(1);
A6 = A(6)+A(1)*centroid(1)^2+A(3)*centroid(2)^2+...
     A(2)*centroid(1)*centroid(2)-A(4)*centroid(1)-A(5)*centroid(2);
A(4) = A4;  A(5) = A5;  A(6) = A6;
A = A/norm(A);


% additional program by Wahyu Caesarendra
% 4/11/2012
% --------------------- left shifted ---------------------------
if A(1)<0 && A(2)<0 && A(3)<0 && A(4)>0 && A(5)>0 && A(6)>0     % 1
        posisi = 2;
elseif A(1)<0 && A(2)<0 && A(3)<0 && A(4)<0 && A(5)<0 && A(6)>0 % 2
        posisi = 2;
elseif A(1)>0 && A(2)>0 && A(3)>0 && A(4)>0 && A(5)>0 && A(6)<0 % 3
        posisi = 2;
elseif A(1)<0 && A(2)<0 && A(3)<0 && A(4)<0 && A(5)>0 && A(6)>0 % 4
        posisi = 2;
elseif A(1)>0 && A(2)>0 && A(3)>0 && A(4)<0 && A(5)<0 && A(6)<0 % 5
        posisi = 2;
```

```
% --------------------- right shifted --------------------------
elseif A(1)>0 && A(2)<0 && A(3)>0 && A(4)<0 && A(5)>0 && A(6)<0 % 1
        posisi = 1;
elseif A(1)>0 && A(2)<0 && A(3)>0 && A(4)>0 && A(5)>0 && A(6)<0 % 2
        posisi = 1;
elseif A(1)<0 && A(2)>0 && A(3)<0 && A(4)>0 && A(5)>0 && A(6)>0 % 3
        posisi = 1;
elseif A(1)<0 && A(2)>0 && A(3)<0 && A(4)<0 && A(5)<0 && A(6)>0 % 4
        posisi = 1;
elseif A(1)<0 && A(2)>0 && A(3)<0 && A(4)<0 && A(5)>0 && A(6)>0 % 5
        posisi = 1;
elseif A(1)<0 && A(2)>0 && A(3)<0 && A(4)>0 && A(5)<0 && A(6)>0 % 6
        posisi = 1;
elseif A(1)>0 && A(2)<0 && A(3)>0 && A(4)>0 && A(5)<0 && A(6)<0 % 7
        posisi = 1;
elseif A(1)>0 && A(2)<0 && A(3)>0 && A(4)<0 && A(5)>0 && A(6)<0 % 8
        posisi = 1;
elseif A(1)>0 && A(2)<0 && A(3)>0 && A(4)<0 && A(5)<0 && A(6)<0 % 9
        posisi = 1;
% ------------------------- center -----------------------------
else
        posisi = 0;
end
end  %  EllipseDirectFit
```

```
function [alpha_bar R] = Resultant(alpha,p)
    % Compute circular mean and resultant length
    % created by Caesar
    % 5/11/2012

    % weight (this should be the diameter of bearing)
    w = ones(size(alpha));

    if nargin <2 || isempty(p)
        % compute weighted sum of cos and sin of angles
        ri = w.*(cos(alpha)+i*sin(alpha));
        r_bar = mean(ri);
        % obtain meanR
        alpha_bar = angle(r_bar); % convert complex value to radian
        % obtain lengthR
        R = abs(r_bar);
    else
        % compute weighted sum of cos and sin of angles
        ri = w.*(cos(p*alpha)+i*sin(p*alpha));
        r_bar = mean(ri);
        % obtain meanR
        alpha_bar = angle(r_bar); % convert complex value to radian
        % obtain lengthR
        R = abs(r_bar);
    end
```

```
function [S s] = circ_var(alpha, w, d, dim)
% s = circ_var(alpha, w, d, dim)
%   Computes circular variance for circular data
%   (equ. 26.17/18, Zar).
%
%   Input:
%     alpha sample of angles in radians
%     [w    number of incidences in case of binned angle data]
%     [d    spacing of bin centers for binned data, if supplied
%           correction factor is used to correct for bias in
%           estimation of r]
%     [dim  compute along this dimension, default is 1]
%
%     If dim argument is specified, all other optional arguments can
be
%     left empty: circ_var(alpha, [], [], dim)
%
%   Output:
%     S     circular variance 1-r
%     s     angular variance 2*(1-r)
%
% PHB 6/7/2008
%
% References:
%   Statistical analysis of circular data, N.I. Fisher
%   Topics in circular statistics, S.R. Jammalamadaka et al.
%   Biostatistical Analysis, J. H. Zar
% Circular Statistics Toolbox for Matlab

% By Philipp Berens, 2009
% berens@tuebingen.mpg.de - www.kyb.mpg.de/~berens/circStat.html

if nargin < 4
  dim = 1;
end

if nargin < 3 || isempty(d)
  % per default do not apply correct for binned data
  d = 0;
end

if nargin < 2 || isempty(w)
  % if no specific weighting has been specified
  % assume no binning has taken place
    w = ones(size(alpha));
else
  if size(w,2) ~= size(alpha,2) || size(w,1) ~= size(alpha,1)
    error('Input dimensions do not match');
  end
end

% compute mean resultant vector length
r = circ_r(alpha);

% apply transformation to var
S = 1 - r;
s = 2 * S;
```

```
function [m1 m2] = circ_skewness(alpha, w, dim)

% [m1 m2] = circ_skewness(alpha,w,dim)
%   Calculates a measure of angular skewness.
%
%   Input:
%     alpha     sample of angles
%     [w        weightings in case of binned angle data]
%     [dim      statistic computed along this dimension, 1]
%
%     If dim argument is specified, all other optional arguments can
be
%     left empty: circ_skewness(alpha, [], dim)
%
%   Output:
%     m1          skewness (from Pewsey)
%     m2          alternative skewness measure (from Fisher)
%
%   References:
%     Pewsey, Metrika, 2004
%     Statistical analysis of circular data, Fisher, p. 34
%
% Circular Statistics Toolbox for Matlab

% By Philipp Berens, 2009
% berens@tuebingen.mpg.de

if nargin < 3
  dim = 1;
end

if nargin < 2 || isempty(w)
  % if no specific weighting has been specified
  % assume no binning has taken place
    w = ones(size(alpha));
else
  if size(w,2) ~= size(alpha,2) || size(w,1) ~= size(alpha,1)
    error('Input dimensions do not match');
  end
end



% compute neccessary values
R = circ_r(alpha);
theta = circ_mean(alpha);
[mp, rho2, mu2] = circ_moment(alpha,w,2,true,dim);
theta2 = repmat(theta, size(alpha)./size(theta));

% compute skewness
m1 = sum(w.*(sin(2*(circ_dist(alpha,theta2)))),dim)./sum(w,dim);
m2 = rho2.*sin(circ_dist(mu2,2*theta))./(1-R).^(3/2);    % (formula
2.29)
```

```
function [kurPewsey kurFisher] = circ_kurtosis(alpha)
% [kPewsey kurFisher] = circ_kurtosis(alpha)
%   Calculates a measure of angular kurtosis.
% Created by Caesar
% 5/11/2012

    % weighting
    w = ones(size(alpha));
    % compute mean and resultant length
    [alpha_bar R] = Resultant(alpha); % mean alpha

    % compute kurtosis from Pewsey
    kurPewsey = mean(cos(2*(alpha - alpha_bar)));

    p = 2; % number of p-moments trigonometric
    [alpha_bar2 R2] = Resultant(alpha,2);

    % compute kurtosis from Fisher
    kurFisher = (R2.*cos(circ_dist(alpha_bar2,2*alpha_bar))-R.^4)./(1-
R).^2;    % (formula 2.30)

end
```

D.9 LLE feature extraction.

```
% LLE feature extraction for vibration slew bearing signal
% 1/1/2013
% created by Wahyu Caesarendra

function n = parameter()

for bulan = 1:6

if bulan == 1
    start_day = 21;
    end_day = 28;
elseif bulan == 2
    start_day = 1;
    end_day = 31;
elseif bulan == 3
    start_day = 1;
    end_day = 26;
elseif bulan == 4
    start_day = 1;
    end_day = 28;
elseif bulan == 5
    start_day = 17;
    end_day = 31;
else bulan == 6
    start_day = 1;
    end_day = 31;
end

baris = 1;
% ================== Loading data ====================
for day = start_day:end_day             % Number of data

    if bulan == 1
        bln = ['february' num2str(day) '.txt']
    elseif bulan == 2
        bln = ['march' num2str(day) '.txt']
    elseif bulan == 3
        bln = ['april' num2str(day) '.txt']
    elseif bulan == 4
        bln = ['may' num2str(day) '.txt']
    elseif bulan == 5
        bln = ['july' num2str(day) '.txt']
    else bulan = 6
        bln = ['august' num2str(day) '.txt']
    end

    raw_data = load(bln);

        feat_counter = 1;
        % ========== Data Loading based selected channel ==========
        for i = 2 % channel 1
            data = raw_data(:,i);
            rpm = 1;            % rotational speed
            dt = 60/(rpm*60); % time interval for 1 rpm
            deg = 60;           % 30deg=5sec, 60deg=10 sec, 90deg=15sec
            maxTime = dt*(deg/360)*60;      % total time for 60 deg
            sf = 4880;
```

```
y = data((48800+1):(48800+sf*maxTime))';
% normalize to zero mean
yy = (y-mean(y))/std(y);

new_data = reshape(yy,sf,maxTime); % for 1 sec data

% Lyapunov exponent every 4880 data points
[row col]=size(new_data);
for j = 1:col
    x = new_data(:,j);
    J = 48; % J is reconstruction delay (1/100)*4880=48.8
    m = 100; % m is the embedding dimension
    miu = 50; % 50
    [lle, d] = lyarosenstein2(x,m,J,miu);
    lambda1(j)=lle;
    lambda(day,j) = lle;
end

  lambda_max(day) = max(lambda1);
  lambda_min(day) = min(lambda1);
  lambda_mean(day) = mean(lambda1);
  positive = find(tanda > 0);  % tanda positif (kode 1)
  negative = find(tanda < 0); % tanda negatif (kode 2)

  angDeg_pos = time2ang(negative,maxTime,deg)';    % time
  to angle (degree) conversion
  rad_pos = ang2rad(angDeg_pos);                   % angle
  (degree) to radian conversion
  angDeg_neg = time2ang(negative,maxTime,deg)';
  rad_neg = ang2rad(angDeg_neg);


% Plot raw data in circular shape
  f = figure(day);
  set(f,'color',[1 1 1]);
% subplot(5,4,[1 2 5 6 9 10])
% subplot(2,2,1)
% time2 = 1/4880:1/4880:maxTime;
% tRad = time2rad(time2,maxTime,deg);     % time to radian
  conversion
% circ_plot4(tRad,yy,'Color','r')

% subplot(5,4,[7 8 11 12])
  subplot(1,2,1)
  circ_plot1(rad_neg,'LineWidth',2,'Color','r'),
% subplot(5,4,[15 16 19 20])
% subplot(2,2,3)
% circ_plot2(rad_neg,'-',20,'LineWidth',2,'Color','r'),

 [alpha_bar1 R1] = Resultant(rad_neg);
 var1 = circ_var(rad_neg);
 [skewPewsey1 skewFisher1] = circ_skewness(rad_neg);
 [kurPewsey1 kurFisher1] = circ_kurtosis(rad_neg);

 % gbr baru
 % subplotHandle = subplot(5,4,[13 14 17 18]);
  subplotHandle = subplot(1,2,2);
  text(0,0.7 ,['Circular Mean        :    ',
  num2str(alpha_bar1)]);
```

```
                % text(0,0.7,['Circular Variance   :    ',
                 num2str(var1)]);
                 text(0,0.5,['Circular Skewness :   ',
                 num2str(skewFisher1)]);
                % text(0,0.4,['Circular skewness2 :  ',
                 num2str(skewFisher1)]);
                 text(0,0.3,['Circular Kurtosis    :    ',
                 num2str(kurFisher1)]);
                % text(0,0,['Circular kurtosis2 :     ',
                 num2str(kurFisher1)]);
                % setting the axes invisibale
                 set(subplotHandle,'Xcolor',[1 1 1]);
                 set(subplotHandle,'Ycolor',[1 1 1]);


                   % ************ Saving the features % ************
                     feature1.mean = alpha_bar1;
                     feature1.var = var1;
                     feature1.skewA = skewPewsey1;
                     feature1.skewB = skewFisher1;

                     feature1.kurA = kurPewsey1;
                     feature1.kurB = kurFisher1;

                     nfile = 1;
                     features1(nfile,1) = feature1.mean;
                     features1(nfile,2) = feature1.var;
                     features1(nfile,3) = feature1.skewA;
                     features1(nfile,4) = feature1.skewB;
                     features1(nfile,5) = feature1.kurA;
                     features1(nfile,6) = feature1.kurB;

                     [ndata, nfeat] = size(features1);

                     total_features1(baris,nfeat*(feat_counter-
                     1)+1:feat_counter*nfeat) = features1;

                     feat_counter = feat_counter+1;
          end
            baris = baris + 1;

    end

cd total_LLE_features

if bulan == 1
    save lambda_Feb.dat lambda -ascii
    save lambda_min_Feb.dat lambda_min -ascii
    save lambda_max_Feb.dat lambda_max -ascii
    save lambda_mean_Feb.dat lambda_mean -ascii
elseif bulan == 2
    save lambda_Mar.dat lambda -ascii
    save lambda_min_Mar.dat lambda_min -ascii
    save lambda_max_Mar.dat lambda_max -ascii
    save lambda_mean_Mar.dat lambda_mean -ascii
elseif bulan == 3
    save lambda_Apr.dat lambda -ascii
    save lambda_min_Apr.dat lambda_min -ascii
    save lambda_max_Apr.dat lambda_max -ascii
    save lambda_mean_Apr.dat lambda_mean -ascii
```

```
elseif bulan == 4
    save lambda_May.dat lambda -ascii
    save lambda_min_May.dat lambda_min -ascii
    save lambda_max_May.dat lambda_max -ascii
    save lambda_mean_May.dat lambda_mean -ascii
elseif bulan == 5
%     save CircFeat1_Jul.dat total_features1 -ascii
    save lambda_Jul.dat lambda -ascii
    save lambda_min_Jul.dat lambda_min -ascii
    save lambda_max_Jul.dat lambda_max -ascii
    save lambda_mean_Jul.dat lambda_mean -ascii
else bulan == 6
%     save CircFeat1_Aug.dat total_features1 -ascii
    save lambda_Aug.dat lambda -ascii
    save lambda_min_Aug.dat lambda_min -ascii
    save lambda_max_Aug.dat lambda_max -ascii
    save lambda_mean_Aug.dat lambda_mean -ascii
end

clear lambda_min
clear lambda_max
clear lambda_mean

cd ..

end
```

```
function [lle, d] = lyarosenstein2(x,m,J,miu)
% d:divergence of nearest trajectories
% x:signal
% J:time delay
% m:embedding dimension

N = length(x);
M = N-(m-1)*J; % M is number of reconstructed signal or number of
phase-space vector
maxiter = 100;
for i = 1:M
    a = i;
    b = i+(m-1)*J;
    c = a:J:b;
    X(i,:) = x(c);  % phase-space matrix
end

for i = 1:M;
    Xrep = repmat(X(i,:),M,1);       % X replicate
    d0 = sqrt(sum((X-Xrep).^2,2));  % Initial Euclidean distance

    %% Rosenstein
    for j = 1:M
        if abs(j-i) <= miu % miu = mean period
            d0(j) = max(d0); % d0_new
        end
    end
    [neardis(i) nearpos(i)] = min(d0);
end

for k = 1:maxiter
    maxind = M-k;
    evolve = 0;
    pnt = 0;
    for j = 1:M
        if j <= maxind && nearpos(j) <= maxind
            % d = sqrt(sum((X(j+k,:)-X(nearpos(j+k),:)).^2,2));
            d = sqrt(sum((X(j+(k-1),:)-X(nearpos(j)+(k-1),:)).^2,2));
             if d ~= 0
                evolve = evolve+log(d);
                pnt = pnt+1;
             end
        end
    end
    if pnt > 0
        d_new(k) = evolve/pnt;
    else
        d_new(k) = 0;
    end
end

% LLE Calculation
fs = 4880;      %sampling frequency
tlinear = 1:maxiter;
F = polyfit(tlinear,d_new(tlinear),1);

lle = fs*F(1);
```

Appendix E: Wideband differential AE sensor calibration chart

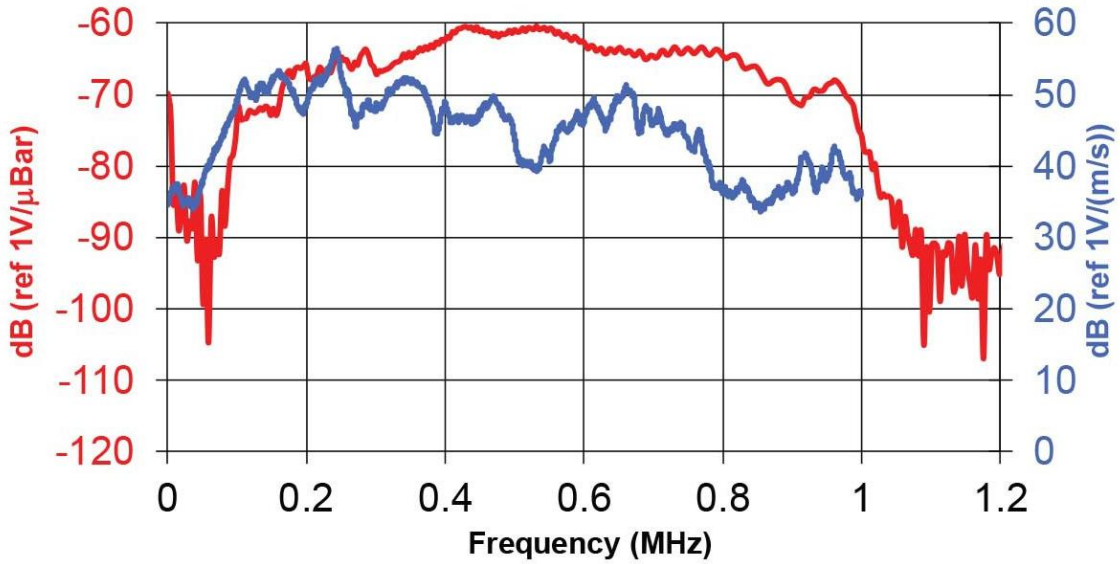

Figure E.1 Wideband differential AE sensor calibration chart [329].

Appendix F: Implementation in online monitoring system based on FTP

F.1 Description

The objective of this project is to facilitate online monitoring to the currently used slew bearing experiment. The resulted software is expected to be able to send the data automatically from one location, to the data centre and then accessed from any other site using the web browser.

The locations involved in this project are divided into 3 main locations. The first one is the 'workshop**',** where the slew bearing being tested is located. There is also the computer which handles the data retrieval from sensors attached on slew bearing test-rig to installed data acquisition hardware and software (PICO). For example, the vibration data collected from accelerometer is composed by 4 different attributes. Whereby each attribute represents each channels attached to the tested bearing. Hence, the daily collected data will be transmitted to the second location.

The second location is the 'data centre/server'. This site will act as the main data storage to be accessed through the whole world. The paid hosting will be further used, since the data transmission and the data size used for data interchange would be enormous. Thus, the bandwidth used and the storage size should be relatively huge as well. Temporarily the free hosting is currently used to test the initial online monitoring system.

The last location is the 'client'**.** *Client* refers to any computer which given the authority to access the data. In this machine, the user will be able to see the graph for the collected data from *data centre*, and to download these data as necessary (if use the paid hosting). Several configurations should be delivered in case of the occurrence of different situations as the project going on.

F.2 Specification

Workshop

Since the vibration data is generated in the machine located in the *workshop,* the control of data format should be done there. Disregarding the process of how the result is yielded, the end resulted data should be in the form of simple human readable file, precisely, TXT or DAT format. Each file will be produced every particular period of time, and each file will contain the readings of the bearing conditions by the machine at that time. Two automatic data acquisition will be conducted at day and night. This will be done by doing two things. First, the executable data acquisition program is written in C language and saved in the EXE format. This is the advantage of PICO DAQ that it can be used not only for human interface but also for automatic way. Second, the automatic data acquisition will be used by running the executable file using Solway's task scheduler shown in Figure F.1. The vibration data are saved in desktop computer where the filename contains the information about date, month and year when the readings are taken.

Initial online monitoring process used free hosting. There is limited data transferred for free hosting. Therefore, the huge file of vibration data should be transformed into less capacity by calculating the useful information. This information is usually called features. In this work, six time domain features are used: root mean square (RMS), shape factor (SF), skewness, kurtosis, crest factor (CF), entropy, histogram lower and histogram upper. The executable MATLAB program is created to do the six feature calculations. This program also runs automatically using Solway's task scheduler approximately every 30 minutes after the automatic data acquisition as shown in Figure F.1. The illustration of automatic data acquisition, automatic feature calculation and online monitoring process are shown in Figure F.4.

The readings as mentioned before are divided into four different channels (channel 1 to channel 4). In other words, each file will contain four values that represent the condition of bearing from four different accelerometer locations, separated by space. As automatic data acquisition will be conducted at two different times (day and night), the feature calculation filename will consist of two data names as well. For example,

the kurtosis feature will be saved as 'kur_1.txt' for day and 'kur_2.txt' for night. Each file will consist of five columns where the first columns will be the date, month and year when the features are calculated. The Second to the fifth columns are the accelerometer channel 1 to accelerometer channel 4. The six different feature calculation data will be temporarily stored in the connected desktop computer. The illustration of data format is shown in Figure F.2 below.

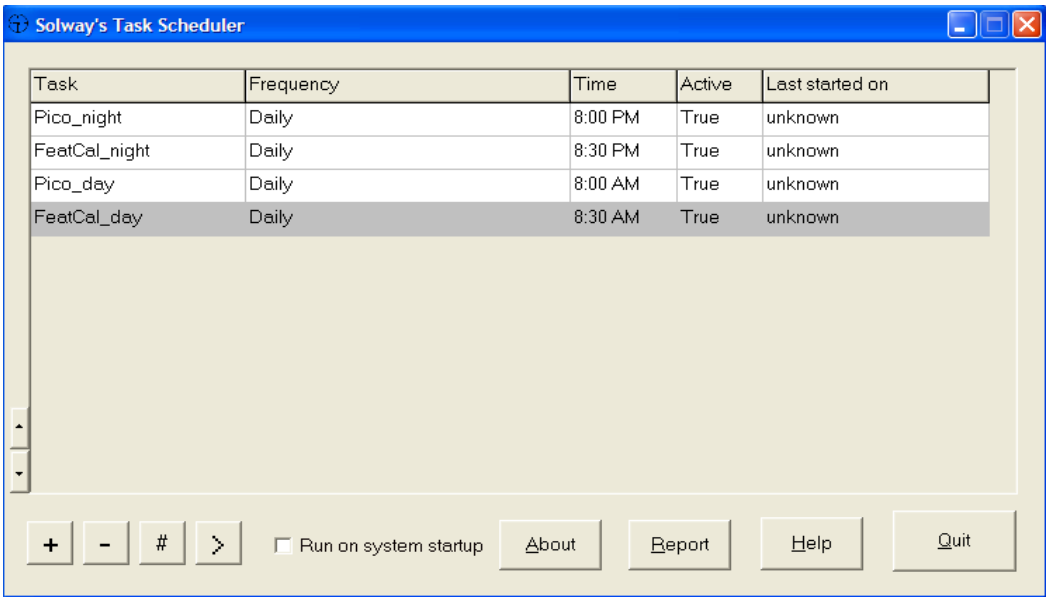

Figure F.1 Solway's task scheduler.

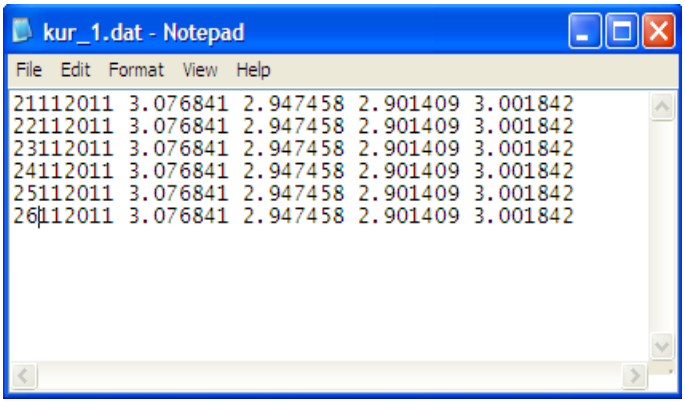

Figure F.2 Example of feature file format.

The above figure is an example of data format for kurtosis feature. The file contains six feature calculations from 21 November 2011 to 26 November 2011. The next feature calculation data will be saved on the last row. This process will run continuously until the measurement stops due to bearing collapse. The first

function of GoodSyns is to identify any changes of the file. In other words, the newly produced data is checked against the existing data in Data Centre. Since the new data is not detected in the server, then it will begin the process of synchronizing between the 2 data sites. This way, it is expected to avoid the probability of data redundancy while maintaining the data being tuned.

The way the data transmitted is using simple File Transfer Protocol (FTP). It is already well known and the software for it is already across the globe. The software should at least be able to do the three major processes which are:

a. Transmit file over FTP
b. Bypass the campus's network using proxy
c. Synchronizing between the 2 data site accordingly.

The three major processes above are solved by using GoodSync software. This software is purchased and installed in desktop computer. The window of GoodSync is shown in Figure F.3.

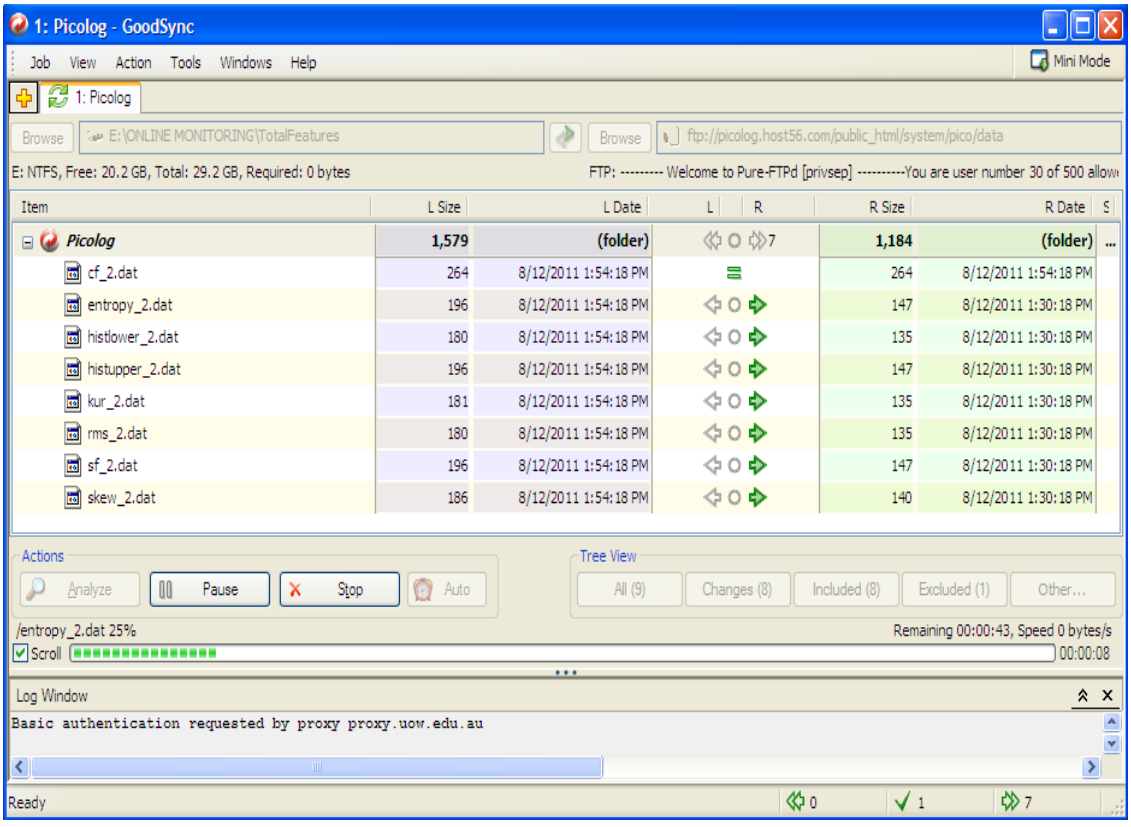

Figure F.3 GoodSync.

Server

The server that is expected to handle a lot of storage and bandwidth sizes to access this site must be reasonable enough (if use paid hosting). Since the transaction including downloading the data from any *client* is done regularly, it is very important to choose a competent hosting site. Most likely, the best choice for this project is the unlimited storage and unlimited bandwidth. The costs are ranged at 4 AUD per month, or greater than that. Moreover, the hosting site should satisfy the following needs:

a. Allow FTP connection to their site
b. Support PHP and MySQL just in Case
c. Again, unlimited storage and bandwidth is favourable

Since the needed data for the *client* site is as the following:

a. Root mean square (RMS)
b. Shape factor (SF)
c. Skewness
d. Kurtosis
e. Crest factor (CF)
f. Entropy
g. Histogram lower and
h. Histogram upper

Then the data must be prepared before fetched by the *client* site. The calculation for each variable will be done in 2 different triggers, automatically and an update button pressed. The first option should check the webpage that is accessed last time. As long as current timestamp and the previous timestamp fall under the same timeframe (frames are like sessions, depend on the FTP frequency), no pre-processor is executed due to definitely no additional raw data. In case the timeframes are different, then the calculations are needed, since we already have new data to be displayed. This way, optimization can be achieved as no unnecessary processes are wasted.

In case of manual update, this button will be provided if and only if the user wishes to do so and not necessarily to do it. Just to reassure the user that the data can be updated at user's wills.

Client

Any computer with internet browser is considered as client. After simple verification the calculated data are then displayed accordingly. The users are given several configurations options to choose what data are preferred to be displayed by default. Users are also allowed to download the data. May it be individually or in several at once. Furthermore, the displayed data is powered by JavaScript to make it more interactive and easier to deal with.

The expected configurations are:

a. Display all data on start-up
b. Download latest data on start-up
c. Only display last 3 days data
d. Etc.

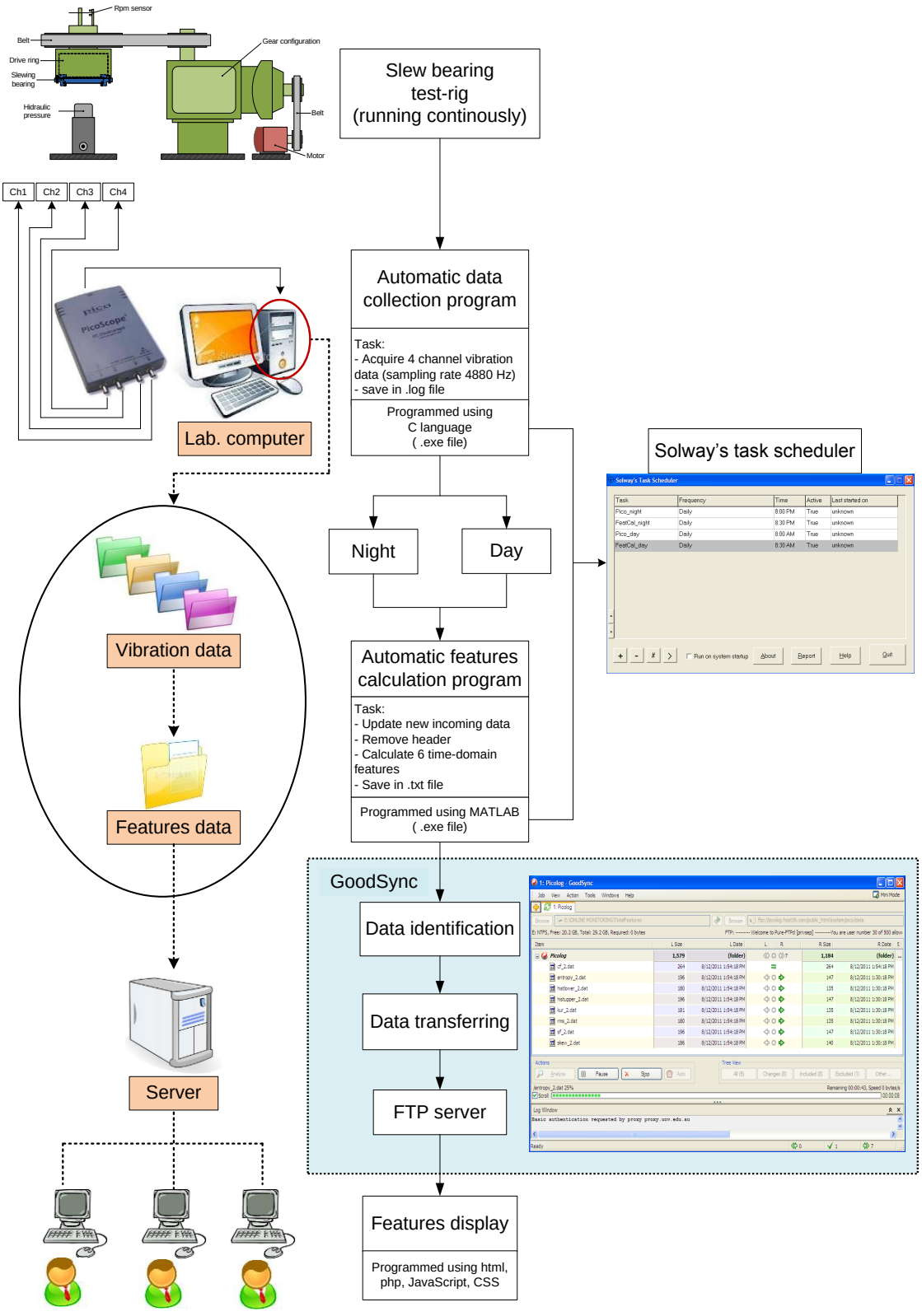

Figure F.4 Online monitoring framework.

F.3 Online monitoring result

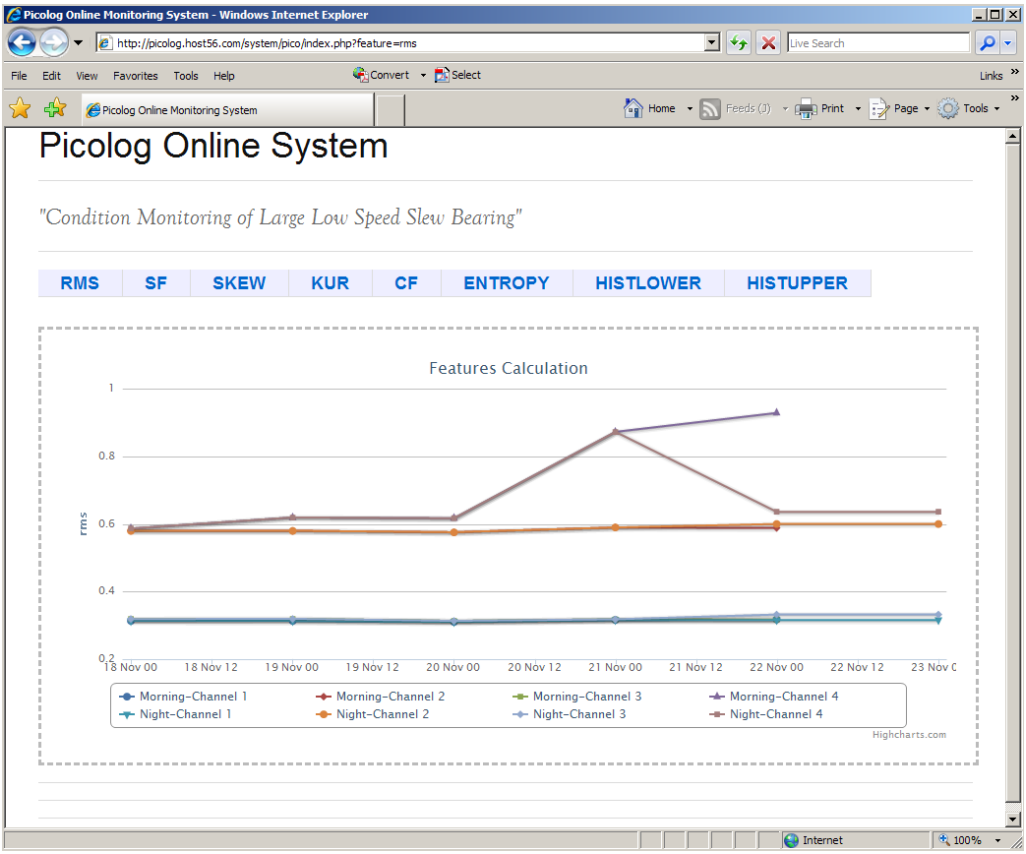

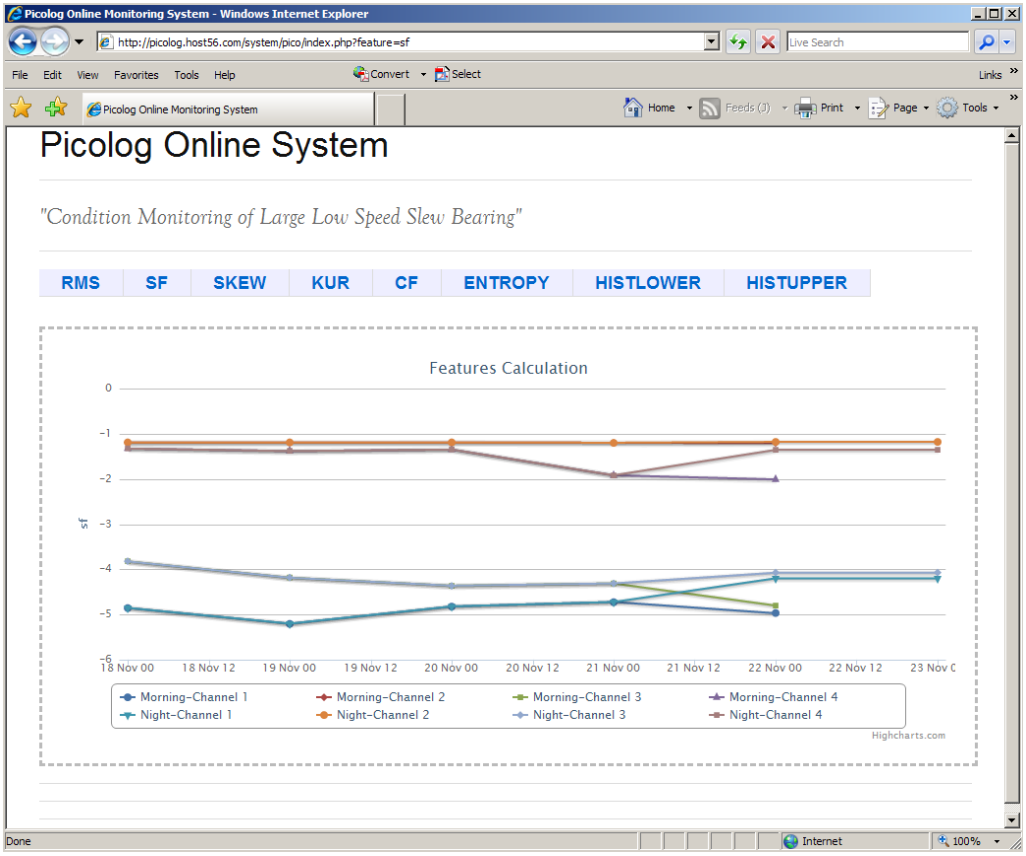

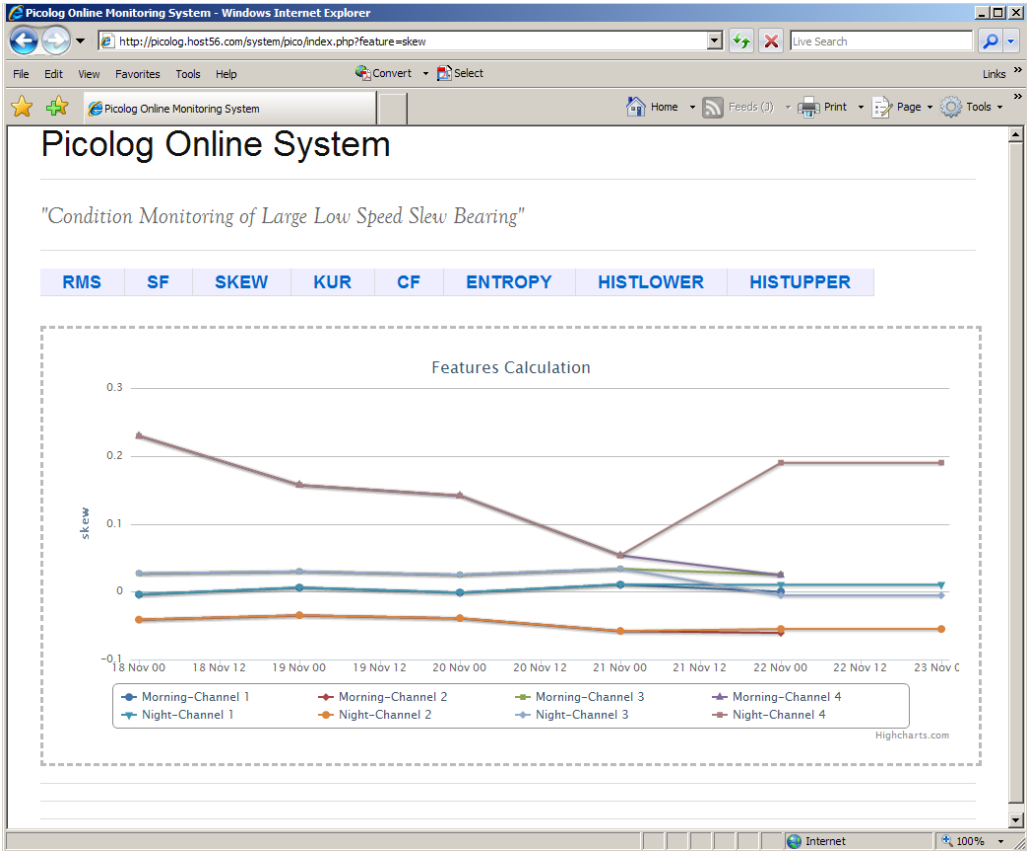
Picolog Online Monitoring System - Windows Internet Explorer
http://picolog.host56.com/system/pico/index.php?feature=skew
Picolog Online System
"Condition Monitoring of Large Low Speed Slew Bearing"
RMS SF SKEW KUR CF ENTROPY HISTLOWER HISTUPPER
Features Calculation
skew
Morning-Channel 1
Morning-Channel 2
Morning-Channel 3
Morning-Channel 4
Night-Channel 1
Night-Channel 2
Night-Channel 3
Night-Channel 4
Highcharts.com

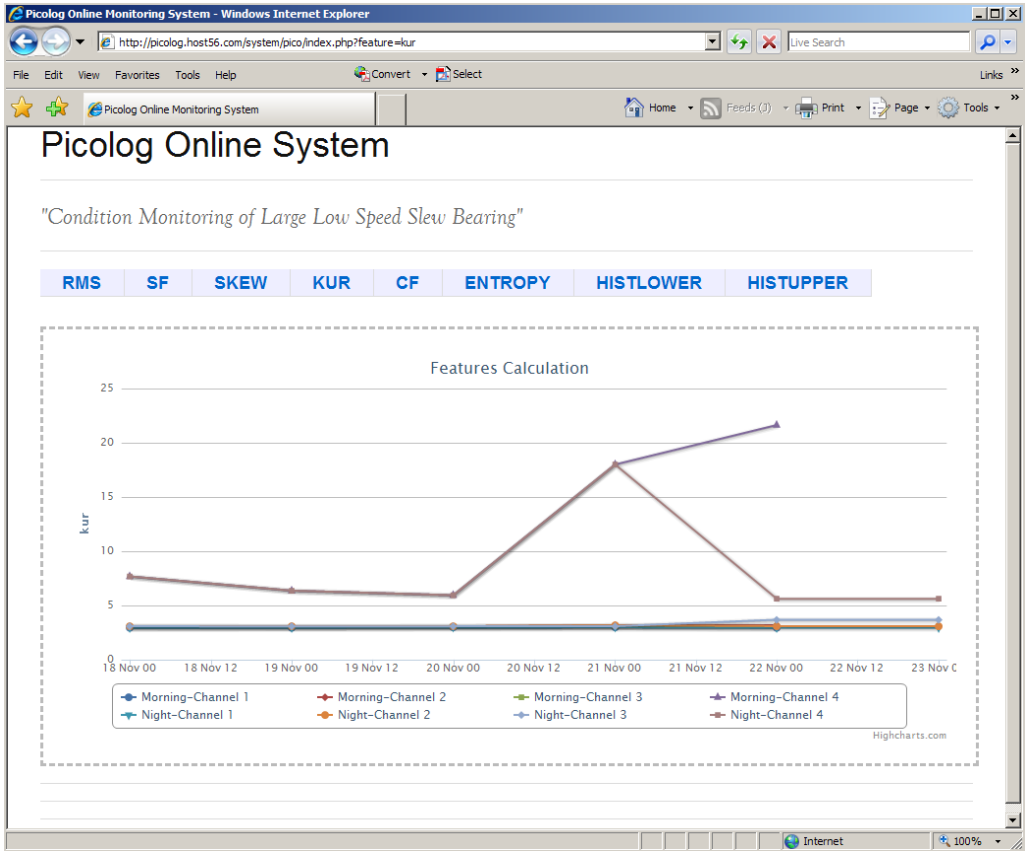
Picolog Online Monitoring System - Windows Internet Explorer
http://picolog.host56.com/system/pico/index.php?feature=kur
Picolog Online System
"Condition Monitoring of Large Low Speed Slew Bearing"
RMS SF SKEW KUR CF ENTROPY HISTLOWER HISTUPPER
Features Calculation
kur
Morning-Channel 1
Morning-Channel 2
Morning-Channel 3
Morning-Channel 4
Night-Channel 1
Night-Channel 2
Night-Channel 3
Night-Channel 4
Highcharts.com